IMMUNOTHERAPY AND IMMUNE REGULATION OF HEAD AND NECK CANCER

EDITED BY: Song Fan, Pablo Parente-Arias, Gary Goldberg and Soldano Ferrone
PUBLISHED IN: Frontiers in Oncology

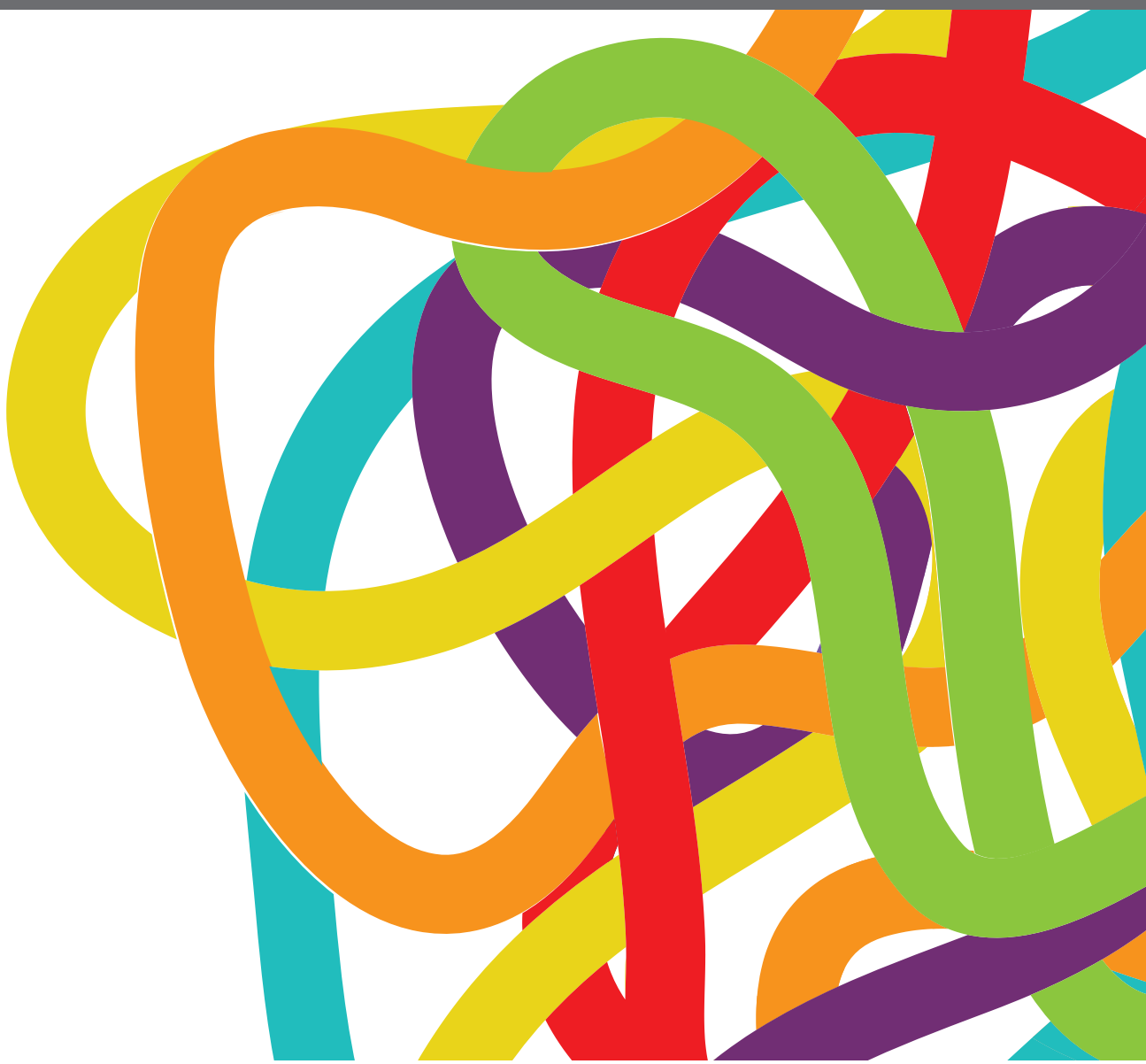

frontiers Research Topics

ISSN 1664-8714
ISBN 978-2-83250-861-9
DOI 10.3389/978-2-83250-861-9

About Frontiers

Frontiers is more than just an open-access publisher of scholarly articles: it is a pioneering approach to the world of academia, radically improving the way scholarly research is managed. The grand vision of Frontiers is a world where all people have an equal opportunity to seek, share and generate knowledge. Frontiers provides immediate and permanent online open access to all its publications, but this alone is not enough to realize our grand goals.

Frontiers Journal Series

The Frontiers Journal Series is a multi-tier and interdisciplinary set of open-access, online journals, promising a paradigm shift from the current review, selection and dissemination processes in academic publishing. All Frontiers journals are driven by researchers for researchers; therefore, they constitute a service to the scholarly community. At the same time, the Frontiers Journal Series operates on a revolutionary invention, the tiered publishing system, initially addressing specific communities of scholars, and gradually climbing up to broader public understanding, thus serving the interests of the lay society, too.

Dedication to Quality

Each Frontiers article is a landmark of the highest quality, thanks to genuinely collaborative interactions between authors and review editors, who include some of the world's best academicians. Research must be certified by peers before entering a stream of knowledge that may eventually reach the public - and shape society; therefore, Frontiers only applies the most rigorous and unbiased reviews.
Frontiers revolutionizes research publishing by freely delivering the most outstanding research, evaluated with no bias from both the academic and social point of view. By applying the most advanced information technologies, Frontiers is catapulting scholarly publishing into a new generation.

What are Frontiers Research Topics?

Frontiers Research Topics are very popular trademarks of the Frontiers Journals Series: they are collections of at least ten articles, all centered on a particular subject. With their unique mix of varied contributions from Original Research to Review Articles, Frontiers Research Topics unify the most influential researchers, the latest key findings and historical advances in a hot research area! Find out more on how to host your own Frontiers Research Topic or contribute to one as an author by contacting the Frontiers Editorial Office: frontiersin.org/about/contact

IMMUNOTHERAPY AND IMMUNE REGULATION OF HEAD AND NECK CANCER

Topic Editors:
Song Fan, Department of Oral & Maxillofacial Surgery, Sun Yat-sen Memorial Hospital, China
Pablo Parente-Arias, A Coruña University Hospital Complex (CHUAC), Spain
Gary Goldberg, Rowan University School of Osteopathic Medicine, United States
Soldano Ferrone, Massachusetts General Hospital, Harvard Medical School, United States

Citation: Fan, S., Parente-Arias, P., Goldberg, G., Ferrone, S., eds. (2022). Immunotherapy and Immune Regulation of Head and Neck Cancer. Lausanne: Frontiers Media SA. doi: 10.3389/978-2-83250-861-9

Table of Contents

frontiers in Oncology

REVIEW
published: 10 September 2021
doi: 10.3389/fonc.2021.744889

The Stromal and Immune Landscape of Nasopharyngeal Carcinoma and Its Implications for Precision Medicine Targeting the Tumor Microenvironment

Lanqi Gong[1,2], *Dora Lai-Wan Kwong*[1,2], *Wei Dai*[1,2], *Pingan Wu*[3], *Yan Wang*[4], *Anne Wing-Mui Lee*[1,2*] *and Xin-Yuan Guan*[1,2*]

[1] Department of Clinical Oncology, Li Ka Shing Faculty of Medicine, The University of Hong Kong, Hong Kong, Hong Kong, SAR China, [2] Department of Clinical Oncology, The University of Hong Kong-Shenzhen Hospital, Shenzhen, China, [3] Department of Surgery, The University of Hong Kong-Shenzhen Hospital, Shenzhen, China, [4] Department of Pathology, The University of Hong Kong-Shenzhen Hospital, Shenzhen, China

The evolution of the tumor microenvironment (TME) is a cancer-dependent and dynamic process. The TME is often a complex ecosystem with immunosuppressive and tumor-promoting functions. Conventional chemotherapy and radiotherapy, primarily focus on inducing tumor apoptosis and hijacking tumor growth, whereas the tumor-protective microenvironment cannot be altered or destructed. Thus, tumor cells can quickly escape from extraneous attack and develop therapeutic resistance, eventually leading to treatment failure. As an Epstein Barr virus (EBV)-associated malignancy, nasopharyngeal carcinoma (NPC) is frequently infiltrated with varied stromal cells, making its microenvironment a highly heterogeneous and suppressive harbor protecting tumor cells from drug penetration, immune attack, and facilitating tumor development. In the last decade, targeted therapy and immunotherapy have emerged as promising options to treat advanced, metastatic, recurrent, and resistant NPC, but lack of understanding of the TME had hindered the therapeutic development and optimization. Single-cell sequencing of NPC-infiltrating cells has recently deciphered stromal composition and functional dynamics in the TME and non-malignant counterpart. In this review, we aim to depict the stromal landscape of NPC in detail based on recent advances, and propose various microenvironment-based approaches for precision therapy.

Keywords: nasophanrygeal carcinoma, tumor microenvionment, precision medicine, single-cell sequencing, immune regulation

OPEN ACCESS

Edited by:
Gary Goldberg,
Rowan University School of Osteopathic Medicine, United States

Reviewed by:
Benjamin E. Gewurz,
Brigham and Women's Hospital and Harvard Medical School, United States
Franz Rödel,
University Hospital Frankfurt, Germany

****Correspondence:***
Anne Wing-Mui Lee
awmlee@hku.hk
Xin-Yuan Guan
xyguan@hku.hk

Specialty section:
This article was submitted to Head and Neck Cancer, a section of the journal Frontiers in Oncology

Received: *21 July 2021*
Accepted: *23 August 2021*
Published: *10 September 2021*

Citation:
Gong L, Kwong DL-W, Dai W, Wu P, Wang Y, Lee AW-M and Guan X-Y (2021) The Stromal and Immune Landscape of Nasopharyngeal Carcinoma and Its Implications for Precision Medicine Targeting the Tumor Microenvironment. Front. Oncol. 11:744889. doi: 10.3389/fonc.2021.744889

INTRODUCTION

NPC is a unique type of cancer in terms of its geographical distribution, differentiation grade and microenvironmental landscape. According to the global cancer statistics in 2020, more than 75% of NPC cases were diagnosed in East and Southeast Asia, especially in southern China (1) (**Figures 1A, B**). People who have ancestors who originally resided in southern China possess a higher possibility of NPC incidences, indicating that NPC pathogenesis might be closely related to epidemiological patterns and genetic susceptibility in certain ethical groups (2). In addition, undifferentiated NPC (The World Health Organization type III histology) is the predominant disease type that constitutes more than 90% of total incidences, in which tumor cells exhibit many stem-cell-like signatures, including CD133, CD44 and ALDH1 (3–6). The NPC microenvironment might provide a supportive niche for such a high portion of undifferentiated cells. Compared with many solid tumors, NPC has the most severe stromal infiltration, possibly because NPC is originated from the nasopharynx that contains secondary/tertiary lymphoid structures (TLSs) and closely associated with EBV infection (7). Even EBV-negative NPC tumors and non-malignant nasopharyngeal tissues are also intensively infiltrated with varied stromal cells, caused by the locoregional lymphoid structures and tumor-mediated mechanism (8, 9). However, the differentiated NPC is significantly less infiltrated with stromal cells, suggesting that pathological status might alter cellular composition in the NPC microenvironment. During the past decades, the tumor heterogeneity and stromal landscape in the NPC microenvironment remain largely unexplored. Only few studies have reported that T cell and myeloid-derived cells are the predominant stromal subtypes in the NPC microenvironment based on hematoxylin and eosin (H&E) staining, immunohistological (IHC) staining and flow cytometry (10–12). Other stromal cells, such as fibroblasts and B cells, have not been comprehensively characterized in the NPC microenvironment yet, but might be associated with stemness, therapeutic resistance, and immune regulation (13, 14). However, these techniques using few gene signatures remain far from sufficient to identify the finer stromal subpopulations and characterize the functional dynamics of those tumor-infiltrating cells on immune suppression and tumor progression.

The lack of understanding of the stromal landscape in NPC significantly hinders the development of precision medicine. Conventional chemotherapy (cisplatin, gemcitabine and fluorouracil) and radiotherapy have been facing obstacles in optimizing the efficacy in locoregional advanced NPC, overcoming acquired resistance, and suffering from long-term toxicities (15–17). Recently, immunotherapy has emerged as a new strategy to treat recurrent, metastatic, and chemo/radio-resistant NPC patients using PD-1 inhibitors, including camrelizumab, pembrolizumab and nivolumab (18–20). Although the PD-1-based therapeutics has been shown effective in phase I/II clinical trials, it has also suffered from patient-specific responsiveness and adaptive resistance after long-term dosage. Resistance to immunotherapy is multifaceted since the functional state of infiltrating stromal cells is dynamic. Thus, in order to optimize precision medicine in NPC patients, it remains essential to comprehensively decipher the stromal landscape in NPC, and to identify patient-specific targets and signatures associated with prognosis and treatment responsiveness (**Figure 1C**).

Single-cell sequencing has provided a powerful platform to analyze the heterogeneous ecosystem in cancer. As yet, research enthusiasm for single-cell sequencing has remained high, and the TME-infiltrating cells in many cancers have been revealed. Single-cell analysis has provided bench-to-bedside guidelines to clinical practice, especially by revealing TME-based targets that can re-activate immune response or inhibit tumor-facilitating effects. However, the single-cell sequencing of NPC only started after 2019, largely due to its low global incidence. So far, single-cell data of NPC have participated in the public repository and contributed to the establishment of large-scale and multi-central cohorts for downstream analysis (21). In this review, we aim to address the stromal landscape in NPC based on recent advances, and subsequently propose a variety of approaches to enhance therapeutic response and patient prognosis *via* specifically targeting the immunosuppressive and tumor-promoting microenvironment.

THE HETEROGENOUS NPC MICROENVIRONMENT SHAPED BY LOCOREGIONAL LYMPHOID INFILTRATION, EBV INFECTION AND TUMOR-MEDIATED RECRUITMENT

NPC is categorized as an inflamed tumor based on its spatial localization of stromal cells with respect to tumor compartments (22). Stromal cells are in close proximity to and in contact with NPC cells, instead of being embedded in the surrounding regions away from the tumor core. Hence, cytokine secretion and ligand-receptor interactions are both involved in the bilateral tumor-stroma interplay. It is also noteworthy that the nasopharynx is one of the first defensive organs against viral and bacterial entry and infection, which makes its underlying microenvironment highly heterogenous and immunogenic prior to malignant transformation.

There exist two major cell lineages in the nasopharyngeal microenvironment, $CD45^+$ immune cells, including T cells, B cells, natural killer cells (NK cells), and myeloid-derived cells, as

Abbreviations: TME, Tumor microenvironment; EBV, Epstein Barr virus; NPC, Nasopharyngeal carcinoma; TLS, Tertiary lymphoid structure; H&E staining, Hematoxylin and eosin staining; IHC staining, Immunohistological staining; NK cell, Natural killer cell; Treg cell, Regulatory T cell; IFN, Interferon; EBNA1, Epstein-Barr nuclear antigen 1; LMP1, Latent membrane protein 1; LMP2, Latent membrane protein 2; EBER, Epstein-Barr encoding region; MDSCs, Myeloid-derived suppressor cells; TCR, T-cell receptor; HNSCC, Head and neck squamous cell carcinoma; HPV, Human papillomavirus; GZM, Granzyme; DC, Dendritic cell; HCC, Hepatocellular carcinoma; NSCLC, Non-small-cell-lung cancer; ESCC, Esophageal squamous cell carcinoma; ECM, Extracellular matrix; FGF2, Fibroblast growth factor 2; FAP, Fibroblast activation protein-α; CAFs, Cancer-associated fibroblasts; FFPE tissue sample, Formalin-fixed paraffin-embedded tissue sample.

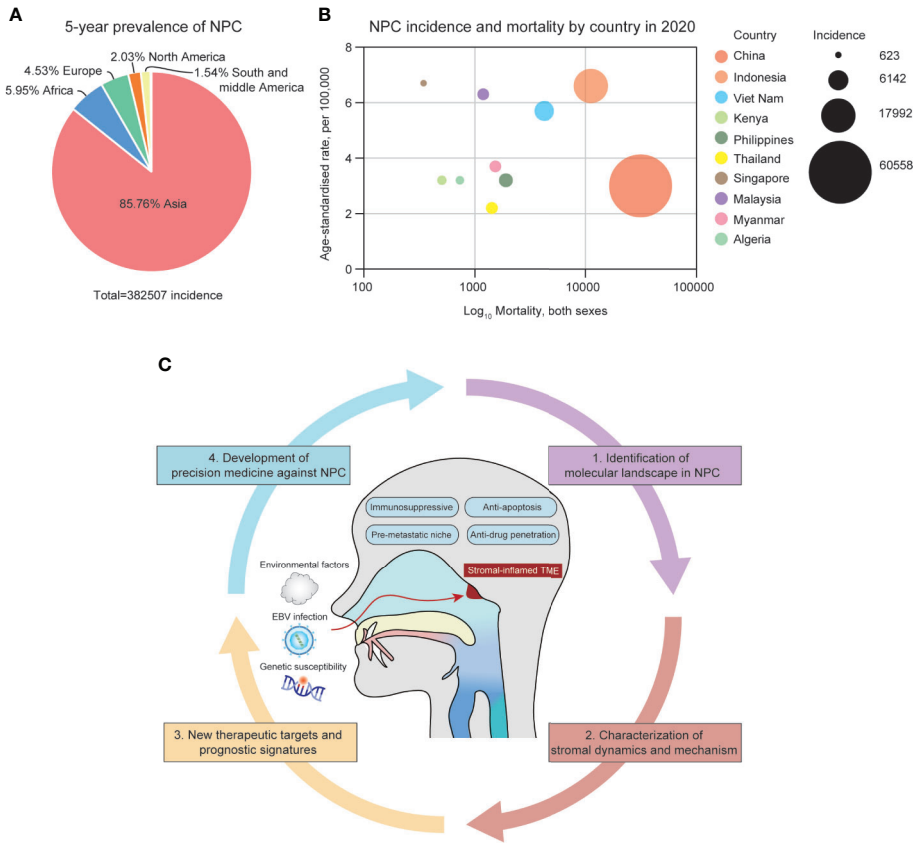

FIGURE 1 | **(A)** The 5-year prevalence of NPC incidences around the globe from 2015-2020. **(B)** The geographical distribution of NPC incidences in Asia, 2020. **(C)** The summary of the NPC microenvironment and focuses of the review.

well as $CD45^-$ non-immune stromal cells, including fibroblasts and endothelial cells. Recent single-cell analysis has revealed that normal nasopharyngeal tissues also have high immune infiltration, especially for T and B lymphocytes (23, 24). Fibroblasts and myeloid-derived cells are hardly seen from normal nasopharyngeal tissues, even those with reactive hyperplasia caused by allergy and inflammation (23, 24). The major stromal landscape between normal nasopharyngeal tissues and malignant nasopharyngeal carcinoma is distinctive. For instance, B cells are highly enriched in the normal nasopharyngeal tissues upon inflammation, whereas T cells, NK cells, myeloid-derived cells and fibroblasts, are more likely to infiltrate the NPC microenvironment (23). Germinal centers are commonly seen in the normal nasopharyngeal tissues, where $CD3^+/CCR7^+$ naïve T cells and $CD19^+/CD27^-$ naïve B cells accumulate and proliferate, causing lamps in the nasopharynx (23, 25). Under non-malignant inflammation, a large portion of those naïve lymphocytes does not differentiate into cytotoxic, memory and regulatory phenotypes. However, the chronic EBV infection and tumor progression result in an increasing number of naïve cells transitioned into an activated state, and eventually become exhausted (26). Retrospective cohort studies have found that 90% of NPC incidences are accompanied by EBV infection, but there still are EBV^- cases where the stromal composition is distinctive from EBV^+ counterparts (27). The abundance of major cell lineages in EBV^- NPC patients, does not significantly differ from the abundance in the EBV^+ microenvironment, but the exhausted and immunoregulatory subtypes, such as $HAVCR2^+/PD\text{-}1^+$ T cells, $CD25^+/FOXP3^+/CTLA4^+$ regulatory T cells (Tregs) and $CD68^+$ myeloid-derived cells are found more enriched in the EBV^+ microenvironment (11, 28). Besides, the functional state of infiltrating immune cells has been greatly influenced by the hyper-activation of interferon (IFN) secretion induced by EBV infection. In the NPC microenvironment, type I and type II IFNs, namely IFN-α and IFN-γ, are activated to combat viral entry and incorporation. Thus, the IFN-α and IFN-γ signaling pathways are activated in almost all the infiltrating immune cells, mainly reflecting in up-regulation of IFN-induced genes, including ISG15, IFI6, IFI44L, IFIT3 and IFITM1 (23). On the contrary, NF-κB signaling is up-regulated in nasopharyngeal tissues upon non-malignant inflammation, but it is also closely associated with inflammation caused by EBV-encoded genes (23). Although IFNs play a vital role in anti-tumor cytotoxicity, previous

studies have reported that chronic IFN activation in the TME hijacks helper T cell response and leads to progressive exhaustion of T cells and persistent infection (29–31). Nevertheless, the molecular mechanism of chronic IFN activation on immune cells needs to be further investigated, including its effect on antigen presentation, T cell differentiation, activation and exhaustion.

EBV infection in NPC is classified as type II latency and contributes to TME remodeling. Type II latency is characterized by the expression of a set of latent genes in NPC, including Epstein-Barr nuclear antigen 1 (EBNA1), latent membrane protein 1 (LMP1), LMP2 and Epstein-Barr encoding region (EBER) RNAs (32, 33). LMP1 and EBNA1 expressed by NPC cells are able to induce PD-L1 up-regulation *via* STAT3 and NF-κB signaling, Treg recruitment *via* CXCL12-CXCR4 chemotaxis, as well as expansion of myeloid-derived suppressor cells (MDSCs) (31, 34, 35). EBV can also infect B cells, however, the infiltrating B cells in the NPC microenvironment are uninfected, indicating that EBV infection on nasopharyngeal epithelial cells may occur prior to B-cell recruitment and accumulation (36). Tumor-mediated recruitment is another mechanism to alter the microenvironmental landscape. NPC cells specifically express cytokine-encoding genes, including CX3CL1, CXCL10, CCL2, CSF1, IL-10 and TGF-β1 that are critical for the recruitment of immune cells from peripheral blood and immune suppression (37, 38). T-cell receptor (TCR) profiling has revealed that $CX3CR1^+$ T cells are migrated from the peripheral blood into the NPC microenvironment *via* CX3CL1-CX3CR1 chemotaxis. Differentiated NPC has higher macrophage infiltration, lower B cell infiltration and worse prognosis compared with undifferentiated NPC (39, 40). Although Longitudinal analysis has suggested that the peripheral myeloid-to-lymphocyte ratio negatively correlated with overall survival in NPC patients, little is known whether the prognosis is directly influenced by the abundance of macrophages and B cells in the TME (41).

Other head and neck squamous cell carcinoma (HNSCC) developed from the oral cavity, oropharynx, hypopharynx, and larynx, also displays an inflamed microenvironmental landscape due to NF-κB activation and immune evasion (42, 43). Human papillomavirus (HPV), instead of EBV, plays a vital role in the immune modulation of HNSCC. HPV^+ HNSCC is infiltrated with a higher number of Tregs, $CD20^+$ B cells, and NK cells, but a lower number of T helper cells than its HPV^- counterpart and non-malignant inflamed tonsil (42, 44). HPV infection also causes T cell dysfunction, possibly *via* the overreaction of IFN-associated signalings and HPV integration into the host genome (42, 45). B cell infiltration in HPV-associated HNSCC is as high as in NPC and similarly correlates to a better prognosis (44). Germinal centers and TLSs are frequently seen in HPV^+ tumors, associated with better patient survival and responsiveness to ICB therapies (44, 46). PD-1/PD-L1 blockades combined with chemotherapeutic drugs such as platinum and fluorouracil have prolonged the overall survival by three months in patients with advanced and metastatic HNSCC (47). However, the objective response rates of nivolumab and pembrolizumab in HNSCC patients are only 15%, significantly lower than in NPC patients (48, 49). The paradigm-shifting therapeutics in NPC, including alleviating viral infection, inactivating Treg-mediated suppression and expanding TLS-associated B cells within the TME, might also be feasible in HPV^+ HNSCC to synergistically promote PD-1/PD-L1 efficacy.

The severe stromal infiltration in the NPC microenvironment is not solely shaped by one factor, but a combination of factors that lead to the phenomenon we have seen in clinical practice. Amidst the complexity of the NPC microenvironment, many therapeutic targets remain effective to modulate the tumor-stroma interplay, which imparts strong influences on tumor progression and therapeutic resistance and responsiveness. For instance, while exhausted and regulatory T and myeloid-derived cells exhibit immunosuppressive function in response to cytokine stimulation and antigen presentation in NPC, they can also be reprogrammed to reinvigorate tumor-specific cytotoxicity *via* pharmacological administration. The plasticity of the NPC microenvironment has offered an approach to specifically re-activate dysfunctional subtypes and in-activate suppressive subtypes to achieve optimal anti-tumor effects, which requires an in-depth understanding of the stromal phenotyping and functional dynamics.

TARGETING T CELLS AND NK CELLS TO REINVIGORATE TUMOR-SPECIFIC IMMUNITY

Tumor survival from the host immune system is one of the critical steps during malignant progression, which can be achieved *via* inhibition of cytotoxic cells and activation of immunosuppressive cells. Naïve T cells are intrinsically enriched around the germinal centers in the nasopharynx. As a consequence of tumor progression, the normal T-cell differentiation and activation processes can be hijacked by NPC cells and eventually result in the dominance of dysfunctional and suppressive T cells in the NPC microenvironment. The inhibitory signatures on $CD8^+$ T cells, including PD-1, HAVCR2 and LAG3 have been found up-regulated by $EpCAM^+HLA\text{-}DR^{High}$ NPC cells *via* ligand-receptor interaction (50). TCR profiling on NPC-derived T cells has validated the presence of activation-to-exhaustion transition, where a portion of activated effector T cells gradually loses its cytotoxic function (23). Indeed, the exhaustion program is dynamic instead of terminally static. Most of the exhausted T cells can still secrete cytotoxic cytokines, particularly IFN-γ and granzymes (GZMs), but at a lower level than fully activated effector cells. Therefore, a high abundance of exhausted and activated T cells usually correlated to better prognosis and higher immunotherapeutic responsiveness in NPC patients (23, 24).

Targeting $CD8^+$ T cells primarily focuses on how to inhibit and reverse the activation-to-exhaustion transition. Targeting inhibitory checkpoint molecules has been shown effective in the context of anti-tumor immunity, in which PD-1 is currently the

only therapeutic target for $CD8^+$ T cells in NPC clinical trials (20, 51). The clinical response rate for PD-1 monotherapy using camrelizumab, nivolumab and pembrolizumab ranges from 20.5% to 34% in phase I/II clinical trials (18–20, 52). Although the response rate for pembrolizumab in NPC (phase I, 25.9%) is significantly higher than in non-small-cell lung cancer (phase I, 19.4%), hepatocellular carcinoma (phase III, 18.4%) and gastroesophageal cancer (phase II, 11.6%), synergistically targeting more highly expressed receptors in NPC-infiltrating exhausted T cells might enhance the anti-tumor immunity of PD-1 monotherapy (53–55). $HAVCR2^{High}$ exhausted T cells had a unique exhaustion program but identical TCR clonotypes with $PD\text{-}1^{High}$ counterparts, indicating that the exhaustion transition is not independent where exhausted T cells are maintained as a homogenous population with fixed molecular signatures (23). Conversely, T cells on an early, intermediate or late exhaustion stage, exhibited phase-specific inhibitory signatures and can be continually transformed from one stage to another upon stimulation. Single-cell sequencing and multiplex immunofluorescence has corroborated that HAVCR2, instead of PD-1, is the predominant inhibitory molecule in the NPC microenvironment (23, 24, 56). BGB-A425, as a humanized anti-Tim-3 (encoded by HAVCR2) antibody, is currently in progress of phase I/II clinical trials treating solid tumors in combination with tislelizumab, which has been shown to augments T-cell response *via* enhancing IFN-γ production and NK-mediated cytotoxicity (57). Galectin-9 (encoded by LGALS9), as the most studied ligand for HAVCR2, is specifically expressed by NPC cells, as an immunosuppressive molecule induced by high intratumoral IFN-β and IFN-γ (58, 59). Inhibition of LGALS9 selectively expands and activates infiltrating exhausted T cells by intervening in the crosstalk between PD-1 and HAVCR2 (59). Targeting IFN-induced LGALS9 up-regulation and secretion in NPC cells might be an alternative approach to overcome the primary and adaptive resistance to the PD-1/PD-L1 therapy.

LAG3 is another predominant inhibitory signature on infiltrating exhausted T cells in the NPC microenvironment (23, 24, 56). Unlike HAVCR2, LAG3 has been found specifically expressed on exhausted $ZNF683^+$ tissue-resident T cells (23). The average abundance of tissue-resident memory T cells in the NPC microenvironment is approximately 10%, two-fold lower than the cytotoxic and exhausted T cells (23). It might be that a substantial amount of infiltrating cytotoxic T cells does not originally reside in the nasopharynx, but is recruited from peripheral blood. As previously stated, $CD8^+/CX3CR1^+$ T cells with minimal cytotoxicity and proliferative capacity are migrated from blood and quickly become exhausted *via* an EBV^+ NPC-secreted cytokine, CX3CL1, constituting the major source of infiltrating $CD8^+$ T cells in the TME (56). In phase I/II clinical trials, the efficacy of LAG3-targeted antibodies, such as MK-4280, TSR-033 and IMP321, are often evaluated in combination with anti-PD-1 and anti-HAVCR2 treatment to promote responsiveness (60, 61). Although therapeutic targeting to HAVCR2 and LAG3 is currently not as mature as to PD-1, we must pay attention that the NPC microenvironment is unique and complicated, which means that we cannot directly adapt a developed therapeutics from other malignancies into NPC treatment. In the future, the combo-therapy synergistically targets PD-1/HAVCR2 or PD-1/LAG3 might become a more effective therapeutic option for NPC patients.

Inactivation of Tregs is also an approach to retrieve immunosurveillance against NPC, which indirectly enhances anti-tumor T cell response. Similar to the exhausted subtypes in the NPC microenvironment, there exist two subtypes of Tregs, resting Tregs and suppressive Tregs, which both have high expression of Treg signatures, including CD25, FOXP3 and IKZF2 (23, 24, 56). The two immunoregulatory subtypes are functionally different since suppressive Tregs possess a higher expression of immune checkpoint CTLA4 and co-stimulatory molecules CD27, TNFRSF4, TNFRSF9 and ICOS (23, 24, 56). Anti-CTLA4 therapy using ipilimumab, has shown effective to improve overall survival in patients with melanoma and hepatocellular carcinoma, but is often used in combination with PD-1 inhibitors (62–65). The efficacy and safety of ipilimumab+nivolumab in NPC is currently under investigation in a phase II clinical trial (NCT03097939). Based on the preliminary data up to February 2020, the partial response rate was 35% with a median duration of response of 5.9 months, which is significantly higher than the responsiveness of PD-1-based monotherapy. The average abundance of $CTLA4^+$ Tregs is approximately 20%, which might explain why NPC is responsive to anti-CTLA4 drugs that relieve Treg-mediated suppression and expedite proliferation of effector T cells (23). In addition, Treg-mediated suppression is largely dependent on CD27-CD70 interaction, which provides co-stimulatory signals critical for naïve-to-Treg differentiation, Treg proliferation and activation. Cusatuzumab (ARGX-110) is a CD70-targeting drug currently under clinical evaluation. Previous *in vitro* studies have demonstrated that blocking $CD70^+$ leukemia and B cell lymphoma cell lines using ARGX-110 can inhibit the activation of Treg and facilitate the anti-tumor immunity exerted by $CD8^+$ effector T cells (66). Most of the solid tumors lack CD70 expression, whereas only hematologic cancers have a high frequency of $CD70^+$ cancer cells. Thus, cusatuzumab is mainly being evaluated in acute myeloid leukemia in phase II clinical trial (67). In the NPC microenvironment, CD70 is highly and specifically expressed on tumor cells rather than T cells and dendritic cells (DCs). The pathological examination has confirmed that more than 80% of NPC cases are CD70 positive (68). Therefore, direct targeting of $CD70^+$ tumor cells might further inhibit Treg accumulation and activation in NPC. However, recent studies have suggested that CD70 deficiency in EBV-infected patients might exacerbate chronic EBV infection and predispose them to lymphoma and immune disorders (69, 70). As CD70 is also expressed on $CD8^+$ effector T cells and activated B cells, lack of functional CD70 might hinder T and B cell-mediated immunity to combat EBV infection and further promote tumor progression. Thus, the safety of anti-CD70 therapy should be carefully examined in humanized animal models prior to clinical translation, for its potential to damage immunocompetence.

Accumulating evidence has suggested that the enrichment of Tregs in the NPC microenvironment is also caused by tumor-mediated recruitment, where $CCR4^+$ and $CCR6^+$ resting Treg are migrated from peripheral blood and activated into a suppressive phenotype *via* tumor-secreted CXCL10, CXCL16, CCL20, and CD70 binding (50, 71, 72). Targeting these Treg-attractive chemokines produced by NPC cells might also alleviate the infiltration of Tregs in the TME and sustain $CD8^+$ cytotoxicity. Additionally, excessive production of IFNs might also contribute to Treg accumulation by hijacking the $CD4^+$ naïve T cell differentiation, since $CD4^+$ IFN-induced T cells in the NPC microenvironment co-express naïve signatures.

LGALS1 has been found highly expressed in suppressive Tregs in the NPC microenvironment and plays a vital role in Treg activation (23). Extracellular galectin-1 (encoded by LGALS1) has been implicated in promoting the suppressive capability of Treg and inducing apoptosis of $CD8^+$ T cell (73). LGALS1-deficient mice showed impeded Treg activity. In T cell subpopulations, LGALS1 is correlated to CD25 expression, indicating it might play a vital role in Treg activation. Blocking and CRISPR-silencing of LGALS1 leads to decreased proliferation and IFN production in T cells (74). LGALS1 has long been considered as one of the key regulators in T-cell homeostasis and inflammation. However, its function in Treg has not been explicitly elucidated. LGALS1 up-regulation in Treg promotes growth arrest and apoptosis and inhibits the secretion of pro-inflammatory cytokines of activated T cells. Thus, it might serve as an immune checkpoint to revert the Treg-mediated suppression *via* partial activation. In HPV^+ and HPV^- head and neck squamous cell carcinoma, LGALS1 blockade has resulted in elevated infiltration of T cells in tumor cores and further enhance response to PD-1 therapy (75). In clear cell renal carcinoma, patients who are responsive to PD-1 therapy possess a higher expression of LGALS1 (76). Thus, inhibition of LGALS1 might synergize with ICB-based monotherapy. TNF-alpha signaling and calcium channel might be regulated by LGALS1 to exert its effect on T cell survival and activation. LGALS1 has also been found expressed on NPC cells, further confirming that NPC cells are actively involved in immune regulation of the TME. Currently, there are no clinically available therapeutic agents that specifically target LGALS1, but targeting LGALS1 in NPC patients remains a feasible approach that worth to be developed in the future.

NK cells are commonly characterized by the high expression of GNLY, and they also express chemokines CCL5, XCL1 and XCL2 responsible for the recruitment of pro-inflammation $CCR5^+/XCR1^+$ DCs (77). Compared with cytotoxic T cell infiltration, NK cells constitute a relatively minor subpopulation (~2% of the total stromal infiltrates) (23). Previous studies have suggested the presence of dysfunctional NK cells with NKG2A, PD-1 and HAVCR2 up-regulation in the TME (78). In the NPC microenvironment, NK cells do not express these exhaustion signatures, instead, NK cells highly express cytotoxic signatures, indicating that NK cells might not be severely influenced by tumor cells and chronic infection (23). It offers a new perspective for anti-tumor immunity which we can expand or recruit immune-activated NK cells to counter the loss-of-function in exhausted T cells. Nevertheless, it remains necessary to evaluate the prognostic value of NK-specific signatures and investigate the mechanism so that we can have a better understanding of the role of NK cells in the NPC microenvironment that might facilitate therapeutic development in the future.

TARGETING B CELLS TO ENHANCE RESPONSE TO IMMUNOTHERAPY

Compared with T cells, significantly fewer B cells are often found in the TME (79). However, single-cell analysis in NPC has shown that B cells are more enriched and diverse than previously reported, and the infiltration and functionality of B cells have emerged as a vital prognostic factor and therapeutic target (23, 24, 56). Increased B cell density in the TME facilitates the establishment of TLSs and promotes responsiveness to PD-1/CTLA4 immunotherapy in melanoma (80, 81). The spatial localization and cell-cell communication have been observed in tumor-associated TLSs, where T cells and B cells can undergo cooperative maturation, activation and clonal expansion. In addition, a higher expression of B cell-associated signatures, including CD79A, CD20, CD27, IGHD, CXCR5 and FCLR4, are associated with increased progression-free survival in NPC patients (23). Enrichment of B cells might be caused *via* CXCL13-CXCR5 chemotaxis from surrounding lymph nodes and peripheral blood into the TME. In the NPC microenvironment, CXCL13 is mainly produced by $CD4^+$ helper T cells and $PD\text{-}1^+$ exhausted T cells, suggesting that exhausted T cells might remain beneficial to the immune modulation *via* the recruitment of $CXCR5^+$ B cells (only plasma B cells are $CXCR5^-$) and TLS development (23). In non-small-cell lung cancer patients who received PD-1 blockade, increased CXCL13 production also has been found in $PD\text{-}1^+$ exhausted T cells with impaired cytotoxicity (82). Considering the positive prognostic value of tumor-infiltrating B cells, it might be an effective adjuvant therapy to increase intratumoral B cells *via* CXCL13-dependent recruitment in NPC patients with low TLS density. Consequently, TLSs provide a harbor for lymphocyte maturation and immune activation. Meanwhile, the molecular function and mechanism of infiltrating B cells and tumor-associated TLSs remain undiscovered owing to relatively few B infiltrates in most malignancies. Thus, NPC can serve as an applicable model to investigate the interplay within T cells, B cells and tumor cells.

A higher abundance of intratumoral B cells is frequently associated with better prognosis in NPC patients, but there exist B subtypes that contribute to worse prognosis (23, 24). Single-cell sequencing of NPC patients and non-malignant counterparts has identified the presence of double-negative B cells (IGHD-/CD27-) in the TME. Double-negative B cells are commonly found in the peripheral blood of patients with autoimmune diseases, such as rheumatoid arthritis and systemic

lupus erythematosus (83–85). Although double-negative B cells represent a rare subpopulation in the normal microenvironment, they have been found expanded in the NPC microenvironment and constituted 12.6% of the total $CD79A^+$ B cells, and correlated to worse prognosis (23). Increased double-negative B cells have also been found in non-small cell lung cancer and negatively correlated to the abundance of pro-inflammation B cells (86). Higher frequencies of double-negative B cells are associated with lymph node and distant metastasis in cancer patients, which might be alleviated or overcome by cisplatin-based chemotherapy (87). Nonetheless, little is known about the function nor the mechanism of double-negative B cell enrichment in the NPC microenvironment because they have not been previously detected in tumor tissues. One recent study has exhibited that double-negative B cells might regulate inflammatory activation and undergo clonal expansion upon antigenic stimulation *via* an extra-follicular maturation pathway (88). Pseudotime trajectory analysis has shown that double-negative B cells are the precursors of matured effector B cells, which can be further differentiated into plasma B cells and memory B cells (23). However, it seems that in the NPC microenvironment, the differentiation of double-negative B cells is hijacked by tumor- or TME-mediated mechanism so that a substantial portion of double-negative B cells are forced to maintain in an intermediately differentiated and ineffective phenotype. Hence, inhibiting the expansion or inducing the differentiation of double-negative B cells in the NPC microenvironment might enhance inflammatory activation. Furthermore, quantifying the intratumoral or peripheral abundance of double-negative B cells in NPC patients might be feasible for patient stratification and prognosis, as well as serve as a biomarker for treatment selection.

Antibody-secreting plasma B cells and $FCLR4^+$ memory B cells represent two terminally differentiated pro-inflammation subtypes in the NPC microenvironment. They are commonly more infiltrated in the TME and correlated to better clinical outcomes, exhibiting their functions in immune survilliance (89). Nevertheless, their abundance is highly patient-specific due to EBV status, since plasma B cells and memory B cells showed increased enrichment and activity in EBV^+ tumors than in EBV^- ones (23). The differentiation and activation of these two subtypes are influenced by chronic IFN-α and IFN-γ production and chemotaxis in the NPC microenvironment (23). In the treatment of autoimmune and infectious diseases, rituximab is used to deplete excessive enrichment of $CD20^+$ B cells (90), whereas, in NPC treatment, we should focus on *in vivo* or *ex vivo* expanding pro-inflammatory B cells, especially in the NPC patients with fewer B infiltrates (91). Previous studies have illustrated that B cell proliferation and maturation can be re-directed *via* CD38-mediated inhibition of mTOR and PI3K signaling (92–94). However, the function of B cells and their associated antibody repositories in NPC is hardly identified and characterized so far. Thus, prior to clinical translation, it remains necessary to understand the crosstalk between plasma B cells/memory B cells and T cell subpopulations so that humoral immune responses stimulated by tumor-infiltrating B cells can facilitate the development of effective anti-tumor immunity within the TME.

TARGETING MYELOID-DERIVED CELLS TO INTERVENE THE TUMOR-STROMA COMMUNICATIONS

Intratumoral myeloid-derived cells are commonly developed from immature monocytes recruited from peripheral blood during tumor progression and viral infection (95, 96). Immature macrophages and monocytes express pan-monocyte markers CD14 and CD68, but they lack functional and polarized signatures such as IL-10. Enrichment of these immature myeloid cells indicates an earlier or less progressive disease status, therefore its abundance is associated with better prognosis in undifferentiated NPC patients (97). Prevalent cell-cell communications have been identified between macrophage and lymphocytes, indicating the strong potential to recruit, activate and suppress innate and adaptive immunity. In the NPC microenvironment, the maturation and polarization of macrophages do not follow the classic M1/M2 model. Instead, the infiltrating macrophages exhibit an M1/M2 coupled pattern, expressing both M1 and M2-polarized signatures, including FCGR2A, FCGR3A, TREM2 and APOC1 (23). The multilateral cell-cell communications between macrophages and lymphocytes are ambiguous due to dynamic functional alterations. For example, $CD163^+$ M2-polarized macrophages in the NPC microenvironment are considered to associate with worse prognosis and facilitate the development of a pre-metastasis niche by secreting pro-angiogenesis cytokines, including VEGF, MMP9, TGFB1 and PLA2G7 (97–99). Hypoxia and IFN signaling are two mechanisms that induce accumulation, maturation and M2 polarization of macrophages, and further induce therapeutic resistance and disease progression in the NPC microenvironment (100). Targeting molecules that are associated with hypoxia and IFN signaling represents a potential therapeutic strategy to minimize the suppressive function of M2 macrophages or enhance the accumulation of monocytes and M1-macrophages in the TME.

DCs are one of the differentiated myeloid subtypes accumulated both in nasopharyngeal hyperplasia and NPC, and responsible for antigen processing and presentation so that T and B cells can be activated (101, 102). For instance, $FCER1A^+$ Langerhans cells and $LGALS2^+$ DCs are tissue-resident DCs located in the epithelium and lymph nodes of the nasopharynx, to capture and recognize the antigens on malignant-transforming nasopharyngeal epithelial cells. Although DCs are a pro-inflammation subtype and significantly correlated to better prognosis in NPC patients, some DCs have been found capable of impairing T-cell and B-cell immunity driven by chronic inflammation and hypoxia (103). In the NPC microenvironment, $LAMP3^+$ DCs with high maturation, immune-regulatory and migration potentials, produce multiple

cytokines, including CCL17, CCL19 and CCL22, to recruit $CCR4^+$ Tregs and $CCR7^+$ naïve T cells (56). $LAMP3^+$ DCs also exhibit reduced immune activation status and elevated suppression status, characterized by high expression of PD-L1, PD-L2, IDO1 and TGFB1. Meanwhile, the immunosuppressive function of $LAMP3^+$ DCs has been validated in hepatocellular carcinoma (HCC) and non-small-cell-lung cancer (NSCLC) where $LAMP3^+$ DCs showed strong interaction with exhausted T cells, Tregs and proliferating T cells *via* CD28/B7 binding and IL-15 signaling (104, 105). Up-regulation of LAMP3 in tumor tissues has been found correlated to worse prognosis in patients with esophageal squamous cell carcinoma (ESCC) (106). Developmental trajectory has revealed that $LAMP3^+$ DCs might be differentiated from immature monocytes during tumor initiation so that NPC cells can escape from initial antigen recognition and immune attack (56). Thus, therapeutic targeting of $LAMP3^+$ DCs might be only feasible in the early stage of NPC development so that effector lymphocytes can more effectively recognize the tumor antigens subsequently induce tumor depletion. However, the function of LAMP3 remains ambiguous since immunosuppressive DCs in metastatic lung adenocarcinoma have shown loss of LAMP3 activation marker expression (107). Although $LAMP3^+$ DCs are common malignancy-associated infiltrates with the ability to restrain T cell function, further *in vivo* and *in vitro* functional assays need to be conducted to validate its regulatory potential.

MDSCs are another type of differentiated monocytes infiltrating in the TME (108). Unlike DCs which are infiltrated both in the malignant and non-malignant nasopharyngeal microenvironment, MDSCs are highly enriched in the NPC microenvironment, indicating the presence of NPC-associated recruitment and differentiation in MDSCs. Previous studies have considered that MDSCs are a dynamically changing myeloid subtype that cannot be accurately characterized *via* genetic profiling (103). Single-cell sequencing has demonstrated that infiltrating MDSCs are lack macrophage and DC-specific signatures, such as CD14 and CD68, but highly express S100A family genes, including FCN1, VCAN, S100A8 and S100A9 (105, 109). Accumulating evidence has suggested that S100A8/S100A9 are pro-inflammation molecules that are elevated in patients with a variety of inflammatory diseases and cancer (110, 111). The expression of S100A8/A9 is closely related to tumor stage, lymph node metastasis and poor prognosis in NPC patients (112). In tumor-bearing mice treated with mAbGB3.1 (10 ug/gm body weight), S100A8/A9 binding and signaling has been blocked and the accumulation of MDSCs in the peripheral blood and secondary lymphoid organs has been reduced (113). $S100A8/A9^+$ MDSCs exert immunosuppressive effects *via* hijacking the differentiation from monocytes into antigen-presenting DCs and pro-inflammation macrophages *via* STAT3 signaling (114). Thus, limiting the accumulation and retention of MDSCs can facilitate the activation of anti-tumor immunity *via* communications with T and B cells, and might further retard NPC progression. Targeting S100A8 and S100A9 *via* siRNA has shown to reduce invasive capability of NPC cells, whereas the silencing effects on TME remodeling remain under-investigated (115).

TARGETING FIBROBLASTS TO MANIPULATE THE TUMOR-PROMOTING EXTRACELLULAR MATRIX

In the NPC microenvironment, $CD45^+$ immune cells usually outnumber tumor cells and $CD45^-$ non-immune stromal cells. Indeed, fibroblasts represent a relatively minor but critical subpopulation that constructs a complex extracellular matrix (ECM). Fibroblasts are rarely infiltrated in non-malignant nasopharyngeal tissues, and hardly recruited in response to acute inflammation. Whereas in the TME, fibroblasts constitute approximately 2% of the total stromal infiltrates in the NPC microenvironment. The abundance of fibroblasts has also been validated *via* multiplex immunohistochemistry. A high density of α-SMA^+ fibroblasts is found in 41.2% of primary NPC biopsies and 83.3% of metastatic NPC tissues. In two independent NPC cohorts, a higher density of α-SMA^+ fibroblasts has been found correlated with shorter overall survival and lower 5-year survival rates in NPC patients, suggesting their utility as an independent prognostic factor (116, 117). Recruitment and accumulation of fibroblasts is a malignancy-dependent process found in varied cancers, since they can develop a tumor-promoting ECM and secrete varied cytokines that facilitate survival and metastasis. The function of ECM is primarily involved with the activation of focal adhesion-related pathways, including FAK/SRC, PI3K/AKT and RhoA/ROCK signaling. The predominant ECM components in the NPC microenvironment are collagen (especially type I collagen), lumican, and fibronectin, which all have a positive impact on angiogenesis and anti-apoptosis (50, 118, 119). Other collagens are also synthesized by intratumoral fibroblasts, such as type III and type IV collagens, but they exhibit patient-specific distribution. Recent advances have suggested that the tumor-parenchyma barrier manipulated by fibroblasts is the first protective shield of tumor cells to attenuate infiltration of T cells and penetration of anti-PD-1 drugs in patients with lung cancer and esophageal cancer (120). Hence, ECM is one of the critical mediators of immune suppression in the NPC microenvironment.

Besides, fibroblasts in the NPC microenvironment can secrete varied growth factors, including EGF, FGF, IGF1, CSF and TGF-β, which can either facilitate tumor progression or immune suppression (121). For example, CSF-1 is a vital factor inducing M0-to-M2 polarization, TGF-β induces differentiation and activation of Tregs, and IGF-1 is positively correlated to tumor sizes in NPC patients (122, 123). Fibroblast growth factor 2 (FGF2) is the upstream molecule of the PI3K/AKT signal pathway and activates proliferation and metastasis of NPC cells so that FGF2/FGFR2 has become a crucial target in the treatment of NPC as well (124). Targeting fibroblasts in the NPC microenvironment might provide significant benefits to chemo and immunotherapy. These fibroblasts can also secrete varied chemokines, such as CXCL9, CXCL10 and CXCL12 which can promote tumor growth and has chemoattractant properties that stimulate the migration of $CXCR3^+/CXCR4^+$ suppressive Tregs and cytotoxic T cells into the NPC microenvironment (24, 56). However, the fibroblasts can quickly inhibit the cytotoxic function of these recruited T cells *via* PD-L2-PD-1 interaction. Some fibroblasts also secret immunosuppressive factor IDO1, which

further regulate T-cell immunity in the NPC microenvironment (24, 56). Targeting fibroblasts with high expression of fibroblast activation protein-α (FAP) in tumor-bearing mice have induced tumor necrosis mediated by IFN-γ and TNF-α, demonstrating that anti-tumor immunity has been reverted upon depletion of these cells (125). Significantly, up-regulated genes in tumor-derived fibroblasts were enriched in IFN response-related pathways (23). Meanwhile, fibroblasts are also considered as one of the vital factors maintaining the differentiation status of NPC cells because they are frequently associated with the epithelial-to-mesenchymal transition (13, 126). Targeting infiltrating fibroblasts might also result in decreasing the cancer stem cell pools in NPC to alleviate therapeutic resistance commonly possessed by high stemness cells (126). CD248 has been found dynamically expressed by cancer-associated fibroblasts (CAFs), and lowly expressed by other stromal cells (127). Although, it might serve as a potential molecular marker and target, the expression and mechanism of CD248 in NPC-infiltrating fibroblasts have not been fully elucidated, due to a low number of fibroblasts captured *via* single-cell sequencing. The current single-cell technique allows to process 20,000 cells per reaction, and it remains insufficient to depict the global mapping of stromal cells with low abundance in the NPC microenvironment. Thus, it is necessary to enrich the $CD45^-$ non-immune stromal cells prior to sequencing so that we can have a maximum yield of fibroblasts to further identify the heterogeneity and molecular signatures of varied fibroblast subpopulations and characterize their functional status.

DISCUSSION

The past two decades have witnessed a tremendous shift from recognizing the tumor as a homogenous entity towards understanding TME as a heterogeneous ecosystem at a single-cell resolution. Recent advances using single-cell sequencing and multiplex immunohistochemistry have deciphered the NPC microenvironment as a tumor-promoting and immunosuppressive harbor. Single cell-cell communication analysis and V(D)J immune profiling has revealed the origin of tumor-infiltrating stromal cells so that we can know the recruitment mechanism and tumor-stroma interplay either from peripheral blood, adjacent lymph nodes and surroundings (**Figure 2** and **Table 1**). Nevertheless, we have seen a lack of functional and clinical investigations on the function and mechanism of T cells, NK cells, B cells, myeloid-derived cells and fibroblasts in the NPC microenvironment. Among these infiltrating stromal subtypes, B cells are the least studied subtype in the TME due to their relatively low infiltration degree in many malignancies. Therefore, we should continue to identify the finer B-cell subpopulations and characterize the functional status of B cell subtypes, since B cells are gradually recognized as a ineligible factor that influences the responsiveness of chemo and immunotherapy (128, 129). Besides stromal compositions in the NPC microenvironment, understanding the spatial orientation of stromal cells is also critical to functional dynamics and clinical translation. The field of spatial single-cell transcriptomics is rapidly evolving to uncover

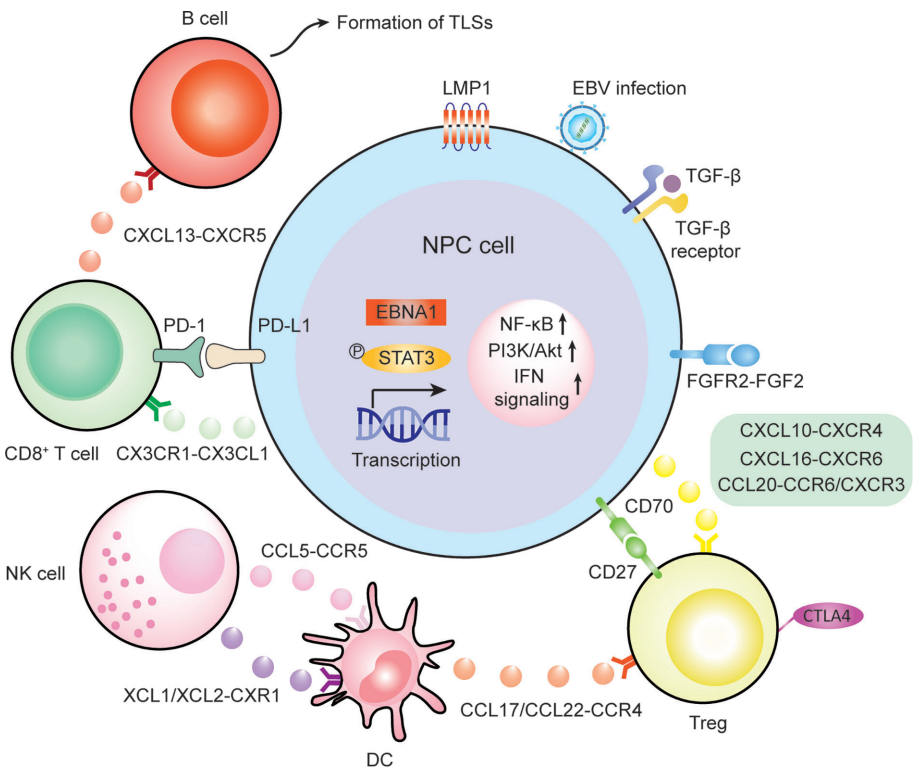

FIGURE 2 | The schematic illustration of cell recruitment and cell-cell interactions in the NPC microenvironment.

TABLE 1 | Novel chemotaxis responsible for cell recruitment in the NPC microenvironment.

Chemotaxis (A-B)	Interacting cell subtype A	Interacting cell subtype B
CX3CL1-CX3CR1	Tumor cells	$CD8^+$ T cells with minimal cytotoxicity
CXCL10-CXCR4	Tumor cells	Treg
CXCL16-CXCR6		
CCL20-CCR6/CXCR3		
CXCL13-CXCR5	Exhausted/helper T cells	B cells, except plasma B cells
XCL1/XCL2-CXR1	NK cells	Pro-inflammatory DCs
CCL5-CCR5		
CCL17/CCL22-CCR4	LAMP3+ DC	Treg
CCL19-CCR7		Naïve T cells
CCL4L2-CCR5	Macrophage	Memory T cells

the locoregional localization of different stromal counterparts from formalin-fixed paraffin-embedded (FFPE) tissue samples (130). It is necessary to map where the cell-cell communication is occurring, but this technique highly relies on tissue quality and technical proficiency. So far, lack of reproducibility which induce high batch-to-batch effect and lower sequencing depth has hindered the feasibility of spatial single-cell transcriptomics. Single-cell sequencing is also currently facing limitations on sequencing depth in which lowly expressed genes cannot be detected even though they are highly important. Finer subpopulations, especially those that are lower than 5% of total cell input, cannot be accurately identified *via* sequencing nor characterized *via* computational algorithm. Thus, it remains necessary to enrich lowly infiltrated stromal cells prior to sequencing *via* flow cytometry and magnetic separation based on known signatures so that higher resolution of the molecular landscape can be reliably analyzed to depict the true molecular landscape and functional dynamics in the human body.

In this review, we have proposed a variety of therapeutic strategies that might enhance immunotherapeutic efficacy *via* direct and indirect remodeling of the NPC microenvironment (**Figure 3** and **Table 2**), which highly relies on recent identification and characterization of molecular targets that are essential for tumor proliferation and progression in NPC. Although some targets cannot be independently utilized as effective therapeutics like anti-PD-1/PD-L1 monotherapy, most of them remain feasible to be used as adjuvant therapies that enhance the efficacy of ongoing monotherapy in NPC patients. We acknowledge that there is a large transition gap between laboratorial investigation and clinical translation, but we believe that rational combinatorial strategies will be one of the most effective therapeutics in the future. However, functional analysis on NPC greatly suffers from the lack of reliable animal models. It is needed to establish a humanized mouse model with a competent human-originated immune system so that NPC-mediated immune regulation can be studied *in vivo* and predict clinical outcomes in NPC patients (131). Currently, NPC organoid is also underdeveloped in multiple groups around the world which can also serve an important alternative to study the function and interaction *in vivo* from

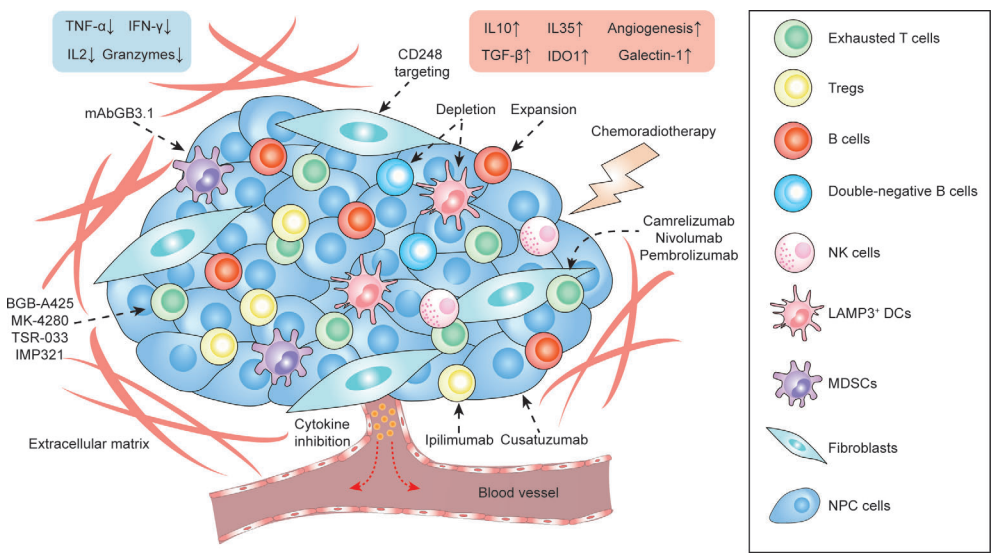

FIGURE 3 | The stromal landscape of NPC at a glance and proposed treatment strategies targeting TME-infiltrating cells.

TABLE 2 | Proposed therapeutic approaches to target tumor-infiltrating cell subtypes in the NPC microenvironment.

Cell subtypes	Molecular targets	Outcomes	Available drugs or approaches
Tregs	CTLA4	Reduced T cell suppression	Ipilimumab
	CD27-CD70		Cusatuzumab
	LGALS1		N/A
Exhausted T cells	PD1-PDL1	Enhanced T cell cytotoxicity	Camrelizumab, Nivolumab, Pembrolizumab
	HAVCR2-LGALS9		BGB-A425
	LAG3		MK-4280, TSR-033, IMP321
$CXCR5^+$ B cells	CXCL13-CXCR5	Enhanced responsiveness to immunotherapy	*Ex vivo* expansion
Double-negative B cells	NA	Better prognosis	Specific depletion/differentiation
DCs	LAMP3	Reduced T cell suppression	Specific depletion
MDSCs	S100A8/S100A9	Reduced chronic inflammation	mAbGB3.1
Fibroblasts	CD248	Inhibited recruitment of endothelial cells and angiogenesis	Targeted therapy

N/A, not applicable.

NPC patient derived tissues, and to study the feasibility and efficacy of proposed therapeutic strategies (132). Due to the intrinsic nature of NPC as a stromal inflamed tumor, it would be better to adapt to local conditions to use tumor infiltrates themselves, instead of primarily focusing on extraneous attack mediated by chemotherapy and radiotherapy. Indeed, optimizing the innate and adaptive immunity to combat tumor progression is the principle of precision medicine and is currently leading the tide in the upcoming decade in cancer treatment. Better defining molecular contributors to an immunosuppressive and tumor-promoting microenvironment constitute an important step, including thorough investigations not only of locoregional stromal infiltration but also of such modifiable factors in peripheral blood, surrounding lymph nodes and metastatic sites. What lies beneath is a complex environment that supports the tumor, and we expect that targeting this foundation will yield the next breakthroughs in cancer therapy with greater efficacy, less toxicity, and less cost of cancer care. The development and use of such pharmaceutical agents targeting signature- and function-characterized populations enable a more personalized approach to NPC treatment.

AUTHOR CONTRIBUTIONS

X-YG and AW-ML supervised and reviewed the manuscript. LG conducted literature review and wrote the manuscript. DL-WK, WD, PW, and YW contributed to the clinical and bioinformatics interpretation of the manuscript. All authors contributed to the article and approved the submitted version.

FUNDING

This work was supported by grants from the Hong Kong Research Grant Council (RGC) grants including GRF (17143716), Collaborative Research Funds (C7065-18GF and C7026-18GF), Theme-based Research Scheme (T12-704/16-R), National Key Sci-Tech Special Project of Infectious Diseases (2013ZX10002-011-005), and The Shenzhen Peacock team project (KQTD20150331172101 53 and KQTD20180411185028 79), X-YG is the Sophie YM Chan Professor in Cancer Research.

REFERENCES

1. Sung H, Ferlay J, Siegel RL, Laversanne M, Soerjomataram I, Jemal A, et al. Global Cancer Statistics 2020: GLOBOCAN Estimates of Incidence and Mortality Worldwide for 36 Cancers in 185 Countries. *CA Cancer J Clin* (2021). doi: 10.3322/caac.21660
2. Chen YP, Chan ATC, Le QT, Blanchard P, Sun Y, Ma J. Nasopharyngeal Carcinoma. *Lancet* (2019) 394(10192):64–80. doi: 10.1016/S0140-6736(19)30956-0
3. Chan AT, Teo PM, Johnson PJ. Nasopharyngeal Carcinoma. *Ann Oncol* (2002) 13(7):1007–15. doi: 10.1093/annonc/mdf179
4. Lun SW, Cheung ST, Cheung PF, To KF, Woo JK, Choy KW, et al. CD44+ Cancer Stem-Like Cells in EBV-Associated Nasopharyngeal Carcinoma. *PloS One* (2012) 7(12):e52426. doi: 10.1371/journal.pone.0052426
5. Wu A, Luo W, Zhang Q, Yang Z, Zhang G, Li S, et al. Aldehyde Dehydrogenase 1, A Functional Marker for Identifying Cancer Stem Cells in Human Nasopharyngeal Carcinoma. *Cancer Lett* (2013) 330(2):181–9. doi: 10.1016/j.canlet.2012.11.046
6. Zhuang HW, Mo TT, Hou WJ, Xiong GX, Zhu XL, Fu QL, et al. Biological Characteristics of CD133(+) Cells in Nasopharyngeal Carcinoma. *Oncol Rep* (2013) 30(1):57–63. doi: 10.3892/or.2013.2408
7. Thompson LD. Update on Nasopharyngeal Carcinoma. *Head Neck Pathol* (2007) 1(1):81–6. doi: 10.1007/s12105-007-0012-7
8. Nicholls JM, Lee VH, Chan SK, Tsang KC, Choi CW, Kwong DL, et al. Negative Plasma Epstein-Barr Virus DNA Nasopharyngeal Carcinoma in an Endemic Region and Its Influence on Liquid Biopsy Screening Programmes. *Br J Cancer* (2019) 121(8):690–8. doi: 10.1038/s41416-019-0575-6
9. Nilsson JS, Sobti A, Swoboda S, Erjefalt JS, Forslund O, Lindstedt M, et al. Immune Phenotypes of Nasopharyngeal Cancer. *Cancers (Basel)* (2020) 12(11):3428. doi: 10.3390/cancers12113428
10. Huang SCM, Tsao SW, Tsang CM. Interplay of Viral Infection, Host Cell Factors and Tumor Microenvironment in the Pathogenesis of Nasopharyngeal Carcinoma. *Cancers (Basel)* (2018) 10(4):106. doi: 10.3390/cancers10040106
11. Ooft ML, van Ipenburg JA, Sanders ME, Kranendonk M, Hofland I, de Bree R, et al. Prognostic Role of Tumour-Associated Macrophages and Regulatory T Cells in EBV-Positive and EBV-Negative Nasopharyngeal Carcinoma. *J Clin Pathol* (2018) 71(3):267–74. doi: 10.1136/jclinpath-2017-204664
12. Chen M, Jin F, Ma L. The Detection and Significance of T Cells in Nasopharyngeal Carcinoma Patients. *J Cancer Res Ther* (2018) 14(Supplement):S331–5. doi: 10.4103/0973-1482.235350
13. Morris MA. Cancer-Associated Fibroblasts in Undifferentiated Nasopharyngeal Carcinoma: A Putative Role for the EBV-Encoded

Oncoprotein, Lmp1. *Pathogens* (2019) 9(1):8. doi: 10.3390/pathogens9010008
14. Gourzones C, Barjon C, Busson P. Host-Tumor Interactions in Nasopharyngeal Carcinomas. *Semin Cancer Biol* (2012) 22(2):127–36. doi: 10.1016/j.semcancer.2012.01.002
15. Blanchard P, Lee A, Marguet S, Leclercq J, Ng WT, Ma J, et al. Chemotherapy and Radiotherapy in Nasopharyngeal Carcinoma: An Update of the MAC-NPC Meta-Analysis. *Lancet Oncol* (2015) 16(6):645–55. doi: 10.1016/S1470-2045(15)70126-9
16. Bhattacharyya T, Babu G, Kainickal CT. Current Role of Chemotherapy in Nonmetastatic Nasopharyngeal Cancer. *J Oncol* (2018) 2018:3725837. doi: 10.1155/2018/3725837
17. Lin JC, Wang WY, Chen KY, Wei YH, Liang WM, Jan JS, et al. Quantification of Plasma Epstein-Barr Virus DNA in Patients With Advanced Nasopharyngeal Carcinoma. *N Engl J Med* (2004) 350 (24):2461–70. doi: 10.1056/NEJMoa032260
18. Hsu C, Lee SH, Ejadi S, Even C, Cohen RB, Le Tourneau C, et al. Safety and Antitumor Activity of Pembrolizumab in Patients With Programmed Death-Ligand 1-Positive Nasopharyngeal Carcinoma: Results of the KEYNOTE-028 Study. *J Clin Oncol* (2017) 35(36):4050–6. doi: 10.1200/JCO.2017.73.3675
19. Lv JW, Li JY, Luo LN, Wang ZX, Chen YP. Comparative Safety and Efficacy of Anti-PD-1 Monotherapy, Chemotherapy Alone, and Their Combination Therapy in Advanced Nasopharyngeal Carcinoma: Findings From Recent Advances in Landmark Trials. *J Immunother Cancer* (2019) 7(1):159. doi: 10.1186/s40425-019-0636-7
20. Masterson L, Howard J, Gonzalez-Cruz J, Jackson C, Barnett C, Overton L, et al. Immune Checkpoint Inhibitors in Advanced Nasopharyngeal Carcinoma: Beyond an Era of Chemoradiation? *Int J Cancer* (2020) 146(8):2305–14. doi: 10.1002/ijc.32869
21. Mints M, Tirosh I. Nasopharyngeal Carcinoma Joins the Single-Cell Party. *Cancer Commun (Lond)* (2020) 40(9):453–5. doi: 10.1002/cac2.12091
22. Binnewies M, Roberts EW, Kersten K, Chan V, Fearon DF, Merad M, et al. Understanding the Tumor Immune Microenvironment (TIME) for Effective Therapy. *Nat Med* (2018) 24(5):541–50. doi: 10.1038/s41591-018-0014-x
23. Gong L, Kwong DL, Dai W, Wu P, Li S, Yan Q, et al. Comprehensive Single-Cell Sequencing Reveals the Stromal Dynamics and Tumor-Specific Characteristics in the Microenvironment of Nasopharyngeal Carcinoma. *Nat Commun* (2021) 12(1):1540. doi: 10.1038/s41467-021-21795-z
24. Chen YP, Yin JH, Li WF, Li HJ, Chen DP, Zhang CJ, et al. Single-Cell Transcriptomics Reveals Regulators Underlying Immune Cell Diversity and Immune Subtypes Associated With Prognosis in Nasopharyngeal Carcinoma. *Cell Res* (2020) 30(11):1024–42. doi: 10.1038/s41422-020-0374-x
25. Chan JK. Virus-Associated Neoplasms of the Nasopharynx and Sinonasal Tract: Diagnostic Problems. *Mod Pathol* (2017) 30(s1):S68–83. doi: 10.1038/modpathol.2016.189
26. Yeung WM, Zong YS, Chiu CT, Chan KH, Sham JS, Choy DT, et al. Epstein-Barr Virus Carriage by Nasopharyngeal Carcinoma *In Situ*. *Int J Cancer* (1993) 53(5):746–50. doi: 10.1002/ijc.2910530507
27. Tsao SW, Tsang CM, Lo KW. Epstein-Barr Virus Infection and Nasopharyngeal Carcinoma. *Philos Trans R Soc Lond B Biol Sci* (2017) 372(1732):20160270. doi: 10.1098/rstb.2016.0270
28. Li J, Zeng XH, Mo HY, Rolen U, Gao YF, Zhang XS, et al. Functional Inactivation of EBV-Specific T-Lymphocytes in Nasopharyngeal Carcinoma: Implications for Tumor Immunotherapy. *PloS One* (2007) 2(11):e1122. doi: 10.1371/journal.pone.0001122
29. Wang Y, Swiecki M, Cella M, Alber G, Schreiber RD, Gilfillan S, et al. Timing and Magnitude of Type I Interferon Responses by Distinct Sensors Impact CD8 T Cell Exhaustion and Chronic Viral Infection. *Cell Host Microbe* (2012) 11(6):631–42. doi: 10.1016/j.chom.2012.05.003
30. Bhat P, Leggatt G, Waterhouse N, Frazer IH. Interferon-Gamma Derived From Cytotoxic Lymphocytes Directly Enhances Their Motility and Cytotoxicity. *Cell Death Dis* (2017) 8(6):e2836. doi: 10.1038/cddis.2017.67
31. Fang W, Zhang J, Hong S, Zhan J, Chen N, Qin T, et al. EBV-Driven LMP1 and IFN-Gamma Up-Regulate PD-L1 in Nasopharyngeal Carcinoma: Implications for Oncotargeted Therapy. *Oncotarget* (2014) 5(23):12189–202. doi: 10.18632/oncotarget.2608
32. Tsao SW, Tramoutanis G, Dawson CW, Lo AK, Huang DP. The Significance of LMP1 Expression in Nasopharyngeal Carcinoma. *Semin Cancer Biol* (2002) 12(6):473–87. doi: 10.1016/s1044579x02000901
33. Hau PM, Lung HL, Wu M, Tsang CM, Wong KL, Mak NK, et al. Targeting Epstein-Barr Virus in Nasopharyngeal Carcinoma. *Front Oncol* (2020) 10:600. doi: 10.3389/fonc.2020.00600
34. Huo S, Luo Y, Deng R, Liu X, Wang J, Wang L, et al. EBV-EBNA1 Constructs an Immunosuppressive Microenvironment for Nasopharyngeal Carcinoma by Promoting the Chemoattraction of Treg Cells. *J Immunother Cancer* (2020) 8(2):e001588. doi: 10.1136/jitc-2020-001588
35. Cai TT, Ye SB, Liu YN, He J, Chen QY, Mai HQ, et al. LMP1-Mediated Glycolysis Induces Myeloid-Derived Suppressor Cell Expansion in Nasopharyngeal Carcinoma. *PloS Pathog* (2017) 13(7):e1006503. doi: 10.1371/journal.ppat.1006503
36. Kang MS, Kieff E. Epstein-Barr Virus Latent Genes. *Exp Mol Med* (2015) 47: e131. doi: 10.1038/emm.2014.84
37. Wang J, Huang H, Lu J, Bi P, Wang F, Liu X, et al. Tumor Cells Induced-M2 Macrophage Favors Accumulation of Treg in Nasopharyngeal Carcinoma. *Int J Clin Exp Pathol* (2017) 10(8):8389–401.
38. Teichmann M, Meyer B, Beck A, Niedobitek G. Expression of the Interferon-Inducible Chemokine IP-10 (CXCL10), A Chemokine With Proposed Anti-Neoplastic Functions, in Hodgkin Lymphoma and Nasopharyngeal Carcinoma. *J Pathol* (2005) 206(1):68–75. doi: 10.1002/path.1745
39. Wu SG, Lian CL, Wang J, Zhang WW, Sun JY, Lin Q, et al. The Effect of Histological Subtypes on Survival Outcome in Nasopharyngeal Carcinoma After Extensive Follow Up. *Ann Transl Med* (2019) 7(23):768. doi: 10.21037/atm.2019.11.75
40. Cheung F, Chan O, Ng WT, Chan L, Lee A, Pang SW. The Prognostic Value of Histological Typing in Nasopharyngeal Carcinoma. *Oral Oncol* (2012) 48 (2):429–33. doi: 10.1016/j.oraloncology.2011.11.017
41. Hopkins R, Xiang W, Marlier D, Au VB, Ching Q, Wu LX, et al. Monocytic Myeloid-Derived Suppressor Cells Underpin Resistance to Adoptive T Cell Therapy in Nasopharyngeal Carcinoma. *Mol Ther* (2021) 29(2):734–43. doi: 10.1016/j.ymthe.2020.09.040
42. Wang HC, Chan LP, Cho SF. Targeting the Immune Microenvironment in the Treatment of Head and Neck Squamous Cell Carcinoma. *Front Oncol* (2019) 9:1084. doi: 10.3389/fonc.2019.01084
43. Ngan HL, Wang L, Lo KW, Lui VWY. Genomic Landscapes of EBV-Associated Nasopharyngeal Carcinoma *vs*. HPV-Associated Head and Neck Cancer. *Cancers (Basel)* (2018) 10(7):210. doi: 10.3390/cancers10070210
44. Ruffin AT, Cillo AR, Tabib T, Liu A, Onkar S, Kunning SR, et al. B Cell Signatures and Tertiary Lymphoid Structures Contribute to Outcome in Head and Neck Squamous Cell Carcinoma. *Nat Commun* (2021) 12(1):3349. doi: 10.1038/s41467-021-23355-x
45. Pinatti LM, Walline HM, Carey TE. Human Papillomavirus Genome Integration and Head and Neck Cancer. *J Dent Res* (2018) 97(6):691–700. doi: 10.1177/0022034517744213
46. Kim SS, Shen S, Miyauchi S, Sanders PD, Franiak-Pietryga I, Mell L, et al. B Cells Improve Overall Survival in HPV-Associated Squamous Cell Carcinomas and Are Activated by Radiation and PD-1 Blockade. *Clin Cancer Res* (2020) 26(13):3345–59. doi: 10.1158/1078-0432.CCR-19-3211
47. Kok VC. Current Understanding of the Mechanisms Underlying Immune Evasion From PD-1/PD-L1 Immune Checkpoint Blockade in Head and Neck Cancer. *Front Oncol* (2020) 10:268. doi: 10.3389/fonc.2020.00268
48. Qiao XW, Jiang J, Pang X, Huang MC, Tang YJ, Liang XH, et al. The Evolving Landscape of PD-1/PD-L1 Pathway in Head and Neck Cancer. *Front Immunol* (2020) 11:1721. doi: 10.3389/fimmu.2020.01721
49. Ribas A, Wolchok JD. Cancer Immunotherapy Using Checkpoint Blockade. *Science* (2018) 359(6382):1350–5. doi: 10.1126/science.aar4060
50. Jin S, Li R, Chen MY, Yu C, Tang LQ, Liu YM, et al. Single-Cell Transcriptomic Analysis Defines the Interplay Between Tumor Cells, Viral Infection, and the Microenvironment in Nasopharyngeal Carcinoma. *Cell Res* (2020) 30(11):950–65. doi: 10.1038/s41422-020-00402-8
51. Das M, Zhu C, Kuchroo VK. Tim-3 and Its Role in Regulating Anti-Tumor Immunity. *Immunol Rev* (2017) 276(1):97–111. doi: 10.1111/imr.12520
52. Ma BBY, Lim WT, Goh BC, Hui EP, Lo KW, Pettinger A, et al. Antitumor Activity of Nivolumab in Recurrent and Metastatic Nasopharyngeal Carcinoma: An International, Multicenter Study of the Mayo Clinic Phase

2 Consortium (NCI-9742). *J Clin Oncol* (2018) 36(14):1412–8. doi: 10.1200/JCO.2017.77.0388
53. Garon EB, Rizvi NA, Hui R, Leighl N, Balmanoukian AS, Eder JP, et al. Pembrolizumab for the Treatment of Non-Small-Cell Lung Cancer. *N Engl J Med* (2015) 372(21):2018–28. doi: 10.1056/NEJMoa1501824
54. Fuchs CS, Doi T, Jang RW, Muro K, Satoh T, Machado M, et al. Safety and Efficacy of Pembrolizumab Monotherapy in Patients With Previously Treated Advanced Gastric and Gastroesophageal Junction Cancer: Phase 2 Clinical KEYNOTE-059 Trial. *JAMA Oncol* (2018) 4(5):e180013. doi: 10.1001/jamaoncol.2018.0013
55. Finn RS, Ryoo BY, Merle P, Kudo M, Bouattour M, Lim HY, et al. Pembrolizumab As Second-Line Therapy in Patients With Advanced Hepatocellular Carcinoma in KEYNOTE-240: A Randomized, Double-Blind, Phase III Trial. *J Clin Oncol* (2020) 38(3):193–202. doi: 10.1200/JCO.19.01307
56. Liu Y, He S, Wang XL, Peng W, Chen QY, Chi DM, et al. Tumour Heterogeneity and Intercellular Networks of Nasopharyngeal Carcinoma at Single Cell Resolution. *Nat Commun* (2021) 12(1):741. doi: 10.1038/s41467-021-21043-4
57. Desai J, Meniawy T, Beagle B, Li Z, Mu S, Denlinger CS, et al. Bgb-A425, An Investigational Anti-TIM-3 Monoclonal Antibody, in Combination With Tislelizumab, An Anti-PD-1 Monoclonal Antibody, in Patients With Advanced Solid Tumors: A Phase I/II Trial in Progress. *J Clin Oncol* (2020) 38. doi: 10.1200/JCO.2020.38.15_suppl.TPS3146
58. Holderried TAW, de Vos L, Bawden EG, Vogt TJ, Dietrich J, Zarbl R, et al. Molecular and Immune Correlates of TIM-3 (HAVCR2) and Galectin 9 (LGALS9) mRNA Expression and DNA Methylation in Melanoma. *Clin Epigenet* (2019) 11(1):161. doi: 10.1186/s13148-019-0752-8
59. Yang R, Sun L, Li CF, Wang YH, Yao J, Li H, et al. Galectin-9 Interacts With PD-1 and TIM-3 to Regulate T Cell Death and Is a Target for Cancer Immunotherapy. *Nat Commun* (2021) 12(1):832. doi: 10.1038/s41467-021-21099-2
60. Ghosh S, Sharma G, Travers J, Kumar S, Choi J, Jun HT, et al. TSR-033, a Novel Therapeutic Antibody Targeting LAG-3, Enhances T-Cell Function and the Activity of PD-1 Blockade *In Vitro* and *In Vivo*. *Mol Cancer Ther* (2019) 18(3):632–41. doi: 10.1158/1535-7163.MCT-18-0836
61. Chen R, Manochakian R, James L, Azzouqa AG, Shi H, Zhang Y, et al. Emerging Therapeutic Agents for Advanced Non-Small Cell Lung Cancer. *J Hematol Oncol* (2020) 13(1):58. doi: 10.1186/s13045-020-00881-7
62. Hodi FS, O'Day SJ, McDermott DF, Weber RW, Sosman JA, Haanen JB, et al. Improved Survival With Ipilimumab in Patients With Metastatic Melanoma. *N Engl J Med* (2010) 363(8):711–23. doi: 10.1056/NEJMoa1003466
63. Overman MJ, McDermott R, Leach JL, Lonardi S, Lenz HJ, Morse MA, et al. Nivolumab in Patients With Metastatic DNA Mismatch Repair-Deficient or Microsatellite Instability-High Colorectal Cancer (CheckMate 142): An Open-Label, Multicentre, Phase 2 Study. *Lancet Oncol* (2017) 18(9):1182–91. doi: 10.1016/S1470-2045(17)30422-9
64. Yau T, Kang YK, Kim TY, El-Khoueiry AB, Santoro A, Sangro B, et al. Efficacy and Safety of Nivolumab Plus Ipilimumab in Patients With Advanced Hepatocellular Carcinoma Previously Treated With Sorafenib: The CheckMate 040 Randomized Clinical Trial. *JAMA Oncol* (2020) 6(11):e204564. doi: 10.1001/jamaoncol.2020.4564
65. Wong JSL, Kwok GGW, Tang V, Li BCW, Leung R, Chiu J, et al. Ipilimumab and Nivolumab/Pembrolizumab in Advanced Hepatocellular Carcinoma Refractory to Prior Immune Checkpoint Inhibitors. *J Immunother Cancer* (2021) 9(2):e001945. doi: 10.1136/jitc-2020-001945
66. Silence K, Dreier T, Moshir M, Ulrichts P, Gabriels SM, Saunders M, et al. ARGX-110, a Highly Potent Antibody Targeting CD70, Eliminates Tumors *via* Both Enhanced ADCC and Immune Checkpoint Blockade. *MAbs* (2014) 6(2):523–32. doi: 10.4161/mabs.27398
67. Riether C, Pabst T, Hopner S, Bacher U, Hinterbrandner M, Banz Y, et al. Targeting CD70 With Cusatuzumab Eliminates Acute Myeloid Leukemia Stem Cells in Patients Treated With Hypomethylating Agents. *Nat Med* (2020) 26(9):1459–67. doi: 10.1038/s41591-020-0910-8
68. Agathanggelou A, Niedobitek G, Chen R, Nicholls J, Yin W, Young LS. Expression of Immune Regulatory Molecules in Epstein-Barr Virus-Associated Nasopharyngeal Carcinomas With Prominent Lymphoid Stroma. Evidence for a Functional Interaction Between Epithelial Tumor Cells and Infiltrating Lymphoid Cells. *Am J Pathol* (1995) 147(4):1152–60.
69. Ghosh S, Kostel Bal S, Edwards ESJ, Pillay B, Jimenez Heredia R, Erol Cipe F, et al. Extended Clinical and Immunological Phenotype and Transplant Outcome in CD27 and CD70 Deficiency. *Blood* (2020) 136(23):2638–55. doi: 10.1182/blood.2020006738
70. Kruger R, Martin E, Dmytrus J, Feiterna-Sperling C, Meisel C, Unterwalder N, et al. CD70 Deficiency Associated With Chronic Epstein-Barr Virus Infection, Recurrent Airway Infections and Severe Gingivitis in a 24-Year-Old Woman. *Front Immunol* (2020) 11:1593. doi: 10.3389/fimmu.2020.01593
71. Mrizak D, Martin N, Barjon C, Jimenez-Pailhes AS, Mustapha R, Niki T, et al. Effect of Nasopharyngeal Carcinoma-Derived Exosomes on Human Regulatory T Cells. *J Natl Cancer Inst* (2015) 107(1):363. doi: 10.1093/jnci/dju363
72. Tang M, Ou N, Li C, Lu A, Li J, Ma L, et al. Expression and Prognostic Significance of Macrophage Inflammatory Protein-3 Alpha and Cystatin A in Nasopharyngeal Carcinoma. *BioMed Res Int* (2015) 2015:617143. doi: 10.1155/2015/617143
73. Wdowiak K, Francuz T, Gallego-Colon E, Ruiz-Agamez N, Kubeczko M, Grochola I, et al. Galectin Targeted Therapy in Oncology: Current Knowledge and Perspectives. *Int J Mol Sci* (2018) 19(1):210. doi: 10.3390/ijms19010210
74. Garin MI, Chu CC, Golshayan D, Cernuda-Morollon E, Wait R, Lechler RI. Galectin-1: A Key Effector of Regulation Mediated by CD4+CD25+ T Cells. *Blood* (2007) 109(5):2058–65. doi: 10.1182/blood-2006-04-016451
75. Nambiar DK, Aguilera T, Cao H, Kwok S, Kong C, Bloomstein J, et al. Galectin-1-Driven T Cell Exclusion in the Tumor Endothelium Promotes Immunotherapy Resistance. *J Clin Invest* (2019) 129(12):5553–67. doi: 10.1172/JCI129025
76. Li Y, Yang S, Yue H, Yuan D, Li L, Zhao J, et al. Unraveling LGALS1 as a Potential Immune Checkpoint and a Predictor of the Response to Anti-PD1 Therapy in Clear Cell Renal Carcinoma. *Pathol Oncol Res* (2020) 26(3):1451–8. doi: 10.1007/s12253-019-00710-4
77. Bottcher JP, Bonavita E, Chakravarty P, Blees H, Cabeza-Cabrerizo M, Sammicheli S, et al. NK Cells Stimulate Recruitment of Cdc1 Into the Tumor Microenvironment Promoting Cancer Immune Control. *Cell* (2018) 172(5):1022–37.e14. doi: 10.1016/j.cell.2018.01.004
78. Bi J, Tian Z. NK Cell Exhaustion. *Front Immunol* (2017) 8:760. doi: 10.3389/fimmu.2017.00760
79. Sharonov GV, Serebrovskaya EO, Yuzhakova DV, Britanova OV, Chudakov DM. B Cells, Plasma Cells and Antibody Repertoires in the Tumour Microenvironment. *Nat Rev Immunol* (2020) 20(5):294–307. doi: 10.1038/s41577-019-0257-x
80. Griss J, Bauer W, Wagner C, Simon M, Chen M, Grabmeier-Pfistershammer K, et al. B Cells Sustain Inflammation and Predict Response to Immune Checkpoint Blockade in Human Melanoma. *Nat Commun* (2019) 10(1):4186. doi: 10.1038/s41467-019-12160-2
81. Helmink BA, Reddy SM, Gao J, Zhang S, Basar R, Thakur R, et al. B Cells and Tertiary Lymphoid Structures Promote Immunotherapy Response. *Nature* (2020) 577(7791):549–55. doi: 10.1038/s41586-019-1922-8
82. Thommen DS, Koelzer VH, Herzig P, Roller A, Trefny M, Dimeloe S, et al. A Transcriptionally and Functionally Distinct PD-1(+) CD8(+) T Cell Pool With Predictive Potential in Non-Small-Cell Lung Cancer Treated With PD-1 Blockade. *Nat Med* (2018) 24(7):994–1004. doi: 10.1038/s41591-018-0057-z
83. Bernard NJ. Double-Negative B Cells. *Nat Rev Rheumatol* (2018) 14(12):684. doi: 10.1038/s41584-018-0113-6
84. Moura RA, Quaresma C, Vieira AR, Goncalves MJ, Polido-Pereira J, Romao VC, et al. B-Cell Phenotype and IgD-CD27- Memory B Cells Are Affected by TNF-Inhibitors and Tocilizumab Treatment in Rheumatoid Arthritis. *PloS One* (2017) 12(9):e0182927. doi: 10.1371/journal.pone.0182927
85. You X, Zhang R, Shao M, He J, Chen J, Liu J, et al. Double Negative B Cell Is Associated With Renal Impairment in Systemic Lupus Erythematosus and Acts as a Marker for Nephritis Remission. *Front Med (Lausanne)* (2020) 7:85. doi: 10.3389/fmed.2020.00085
86. Centuori SM, Gomes CJ, Kim SS, Putnam CW, Larsen BT, Garland LL, et al. Double-Negative (CD27(-)IgD(-)) B Cells Are Expanded in NSCLC and

Inversely Correlate With Affinity-Matured B Cell Populations. *J Transl Med* (2018) 16(1):30. doi: 10.1186/s12967-018-1404-z
87. Gu Y, Liu Y, Fu L, Zhai L, Zhu J, Han Y, et al. Tumor-Educated B Cells Selectively Promote Breast Cancer Lymph Node Metastasis by HSPA4-Targeting IgG. *Nat Med* (2019) 25(2):312–22. doi: 10.1038/s41591-018-0309-y
88. Ruschil C, Gabernet G, Lepennetier G, Heumos S, Kaminski M, Hracsko Z, et al. Specific Induction of Double Negative B Cells During Protective and Pathogenic Immune Responses. *Front Immunol* (2020) 11:606338. doi: 10.3389/fimmu.2020.606338
89. Garaud S, Buisseret L, Solinas C, Gu-Trantien C, de Wind A, Van den Eynden G, et al. Tumor Infiltrating B-Cells Signal Functional Humoral Immune Responses in Breast Cancer. *JCI Insight* (2019) 5(18):e129641. doi: 10.1172/jci.insight.129641
90. Lee DSW, Rojas OL, Gommerman JL. B Cell Depletion Therapies in Autoimmune Disease: Advances and Mechanistic Insights. *Nat Rev Drug Discov* (2021) 20(3):179–99. doi: 10.1038/s41573-020-00092-2
91. Hofmann K, Clauder AK, Manz RA. Targeting B Cells and Plasma Cells in Autoimmune Diseases. *Front Immunol* (2018) 9:835. doi: 10.3389/fimmu.2018.00835
92. Benhamron S, Tirosh B. Direct Activation of mTOR in B Lymphocytes Confers Impairment in B-Cell Maturation Andloss of Marginal Zone B Cells. *Eur J Immunol* (2011) 41(8):2390–6. doi: 10.1002/eji.201041336
93. Oluwadara O, Barkhordarian A, Giacomelli L, Brant X, Chiappelli F. Immune Surveillance of Nasopharyngeal Carcinoma (NpC). *Bioinformation* (2011) 7(5):271–5. doi: 10.6026/97320630007271
94. Silvennoinen O, Nishigaki H, Kitanaka A, Kumagai M, Ito C, Malavasi F, et al. CD38 Signal Transduction in Human B Cell Precursors. Rapid Induction of Tyrosine Phosphorylation, Activation of Syk Tyrosine Kinase, and Phosphorylation of Phospholipase C-Gamma and Phosphatidylinositol 3-Kinase. *J Immunol* (1996) 156(1):100–7.
95. Schmid MC, Varner JA. Myeloid Cells in the Tumor Microenvironment: Modulation of Tumor Angiogenesis and Tumor Inflammation. *J Oncol* (2010) 2010:201026. doi: 10.1155/2010/201026
96. Schupp J, Krebs FK, Zimmer N, Trzeciak E, Schuppan D, Tuettenberg A. Targeting Myeloid Cells in the Tumor Sustaining Microenvironment. *Cell Immunol* (2019) 343:103713. doi: 10.1016/j.cellimm.2017.10.013
97. Chen YL. Prognostic Significance of Tumor-Associated Macrophages in Patients With Nasopharyngeal Carcinoma: A Meta-Analysis. *Med (Baltimore)* (2020) 99(39):e21999. doi: 10.1097/MD.0000000000021999
98. Low HB, Png CW, Li C, Wang Y, Wong SB, Zhang Y. Monocyte-Derived Factors Including PLA2G7 Induced by Macrophage-Nasopharyngeal Carcinoma Cell Interaction Promote Tumor Cell Invasiveness. *Oncotarget* (2016) 7(34):55473–90. doi: 10.18632/oncotarget.10980
99. Riabov V, Gudima A, Wang N, Mickley A, Orekhov A, Kzhyshkowska J. Role of Tumor Associated Macrophages in Tumor Angiogenesis and Lymphangiogenesis. *Front Physiol* (2014) 5:75. doi: 10.3389/fphys.2014.00075
100. Hong B, Lui VW, Hashiguchi M, Hui EP, Chan AT. Targeting Tumor Hypoxia in Nasopharyngeal Carcinoma. *Head Neck* (2013) 35(1):133–45. doi: 10.1002/hed.21877
101. Nilsson JS, Abolhalaj M, Lundberg K, Lindstedt M, Greiff L. Dendritic Cell Subpopulations in Nasopharyngeal Cancer. *Oncol Lett* (2019) 17(2):2557–61. doi: 10.3892/ol.2018.9835
102. Gabrilovich DI, Ostrand-Rosenberg S, Bronte V. Coordinated Regulation of Myeloid Cells by Tumours. *Nat Rev Immunol* (2012) 12(4):253–68. doi: 10.1038/nri3175
103. Balkwill FR, Capasso M, Hagemann T. The Tumor Microenvironment at a Glance. *J Cell Sci* (2012) 125(Pt 23):5591–6. doi: 10.1242/jcs.116392
104. Maier B, Leader AM, Chen ST, Tung N, Chang C, LeBerichel J, et al. A Conserved Dendritic-Cell Regulatory Program Limits Antitumour Immunity. *Nature* (2020) 580(7802):257–62. doi: 10.1038/s41586-020-2134-y
105. Zhang Q, He Y, Luo N, Patel SJ, Han Y, Gao R, et al. Landscape and Dynamics of Single Immune Cells in Hepatocellular Carcinoma. *Cell* (2019) 179(4):829–45.e20. doi: 10.1016/j.cell.2019.10.003
106. Liao X, Chen Y, Liu D, Li F, Li X, Jia W. High Expression of LAMP3 Is a Novel Biomarker of Poor Prognosis in Patients With Esophageal Squamous Cell Carcinoma. *Int J Mol Sci* (2015) 16(8):17655–67. doi: 10.3390/ijms160817655
107. Kim N, Kim HK, Lee K, Hong Y, Cho JH, Choi JW, et al. Single-Cell RNA Sequencing Demonstrates the Molecular and Cellular Reprogramming of Metastatic Lung Adenocarcinoma. *Nat Commun* (2020) 11(1):2285. doi: 10.1038/s41467-020-16164-1
108. Marvel D, Gabrilovich DI. Myeloid-Derived Suppressor Cells in the Tumor Microenvironment: Expect the Unexpected. *J Clin Invest* (2015) 125(9):3356–64. doi: 10.1172/JCI80005
109. Ostrand-Rosenberg S, Sinha P. Myeloid-Derived Suppressor Cells: Linking Inflammation and Cancer. *J Immunol* (2009) 182(8):4499–506. doi: 10.4049/jimmunol.0802740
110. Foell D, Frosch M, Sorg C, Roth J. Phagocyte-Specific Calcium-Binding S100 Proteins as Clinical Laboratory Markers of Inflammation. *Clin Chim Acta* (2004) 344(1-2):37–51. doi: 10.1016/j.cccn.2004.02.023
111. Gebhardt C, Nemeth J, Angel P, Hess J. S100A8 and S100A9 in Inflammation and Cancer. *Biochem Pharmacol* (2006) 72(11):1622–31. doi: 10.1016/j.bcp.2006.05.017
112. Hu W, Wang C, Ye L, Chen J, Chen X, Gu L, et al. Correlation of Expressions of S100A8 and S100A9 and Its Prognostic Potential in Nasopharyngeal Carcinoma. *Trop J Pharm Res* (2017) 16(11):2577–83. doi: 10.4314/tjpr.v16i11.2
113. Sinha P, Okoro C, Foell D, Freeze HH, Ostrand-Rosenberg S, Srikrishna G. Proinflammatory S100 Proteins Regulate the Accumulation of Myeloid-Derived Suppressor Cells. *J Immunol* (2008) 181(7):4666–75. doi: 10.4049/jimmunol.181.7.4666
114. Cheng P, Corzo CA, Luetteke N, Yu B, Nagaraj S, Bui MM, et al. Inhibition of Dendritic Cell Differentiation and Accumulation of Myeloid-Derived Suppressor Cells in Cancer Is Regulated by S100A9 Protein. *J Exp Med* (2008) 205(10):2235–49. doi: 10.1084/jem.20080132
115. Yan LL, Huang YJ, Yi X, Yan XM, Cai Y, He Q, et al. Effects of Silencing S100A8 and S100A9 With Small Interfering RNA on the Migration of CNE1 Nasopharyngeal Carcinoma Cells. *Oncol Lett* (2015) 9(6):2534–40. doi: 10.3892/ol.2015.3090
116. Chen J, Yang P, Xiao Y, Zhang Y, Liu J, Xie D, et al. Overexpression of Alpha-Sma-Positive Fibroblasts (CAFs) in Nasopharyngeal Carcinoma Predicts Poor Prognosis. *J Cancer* (2017) 8(18):3897–902. doi: 10.7150/jca.20324
117. Yu Y, Ke L, Lv X, Ling YH, Lu J, Liang H, et al. The Prognostic Significance of Carcinoma-Associated Fibroblasts and Tumor-Associated Macrophages in Nasopharyngeal Carcinoma. *Cancer Manag Res* (2018) 10:1935–46. doi: 10.2147/CMAR.S167071
118. Kang Y, He W, Ren C, Qiao J, Guo Q, Hu J, et al. Advances in Targeted Therapy Mainly Based on Signal Pathways for Nasopharyngeal Carcinoma. *Signal Transduct Target Ther* (2020) 5(1):245. doi: 10.1038/s41392-020-00340-2
119. Yang X, Wu Q, Wu F, Zhong Y. Differential Expression of COL4A3 and Collagen in Upward and Downward Progressing Types of Nasopharyngeal Carcinoma. *Oncol Lett* (2021) 21(3):223. doi: 10.3892/ol.2021.12484
120. Li L, Wei JR, Dong J, Lin QG, Tang H, Jia YX, et al. Laminin Gamma2-Mediating T Cell Exclusion Attenuates Response to Anti-PD-1 Therapy. *Sci Adv* (2021) 7(6):eabc8346. doi: 10.1126/sciadv.abc8346
121. Ge S, Mao Y, Yi Y, Xie D, Chen Z, Xiao Z. Comparative Proteomic Analysis of Secreted Proteins From Nasopharyngeal Carcinoma-Associated Stromal Fibroblasts and Normal Fibroblasts. *Exp Ther Med* (2012) 3(5):857–60. doi: 10.3892/etm.2012.483
122. Wang Y, Lyu Z, Qin Y, Wang X, Sun L, Zhang Y, et al. FOXO1 Promotes Tumor Progression by Increased M2 Macrophage Infiltration in Esophageal Squamous Cell Carcinoma. *Theranostics* (2020) 10(25):11535–48. doi: 10.7150/thno.45261
123. M'Hamdi H, Baizig NM, ELHadj OE, M'Hamdi N, Attia Z, Gritli S, et al. Usefulness of IGF-1 Serum Levels as Diagnostic Marker of Nasopharyngeal Carcinoma. *Immunobiology* (2016) 221(11):1304–8. doi: 10.1016/j.imbio.2016.05.008
124. Xu M, Tian GL, Hao CC, Shi M, Zha DJ, Liang K. MicroRNA-29 Targets FGF2 and Inhibits the Proliferation, Migration and Invasion of Nasopharyngeal Carcinoma Cells *via* PI3K/AKT Signaling Pathway. *Eur Rev Med Pharmacol Sci* (2020) 24(13):7199. doi: 10.26355/eurrev_202007_21849

125. Kraman M, Bambrough PJ, Arnold JN, Roberts EW, Magiera L, Jones JO, et al. Suppression of Antitumor Immunity by Stromal Cells Expressing Fibroblast Activation Protein-Alpha. *Science* (2010) 330(6005):827–30. doi: 10.1126/science.1195300
126. Huang W, Zhang L, Yang M, Wu X, Wang X, Huang W, et al. Cancer-Associated Fibroblasts Promote the Survival of Irradiated Nasopharyngeal Carcinoma Cells *via* the NF-kappaB Pathway. *J Exp Clin Cancer Res* (2021) 40(1):87. doi: 10.1186/s13046-021-01878-x
127. Teicher BA. CD248: A Therapeutic Target in Cancer and Fibrotic Diseases. *Oncotarget* (2019) 10(9):993–1009. doi: 10.18632/oncotarget.26590
128. Petitprez F, de Reynies A, Keung EZ, Chen TW, Sun CM, Calderaro J, et al. B Cells Are Associated With Survival and Immunotherapy Response in Sarcoma. *Nature* (2020) 577(7791):556–60. doi: 10.1038/s41586-019-1906-8
129. Increased B-Cell ICOSL Expression Improves Chemotherapy Response. *Cancer Discov* (2020) 10(9):OF8. doi: 10.1158/2159-8290.CD-RW2020-039
130. Andersson A, Bergenstrahle J, Asp M, Bergenstrahle L, Jurek A, Fernandez Navarro J, et al. Single-Cell and Spatial Transcriptomics Enables Probabilistic Inference of Cell Type Topography. *Commun Biol* (2020) 3 (1):565. doi: 10.1038/s42003-020-01247-y
131. Liu WN, Fong SY, Tan WWS, Tan SY, Liu M, Cheng JY, et al. Establishment and Characterization of Humanized Mouse NPC-PDX Model for Testing Immunotherapy. *Cancers (Basel)* (2020) 12(4):1025. doi: 10.3390/cancers12041025
132. Lucky SS, Law M, Lui MH, Mong J, Shi J, Yu S, et al. Patient-Derived Nasopharyngeal Cancer Organoids for Disease Modeling and Radiation Dose Optimization. *Front Oncol* (2021) 11:622244. doi: 10.3389/fonc.2021.622244

Conflict of Interest: The authors declare that the research was conducted in the absence of any commercial or financial relationships that could be construed as a potential conflict of interest.

Publisher's Note: All claims expressed in this article are solely those of the authors and do not necessarily represent those of their affiliated organizations, or those of the publisher, the editors and the reviewers. Any product that may be evaluated in this article, or claim that may be made by its manufacturer, is not guaranteed or endorsed by the publisher.

frontiers in Oncology

ORIGINAL RESEARCH
published: 28 September 2021
doi: 10.3389/fonc.2021.728040

Positron Emission Tomography-Computed Tomography Parameters Predict Efficacy of Immunotherapy in Head and Neck Squamous Cell Carcinomas

Songtao Zhang, Runfang Zhang, Wenbo Gong, Chao Wang, Chen Zeng, Yifei Zhai, Qigen Fang and Liyuan Dai*

Department of Thyroid and Head Neck, Affiliated Cancer Hospital of Zhengzhou University, Henan Cancer Hospital, Zhengzhou, China

OPEN ACCESS

Edited by:
Pablo Parente-Arias, A Coruña University Hospital Complex (CHUAC), Spain

Reviewed by:
Miguel Mayo, Complexo Hospitalario Universitario A Coruña, Spain
Alberto Carral-Maseda, Lucus Augusti University Hospital, Spain

***Correspondence:**
Songtao Zhang
zhyy143@126.com

Specialty section:
This article was submitted to Head and Neck Cancer, a section of the journal Frontiers in Oncology

Received: *20 June 2021*
Accepted: *31 August 2021*
Published: *28 September 2021*

Citation:
Zhang S, Zhang R, Gong W, Wang C, Zeng C, Zhai Y, Du W, Fang Q and Dai L (2021) Positron Emission Tomography-Computed Tomography Parameters Predict Efficacy of Immunotherapy in Head and Neck Squamous Cell Carcinomas. Front. Oncol. 11:728040. doi: 10.3389/fonc.2021.728040

Background: This study aims to assess the association between positron emission tomography-computed tomography (PET-CT) parameters and the response to immune checkpoint inhibitors in unresectable head and neck squamous cell carcinoma (HNSCC).

Methods: A total of 105 patients receiving immunotherapy (pembrolizumab or sintilimab with/without cisplatin) were retrospectively enrolled in this study; pretreatment data regarding metabolic tumor volume (MTV) and maximum standardized uptake value (SUVmax) were collected. The primary interest of the study was objective response rate (ORR), and the secondary was progression–free survival (PFS).

Results: The mean total MTV was 40.6 cm^3 (range: 8.5–100.3), ORRs in tumors with total MTV of ≥40.6 and <40.6 cm^3 were 43.1% and 23.1%, respectively; the difference was statistically significant ($p = 0.018$). Survival analysis indicated similar PFS rates in the two groups ($p = 0.057$). The mean total SUVmax was 12.5, ORRs in tumors with total SUVmax ≥12.5 and <12.5 were 40.0% and 26.0%, respectively; the difference was not significant ($p = 0.092$). Survival analysis reported patients with total SUVmax of ≥12.5 had significantly worse PFS ($p = 0.001$) than patients with total SUVmax of <12.5.

Conclusions: In HNSCC, total MTV ≥40.6 cm^3 translated into improved clinical response but not into better PFS; total SUVmax had no effect on clinical response, but total SUVmax ≥12.5 was associated with worse PFS.

Keywords: PD-1 inhibitor, immunotherapy, head and neck squamous cell carcinoma, metabolic tumor volume, SUVmax

INTRODUCTION

Head and neck squamous cell carcinoma (HNSCC) is the seventh commonest malignancy in the world (1), even treated with multiple procedures, numerous patients develop locoregional recurrence and/or distant metastasis and can only receive palliative chemotherapy if there is no chance of salvage surgery (2). The emergence of immune checkpoint inhibitors, of which PD-1 inhibitor is the prototype, greatly reformed the treatment blueprint. Burtness et al. (3) analyzed the definite treatment role of pembrolizumab in 882 patients with untreated incurable HNSCC, and noted that in the combined positive score (CPS) of 20 or more patients, pembrolizumab alone improved overall survival (OS) compared with those on cetuximab with chemotherapy (14.9 *vs*. 10.7 months); in the CPS of one or more patients, pembrolizumab with chemotherapy achieved longer OS time than other regimen. Recently, the Food and Drug Administration (FDA) approved the use of PD-1 inhibitor (pembrolizumab) with or without cisplatin as the first-line therapy for recurrent or metastatic HNSCC (4).

However, the overall response rate to PD-1 inhibitor monotherapy is about 20%; thus, there is a need to identify biomarkers that will help with patient selection (5). Some researchers have analyzed the predictive value of PD-L1 expression (6), peripheral lymphocyte counts (7), total tumor burden (8), and gut microbiome (9) in PD-1-based immunotherapy efficacy, although this is still controversial.

PET-CT is widely used for detecting disease metastasis in clinical practice, and its parameters including maximum standard uptake value (SUVmax) and metabolic tumor volume (MTV), are significantly associated with patient survival in HNSCC (10, 11).

Therefore, this study aims to assess the association between PET-CT parameters and response to immune checkpoint inhibitors in unresectable HNSCC.

MATERIALS AND METHODS

Ethical Consideration

Our hospital institutional research committee approved our study, and all participants signed an informed consent agreement. All methods were performed in accordance with the relevant guidelines and regulations. All procedures performed in studies involving human participants were in accordance with the ethical standards of the institutional and/or national research committee and the 1964 Helsinki Declaration and its later amendments or comparable ethical standards.

Patient Selection

Between January 2018 and January 2021, medical records of HNSCC patients were retrospectively reviewed; inclusion criteria were as follows: those with disease defined as unresectable; those who received pembrolizumab or sintilimab with/without cisplatin (docetaxel 75 mg/m^2 and cisplatin 100 mg/m^2, on day 1; fluorouracil by continuous infusion 1,000 mg/m^2, on days 1 to 5, TPF) as palliative treatment after multidisciplinary consultation, based on Chinese Society of Clinical Oncology guidelines for recurrent and metastatic HNSCC; those who had a PET-CT scan performed within 1 week prior to treatment. Patients were excluded if they had insufficient follow-up data or had received other treatment for the primary or recurrent disease. Information regarding demographic and pathologic data, Eastern Cooperative Oncology Group (ECOG) performance, PET-CT parameters, prior treatment, and follow-up was extracted and analyzed.

Palliative Treatment

Pembrolizumab (Keytruda, Merck & Co, Kenilworth, NJ, USA) or sintilimab (Daboshu, Innovent Biologics, Suzhou, China) was used solely or concurrently with TPF chemotherapy based on comprehensive consideration of the patient's economic status and willingness, health condition, PD-L1 expression, and so on for HNSCC patients from January 2018. Pembrolizumab or sintilimab was given intravenously at a dose of 200 mg every 3 weeks until intolerable toxicity or disease progression occurred. Six cycles of TPF chemotherapy was given.

Immunohistochemical Analysis

From July 2013, immunohistochemical analysis of p16 (Wuhan Boster Biotechnology Co., Ltd., Wuhan, China) was performed for every patient with HNSCC. The level of positivity of p16 overexpression was consistent with that in previous studies (12): 0–+, defined as less than 25% tumor staining; ++, defined as 25%–50% tumor staining; +++, defined as 50%–75% tumor staining; and ++++, defined as more than 75% tumor staining. Tumors with +++ and ++++ were classified as having p16 positivity.

PD-L1 expression was assessed using the 22C3 pharmDx assay (DAKO, Glostrup, Denmark) and calculated by CPS, it was defined as the number of PD-L1-positive cells divided by the total number of tumor cells ×100; a minimum of 100 viable tumor cells must have been present for the specimen to be considered evaluable (3).

Important Variable Definitions

A current smoker was defined as one who had smoked at least 10 cigarettes per day for at least 10 years, a former smoker was defined as one who had quit smoking for at least 2 years prior to this study, a never smoker was defined as one who had smoked no more than 100 cigarettes in his lifetime (13). Total SUVmax was calculated as the sum of the SUVmax of all measurable lesions by RECIST, version 1 (14). Total MTV was calculated as the sum of the MTV of all measurable lesions by RECIST, version 1 (14).

PET-CT Scheme

PET-CT (GE Healthcare, Milwaukee, WI, USA) was performed by several scanners. Before the scan, patients were required to fast for at least 6 h. If glucose levels were >200 mg/dl, PET-CT scan was postponed. Every patient received 10–20 mCi of [^{18}F] FDG dosed according to his or her weight. Axial PET and diagnostic CT images were obtained from the calvarial vertex

through the upper thighs after urinary voiding. Emission images were obtained after radiopharmaceutical injection, 60 min later. During the CT scan, there was no contrast medium used. The images were reconstructed to the thickness of a 2.5-mm slice. The SUVmax was measured for all suspicious lesions. For every suspicious lesion, the isocontour region of interest centered on the maximum value pixel was drawn automatically with workstation tools generating the SUV max of the region. A SUVmax cutoff of 2.5 MBq/g was used to indicate malignancy.

Follow-Up Protocol

The patient was usually examined by palpation and image assessment after every two to four cycles of treatment; timely evaluation was performed if there was any new sign of disease progression or other complications.

Study Endpoint

The primary study interest was objective response rate (ORR); the secondary interest included progression–free survival (PFS) and OS. Responses were formulated as complete response (CR), partial response (PR), stable disease (SD), and progressive disease (PD) according to RECIST, version 1 (14), and were assessed every 8 weeks, with the overall treatment response defined as the best response recorded from the initial treatment to disease progression or death. The ORR referred to the proportion of patients achieving CR or PR. PFS was calculated as the time from the date of diagnosis to documented disease progression, or death from any cause. OS was calculated as the time from the date of diagnosis until death from any cause (3).

Statistical Analysis

The Chi-square test (univariate analysis) was used to analyze the association between clinicopathologic variables, PET-CT parameters, and ORR, and the factors which were significant in univariate analyses were then analyzed in multivariate analysis to detect the independent predictors. The Kaplan-Meier method was used to compare the PFS and OS. Cox model was used to determine the independent prognostic factors. All statistical analyses were performed using SPSS 20.0, and a $p < 0.05$ was considered to be significant.

RESULTS

Baseline Data

In the 105 patients, 75 (71.4%) were male and 30 (28.6%) were female with a mean age of 56.8 years (range: 38–79). Twenty-nine (27.6%) of them had an ECOG score of 0, 61 (58.1%) had a score of 1, and 15 (14.3%) had a score of 2. Twenty (19.0%) patients were current smokers, 61 (58.1%) were former smokers, and 24 (22.9%) were never smokers. Thirty-five (33.3%) patients had a primary disease, 70 (66.7%) had recurrent/metastatic disease, and had all received prior treatment in form of surgery or radiotherapy; 35 of them had also received chemotherapy. Primary tumors were located in the oral cavity in 20 (19.0%) patients, in the oropharynx in 31 (29.5%), in the larynx in 32 (30.5%), and in the hypopharynx in 22 (21.0%). Positivity of p16 occurred in 11 (10.5%) patients. The mean total SUVmax was 12.5 (range: 4.7–48.6), while the mean total MTV was 40.6 cm^3 (range: 8.5–100.3). Fourteen (13.3%) patients had a CPS of less than 1, 66 (62.9%) had a CPS greater than 1 but less than 20, and 25 (23.8%) had a CPS no less than 20. Forty-six (43.8%) patients received immunotherapy alone, and 59 (56.2%) received both immunotherapy and TPF chemotherapy (**Table 1**).

Response to Treatment and Its Potential Predictors

A total of 35 patients showed positive clinical response; there were four cases of CR and 31 cases of PR, the overall ORR was 33.3%, and SD and PD occurred in 15 (14.3%) and 55 (52.4%) patients, respectively.

Tumors with p16 positivity had an ORR of 72.7%, which was significantly higher than 28.7% in tumors without p16 positivity ($p = 0.006$). The ORRs in tumors with total MTV ≥40.6 cm^3 and<40.6 cm^3 were 43.1% and 23.1%, respectively; the difference

TABLE 1 | Baseline data of the enrolled 105 patients.

Parameter	*N* (%)
Age	
<40	3 (2.9%)
≥40	102 (97.1%)
Sex	
Male	75 (71.4%)
Female	30 (28.6%)
Eastern Cooperative Oncology Group score	
0	29 (27.6%)
1	61 (58.1%)
2	15 (14.3%)
Smoker	
Current	20 (19.0%)
Former	61 (58.1%)
Never	24 (22.9%)
Disease classification	
Primary	35 (33.3%)
Recurrent/metastatic	70 (66.7%)
Prior treatment	
None	35 (33.3%)
Surgery, radiotherapy	35 (33.3%)
Surgery, chemoradiotherapy	35 (33.3%)
Primary tumor site	
Oral cavity	20 (19.0%)
Oropharynx	31 (29.5%)
Larynx	32 (30.5%)
Hypopharynx	22 (21.0%)
Positivity of p16	11 (10.5%)
Total SUVmax	
<12.5	50 (47.6%)
≥12.5	55 (52.4%)
Total MTV (cm^3)	
<40.6	47 (44.8%)
≥40.6	58 (55.2%)
Combined positive score	
<1	14 (13.3%)
1–20	66 (62.9%)
≥20	25 (23.8%)
Palliative treatment	
PD-1 inhibitor	46 (43.8%)
PD-1 inhibitor + TPF	59 (56.2%)

SUVmax, max standard uptake value; MTV, metabolic tumor volume; TPF, docetaxel + cisplatin + fluorouracil.

was significant (p = 0.018). In tumors with CPS ≥20, the ORR was 52.0%, it was apparently higher than those of the other two subgroups (p = 0.044). Compared with immunotherapy alone, the addition of TPF yielded a significantly increased ORR of 42.4% (p = 0.026). The ORRs in tumors with total SUVmax ≥12.5 and<12.5 were 40.0% and 26.0%, respectively; the difference was not significant (p = 0.092). Moreover, the treatment response had no association with age, sex, ECOG score, or smoking status (all p > 0.05) (**Table 2**). In further multivariate analysis, the factor total MTV remained an independent predictor of response (**Table 3**).

TABLE 2 | Univariate analysis of the association between general variables and treatment response in the 105 patients.

Variables	Response (CR/PR) *N* = 35	Nonresponse (SD/PD) *N* = 70	*p*-Value
Age			
<40	0	3 (100%)	
≥40	35 (34.3%)	67 (65.7%)	0.549
Sex			
Male	23 (30.7%)	52 (69.3%)	
Female	12 (40.0%)	18 (60.0%)	0.359
ECOG[#]			
0	9 (31.0%)	20 (69.0%)	
1	22 (36.1%)	39 (63.9%)	
2	4 (26.7%)	11 (73.3%)	0.751
Smoker			
Current	7 (35.0%)	13 (65.0%)	
Former	20 (32.8%)	41 (67.2%)	
Never	8 (33.3%)	16 (67.7%)	0.984
Disease classification			
Primary	13 (37.1%)	22 (62.9%)	
Recurrent/metastatic	22 (31.4%)	48 (68.6%)	0.693
Prior treatment			
None	13 (37.1%)	22 (62.9%)	
Surgery + radiotherapy	11 (31.4%)	24 (68.6%)	
Surgery + chemoradiotherapy	11 (31.4%)	24 (68.6%)	0.842
Primary tumor site			
Oral cavity	7 (35.0%)	13 (65.0%)	
Oropharynx	13 (41.9%)	18 (58.1%)	
Larynx	10 (31.3%)	22 (68.7%)	
Hypopharynx	5 (22.7%)	17 (77.3%)	0.525
p16			
Positive	8 (72.7%)	3 (27.3%)	
Negative	27 (28.7%)	67 (71.3%)	0.006
Total SUVmax			
<12.5	13 (26.0%)	37 (74.0%)	
≥12.5	22 (40.0%)	33 (60.0%)	0.092
Total MTV (cm^3)			
<40.6	10 (21.3%)	37 (78.7%)	
≥40.6	25 (43.1%)	33 (56.9%)	0.018
Combined positive score			
<1	2 (14.3%)	12 (85.7%)	
1–20	20 (30.3%)	46 (69.7%)	
≥20	13 (52.0%)	12 (48.0%)	0.044
Drug combination			
None	10 (21.7%)	36 (78.3%)	
TPF	25 (42.4%)	34 (57.6%)	0.026

ECOG, Eastern Cooperative Oncology Group score; SUVmax, max standard uptake value; MTV, metabolic tumor volume; TPF, docetaxel + cisplatin + fluorouracil; CR/PR, complete response/partial response; SD/PD, stable disease/progressive disease.

TABLE 3 | Multivariate analysis of the association between general variables and treatment response in the 105 patients.

Variable	Predictor for response	
	p-Value	OR [95% CI]
p16 (positive *vs*. negative)	0.356	2.16 [0.762–6.448]
Total MTV (≥40.6 *vs*. <40.6)	0.004	4.326 [1.327–8.332]
Combined positive score		
<1		
1–20	0.032	2.198 [1.032–5.432]
≥20	0.002	6.438 [1.983–15.725]
Drug combination (TPF *vs*. none)	0.017	3.218 [1.836–7.338]

MTV, metabolic tumor volume; TPF, docetaxel + cisplatin + fluorouracil.

Toxicity to Treatment

Adverse events occurred in all patients, with 268 grades 1–2 events and 12 grades 3–4 events. The most common grades 1–2 and grades 3–4 events were anorexia and neutropenia, respectively. Two patients died of serious adverse reaction (**Table 4**).

PFS and OS

After a mean follow-up time of 20.3 months (range: 2–36), the 2-year PFS rate was 31% in patients with total MTV <40.6 cm^3, and 21% in those with total MTV ≥40.6 cm^3; the difference was not significant (p = 0.057, **Figure 1**). The 2-year PFS rate was 39% in patients with total SUVmax <12.5, and 14% in those with total SUVmax ≥12.5, the difference was significant (p = 0.001, **Figure 2**). Further Cox model confirmed the independence of total SUVmax in decreasing the PFS (**Table 5**).

The 2-year OS rate was 62% in patients with total MTV <40.6 cm^3, and 42% in those with total MTV ≥40.6 cm^3, the difference was significant (p = 0.017, **Figure 3**). The 2-year OS rate was 60% in patients with total SUVmax <12.5, and 42% in those with total SUVmax ≥12.5; the difference was not significant (p = 0.071, **Figure 4**). Further Cox model confirmed the independence of total MTV in decreasing the OS (**Table 5**).

TABLE 4 | Adverse events in the 105 patients.

Event	Number (%)	
	Grades 1–2	Grades 3–4
Anorexia	57 (54.3%)	
Nausea	43 (41.0%)	
Fatigue	40 (38.1%)	
Constipation	35 (33.3%)	
Stomatitis	29 (27.6%)	
Hypothyroidism	15 (14.3%)	
Diarrhea	10 (9.5%)	
Neutropenia	9 (8.6%)	5 (4.8%)
Thrombocytopenia	7 (6.7%)	3 (2.9%)
Vomiting	6 (5.7%)	
Pneumonia	4 (3.8%)	2 (1.9%)
Peripheral neuropathy	3 (2.9%)	
Pyrexia	3 (2.9%)	1 (1.0%)
Venous thrombosis	3 (2.9%)	1 (1.0%)
Dizziness	2 (1.9%)	
Cough	2 (1.9%)	

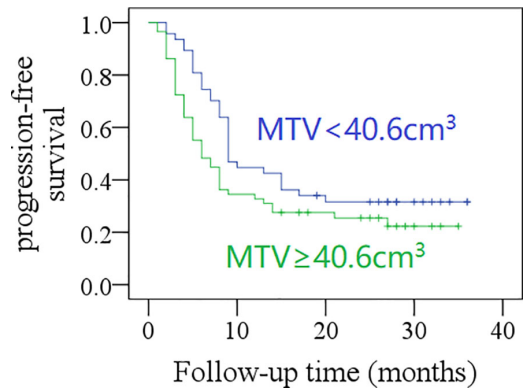

FIGURE 1 | Comparison of progression-free survival in patients with different total metabolic tumor volumes (MTV) (p = 0.057).

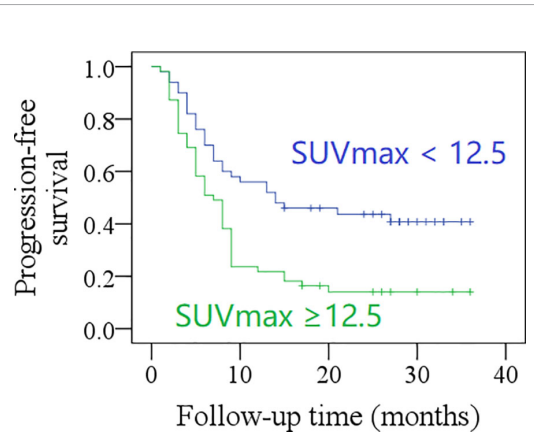

FIGURE 2 | Comparison of progression-free survival in patients with different total maximum standard uptake values (SUVmax) (p = 0.001).

DISCUSSION

The most important finding in this study is that total MTV was associated with the efficacy of PD-1 inhibitor in unresectable HNSCC, but this could not translate into better PFS. Furthermore, total SUVmax had little effect on treatment response to immunotherapy, but total SUVmax ≥12.5 was related to worse PFS.

Several researchers had aimed to explore biomarkers that will predict the efficacy of immunotherapy including PD-L1 expression, tumor mutation burden (15), microbiome (9), and neutrophil/lymphocyte ratio (NLR) (16). Ferris et al. (17) analyzed the OS rates in 240 patients receiving nivolumab with different PD-L1 expression levels and found that the two groups (<1% *vs.* ≥1%) had similar estimated OS rates at 18, 24, and 30 months. However, in a study by Burtness et al. (3), patients with CPS >20 had the highest OS rate after treatment with

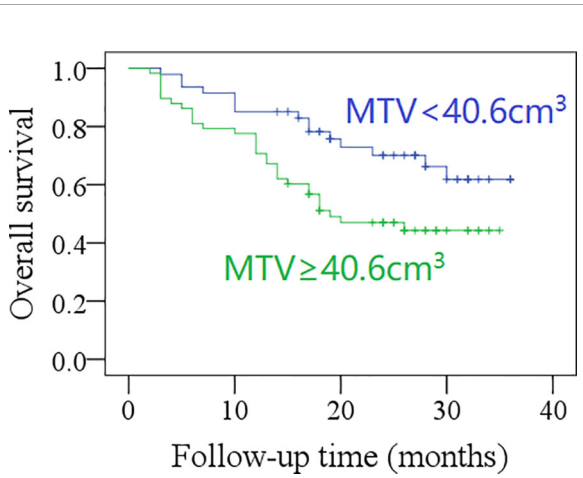

FIGURE 3 | Comparison of overall survival in patients with different total metabolic tumor volumes (MTV) (p = 0.017).

TABLE 5 | Univariate analysis and Cox model for progression-free survival (PFS) and overall survival (OS).

Variables	PFS			OS		
	Univariate	Cox model		Univariate	Cox model	
	p-Value	*p*-Value	HR [95% CI]	*p*-Value	*p*-Value	HR [95%CI]
Age	0.367			0.631		
Sex	0.167			0.432		
ECOG	0.641			0.048		
Smoker	0.222			0.254		
Tumor site	0.107			0.189		
p16	0.049	0.023	0.82 [0.67–0.98]	0.667		
Total SUVmax	0.001	0.014	2.76 [1.25–5.89]	0.071		
Total MTV	0.057			0.017	0.018	3.86 [1.35–7.88]
CPS				0.099		
<1						
1–20		0.087	0.88 [0.42–1.05]			
≥20	0.002	0.004	0.68 [0.37–0.83]			
Chemotherapy	0.035	0.034	0.86 [0.67–0.99]	0.032	0.077	0.98 [0.46–1.28]

ECOG, Eastern Cooperative Oncology Group score; Total SUVmax, total max standard uptake value; Total MTV, total metabolic tumor volume; CPS, combined positive score.

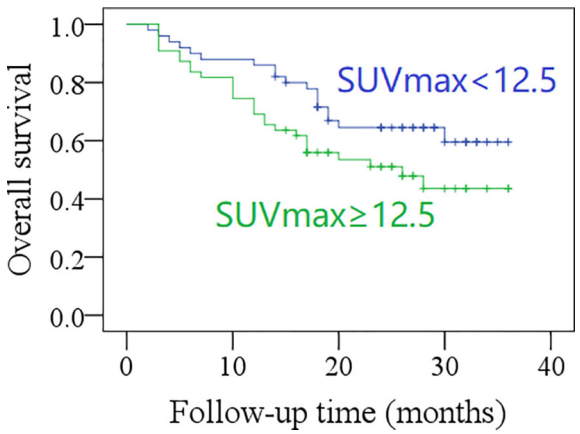

FIGURE 4 | Comparison of overall survival in patients with different total maximum standard uptake values (SUVmax) (p = 0.071).

pembrolizumab alone, and patients with CPS ranging from 1 to 20 had superior OS after being treated with chemotherapy and pembrolizumab rather than pembrolizumab alone. Additionally, Rizvi et al. (15) found that improved objective response, durable clinical benefit, and progression-free survival were noted in tumors with higher nonsynonymous mutation burden in nonsmall cell lung cancer. Routy et al. (9) presented in animal models that primary resistance to immunotherapy was attributable to abnormal gut microbiome composition, and that oral supplementation with *Akkermansia muciniphila* after fecal microbiota transplantation with nonresponder feces restored the efficacy of PD-1 blockade. However, both of them were not applicable in clinical practice. Some authors have assessed the role of blood cell count in immunotherapy, such as NLR; Park et al. (16) found that low NLR at week 6 of therapy and decreased NLR during treatment were both associated with a longer PFS in advanced HNSCC, but as previously stated, the NLR was a nonspecific index, easily affected by local or system inflammation (18). Therefore, continuous exploration for a reliable predictive biomarker for immunotherapy is required.

MTV was a commonly analyzed parameter of PET-CT; it referred to the volume of tumor tissue with high metabolic activity. Our previous studies have confirmed its negative effect on disease prognosis in HNSCC (11), but whether it is associated with the efficacy of immunotherapy in HNSCC remains unknown. We were the first to find that tumors with greater total MTV have better ORR than those with smaller total MTV, and that the improved treatment response contributed to similar PFS rates in the two groups; the finding was very interesting, on the one hand, usually the MTV reflected the tumor burden, it took length diameter and depth of invasion into consideration. Sridharan et al. (8) introduced a different calculation method, which was defined as the sum of the largest diameter of all measurable lesions; the median tumor burden was 5.4 cm and had no relationship with clinical pathologic variables, and tumor burden >5.4 cm was inversely correlated with clinical benefit of immunotherapy and OS. However, in a study by Suzuki et al. (19), which used the same concept of tumor burden, the authors did not report the aforementioned association. These inconsistencies in the reports might have uncovered the inferiority of tumor burden calculation using tumor diameter. On the other hand, the MTV also reflected the functional and biologic status of the tumor due to the biologic features of glucose. High total MTV means a more advanced HNSCC, which is likely to have PD-L1 overexpression (20). Negative prognostic effect of MTV on surgically treated HNSCC has been extensively reported (11), with greater MTV usually related to increased possibility of lymph node metastasis, higher tumor stage, worse disease control and poor prognosis; our study noted after immunotherapy that there was no significant difference regarding PFS between patients with different total MTVs. This indicates the reliability of total MTV in predicting immunotherapy efficacy. However, in a report by Seban et al. (21) who enrolled 63 patients with advanced nonsmall cell lung cancer, high total MTV (>83 cm^3) was likely to decrease the treatment response rate. As for metastatic melanoma treated with anti-PD-1 therapy, Nakamoto et al. (22) did not comment on whether the clinical benefit of immunotherapy was affected by MTV. These conflicting results might be mostly due to the differences in research objects.

SUVmax was another important parameter of PET-CT, which refers to the ability of tumor tissues to take up tracers; in general, the higher the SUVmax, the higher the possibility and degree of malignancy. A number of researchers have described that patients with high SUVmax were more likely to have larger tumors, advanced stage disease, and poor prognosis (10, 23, 24). Whether or not SUVmax can be used for guiding immunotherapy was never analyzed in patients with HNSCC before, although some researchers have assessed its predictive value in lung cancer (21) and melanoma (22). Both studies concluded that there was no association between SUVmax and clinical response, and we would also like to confirm this negative relationship in HNSCC.

Limitations in this study must be acknowledged: first, its retrospective nature had inherent bias; second, our sample size was small, which decreased our statistic power; third, our follow-up time was limited, there might be more interesting findings in the future; fourth, PD-1 inhibitors consisted of two different drugs in this study, both of which had been confirmed to have good ability of binding to receptor PD-L1 (3, 25).

In summary, in HNSCC, total MTV of ≥40.6 cm^3 was related to improved clinical response but did not translate into better PFS; total SUVmax had no effect on clinical response but total SUVmax ≥12.5 was associated with worse PFS.

DATA AVAILABILITY STATEMENT

The original contributions presented in the study are included in the article/**Supplementary Material**. Further inquiries can be directed to the corresponding author.

ETHICS STATEMENT

Henan Cancer hospital institutional research committee approved our study, and all participants signed an informed consent agreement. The patients/participants provided their written informed consent to participate in this study.

AUTHOR CONTRIBUTIONS

All authors have contributed to the concept design, data collection, data analysis, manuscript writing, and manuscript revision. All authors contributed to the article and approved the submitted version.

REFERENCES

1. Ferlay J, Colombet M, Soerjomataram I, Mathers C, Parkin DM, Piñeros M, et al. Estimating the Global Cancer Incidence and Mortality in 2018: GLOBOCAN Sources and Methods. *Int J Cancer* (2019) 144:1941–53. doi: 10.1002/ijc.31937
2. Szturz P, Vermorken JB. Management of Recurrent and Metastatic Oral Cavity Cancer: Raising the Bar a Step Higher. *Oral Oncol* (2020) 144:104492. doi: 10.1016/j.oraloncology.2019.104492
3. Burtness B, Harrington KJ, Greil R, Soulières D, Tahara M, de Castro G Jr, et al. Pembrolizumab Alone or With Chemotherapy *Versus* Cetuximab With Chemotherapy for Recurrent or Metastatic Squamous Cell Carcinoma of the Head and Neck (KEYNOTE-048): A Randomised, Open-Label, Phase 3 Study. *Lancet* (2019) 394:1915–28. doi: 10.1016/S0140-6736(19)32591-7
4. Cohen EEW, Bell RB, Bifulco CB, Burtness B, Gillison ML, Harrington KJ, et al. The Society for Immunotherapy of Cancer Consensus Statement on Immunotherapy for the Treatment of Squamous Cell Carcinoma of the Head and Neck (HNSCC). *J Immunother Cancer* (2019) 7:184. doi: 10.1186/s40425-019-0662-5
5. Moskovitz J, Moy J, Ferris RL. Immunotherapy for Head and Neck Squamous Cell Carcinoma. *Curr Oncol Rep* (2018) 20:22. doi: 10.1007/s11912-018-0654-5
6. Hanna GJ, Lizotte P, Cavanaugh M, Kuo FC, Shivdasani P, Frieden A, et al. Frameshift Events Predict Anti-PD-1/L1 Response in Head and Neck Cancer. *JCI Insight* (2018) 3:e98811. doi: 10.1172/jci.insight.98811
7. Park JC, Durbeck J, Clark JR. Predictive Value of Peripheral Lymphocyte Counts for Immune Checkpoint Inhibitor Efficacy in Advanced Head and Neck Squamous Cell Carcinoma. *Mol Clin Oncol* (2020) 13:87. doi: 10.3892/mco.2020.2157
8. Sridharan V, Rahman RM, Huang RY, Chau NG, Lorch JH, Uppaluri R, et al. Radiologic Predictors of Immune Checkpoint Inhibitor Response in Advanced Head and Neck Squamous Cell Carcinoma. *Oral Oncol* (2018) 85:29–34. doi: 10.1016/j.oraloncology.2018.08.005
9. Routy B, Le Chatelier E, Derosa L, Duong CPM, Alou MT, Daillère R, et al. Gut Microbiome Influences Efficacy of PD-1-Based Immunotherapy Against Epithelial Tumors. *Science* (2018) 359:91–7. doi: 10.1126/science.aan3706
10. Xu C, Li H, Seng D, Liu F. Significance of SUV Max for Predicting Occult Lymph Node Metastasis and Prognosis in Early-Stage Tongue Squamous Cell Carcinoma. *J Oncol* (2020) 2020:6241637. doi: 10.1155/2020/6241637
11. Yang L, Liu F, Wu Y, Fang Q, Zhang X, Du W, et al. Predictive Value of Occult Metastasis and Survival Significance of Metabolic Tumor Volume Determined by PET-CT in Ct1-2N0 Squamous Cell Carcinoma of the Tongue. *Front Oncol* (2020) 10:542530. doi: 10.3389/fonc.2020.542530
12. Dahlstrom KR, Little JA, Zafereo ME, Lung M, Wei Q, Sturgis EM. Squamous Cell Carcinoma of the Head and Neck in Never Smoker-Never Drinkers: A Descriptive Epidemiologic Study. *Head Neck* (2008) 30:75–84. doi: 10.1002/hed.20664
13. Bachar G, Hod R, Goldstein DP, Irish JC, Gullane PJ, Brown D, et al. Outcome of Oral Tongue Squamous Cell Carcinoma in Patients With and Without Known Risk Factors. *Oral Oncol* (2011) 47:45–50. doi: 10.1016/j.oraloncology.2010.11.003
14. Therasse P, Arbuck SG, Eisenhauer EA, Wanders J, Kaplan RS, Rubinstein L, et al. New Guidelines to Evaluate the Response to Treatment in Solid Tumors. European Organization for Research and Treatment of Cancer, National Cancer Institute of the United States, National Cancer Institute of Canada. *J Natl Cancer Inst* (2000) 92:205–16. doi: 10.1093/jnci/92.3.205
15. Rizvi NA, Hellmann MD, Snyder A, Kvistborg P, Makarov V, Havel JJ, et al. Cancer Immunology. Mutational Landscape Determines Sensitivity to PD-1 Blockade in Non-Small Cell Lung Cancer. *Science* (2015) 348:124–8. doi: 10.1126/science.aaa1348
16. Ho WJ, Yarchoan M, Hopkins A, Mehra R, Grossman S, Kang H. Association Between Pretreatment Lymphocyte Count and Response to PD1 Inhibitors in Head and Neck Squamous Cell Carcinomas. *J Immunother Cancer* (2018) 6:84. doi: 10.1186/s40425-018-0395-x
17. Ferris RL, Blumenschein G Jr, Fayette J, Guigay J, Colevas AD, Licitra L, et al. Nivolumab *vs* Investigator's Choice in Recurrent or Metastatic Squamous Cell Carcinoma of the Head and Neck: 2-Year Long-Term Survival Update of CheckMate 141 With Analyses by Tumor PD-L1 Expression. *Oral Oncol* (2018) 81:45–51. doi: 10.1016/j.oraloncology.2018.04.008
18. Xu C, Yuan J, Du W, Wu J, Fang Q, Zhang X, et al. Significance of the Neutrophil-To-Lymphocyte Ratio in P16-Negative Squamous Cell Carcinoma of Unknown Primary in Head and Neck. *Front Oncol* (2020) 10:39. doi: 10.3389/fonc.2020.00039
19. Suzuki C, Kiyota N, Imamura Y, Rikitake J, Sai S, Koyama T, et al. Effect of Tumor Burden and Growth Rate on Treatment Outcomes of Nivolumab in Head and Neck Cancer. *Int J Clin Oncol* (2020) 25:1270–7. doi: 10.1007/s10147-020-01669-y
20. Lenouvel D, González-Moles MÁ, Ruiz-Ávila I, Gonzalez-Ruiz L, Gonzalez-Ruiz I, Ramos-García P. Prognostic and Clinicopathological Significance of PD-L1 Overexpression in Oral Squamous Cell Carcinoma: A Systematic Review and Comprehensive Meta-Analysis. *Oral Oncol* (2020) 106:104722. doi: 10.1016/j.oraloncology.2020.104722
21. Seban RD, Assie JB, Giroux-Leprieur E, Massiani MA, Soussan M, Bonardel G, et al. FDG-PET Biomarkers Associated With Long-Term Benefit From First-Line Immunotherapy in Patients With Advanced Non-Small Cell Lung Cancer. *Ann Nucl Med* (2020) 34:968–74. doi: 10.1007/s12149-020-01539-7
22. Nakamoto R, Zaba LC, Liang T, Reddy SA, Davidzon G, Aparici CM, et al. Prognostic Value of Bone Marrow Metabolism on Pretreatment 18F-FDG PET/CT in Patients With Metastatic Melanoma Treated With Anti-PD-1 Therapy. *J Nucl Med* (2021). doi: 10.2967/jnumed.120.254482
23. Surov A, Meyer HJ, Höhn AK, Wienke A, Sabri O, Purz S. Combined Parameter SUVmax/ADCmean Predicts Microvessel Density in Head and Neck Squamous Cell Carcinoma. *Preliminary results Oral Oncol* (2020) 101:104355. doi: 10.1016/j.oraloncology.2019.06.036
24. Bae MR, Roh JL, Kim JS, Choi SH, Nam SY, Kim SY. Prediction of Cervical Metastasis and Survival in Cn0 Oral Cavity Cancer Using Tumour 18F-FDG PET/CT Functional Parameters. *J Cancer Res Clin Oncol* (2020) 146:3341–8. doi: 10.1007/s00432-020-03313-8
25. Yang Y, Wang Z, Fang J, Yu Q, Han B, Cang S, et al. Efficacy and Safety of Sintilimab Plus Pemetrexed and Platinum as First-Line Treatment for Locally Advanced or Metastatic Nonsquamous NSCLC: A Randomized, Double-Blind, Phase 3 Study (Oncology Program by InnovENT Anti-PD-1-11). *J Thorac Oncol* (2020) 15:1636–46. doi: 10.1016/j.jtho.2020.07.014

Conflict of Interest: The authors declare that the research was conducted in the absence of any commercial or financial relationships that could be construed as a potential conflict of interest.

frontiers in Oncology

ORIGINAL RESEARCH
published: 26 November 2021
doi: 10.3389/fonc.2021.760861

Carnosic Acid Suppresses the Development of Oral Squamous Cell Carcinoma *via* Mitochondrial-Mediated Apoptosis

Fenghe Min[1,2,3†], *Xin Liu*[3†], *Yuan Li*[3], *Mingyuan Dong*[3], *Yidi Qu*[3] *and Weiwei Liu*[1,2*]

[1] Department of Oral and Maxillofacial Surgery, Hospital of Stomatology, Jilin University, Changchun, China, [2] Jilin Provincial Key Laboratory of Tooth Development and Bone Remodeling, Changchun, China, [3] School of Life Sciences, Jilin University, Changchun, China

OPEN ACCESS

Edited by:
Song Fan,
Sun Yat-sen Memorial Hospital, China

Reviewed by:
Da Liu,
Changchun University of Chinese Medicine, China
Sebastiaan De Visscher,
University Medical Center Groningen, Netherlands
Guangqi Song,
Fudan University, China

***Correspondence:**
Weiwei Liu
liuweiw@jlu.edu.cn

[†]These authors have contributed equally to this work and share first authorship

Specialty section:
This article was submitted to Head and Neck Cancer, a section of the journal Frontiers in Oncology

Received: 18 August 2021
Accepted: 08 November 2021
Published: 26 November 2021

Citation:
Min F, Liu X, Li Y, Dong M, Qu Y and Liu W (2021) Carnosic Acid Suppresses the Development of Oral Squamous Cell Carcinoma via Mitochondrial-Mediated Apoptosis. Front. Oncol. 11:760861. doi: 10.3389/fonc.2021.760861

Oral squamous cell carcinoma (OSCC) predominantly consists of squamous cells and is the tumor with the highest incidence of the head and neck. Carnosic acid (CA), a natural monomer drug obtained from rosemary and salvia, shows various pharmacological effects, including of tumor development. This study aimed to assess for an effect of CA on the development of OSCC and the underlying mechanisms. In CAL27 and SCC9 cells, CA inhibited cell proliferation and migration, increased intracellular levels of reactive oxygen species (ROS) and Ca^{2+}, decreased the mitochondrial membrane potential (MMP), and promoted apoptosis. In CAL27- and SCC9-xenotransplanted BALB/c nude mice, CA inhibited the tumor growth without affecting the body weight and tissue morphology. CA upregulated Bax, Bad, cleaved Caspase-3 and -9 levels, and the cleaved PARP1/PARP1 ratio but downregulated Bcl-2 in CA-treated OSCC cells and OSCC cells-xenotransplanted BALB/c nude mice. These results indicate that CA suppresses OSCC at least *via* the mitochondrial apoptotic pathway and offers this natural compound as a potential therapeutic against OSCC.

Keywords: carnosic acid, oral squamous cell carcinoma, reactive oxygen species, mitochondria, apoptosis

INTRODUCTION

Oral cancer is any malignant tumor caused by abnormal changes in the oral mucosa. The cases are predominantly linked to oral squamous cell carcinoma (OSCC) and rarely to salivary-gland cancers (1, 2). OSCC is a typical head and neck cancer, accounting for 2.8% of all the cancers in the world (3). Due to its high incidence, > 200,000 die from OSCC worldwide every year (3). Most patients have an unfavorable prognosis due to the anatomical location of this cancer, lymph node metastasis, or recurrence (4, 5). Smoking, drinking, and betel nut chewing are considered to be responsible for the development of OSCC (6, 7).

Apoptosis is a form of programmed cell death, mediated by multiple genes and cytokines, and constitutes an important target pathway to kill tumor cells (8, 9). Cellular stress, DNA damage, and developmental signals all activate the endogenous apoptotic pathway (9–11). Mitochondria are the primary source of intracellular reactive oxygen species (ROS) (12), which are oxygen-containing

free radicals. ROS affect the influx of Ca^{2+} into cells and cellular calcium stores, and Ca^{2+} increases the production of ROS (13). The accumulation of ROS and Ca^{2+} regulates the access through the mitochondrial permeability transition pore (mPTP) and decreases the potential while increasing the permeability of the mitochondrial membrane, whereby cytochrome c (Cyt-c) is released into the cytoplasm and activate the mitochondrial apoptotic pathway (14–16). B-cell lymphoma 2 (Bcl-2) family proteins are involved in this process. When the permeability of the mitochondrial membrane increases, apoptotic bodies translocate from the mitochondria to the cytoplasm and consequently activate caspase-family proteins, causing DNA damage and ultimately leading to apoptosis (17–19).

Currently, OSCC is treated *via* surgery, radiotherapy, and chemotherapy (20, 21). However, surgery is only applicable to early lesions and has a poor prognosis. Radiotherapy and chemotherapy may cause osteoradionecrosis (ORN), myelosuppression, and organ damage, significantly affecting the life qualities of patients (22). Thus, novel drugs with high efficacy and low toxicity are urgently needed. Recently, natural compounds have increasingly attracted attention and have been widely used to develop anticancer drugs (23). Carnosic acid (CA), a phenolic diterpene compound, is mainly found in labyrinthine plants and has been shown to have various pharmacological effects, such as antioxidant, antitumor, anti-inflammatory, and neuroprotective effects (24–27). CA induced apoptosis in hepatocellular carcinoma cells through the ROS-mediated mitochondrial pathway (28). It has also been shown to induce apoptosis in human gastric cancer cells by activating the protein kinase B/mammalian target of rapamycin (Akt/mTOR) signaling pathway (29). CA induced apoptosis of HCT116 cells by inhibiting the STAT3 signaling pathway (30). Moreover, CA synergized the anti-lung cancer effect of cisplatin and the anti-breast cancer effect of Trastuzumab (31–33). However, there are no relevant reports on the effect of CA in OSCC. Thus, this study assessed whether CA can suppress the development of OSCC.

MATERIALS AND METHODS

Cell Culture

CAL27 (CRL-2095) and SCC9 (CRL-1629) cells (human OSCC cell lines) were obtained from the American Type Culture Collection (ATCC) and cultured in Dulbecco's Modified Eagle Medium (DMEM) (Gibco, Grand Island, New York, USA) and DMEM/F12 (Hyclone, Logan, Utah, USA) at 37°C with 5% CO_2, respectively. The two media contained 10% fetal bovine serum (FBS) (Procell Life Science&Technology Co., Ltd., Wuhan, Hubei, China), 1% penicillin and streptomycin (Sigma-Aldrich, Saint Louis, Missouri, USA), and 0.1% plasmocin prophylactic (*In vivo*gen, San Diego, California, USA).

Cell Viability Assay

CAL27 and SCC9 cells at the logarithmic growth phase were plated into 96-well plates at a density of 8×10^3 cells per well and cultured for 24 h. Then, the cells were incubated with 0, 5, 10, 20, 30, 40, 60, or 80 μM CA (B21175, Shanghai Yuanye Biological Technology Co., Ltd., Shanghai, China), which had been dissolved in dimethyl sulfoxide (DMSO) (Sinopharm Chemical Reagent Co., Ltd., Shanghai, China). The final concentration of DMSO in the culture was ≤ 0.1%. After 24 h of CA treatment, the cells in each well were incubated with 10 μL of 5 mg/mL 3-(4,5-dimethylthiazolyl-2)-2,5-diphenyltetrazolium bromide (MTT) (S19063, Source Leaf Biological Technology Co., Ltd., Shanghai, China) for 4 h. Afterward, the culture supernatant was discarded, and 150 μL DMSO was used to dissolve the formazan crystals in each well. Absorbance of the samples was measured at 490 nm using an Enzyme-labeled Instrument (HBS-1096A, NanJing DeTie Laboratory Equipment Co., Ltd., Nanjing, Jiangsu, China).

Migration Assay

CAL27 and SCC9 cells at the logarithmic growth phase were plated into 6-well plates at a density of 3×10^5 cells per well. When the cells reached > 90% confluence, they were scraped using a syringe needle and then cultured with CA (30 and 15 μM for CAL27 and SCC29 cells, respectively) for 0, 12 and 24 h. Fluorescence microscope (Eclipse TE 2000-S, Nikon Corp., Tokyo, Japan) and quantifiable ImageJ software were used to analyze the influence of CA on OSCC cells migration.

Apoptosis Assay

CAL27 and SCC9 cells at the logarithmic growth phase were plated into 6-well plates at a density of 2.5×10^5 cells per well and incubated in an incubator at 37°C with 5% CO_2 for 24 h. Next, the CAL27 and SCC9 cells were incubated with 30 and 15 μM CA for 12 h, respectively. Afterward, the cells were processed using the eBioscietm Annexin V-FITC Apop Kit (BMS500FI-100, Invitrogen, Carlsbad, California, USA) according to the instructions of the manufacturer and analyzed using a CytoFLEX Flow Cytometer (C02945, Beckman Coulter, Inc. Brea, Carlsbad, California, USA).

Mitochondrial Membrane Potential (MMP) Assay

CAL27 and SCC9 cells at the logarithmic growth phase were plated into 6-well plates at a density of 2.5×10^5 cells per well and cultured for 24 h. Subsequently, the CAL27 and SCC9 cells were incubated with 30 and 15 μM CA for 12 h, respectively. Afterward, the cells were washed with phosphate-buffered saline (PBS) three times and then incubated with 5 mg/mL 5,5′,6,6′-Tetrachloro-1,1′,3,3′-tetraethyl-benzimidazolylcarbocyanine iodide (JC-1) (C2006, Beyotime Biotechnology, Shanghai, China) for 20 min. Fluorescence intensity of the samples was measured using a fluorescence microscope (Eclipse TE 2000-S, Nikon Corp., Tokyo, Japan), and the related data were quantitatively analyzed using ImageJ software.

Quantitation of Intracellular ROS and Ca^{2+}

CAL27 and SCC9 cells at the logarithmic growth phase were plated into 6-well plates at a density of 2.5×10^5 cells per well and

then incubated for 24 h. Afterward, the CAL27 and SCC9 cells were exposed to 30 and 15 μM CA for 12 h, respectively. The cells were incubated with 10 μM DFCH-DA for 30 min, and the intracellular ROS levels were measured using the Reactive Oxygen Species (ROS) Assay Kit (S0033S, Beyotime Biotechnology, Shanghai, China) according to the instructions of the manufacturer.

For Ca^{2+} detection, the cells were incubated with 1 μM Fluo-4AM (S1060, Beyotime Biotechnology, Shanghai, China) for 40 min. Afterward, the culture supernatant was discarded, and the cells were washed three times with PBS. Fluorescence intensity of the samples was measured using a fluorescence microscope (Eclipse TE 2000-S, Nikon Corp., Tokyo, Japan), and the related data were quantitatively analyzed using ImageJ software.

Transmission Electron Microscopy (TEM) Analysis

The incubation and CA treatment protocols of CAL27 and SCC9 cells were the same as *2.6 Quantitation of intracellular ROS and* Ca^{2+}.The collected cells were fixed at 4°C for 4 h, embedded in 1% agarose solution, and then fixed in 1% osmium tetroxide for the secondary fixation. After dehydration with ethanol, the cells were embedded in the embedding plate and polymerized for 48 h. The ultra-microtome (Leica UC7, Leica, Weztlar, Germany) was used to cut the resin blocks into 60-80 nm and loaded the slices on a 150-mesh cuprum grids. After the sections were stained with uranyl acetate and lead citrate, images were captured using a transmission electron microscope (H-7650, HITACHI, Japan).

CAL27- and SCC9-Xenograft Models

All the animal experiments were conducted under the guidance of the Animal Ethics and Welfare Committee of Jilin University (NO. SY202101004). Male BALB/c nude mice (5 weeks old) (Wei-tongli-hua Laboratory Animal Technology Company, Beijing, China) were provided with sufficient food and water and maintained at 23 ± 1°C under 12 h/12 h light/dark cycle.

CAL27 and SCC9 cells (1×10^7) were subcutaneously inoculated into the right dorsum of BALB/c nude mice. When the tumor volume reached 100 mm^3, the mice in each group were randomly divided into two sub-groups (n = 6 per sub-group) and intraperitoneally injected every other day for 14 d with the physiological saline containing < 0.1% DMSO (control mice) or 20 mg/kg of CA dissolved in DMSO with a final concentration of < 0.1% (CA-treated mice). The volumes of the tumors and the body weights of the mice were measured before each administration. Tumor volume was calculated according to the following formula: length (mm) × [width (mm)]^2 × 0.5. After the last treatment, the mice were euthanized *via* carbon-dioxide asphyxiation. The tumors were removed and homogenized for western blot analysis. Peripheral-blood samples were collected from the mice for blood analyses using an automatic blood analyzer. The tumor, heart, liver, spleen, and kidney of the mice were fixed in 4% polyformaldehyde (POM) (AR0211, Dingguo Changsheng Biotechnology Co., Ltd., Beijing, China) for 48 h for histopathological examination.

Histopathological Examination

Following the POM fixation, the samples were embedded in paraffin and then sectioned at 5 μm thickness by using a microtome (Leica, Wetzlar, Germany). The sections were stained with hematoxylin and eosin by using a standard protocol. After the slices were dehydrated and cleared with ethanol and xylene, images were captured using an Eclipse TE 2000-S fluorescence microscope (Nikon Corp., Tokyo, Japan).

Terminal Deoxynucleotidyl Transferase-Mediated dUTP *In Situ* Nick End Labelling (TUNEL) Assay

The paraffin sections prepared from tumor tissues were deparaffinized and repaired with proteinase K. After breaking the membrane with 0.1% triton, terminal deoxynucleotidyl transferase (Tdt) enzyme and dUTP were added according to the instructions of TUNEL assay kit (G1205, Servicebio technology Co., Ltd., Wuhan, China), and incubated at 37°C for 2 h. The nuclei were stained with 2-(4-Amidinophenyl)-6-indolecarbamidine dihydrochloride (DAPI) and incubated in the dark for 10 minutes. Fluorescent images were captured using an Eclipse TE 2000-S fluorescence microscope (Nikon Corp., Tokyo, Japan).

Western Blot Analysis

CAL27 and SCC9 cells at the logarithmic growth phase were plated into 6-well plates at a density of 2.5×10^5 cells per well and cultured for 24 h. Afterward, the CAL27 and SCC9 cells were treated with 30 and 15 μM of CA for 24 h, respectively. The treated cells and the tumor tissues obtained from the BALB/c nude mice were homogenized using the RIPA Lysis Buffer (PC101, EpiZyme, Shanghai, China). The total-protein concentrations of the samples were measured using a Standard BCA Protein Assay Kit (23225, Thermo Fisher Scientific, Waltham, Massachusetts, USA) following the manufacturer's instructions. Lysates with 30–40 μg total protein were electrophoresed using the One-Step PAGE Gel Fast Preparation Kit (PG213, EpiZyme, Shanghai, China) at 90–120 V and then transferred onto a PVDF membranes (Merck Millipore, Billerica, MA, USA) at 100 V for 2 h. The membranes were blocked with the NcmBlot blocking buffer (P30500, NCM Biotech, Suzhou, Jiangsu, China) and then incubated overnight at 4 °C with antibodies against Cleaved poly (ADP-Ribose) polymerase (PARP1) (A19612), PARP1 (A19596), Cleaved Caspase-3 (A2156), Caspase-3 (A2156), Caspase-9 (A2636), Bad (A19595), Bax (A19684) (all from ABclonal Technology Co., Ltd., Wuhan, Hubei, China); Cleaved Caspase-9 (Asp315, Cell Signaling Technology, Boston, Massachusetts, USA); B-cell lymphoma-2 (Bcl-2) (BSM-33047M, Beijing Biosynthesis Biotechnology Co., Ltd., Beijing, China); and Glyceraldehyde-3-phosphate dehydrogenase (GAPDH) (SY0102, Elabscience Biotechnology Co., Ltd., Wuhan, Hubei, China). After washing the membranes with TBST, they were incubated at 4°C for 4 h with the corresponding goat anti-rabbit IgG (H+L) (peroxidase/HRP-conjugated) (E-AB-1003) or anti-mouse IgG (H+L)

(peroxidase/HRP-conjugated) (E-AB-1001) (Elabscience Biotechnology Co., Ltd., Wuhan, Hubei, China). The protein signals were detected using electrochemiluminescence (ECL) detection kits (Merck Millipore, Billerica, MA, USA), and the signal intensities were quantified using ImageJ software.

Statistical Analysis

The statistical significance of the differences between the control and CA-treatment groups was determined using one-way analysis of variance (ANOVA). *Post-hoc* multiple comparisons (Dunn's test) were performed using DSS 25.0 software (IBM Corporation, Armonk, New York, USA). $P < 0.05$ was considered significant.

RESULTS

CA Induced Apoptosis in OSCC Cells *via* the Mitochondrial Pathway

CA significantly inhibited the viability of the OSCC cell lines CAL27 and SCC9 (IC_{50} 34.66 and 13.23 μM, respectively) ($P < 0.05$, **Figure 1A**). CA increased the early/late apoptosis of CAL27

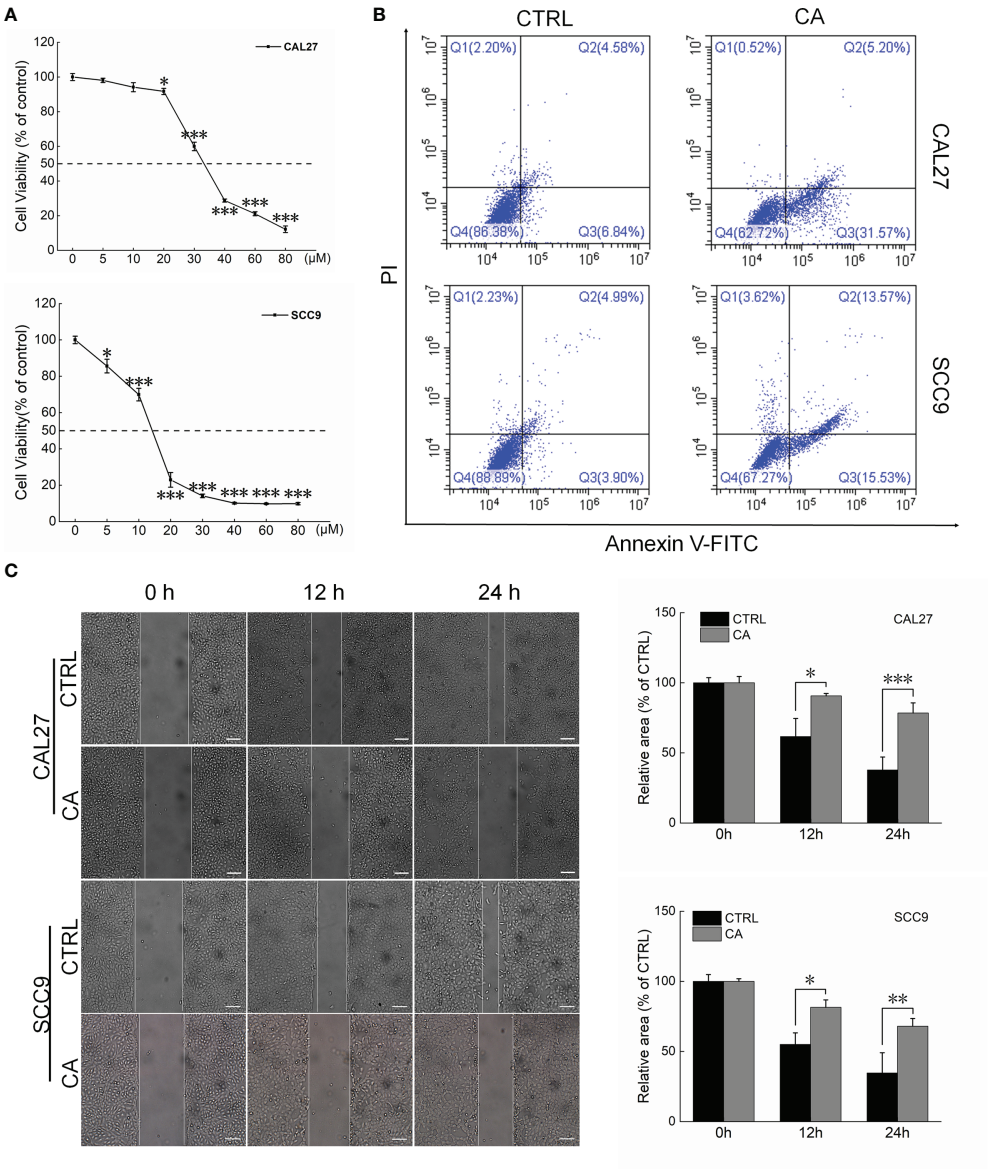

FIGURE 1 | CA treatment affected the cell viability and promoted apoptosis in OSCC cells. **(A)** CA treatment for 24 h reduced the viability of CAL27 and SCC9 cells in a dose-dependent manner ($n = 3$). **(B)** CA treatment increased the apoptosis rates of CAL27 and SCC9 cells ($n = 3$). **(C)** CA treatment significantly inhibited the migration of CAL27 and SCC9 cells over time ($n = 3$) (200× magnification, scale bar: 50 μm). The data are expressed as mean ± SEM. $^{*}P < 0.05$, $^{**}P < 0.01$ and $^{***}P < 0.001$ *versus* the control cells.

and SCC9 cells to 36.77% and 29.1%, respectively (**Figure 1B**). The migration of OSCC cells was time-dependent. Compared with the control cells, CA treatment significantly inhibited the migration ability of these OSCC cells ($P < 0.05$, **Figure 1C**).

After CAL27 and SCC9 cells were incubated with CA for 12 h, increased green fluorescence intensity was observed, indicating that CA increased the ROS levels ($P < 0.001$, **Figure 2A**) and Ca^{2+} influx ($P < 0.001$, **Figure 2B**) in OSCC cells. Moreover, the measurement of mitochondrial membrane potential proved that after OSCC cells were exposed to CA, more green fluorescence from JC-1 monomer was observed, the intensity of the red fluorescence aggregated in the matrix of the mitochondria decreased, and the red/green fluorescence ratio was significantly reduced by > 60% in the CA-treated cells ($P < 0.01$, **Figure 2C**), indicating that the level of mitochondrial depolarization increased, and the MMP decreased, and thus the cells were in the early apoptotic stage. The images obtained by TEM showed that the mitochondrial cristae of CAL27 and SCC9 cells were arranged neatly and densely (**Figure 2D**). After CA incubation, the mitochondria were severely swollen, the matrix was dissolved, and the mitochondrial cristae was missing and accompanied by vacuoles (**Figure 2D**). The administration of CA affected the structure and function of mitochondria.

In CA-exposed CAL27 and SCC9 cells, the ratios of the levels of Cleaved PARP1, Caspase-3, and Caspase-9 to total PARP1, Caspase-3, and Caspase-9 levels, respectively, were increased ($P < 0.05$, **Figure 3**). Additionally, Bcl-2 was downregulated, whereas Bax and Bad were upregulated ($P < 0.01$, **Figure 3**). These *in vitro* results preliminarily showed that CA induced apoptosis in OSCC cells by reducing the MMP.

CA Inhibited the Growth of CAL27- and SCC9-Xenotransplants by Inducing Their Apoptosis

In CAL27- and SCC9-xenotransplanted BALB/c nude mice, CA treatment for 14 d significantly inhibited the tumor growth ($P < 0.01$, **Figures 4A–C** and **5A–C**) without affecting the body weights or organ indices of the animals (**Figures 4D** and **5D**; **Table S1**). Compared with CTRL mice, the green fluorescence in tumor tissues enhanced, in other words, the number of TUNEL positive cells increased after CA administration, indicating that CA administration promoted tumor tissue apoptosis (**Figures 4E** and **5E**). The cardiomyocytes and hepatocytes of the animals were still neatly arranged, the spleen had no significant infiltration of inflammatory cells, and the glomeruli had no obvious lesions, indicating that CA did not impact the histological features of the mice (**Figures 4F** and **5F**).

Results from the peripheral-blood analyses indicated increased monocyte number and decreased platelet distribution width (PDWcv) in the SCC9-xenotransplanted BALB/c nude mice ($P < 0.05$, **Tables S2**). No significant changes in other

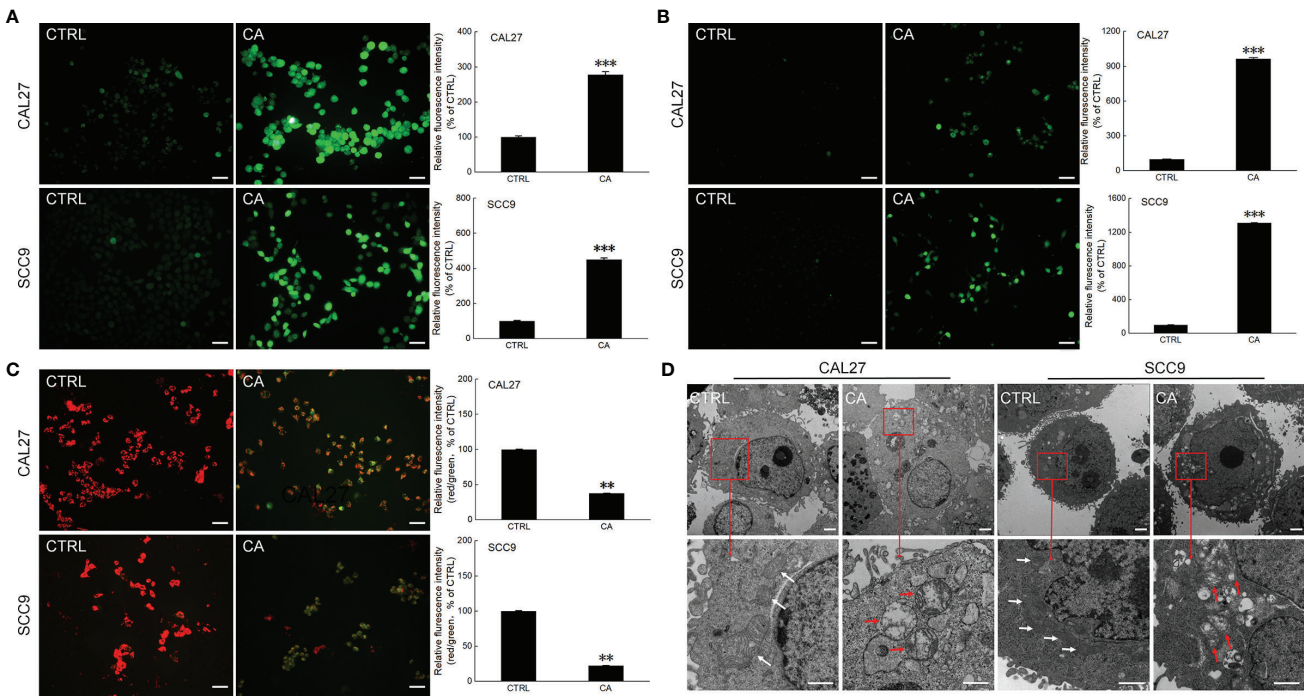

FIGURE 2 | CA treatment affected the mitochondrial function in OSCC cells. CA treatment increased the intracellular **(A)** ROS and **(B)** Ca^{2+} levels and induced the **(C)** dissipation of the MMP in CAL27 and SCC9 cells ($n = 3$, 200× magnification, scale bar: 50 μm). **(D)** CA affected the structure of the mitochondria in OSCC cells observed by transmission electron microscope (TEM) ($n = 3$, 700× magnification, scale bar: 5.0 μm; 3000× magnification, scale bar: 1.0 μm). The quantitation results are expressed as percentages relative to the levels in the corresponding control cells, and the data are expressed as mean ± SEM. $^{**}P < 0.01$ and $^{***}P < 0.001$ *versus* the control levels.

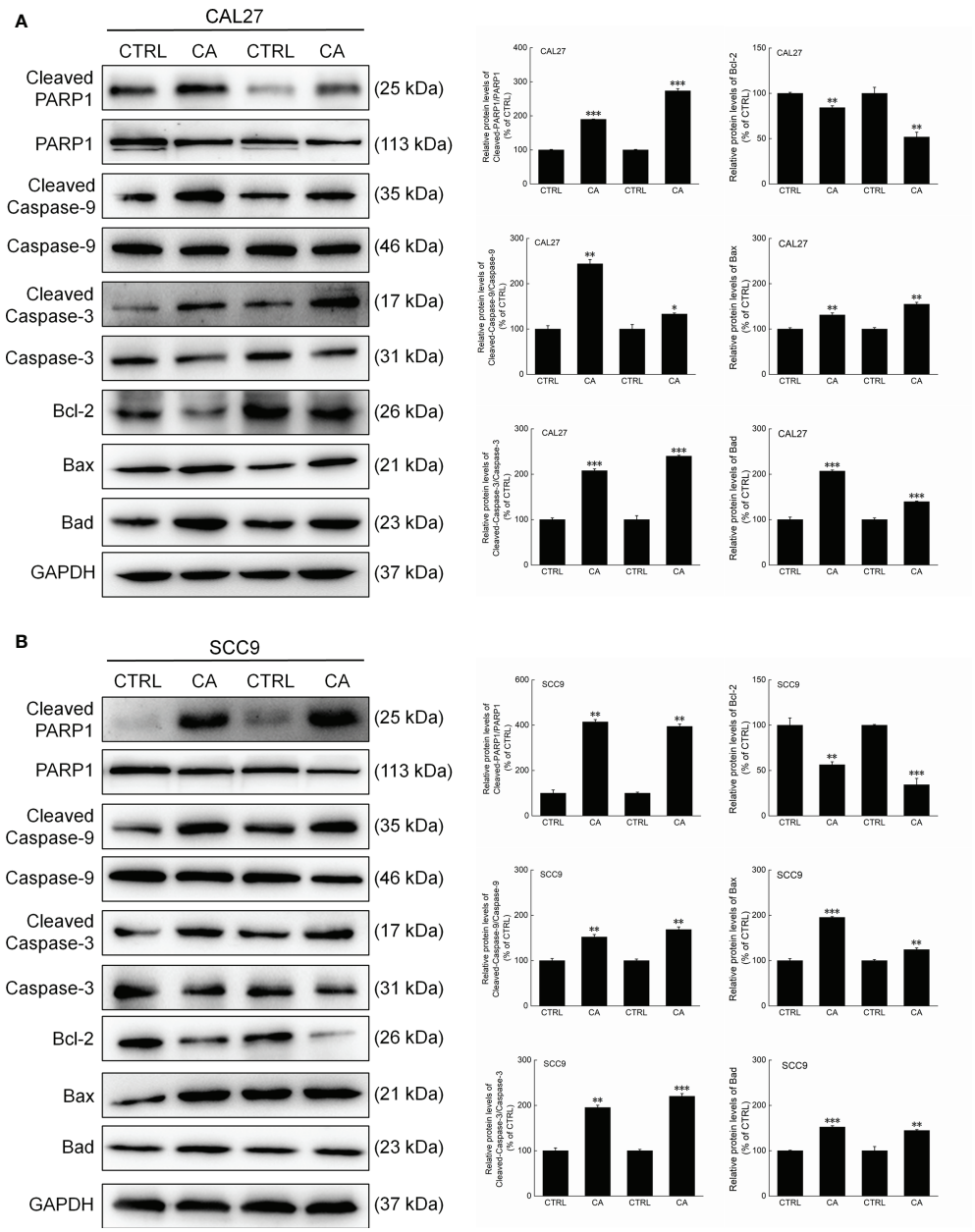

FIGURE 3 | CA treatment changed the levels of apoptosis-related proteins in OSCC cells. CA treatment significantly enhanced the ratios of Cleaved PARP1/PARP1, Cleaved Caspase-3/Caspase-3, and Cleaved Caspase-9/Caspase-9; downregulated Bcl-2 and upregulated Bax and Bad in **(A)** CAL27 and **(B)** SCC9 cells ($n = 3$). The target-protein levels were normalized using the GAPDH levels, and the data are expressed as mean ± SEM. $^{*}P < 0.05$, $^{**}P < 0.01$ and $^{***}P < 0.001$ *versus* CTRL cells.

indicators were found in the mice transplanted with the OSCC cells (**Tables S2**).

Consistent with the *in vitro* results, CA administration for 14 d increased the ratios of the levels of Cleaved PARP1, Caspase-3, and Caspase-9 to total PARP1, Caspase-3, and Caspase-9 levels in the xenografts, respectively ($P < 0.01$, **Figure 6**). Furthermore, Bax and Bad were upregulated, whereas Bcl-2 was downregulated ($P < 0.05$, **Figure 6**).

DISCUSSION

The use of natural compounds against cancer has recently attracted much attention due to their high efficacy and low toxicity (23, 34). CA is a phenolic diterpene with anti-cancer effects on hepatocellular carcinoma cells (28, 35) and gastric cancer cells (29). In this study, we showed that CA induced apoptosis in CAL27 and SCC9 cells *in vitro* as well as in the

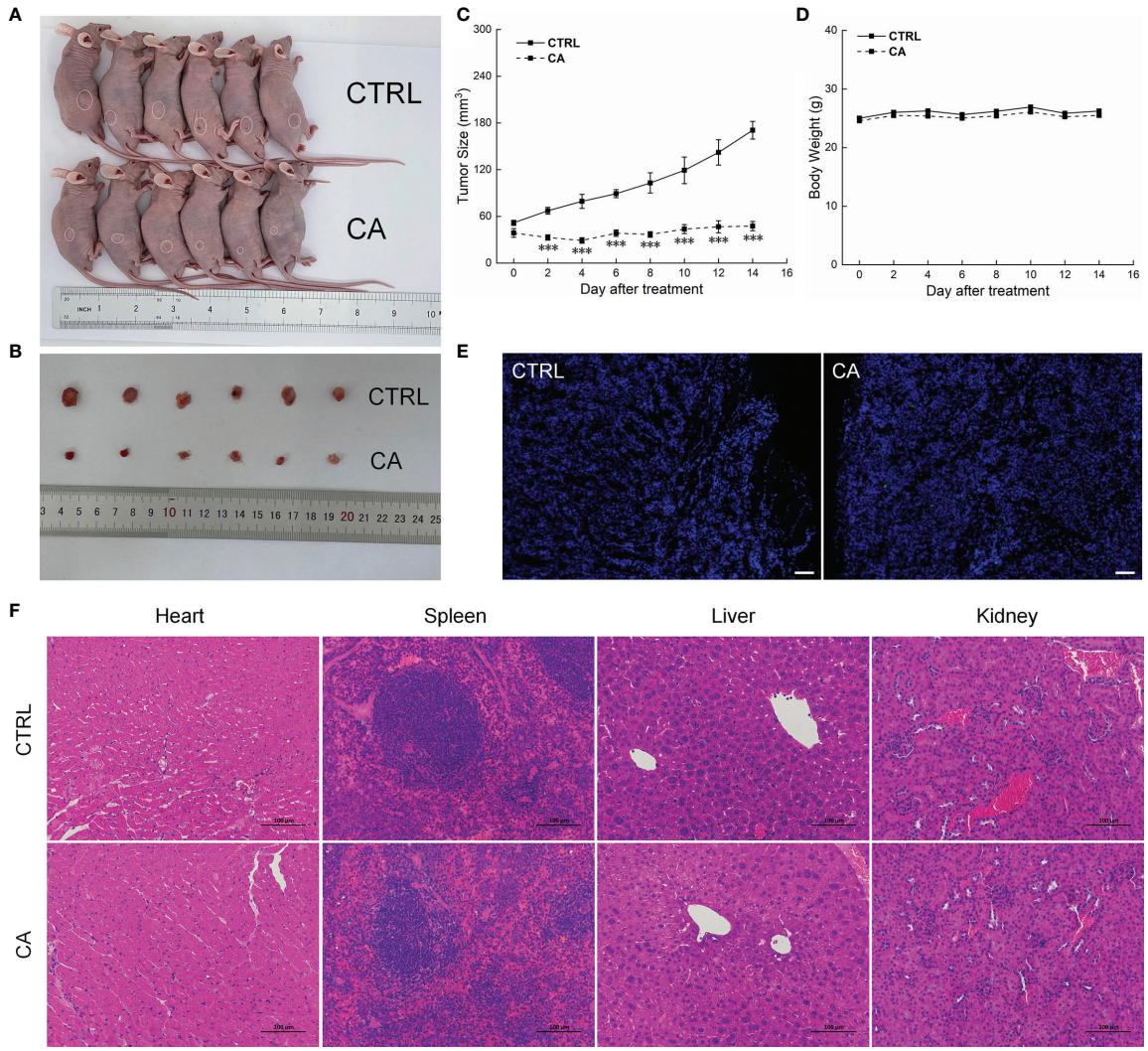

FIGURE 4 | CA treatment inhibited the tumor growth in BALB/c nude mice transplanted with CAL27 cells. CA treatment significantly reduced tumor volumes in **(A)** tumor-bearing BALB/c nude mice and **(B)** tumor tissues collected from the control (CTRL) and CA-treated groups and **(C)** decelerated the tumor growth without affecting **(D)** the body weight of the mice (n = 6). **(E)** The apoptosis of tumor tissues increased after CA treatment (n = 3) (200× magnification, scale bar: 50 μm), while **(F)** the heart, spleen, liver, and kidney showed no histological abnormality (n = 3) (200× magnification, scale bar: 100 μm). Green fluorescence locates apoptotic cells. The data are expressed as mean ± SEM. ***P < 0.001 *versus* the CTRL group.

corresponding xenotransplants in BALB/c nude mice through the mitochondrial apoptotic pathway. Moreover, the CA administration to the xenotransplanted mice did not cause any obvious adverse effect on the mice.

As an area for oxidative respiration, the morphology of mitochondria and cristae compartments are closely related to energy metabolism. The critical functions of the mitochondria include cellular energy metabolism, ROS production, mitochondrial Ca^{2+} release, and apoptosis (36). Dysregulation of these functions may lead to the occurrence and development of various diseases, including cancers (37). ROS, by-products of the oxidative metabolism (38), are mainly produced by the electron transport chain (ETC) and play vital roles in apoptosis as well as cell proliferation, differentiation, and metabolism (39). ROS are considered a double-edged sword in tumor cells. Although low levels of ROS may promote cell proliferation, high levels cause oxidative damage, resulting in cell death (37).

Ca^{2+} is a multifunctional second messenger that plays an essential role in the production of ROS (39). Ca^{2+} in the mitochondria promotes the production of ATP and ROS. After Ca^{2+} activation, ROS are directly generated from glycerol phosphate and α-KGDH. Additionally, Ca^{2+} also leads to ROS production by inhibiting complex IV (40–43). Long-term excessive accumulation of mitochondrial Ca^{2+} may trigger mPTP opening, thereby decreasing the MMP and inducing apoptosis (43, 44). Therefore, the balance between ROS and

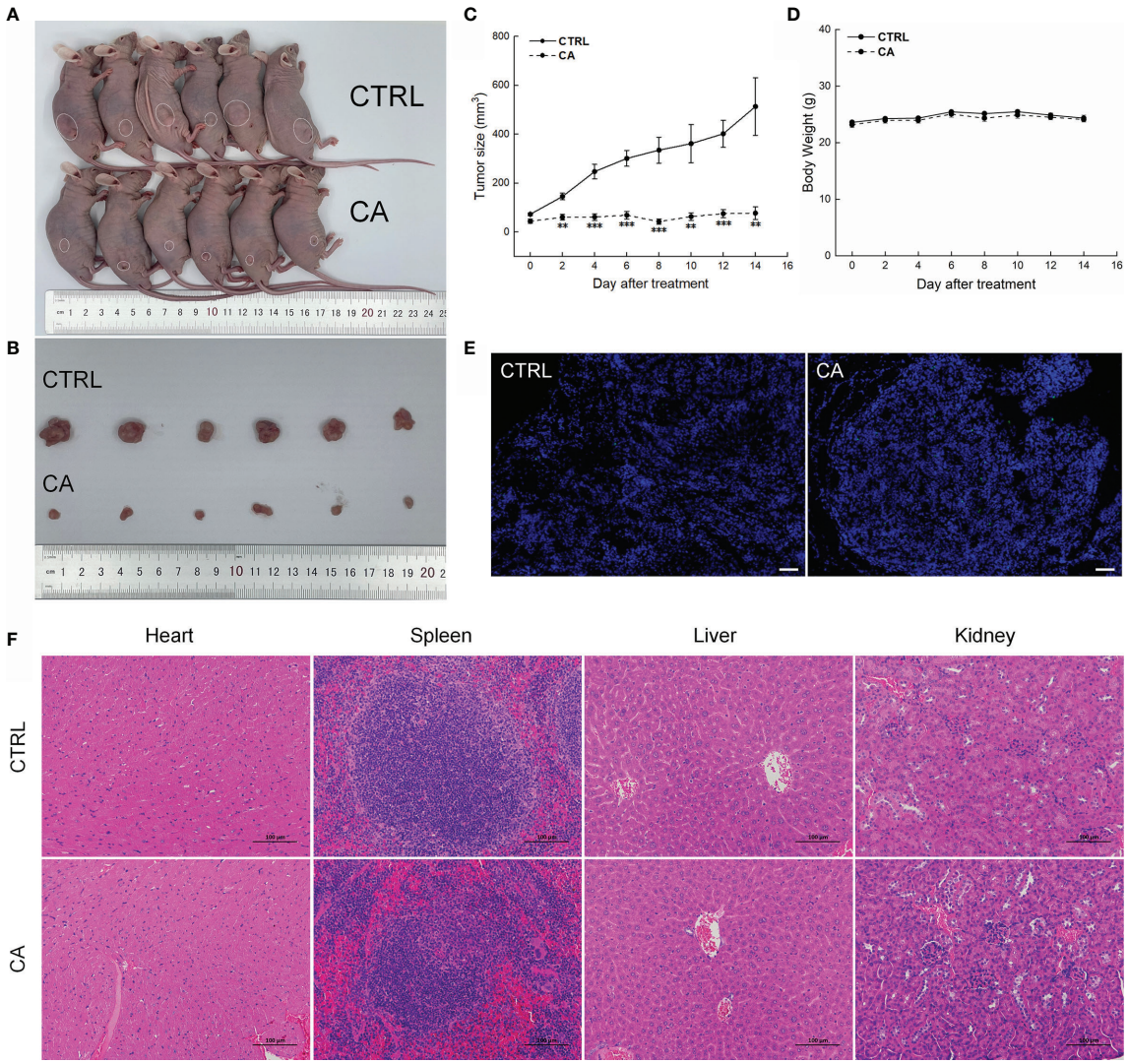

FIGURE 5 | CA treatment inhibited the tumor growth in BALB/c nude mice transplanted with SCC9 cells. CA treatment significantly reduced tumor volumes in **(A)** tumor-bearing BALB/c nude mice and **(B)** tumor tissues collected from the control (CTRL) and CA-treated groups and **(C)** decelerated the tumor growth without affecting **(D)** the body weight of the mice (n = 6). **(E)** The apoptosis of tumor tissues increased after CA treatment (n = 3) (200× magnification, scale bar: 50 μm), while **(F)** the heart, spleen, liver, and kidney showed no histological abnormality (n = 3) (200× magnification, scale bar: 100 μm). Green fluorescence locates apoptotic cells. $^{**}P < 0.01$ and $^{***}P < 0.001$ *versus* the CTRL group.

Ca^{2+} levels is essential for mitochondrial functions. CA significantly increased the levels of ROS and CA^{2+} in CAL27 and SCC9 cells, and these increases were accompanied by decreased MMP, destroyed cristae structure of mitochondria and increased apoptosis.

Apoptosis-related disorders can promote the development of cancer (45). Inducing apoptosis in cancer cells by modulating the related signal transduction cascade is one of the strategies to inhibit tumor development (46). Cell-death inducers, such as Ca^{2+} and ROS, activate the endogenous apoptosis (36, 47). In this process, the anti-apoptotic Bcl-2 family proteins are displaced, and the pro-apoptotic proteins Bax and Bad translocate to the mitochondrial outer membrane (OMM) and regulate the mitochondrial outer membrane permeability (MOMP) (48, 49). The formation of Bax and Bad oligomers in the OMM and the excessive accumulation of ROS and Ca^{2+} promote the formation of membrane voids and decrease the MMP (48, 49). Consequently, pro-apoptotic cytokines, including Cyt C, apoptosis-inducing factor (AIF), and second mitochondria-derived activator of caspases (SMAC), are released into the cytoplasm from the mitochondria (50). Cyt C binds to apoptotic protease-activating factor 1 (APAF1) to form a polymer and activates Caspase-9, thereby forming apoptotic bodies. Cleaved Caspase-9 activates Caspase-3, and activation of Caspase-3 is an essential indicator of apoptosis. Activated Caspase-3 cleaves PARP1, which then promotes apoptosis by inducing DNA double-strand breaks (51–54). Flow cytometry and TUNEL

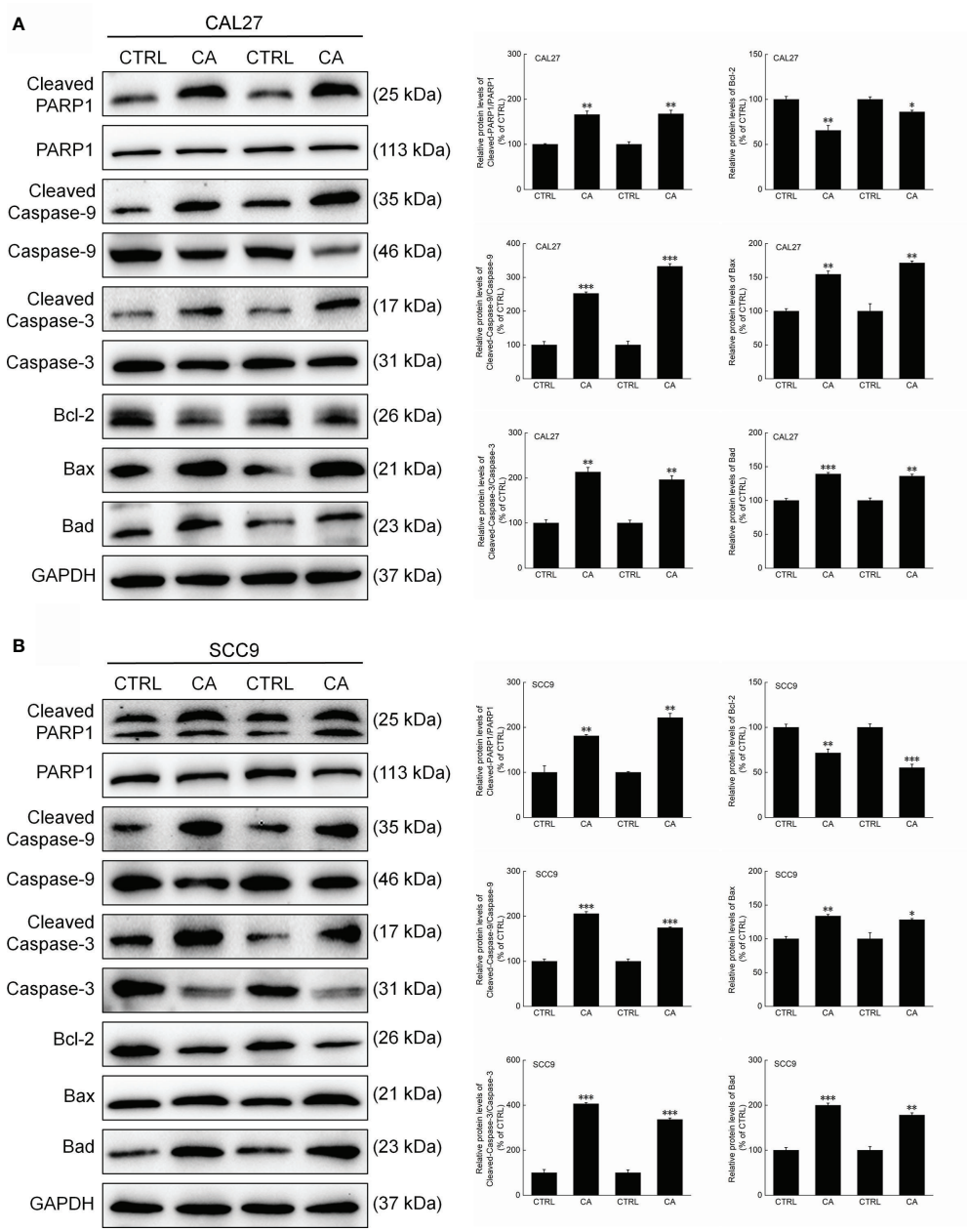

FIGURE 6 | CA treatment changed the levels of apoptosis-related proteins in the tumor tissues collected from the BALB/c nude mice transplanted with OSCC cells. CA treatment significantly enhanced the ratios of Cleaved PARP1/PARP1, Cleaved Caspase-3/Caspase-3, and Cleaved Caspase-9/Caspase-9; downregulated Bcl-2 and upregulated Bax and Bad in the **(A)** CAL27- and **(B)** SCC9-xenografts in BALB/c nude mice (n = 3). The target-protein levels were normalized using the GAPDH levels, and the data are expressed as mean ± SEM. $^{*}P < 0.05$, $^{**}P < 0.01$ and $^{***}P < 0.001$ *versus* CTRL group.

staining first proved the pro-apoptotic effect of CA, and then found that CA significantly downregulated Bcl-2 and upregulated Bax, Bad, Cleaved PARP1, and Cleaved caspase-3 and -9 in OSCC cells *in vitro* as well as in the xenotransplant models. Collectively, these results indicate that CA exerts its anti-OSCC effect through the mitochondrial apoptotic pathway.

This study has some limitations. The development of tumors is related to the proliferation of tumor cells and tumor microenvironment. This study only proved that CA induced tumor cells apoptosis, but the regulation between CA and tumor microenvironment still needs to be further explored. In the peripheral blood of the CA-treated mice transplanted with OSCC cells, an increase in the number of monocytes and a decrease in PDWCV were noted. Whether there is anemia or infection in the mice and their relationship with the tumor microenvironment require further analyses.

CONCLUSION

This study showed that CA inhibited cell proliferation and migration and induced apoptosis in CAL27 and SCC9 cells by upregulating intracellular ROS and Ca^{2+} and thereby reducing the MMP. Importantly, CA inhibited the tumor growth in BALB/c nude mice transplanted with OSCC cells. The *in vivo* and *in vitro* data presented here indicate that CA suppresses the development of OSCC through the mitochondrial apoptotic pathway. Our findings provide that CA has a valuable pharmacological effect in OSCC cells and OSCC cells-xenotransplanted BALB/c nude mice.

DATA AVAILABILITY STATEMENT

The original contributions presented in the study are included in the article/**Supplementary Material**. Further inquiries can be directed to the corresponding author.

ETHICS STATEMENT

The animal study was reviewed and approved by Animal Ethics and Welfare Committee of Jilin University.

AUTHOR CONTRIBUTIONS

FM and XL contributed equally to this work. MD, YL, and YQ assisted in the experiments. FM and XL prepared the manuscript. WL, FM, and XL revised and drafted the manuscript. WL provided the funding for the study. All authors contributed to the article and approved the submitted version.

FUNDING

This work was supported by the International Science and Technology Cooperation Project of Jilin Province Science and Technology Department, China (20200801077GH); Science and Technology Project of Jilin Provincial Department of Finance, China (JCSZ2019378-8); Natural Science Fund Project of Jilin Provincial Science and Technology Department, China (20200201416JC); Changchun Scientfic and Technological Development Program.

SUPPLEMENTARY MATERIAL

The Supplementary Material for this article can be found online at: https://www.frontiersin.org/articles/10.3389/fonc.2021.760861/full#supplementary-material

REFERENCES

1. Nguyen CTK, Sawangarun W, Mandasari M, Morita K, Harada H, Kayamori K, et al. AIRE is Induced in Oral Squamous Cell Carcinoma and Promotes Cancer Gene Expression. *PloS One* (2020) 15(2):e0222689. doi: 10.1371/journal.pone.0222689
2. Park SI, Park W, Choi S, Jang Y, Kim H, Kim S, et al. Clinical Outcome of Minor Salivary Gland Cancers in the Oral Cavity: A Comparative Analysis With Squamous Cell Carcinomas of the Oral Cavity. *Front Oncol* (2020) 10:881. doi: 10.3389/fonc.2020.00881
3. Sung H, Ferlay J, Siegel RL, Laversanne M, Soerjomataram I, Jemal A, et al. Global Cancer Statistics 2020: GLOBOCAN Estimates of Incidence and Mortality Worldwide for 36 Cancers in 185 Countries. *CA: Cancer J Clin* (2021) 71(3):209–49. doi: 10.3322/caac.21660
4. Kang Y, Zhang Y, Sun Y. MicroRNA198 Suppresses Tumour Growth and Metastasis in Oral Squamous Cell Carcinoma by Targeting CDK4. *Int J Oncol* (2021) 59(1):39. doi: 10.3892/ijo.2021.5219
5. Wan S, Wu H, Li H, Deng W, Xiao Y, Wu C, et al. Overexpression of PREX1 in Oral Squamous Cell Carcinoma Indicates Poor Prognosis. *J Mol Histol* (2020) 51(5):531–40. doi: 10.1007/s10735-020-09901-9
6. Li C, Shen Z, Bavarian R, Yang F, Bhattacharya A. Oral Cancer. *Surg Oncol Clin N Am* (2020) 29(1):127–44. doi: 10.1016/j.soc.2019.08.010
7. Jiang X, Wu J, Wang J, Huang R. Tobacco and Oral Squamous Cell Carcinoma: A Review of Carcinogenic Pathways. *Tob Induc Dis* (2019) 17:29. doi: 10.18332/tid/105844
8. Wong RSY. Apoptosis in Cancer: From Pathogenesis to Treatment. *J Exp Clin Canc Res* (2011) 30(1):87–7. doi: 10.1186/1756-9966-30-87
9. Huang Y, Zhou Z, Zhang J, Hao Z, He Y, Wu Z, et al. lncRNA MALAT1 Participates in Metformin Inhibiting the Proliferation of Breast Cancer Cell. *J Cell Mol Med* (2021) 25(15):7135–45. doi: 10.1111/jcmm.16742
10. Huang X, Ou C, Shu Y, Wang Y, Gong S, Luo R, et al. A Self-Sustained Nanoplatform Reverses TRAIL-Resistance of Pancreatic Cancer Through Coactivating of Exogenous and Endogenous Apoptotic Pathway. *Biomaterials* (2021) 272:120795. doi: 10.1016/j.biomaterials.2021.120795
11. Huang Y, Yuan K, Tang M, Yue J, Bao L, Wu S, et al. Melatonin Inhibiting the Survival of Human Gastric Cancer Cells Under ER Stress Involving Autophagy and Ras-Raf-MAPK Signalling. *J Cell Mol Med* (2021) 25(3):1480–92. doi: 10.1111/jcmm.16237
12. Moloney JN, Cotter TG. ROS Signalling in the Biology of Cancer. *Semin Cell Dev Biol* (2018) 80:50–64. doi: 10.1016/j.semcdb.2017.05.023
13. Görlach A, Bertram K, Hudecova S, Krizanova O. Calcium and ROS: A Mutual Interplay. *Redox Biol* (2015) 6:260–71. doi: 10.1016/j.redox.2015.08.010
14. Devnarain N, Tiloke C, Nagiah S, Chuturgoon AA. Fusaric Acid Induces Oxidative Stress and Apoptosis in Human Cancerous Oesophageal SNO Cells. *Toxicon* (2017) 126:4–11. doi: 10.1016/j.toxicon.2016.12.006
15. Wang H, Xu W. Mito-Methyl Coumarin, a Novel Mitochondria-Targeted Drug With Great Antitumor Potential was Synthesized. *Biochem Bioph Res Co* (2017) 489(1):1–7. doi: 10.1016/j.bbrc.2017.05.116
16. Qi H, Li X, Jin Z, Simmen T, Shuai J. The Oscillation Amplitude, Not the Frequency of Cytosolic Calcium, Regulates Apoptosis Induction. *iScience* (2020) 23(11):101671–1. doi: 10.1016/j.isci.2020.101671
17. Kulyar MF, Yao W, Ding Y, Du H, Li K, Zhang L, et al. Cluster of Differentiation 147 (CD147) Expression is Linked With Thiram Induced Chondrocyte's Apoptosis *via* Bcl-2/Bax/Caspase-3 Signalling in Tibial Growth Plate Under Chlorogenic Acid Repercussion. *Ecotox Environ Safe* (2021) 213:112059. doi: 10.1016/j.ecoenv.2021.112059
18. Fan X, Chen X, Liu Y, Zhong H, Jiang F, Liu Y. Oxidative Stress-Mediated Intrinsic Apoptosis in Human Promyelocytic Leukemia HL-60 Cells Induced by Organic Arsenicals. *Sci Rep UK* (2016) 6(1):29865. doi: 10.1038/srep29865
19. Zahedifard M, Lafta Faraj F, Paydar M, Yeng Looi C, Hajrezaei M, Hasanpourghadi M, et al. Synthesis, Characterization and Apoptotic Activity of Quinazolinone Schiff Base Derivatives Toward MCF-7 Cells *via* Intrinsic and Extrinsic Apoptosis Pathways. *Sci Rep UK* (2015) 5(1):1544. doi: 10.1038/srep11544
20. Wang H, Tang J, Wang Y, Farooqi AA, Yen C, Yuan SF, et al. Manoalide Preferentially Provides Antiproliferation of Oral Cancer Cells by Oxidative Stress-Mediated Apoptosis and DNA Damage. *Cancers* (2019) 11(9):1303. doi: 10.3390/cancers11091303

21. Tang Q, Cheng B, Xie M, Chen Y, Zhao J, Zhou X, et al. Circadian Clock GeneBmal1 Inhibits Tumorigenesis and Increases Paclitaxel Sensitivity in Tongue Squamous Cell Carcinoma. *Cancer Res* (2017) 77(2):532–44. doi: 10.1158/0008-5472.CAN-16-1322
22. Demian NM, Shum JW, Kessel IL, Eid A. Oral Surgery in Patients Undergoing Chemoradiation Therapy. *Oral Maxil Surg Clin* (2014) 26(2):193–207. doi: 10.1016/j.coms.2014.01.006
23. Majolo F, de Oliveira Becker Delwing LK, Marmitt DJ, Bustamante-Filho IC, Goettert MI. Medicinal Plants and Bioactive Natural Compounds for Cancer Treatment: Important Advances for Drug Discovery. *Phytochem Lett* (2019) 31:196–207. doi: 10.1016/j.phytol.2019.04.003
24. de Oliveira MR. The Dietary Components Carnosic Acid and Carnosol as Neuroprotective Agents: A Mechanistic View. *Mol Neurobiol* (2016) 53 (9):6155–68. doi: 10.1007/s12035-015-9519-1
25. Shin HB, Choi MS, Ryu B, Lee NR, Kim HI, Choi HE, et al. Antiviral Activity of Carnosic Acid Against Respiratory Syncytial Virus. *Virol J* (2013) 10:303. doi: 10.1186/1743-422X-10-303
26. Rajasekaran D, Manoharan S, Silvan S, Vasudevana K, Baskaran N, Palanimuthu D. Proapoptotic, Anti-Cell Proliferative, Anti-Inflammatory And Antiangiogenic Potential Of Carnosic Acid During 7,12 Dimethylbenz[A]Anthracene-Induced Hamster Buccal Pouch Carcinogenesis. *Afr J Tradit Complement Altern Medicines* (2012) 10(1):102–112. doi: 10.4314/ajtcam.v10i1.14
27. Manoharan S, VasanthaSelvan M, Silvan S, Baskaran N, Kumar Singh A, Vinoth Kumar V. Carnosic Acid: A Potent Chemopreventive Agent Against Oral Carcinogenesis. *Chem Biol Interact* (2010) 188(3):616–22. doi: 10.1016/j.cbi.2010.08.009
28. Zhang X, Chen Y, Cai G, Li X, Wang D. Carnosic Acid Induces Apoptosis of Hepatocellular Carcinoma Cells *via* ROS-Mediated Mitochondrial Pathway. *Chem Biol Interact* (2017) 277:91–100. doi: 10.1016/j.cbi.2017.09.005
29. Gao Q, Liu H, Yao Y, Geng L, Zhang X, Jiang L, et al. Carnosic Acid Induces Autophagic Cell Death Through Inhibition of the Akt/mTOR Pathway in Human Hepatoma Cells. *J Appl Toxicol* (2015) 35(5):485–92. doi: 10.1002/jat.3049
30. Kim D, Park K, Chae IG, Kundu J, Kim E, Kundu JK, et al. Carnosic Acid Inhibits STAT3 Signaling and Induces Apoptosis Through Generation of ROS in Human Colon Cancer HCT116 Cells. *Mol Carcinogen* (2016) 55(6):1096–110. doi: 10.1002/mc.22353
31. Liu W, Wu TC, Hong DM, Hu Y, Fan T, Guo WJ, et al. Carnosic Acid Enhances the Anti-Lung Cancer Effect of Cisplatin by Inhibiting Myeloid-Derived Suppressor Cells. *Chin J Nat Med* (2018) 16():907–15. doi: 10.1016/s1875-5364(18)30132-8
32. D'Alesio C, Bellese G, Gagliani MC, Aiello C, Grasselli E, Marcocci G, et al. Cooperative Antitumor Activities of Carnosic Acid and Trastuzumab in ERBB2(+) Breast Cancer Cells. *J Exp Clin Cancer Res* (2017) 36(1):154. doi: 10.1186/s13046-017-0615-0
33. Gonzalez-Vallinas M, Molina S, Vicente G, Sanchez-Martinez R, Vargas T, Garcia-Risco MR, et al. Modulation of Estrogen and Epidermal Growth Factor Receptors by Rosemary Extract in Breast Cancer Cells. *Electrophoresis* (2014) 35(11):1719–27. doi: 10.1002/elps.201400011
34. El-Huneidi W, Bajbouj K, Muhammad JS, Vinod A, Shafarin J, Khoder G, et al. Carnosic Acid Induces Apoptosis and Inhibits Akt/mTOR Signaling in Human Gastric Cancer Cell Lines. *Pharmaceuticals* (2021) 14(3):230. doi: 10.3390/ph14030230
35. Sánchez-Camargo A, García-Cañas V, Herrero M, Cifuentes A, Ibáñez E. Comparative Study of Green Sub- and Supercritical Processes to Obtain Carnosic Acid and Carnosol-Enriched Rosemary Extracts With *in Vitro* Anti-Proliferative Activity on Colon Cancer Cells. *Int J Mol Sci* (2016) 17(12):2046. doi: 10.3390/ijms17122046
36. Dong Z, Shanmughapriya S, Tomar D, Siddiqui N, Lynch S, Nemani N, et al. Mitochondrial Ca 2+ Uniporter Is a Mitochondrial Luminal Redox Sensor That Augments MCU Channel Activity. *Mol Cell* (2017) 65(6):1014–28.e7. doi: 10.1016/j.molcel.2017.01.032
37. Zaidieh T, Smith JR, Ball KE, An Q. ROS as a Novel Indicator to Predict Anticancer Drug Efficacy. *BMC Cancer* (2019) 19(1):1224. doi: 10.1186/s12885-019-6438-y
38. Wang S, Ma X, Yuan X, Yu B, Xu Y, Liu H. Discovery of New [1,2,4] Triazolo [1,5-A]Pyrimidine Derivatives That Kill Gastric Cancer Cells *via* the Mitochondria Pathway. *Eur J Med Chem* (2020) 203:112630. doi: 10.1016/j.ejmech.2020.112630
39. Sabharwal SS, Schumacker PT. Mitochondrial ROS in Cancer: Initiators, Amplifiers or an Achilles' Heel? *Nat Rev Cancer* (2014) 14(11):709–21. doi: 10.1038/nrc3803
40. Crack PJ, Taylor JM. Reactive Oxygen Species and the Modulation of Stroke☆. *Free Radical Bio Med* (2005) 38(11):1433–44. doi: 10.1016/j.freeradbiomed.2005.01.019
41. Denton RM. Regulation of Mitochondrial Dehydrogenases by Calcium Ions. *Biochim Biophys Acta (BBA) - Bioenergetics* (2009) 1787(11):1309–16. doi: 10.1016/j.bbabio.2009.01.005
42. Iosub R, Avitabile D, Grant L, Tsaneva-Atanasova K, Kennedy HJ. Calcium-Induced Calcium Release During Action Potential Firing in Developing Inner Hair Cells. *Biophys J* (2015) 108(5):1003–12. doi: 10.1016/j.bpj.2014.11.3489
43. Feno S, Butera G, Vecellio Reane D, Rizzuto R, Raffaello A. Crosstalk Between Calcium and ROS in Pathophysiological Conditions. *Oxid Med Cell Longev* (2019) 2019:1–18. doi: 10.1155/2019/9324018
44. Wang K, Chen B, Yin T, Zhan Y, Lu Y, Zhang Y, et al. N-Methylparoxetine Blocked Autophagic Flux and Induced Apoptosis by Activating ROS-MAPK Pathway in Non-Small Cell Lung Cancer Cells. *Int J Mol Sci* (2019) 20 (14):3415. doi: 10.3390/ijms20143415
45. Choo Z, Loh A, Chen ZX. Destined to Die: Apoptosis and Pediatric Cancers. *Cancers (Basel)* (2019) 11(11):1623. doi: 10.3390/cancers11111623
46. Abotaleb M, Samuel S, Varghese E, Varghese S, Kubatka P, Liskova A, et al. Flavonoids in Cancer and Apoptosis. *Cancers* (2019) 11(1):28. doi: 10.3390/cancers11010028
47. Pinton P, Ferrari D, Rapizzi E, Di Virgilio F, Pozzan T, Rizzuto R. The Ca2+ Concentration of the Endoplasmic Reticulum is a Key Determinant of Ceramide-Induced Apoptosis: Signi®Cance for the Molecular Mechanism of Bcl-2 Action. *EMBO J* (2001) 20(11):2690–701. doi: 10.1093/emboj/20.11.2690
48. Jiaxin S, Shengchen W, Yirong C, Shuting W, Shu L. Cadmium Exposure Induces Apoptosis, Inflammation and Immunosuppression Through CYPs Activation and Antioxidant Dysfunction in Common Carp Neutrophils. *Fish Shellfish Immun* (2020) 99:284–90. doi: 10.1016/j.fsi.2020.02.015
49. Tang KK, Liu XY, Wang ZY, Qu KC, Fan RF. Trehalose Alleviates Cadmium-Induced Brain Damage by Ameliorating Oxidative Stress, Autophagy Inhibition, and Apoptosis. *Metallomics* (2019) 11(12):2043–51. doi: 10.1039/c9mt00227h
50. Daugas E, Elia AJ, Joza N, Stanford WL, Kong Y, Ravagnan L, et al. Essential Role of the Mitochondrial Apoptosis-Inducing Factor in Programmed Cell Death. *Nat (London)* (2001) 410(6828):549–54. doi: 10.1038/35069004
51. Xu Y, Li Z, Zhang S, Zhang H, Teng X. miR-187-5p/Apaf-1 Axis was Involved in Oxidative Stress-Mediated Apoptosis Caused by Ammonia *via* Mitochondrial Pathway in Chicken Livers. *Toxicol Appl Pharm* (2020) 388:114869. doi: 10.1016/j.taap.2019.114869
52. Wang S, Chi Q, Hu X, Cong Y, Li S. Hydrogen Sulfide-Induced Oxidative Stress Leads to Excessive Mitochondrial Fission to Activate Apoptosis in Broiler Myocardia. *Ecotox Environ Safe* (2019) 183:109578. doi: 10.1016/j.ecoenv.2019.109578
53. Mahapatra G, Varughese A, Ji Q, Lee I, Liu J, Vaishnav A, et al. Phosphorylation of Cytochrome C Threonine 28 Regulates Electron Transport Chain Activity in Kidney. *J Biol Chem* (2017) 292(1):64–79. doi: 10.1074/jbc.M116.744664
54. Simbulan-Rosenthal CM, Rosenthal DS, Iyer S, Boulares H, Smulson ME. Involvement of PARP and Poly(ADP-Ribosyl)Ation in the Early Stages of Apoptosis and DNA Replication. *Mol Cell Biochem* (1999) 193(1):137–48. doi: 10.1023/A:1006988832729

Conflict of Interest: The authors declare that the research was conducted in the absence of any commercial or financial relationships that could be construed as a potential conflict of interest.

Publisher's Note: All claims expressed in this article are solely those of the authors and do not necessarily represent those of their affiliated organizations, or those of the publisher, the editors and the reviewers. Any product that may be evaluated in this article, or claim that may be made by its manufacturer, is not guaranteed or endorsed by the publisher.

frontiers in Oncology

ORIGINAL RESEARCH
published: 06 December 2021
doi: 10.3389/fonc.2021.759528

Overexpression of B7-H3 Is Associated With Poor Prognosis in Laryngeal Cancer

Yixuan Li[1†], *Qian Cai*[1†], *Ximing Shen*[2], *Xiaoting Chen*[1] *and Zhong Guan*[1*]

[1] Department of Otolaryngology, Sun Yat-sen Memorial Hospital, Sun Yat-sen University, Guangzhou, China, [2] Department of Pathology, Sun Yat-sen Memorial Hospital, Sun Yat-sen University, Guangzhou, China

The immune checkpoint molecule, B7-H3, which belongs to the B7 family, has been shown to be overexpressed in various cancers. Its role in tumors is not well defined, and many studies suggest that it is associated with poor clinical outcomes. The effect of B7-H3 on laryngeal cancer has not been reported. This study investigated the expression of B7-H3 in laryngeal squamous cell carcinoma (LSCC), and its relationship with clinicopathological factors and prognosis of LSCC patients. The gene expression quantification data and clinical data of LSCC retrieved from The Cancer Genome Atlas (TCGA) and Gene Expression Omnibus (GEO) database were analyzed to determine the diagnostic and prognostic roles of B7-H3. Quantitative real-time polymerase chain reaction (qRT-PCR) was then performed to determine the gene expression level of B7-H3 between LSCC tissues and paired normal adjacent tissues. In addition, TCGA RNA-seq data was analyzed to evaluate the expression level of B7 family genes. Next, the protein expression of B7-H3 and CD8 in LSCC was determined using immunohistochemistry and immunofluorescence. qRT-PCR results showed that the expression level of B7-H3 mRNA was significantly higher in LSCC tissues than in adjacent normal tissues. Similar results were obtained from the TCGA analysis. The expression of B7-H3 was significantly associated with T stage, lymph node metastasis, and pathological tumor node metastasis (TNM) stage, and it was also an independent factor influencing the overall survival time (OS) of patients with LSCC. In addition, B7-H3 was negatively correlated with $CD8^+$T cells. These results show that B7-H3 is upregulated in LSCC. Therefore, B7-H3 may serve as a biomarker of poor prognosis and a promising therapeutic target in LSCC.

Keywords: B7-H3, biomarker, LSCC - laryngeal squamous cell carcinoma, diagnosis, prognosis

OPEN ACCESS

Edited by:
Pablo Parente-Arias, A Coruña University Hospital Complex (CHUAC), Spain

Reviewed by:
Christos K. Kontos, National and Kapodistrian University of Athens, Greece
Chongchang Zhou, Ningbo Medical Centre Li Huili Hospital, China

***Correspondence:**
Zhong Guan
gzhong@mail.sysu.edu.cn

[†]These authors have contributed equally to this work

Specialty section:
This article was submitted to Head and Neck Cancer, a section of the journal Frontiers in Oncology

Received: *16 August 2021*
Accepted: *12 October 2021*
Published: *06 December 2021*

Citation:
Li Y, Cai Q, Shen X, Chen X and Guan Z (2021) Overexpression of B7-H3 Is Associated With Poor Prognosis in Laryngeal Cancer. Front. Oncol. 11:759528. doi: 10.3389/fonc.2021.759528

INTRODUCTION

Laryngeal cancer is ranked as the second most prevalent head and neck tumor after lip and oral cavity cancers worldwide (1). A previous study reported that the incidence and number of deaths due to laryngeal cancer increased steadily from 1997 to 2017 worldwide (2). The main causes of deaths due to this cancer are tumor recurrence and distant metastasis. To date, there is no effective

treatment method for advanced laryngeal cancer. This calls for in-depth research to identify new diagnostic biomarkers and therapeutic targets in laryngeal cancer.

As a member of the newly discovered immunomodulatory protein B7 family, B7-H3 has been found to play an important role in a variety of tumors and immune diseases. One study reported that B7-H3 can regulate activation of T cells and promote secretion of inflammatory factors (3). Recent studies have also confirmed that B7-H3 has an immunosuppressive function in several cancers (4, 5), including non-small cell lung cancer (6), breast cancer (7), and other tumors. In these cancers, it affects the prognosis of patients. Moreover, evidence suggests that overexpression of B7-H3 is closely associated with tumor cell apoptosis, cell metabolism, tumor angiogenesis, tumor drug resistance, and other aspects (8–11). However, the role of B7-H3 in laryngeal cancer has not been elucidated.

Therefore, this study investigated the expression level of B7-H3 in laryngeal squamous cell carcinoma (LSCC) tissues, and explored its association with clinicopathological features, cancer prognosis, and tumor-infiltrating $CD8^+$ T cells. In addition, clinical results were combined with data retrieved from The Cancer Genome Atlas (TCGA) to determine the functions of B7-H3 on LSCC. To the best of our knowledge, this is the first study that has elaborated the role of B7-H3 in laryngeal cancer.

MATERIALS AND METHODS

Data Retrieval and Determination of Differential Expression of B7 Family mRNAs

Clinical characteristics and gene expression data of LSCC patients of the HTSeq-FPKM type were acquired from *TCGA* (http://tcga-data.nci.nih.gov/tcga/) and *GEO* (https://www.ncbi.nlm.nih.gov/geo/) on 4th May 2021. The mRNA expression data of LSCC patients was also downloaded from the TCGA database and used to determine differentially expressed genes (DEGs) of B7 family in LSCC tissues. All samples were analyzed using the bioconductor package of edgeR. Results were visualized using gplots packages in R software (version 3.0.1.2). The DEGs were identified using |log2-fold change| ≥ 1.0 as the cut-off. Next, the survival R package was used to generate Kaplan-Meier survival curves of the DEGs, with $P< 0.05$ being the cut-off for statistical significance.

Patients and Clinical Samples

A total of 122 laryngeal cancer patients who underwent surgery between December 2012 and November 2015 were included in this study. The included patients met the following inclusion criteria: underwent surgery as the first treatment, preoperative pathological diagnosis was laryngeal squamous cell carcinoma, and did not receive preoperative radiotherapy, chemotherapy or other treatments. Exclusion criteria were: patients with other tumors or recurrent tumors and patients with other severe diseases or autoimmune disease. All patients were followed up for at least five years. During surgery, paired fresh laryngeal cancer specimens and normal adjacent tissues were collected from 12 patients. Patient clinicopathological variables were collected by reviewing medical records. Data extracted included: age, sex, primary tumor site, tumor differentiation, TNM stage, smoking index, and alcohol consumption. The TNM stage was defined according to the American Joint Committee on Cancer (*AJCC*). Overall survival (OS) was defined as the period from the date of surgery to the time of death or last follow-up, which was 1st November 2020. This study was approved by the institutional ethical review board of Sun Yat-Sen Memorial Hospital and signed informed consent form was obtained from all patients before the study.

RNA Extraction and Real-Time Quantitative PCR

Total RNA was extracted from homogenized frozen tissues using TRIzol reagent (Guangzhou IGE Bio.) and reverse transcribed to cDNA using a RevertAid First Strand cDNA Synthesis Kit (Guangzhou IGE Bio.) according to the manufacturer's instructions. Next, quantitative real-time polymerase chain reaction (qRT-PCR) was performed on a Roche LightCycler 480 Real-Time PCR system using a SYBR Premix Ex Taq (Takara) according to the manufacturer's instructions. The reaction protocol was as follows:1 min at 95°C, 40 cycles of 10 seconds at 95°C and 12 min at 60°C, and finally a 65°C to 95°C ramp up to determine the melting curve. Relative mRNA level of B7-H3 was normalized to that of GAPDH mRNA. The relative mRNA expression was calculated using the comparative $2^{-\triangle\triangle Ct}$ method.

Immunohistochemistry

A total of 152 wax samples, including 122 LSCC samples and 30 adjacent normal tissues, were obtained from the pathology department of Sun Yat-sen Memorial Hospital. All samples were deparaffinized and rehydrated through a series of alcohol baths: 100% xylene (2×20 min), 100% ethanol (2×5 min), 95% ethanol, 80% ethanol, 75% ethanol and H_2O (1×2 min each). Next, the samples were incubated in 10 mM sodium citrate buffer (pH 6.0) for antigen retrieval, followed by incubation with goat anti-human B7-H3 antibody (Cell Signaling Technology, 1:50) overnight at 4°C. Finally, 24 samples were further incubated with CD8 antibody (Cell Signaling Technology, 1:100) overnight at 4°C.

Evaluation of Immunohistological Staining

The staining intensity of B7-H3 was evaluated by two experienced pathologists using an independent double-blind method. Ten high-power fields (magnification×200) were selected to examine the positively stained area. The intensity of stained area was scored as follows: negative (0), weak (1), moderate (2), and strong (3). In addition, the percentage of positively stained cells was scored as: 0% to 5% (0), 6% to 25% (1), 26% to 50% (2), and >50% (3). To calculate the weighted scores for each section, the percentage of stained cells was multiplied with the staining intensity scores. Subsequently, a score of 4 was used as the cut-off to distinguish low B7-H3 expression low (<4) from high expression (≥4). The number of

$CD8^+$ T-cells in LSCC tissues was counted in three randomly selected tumor areas at a magnification of ×200. The average count was finally.

Double Immunofluorescence Staining

Paraffin-embedded (FFPE) slides of LSCC tissues were dewaxed, rehydrated, and incubated in the retrieval buffer solution for antigen retrieval as described above. Next, the samples were incubated with a mixture of two primary antibodies [B7-H3 (goat antibody) and CD8 (rabbit antibody)] overnight at 4°C, followed by a mixture of FITC- and Cy3-conjugated secondary antibodies. The cell nuclei were counterstained blue with a DAPI solution. Images were acquired from at least three randomly high-power fields using the Olympus BX51 microscope at the appropriate excitation wavelength for the fluorophore.

Statistical Analysis

All statistical analyses were performed using SPSS version 25.0 (IBM, Armonk New York). Data are presented as the mean ± S.E.M. Wilcoxon rank sum test was used to compare mRNA expression level between LSCC and noncancerous tissues. Categorical variables were analyzed using Fisher's exact or Pearson's chi-squared test. Moreover, the overall survival (OS) curve of patients was estimated using the Kaplan-Meier method. Univariate and multivariate analysis for hazard estimation was done using Cox regression. A $P < 0.05$ was considered statistically significant, and GraphPad Prism software version 8.0 was used to generate the figures.

RESULTS

Identification of Differentially Expressed Genes of B7 Family in LSCC Tissues

To identify the association of B7 family genes with prognosis of LSCC, the RNA-Seq data of 32 LSCC samples and 7 normal tissues were obtained from the TCGA database. The mRNA expression profiles of seven B7 family genes were also extracted from the database and are shown in **Figure 1A**. Among them, *B7-1*, *B7-DC*, and *B7-H3* were up-regulated in LSCC tissues (absolute logFC≥2.0, adjusted p<0.05). To validate results from TCGA, we used the GEO data for LSCC patients. The results also indicated significant upregulation of *B7-1*, *B7-DC*, and *B7-H3 in LSCC* samples compared to normal levels (**Figure 1B**). Kaplan-Meier analysis showed that none of them was significantly correlated with OS (P>0.05, **Figure 1C**). However, patients with high B7-H3 expression had shorter OS time than patients with low B7-H3 expression.

B7-H3 Is Overexpressed in LSCC Tissues

Next, the mRNA expression level of B7-H3 in LSCC and adjacent normal tissues (n=12) was determined. Results showed that expression of B7-H3 mRNA was significantly higher in LSCC tissues than in adjacent normal tissues (P< 0.01, **Figure 2**).

In addition, IHC was performed on 122 wax LSCC samples and 30 wax adjacent normal tissues to further evaluate the role of B7-H3. B7-H3 positive staining was mainly found in membranes of cancer cells and partially in the cytoplasm. However, central keratinized area of cancer nests was negatively stained. The positive expression of B7-H3 was also found in tumor-infiltrating immune cells. Results indicated that the expression of B7-H3 was significantly higher in LSCC tissues than in the adjacent normal tissues (**Figure 3**), suggesting that B7-H3 is overexpressed in LSCC.

Correlation of B7-H3 Expression With Clinicopathological Features of LSCC Patients

Among the 122 LSCC cases, 75 (61.5%) stained strongly positive for B7-H3. **Table 1**, shows that the expression of B7-H3 in LSCC correlated with T stage, lymph node metastasis, and TNM stage (P<0.05), but not with age, sex, tumor location, pathological differentiation, alcohol consumption, smoking, or cancer recurrence.

Overexpression of B7-H3 Confers Poor Prognosis to LSCC Patients

The median follow-up was 75.0 months in the total cohort. A Kaplan–Meier curve showed that overexpression of B7-H3 was significantly associated with poor prognosis at 60 months (P = 0.003, **Figure 4**). Next, univariate and multivariate Cox regression analyses were performed to determine whether B7-H3 is an independent prognostic factor for OS. Univariate analyses showed that T stage (P=0.039), lymph node metastasis (P=0.002), alcohol consumption (P=0.023), cancer recurrence (P=0.021), and B7-H3 expression (P=0.045) had a significant association with OS. On the other hand, multivariate analysis indicated that lymph node metastasis, alcohol consumption, cancer recurrence, and B7-H3 expression (P=0.038) were independent factors influencing the OS (**Table 2**). Collectively, these results suggest that overexpression of B7-H3 is significantly associated with poor prognosis.

Relationship Between B7-H3 Expression and Infiltration of $CD8^+$ T Cells

Furthermore, we analyzed a TCGA cohort with head and neck squamous cell carcinoma (HNSCC) individuals using six different algorithms and found that the expression of B7-H3 was inversely correlated with the infiltration level of $CD8^+$ T cells (**Figure 5**). To determine the potential relationship between B7-H3 expression and tumor infiltrating $CD8^+$ T cells in LSCC, immunohistochemical staining was performed in 24 cases for CD8. Results showed that the number of $CD8^+$ T cells per 3HPF of high B7-H*3* expression cases ranged from 50 to 238 (mean ± SD: 130 ± 58.2), and the number of low B7-H3 expression cases ranged from 111 to 381 (mean ± SD: 239 ± 87.0), indicating significant differences (**Figure 6**). Given that previous IHC results showed a positive expression of B7-H3 in tumor-infiltrating immune cells, immunofluorescence was further performed to examine B7-H3 expression in $CD8^+$ T cells. The results revealed a trend toward higher stroma $CD8^+$ T-cell infiltration in the tumors relative to lower B7-H3 expression (**Figure 7**). However, B7-H3 was not detected in $CD8^+$ T cells.

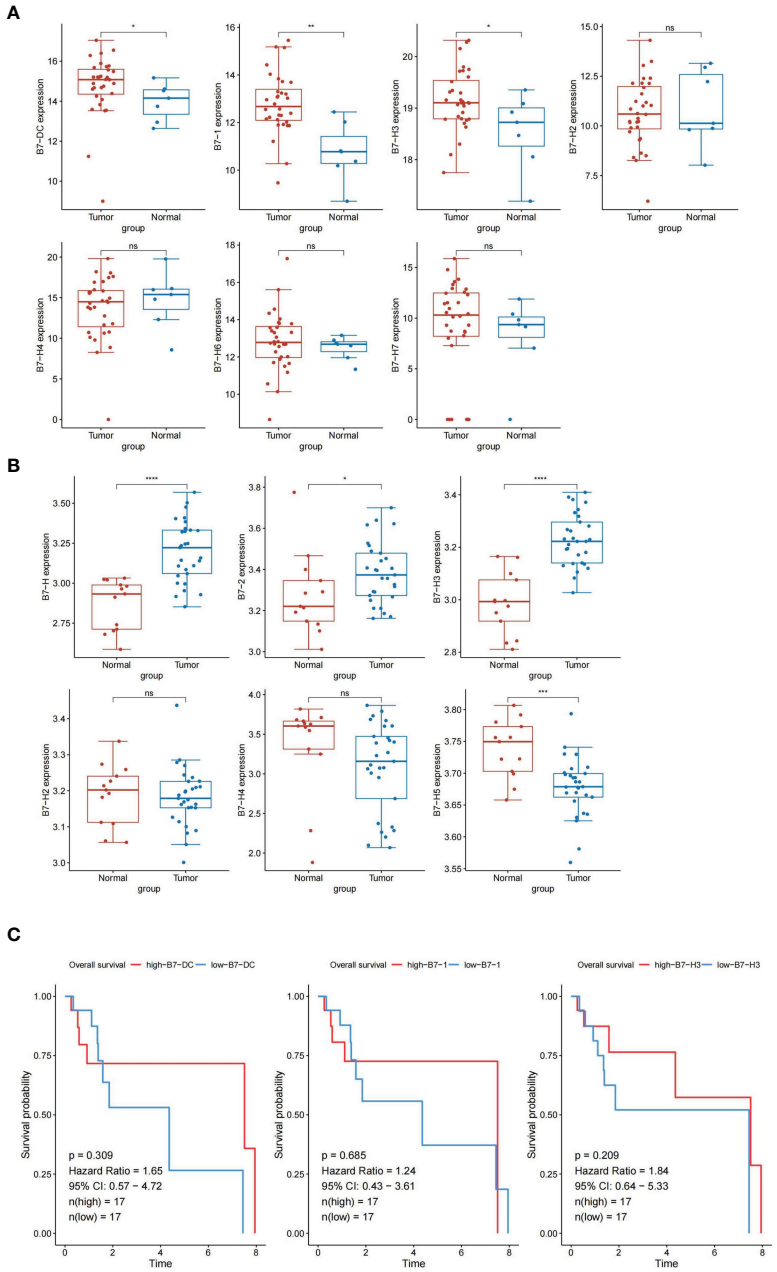

FIGURE 1 | The expression levels of B7 family members in LSCC samples and normal tissues. The data was obtained from TCGA database **(A)** and GEO database **(B)**. ns, not significant, *$p < 0.05$, **$p < 0.01$, ***$p < 0.001$,****$p < 0.0001$. Overall survival of LSCC patients grouped based on *B7-1*, *B7-DC*, and *B7-H3* expression level by Kaplan-Meier analysis **(C)**. $p < 0.05$ considered as significant.

Collectively, these results suggest that B7-H3 is negatively correlated with $CD8^+$ T-cell infiltrate density.

DISCUSSION

Previous studies have reported that B7 family ligands are overexpressed in many types of malignancies and B7-H3 is highly expressed in HNSCC (12–14). This study examined the expression of a set of B7 family genes in LSCC tissues using TCGA and GEO cohorts. It was found that three DEGs including B7-H3 were upregulated in LSCC tissues. According to our PCR analysis, B7-H3 mRNA was also overexpressed in LSCC tissues. Furthermore, results of IHC test revealed that high B7-H3 expression level was associated with advanced T stage, lymph node metastasis, and advanced TNM stage. Moreover, high B7-H3 expression level was correlated with poor prognosis of LSCC. To the best of our knowledge, this study provides the first

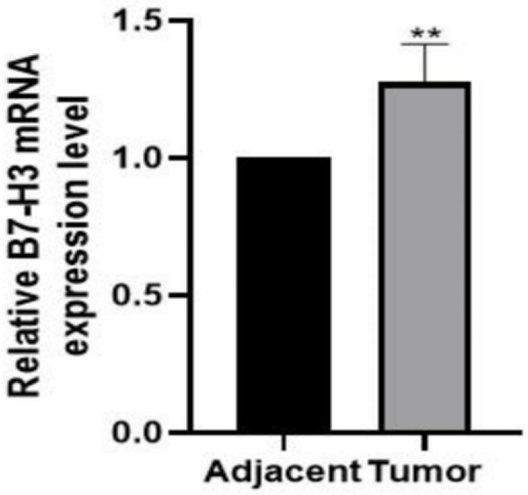

FIGURE 2 | Overexpression of B7-H3 in LSCC tissues compared with noncancerous tissues. B7-H3 mRNA was tested by qRT-PCR, relative to the internal endogenous control GAPDH. B7-H3 show significant increase in expression in LSCC compared to noncancerous tissues. $^{**}p < 0.01$ (n = 12).

evidence that overexpression of B7-H3 can be used to predict the prognosis of patients with LSCC.

As a novel member of B7 family ligands, B7-H3 has been identified as an immune checkpoint in many types of cancers. It has been detected in several cancers, including melanoma, oral squamous carcinoma, colorectal cancer, and numerous cancers (10, 15–22). Overexpression of B7-H3 is associated with poor prognosis in most cancers. Previous studies demonstrated that B7-H3 was highly expressed in HNSCC tissues and thus it may be a prognostic marker (5, 14, 16). However, the role of B7-H3 in LSCC has not been elucidated. In this study, we investigated the expression of B7-H3 in LSCC tissues, and found that B7-H3 was extensively expressed on membranes of cancer cells and slightly expressed in the cytoplasm. In addition, B7-H3 was highly expressed at the invasive front of tumor. Recent studies have reported that high expression of B7-H3 is associated with adverse clinicopathologic features and poor survival. In the present study, B7-H3 was found to be associated with advanced T stage, lymph node metastasis, and advanced TNM stage (III-IV), indicating that B7-H3 may regulate LSCC progression. However, B7-H3 was not correlated with recurrence in LSCC, unlike the results obtained for glioblastoma (23) and some other cancers (24, 25). Therefore,

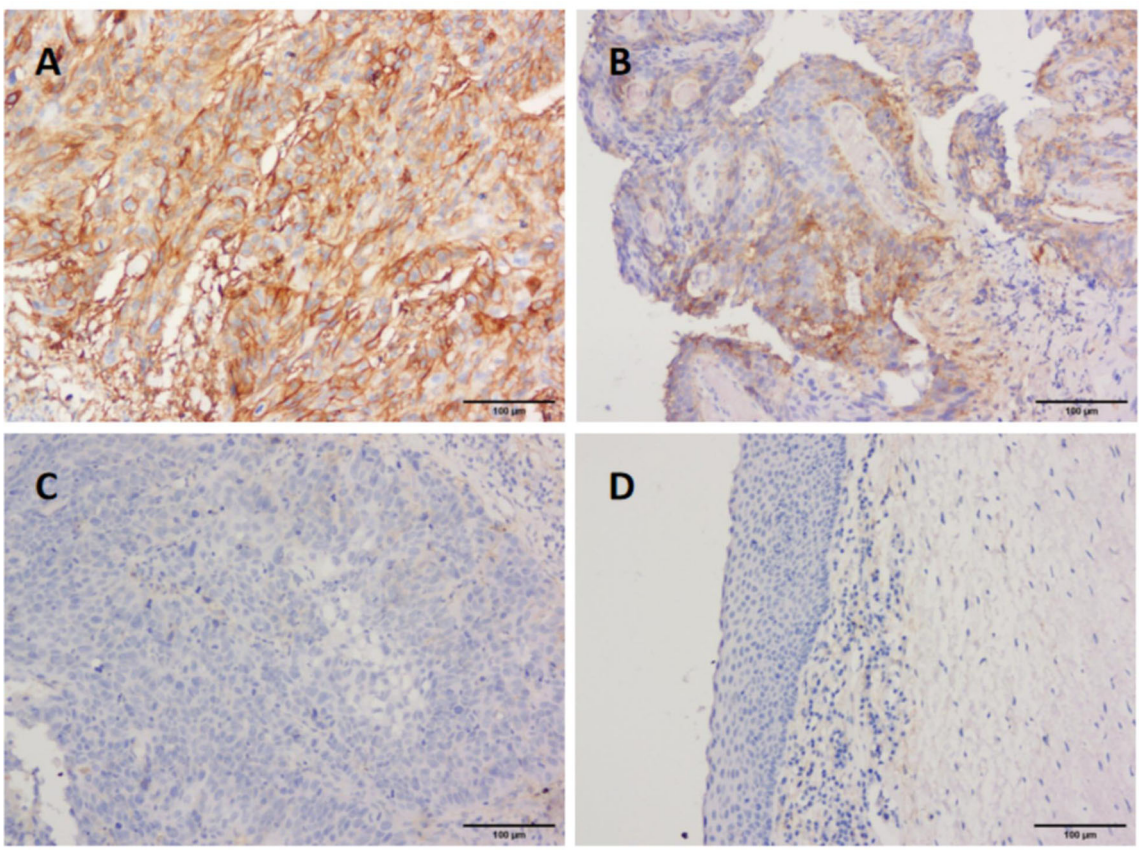

FIGURE 3 | Immunohistological staining of LSCC tissues for B7-H3 expression. Representative tissues of, strong staining **(A)**, moderate **(B)**, weak **(C)**, and adjacent normal tissues **(D)** for B7-H3 expression in LSCC samples. (magnification ×200).

TABLE 1 | Clinicopathological factors associated with B7-H3 expression levels.

Clinicopathological Features	n	B7-H3 expression		P
		low (≤3)	high (>3)	
gender				
male	118	45	73	0.632
female	4	2	2	
age				
<60	54	22	32	0.654
≥60	68	25	43	
T stage				
T1+T2	86	38	48	0.047
T3+T4	36	9	27	
lymph node metastasis				
N0	105	45	60	0.015
N+	17	2	15	
TNM stage				
I+II	81	39	42	0.002
III+IV	41	8	33	
pathological differentiation				
high	57	25	32	0.257
moderate,low	65	22	43	
alcohol consumption				
positive	33	14	19	0.59
negative	89	33	56	
smoking index				
<400	38	15	23	0.885
≥400	84	32	52	
recurrence				
positive	17	6	11	0.768
negative	105	41	64	

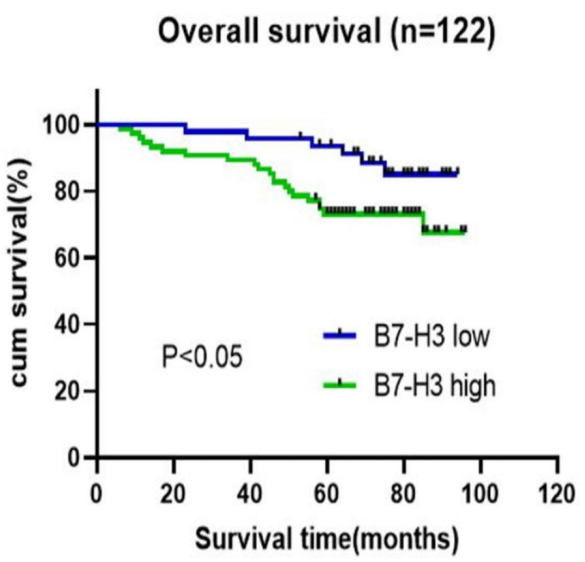

FIGURE 4 | Survival analysis of correlation of overexpression of B7-H3 and overall survival in LSCC patients. The overall survival rate was calculated with Kaplan-Meier method and compared with log-rank test (n=122).

we will continue to follow up these patients to observe the possibility of recurrence. Next, the ability of B7-H3 to predict the prognosis of patients was tested. Results showed that B7-H3 was significantly associated with poor prognosis, suggesting that it might be an independent predictor of OS. Overall, this study reveals that B7-H3 may be used as a marker for predicting the prognosis of LSCC. While, as the adjacent tumor sample cohort size was limited, larger cohorts are required to validate these observations in the future.

As an immune checkpoint, B7-H3 acts as a costimulatory and coinhibitory molecule that influence T cell proliferation (26). Chapoval et al. (3) reported that B7-H3 promoted proliferation of both $CD4^+$ and $CD8^+$ T-cells, and enhanced function of the cytotoxic T-cell (CTL). However, some studies have shown that B7-H3 has a negative effect on proliferation of T-cells (27, 28). Similarly, B7-H3 was inversely associated with the infiltration of $CD8^+$ T cells, and B7-H3 blockade decreased the number of cancer stem cells in HNSCC (29). In this study, IHC staining results revealed that immune cells in the stromal tissue stained positive for B7-H3. To further determine the relationship between B7-H3 and $CD8^+$ T cell infiltration, immunofluorescence staining experiment was done and tissues were examined under a confocal microscope. It was found that $CD8^+$ infiltration was mainly occurred in stromal areas and

TABLE 2 | Univariate and Multivariate Cox proportional hazards analysis for overall survival in 122 LSCC patients.

Variable	Group	Univariate Cox regression		Multivariate Cox regression	
		HR (95%CI)	*P* value	HR (95%CI)	*P* value
age	>60 (*vs.*≤60)	0.789 (0.348-1.789)	0.259		
gender	Male (*vs.* female)	0.696 (0.094-5.172)	0.776		
smoking index	≥400 (*vs.*<400)	1.346 (0.53-3.413)	0.556		
pathological differentiation	well (*vs.*moderate,low)	1.735 (0.735-4.094)	0.303		
T stage	T3+T4 (*vs.* T1+T2)	2.182 (0.956-4.978)	0.039	1.774 (0.696-4.521)	0.23
lymph node metastasis	N+ (*vs.* N0)	3.809 (1.564-9.277)	0.002	5.708 (1.974-16.506)	0.001
alcohol consumption	Positive (*vs.* negative)	2.747 (1.204-6.267)	0.023	4.571 (1.829-11.425)	0.001
recurrence	Positive (*vs.* negative)	2.758 (1.134-6.71)	0.021	5.54 (2.036-15.079)	0.001
B7-H3	low (*vs.* strong)	3.423 (1.164-10.067)	0.045	3.08 (1.066-8.899)	0.038

HR, hazard ratio; CI, confidence interval.

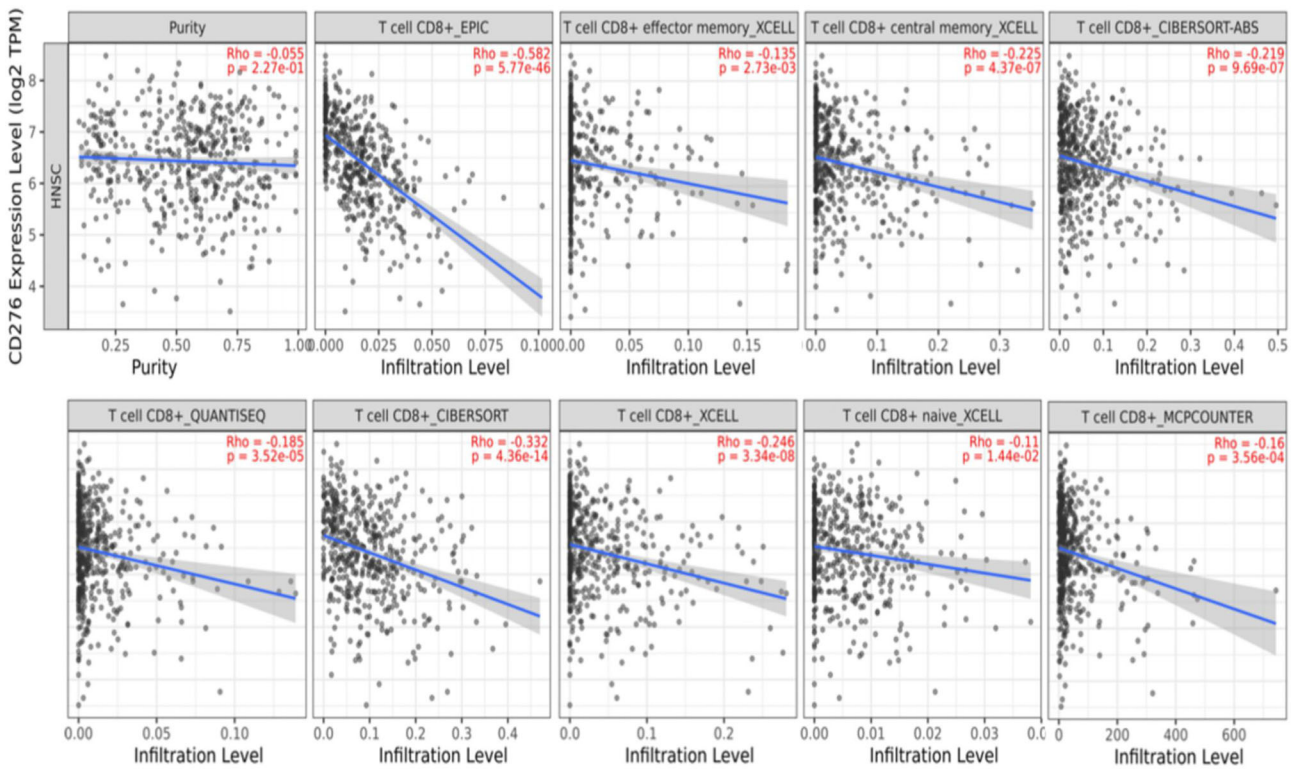

FIGURE 5 | Correlation of B7-H3 expression with infiltration of $CD8^+$ T cells. The data was obtained from TCGA HNSCC datasets and analyzed by 6 different algorithms from TIMER 2.0.

positive staining for B7-H3 was mostly seen in tumor tissues. In addition, low B7-H3 expression was associated with high $CD8^+$ infiltration. However, B7-H3 was not expressed on $CD8^+$ T cells. Similar results were obtained from IHC staining tests. $CD8^+$ T lymphocytes have been shown to be correlated with good prognosis in many cancer types and may be an independent favorable prognostic factor in HNSCC (30). Based on results of this study and previous studies (4, 19, 25), we infer that B7-H3 might inhibit proliferation of $CD8^+$ T cells and impair antitumor immunity in LSCC. However, the specific mechanism of B7-H3 regulating $CD8^+$ T cells infiltration needs further study.

In this study, although B7-H3 was found to be highly expressed in LSCC and associated with poor prognosis, the underlying molecular mechanism was not elucidated. However, we hypothesized that B7-H3 may inhibit $CD8^+$T cells infiltration, hereby promote tumor immune escape. Similarly, a recent study reported that inhibition of B7-H3×m4-1BB suppressed tumor growth and increased the number of terminally differentiated

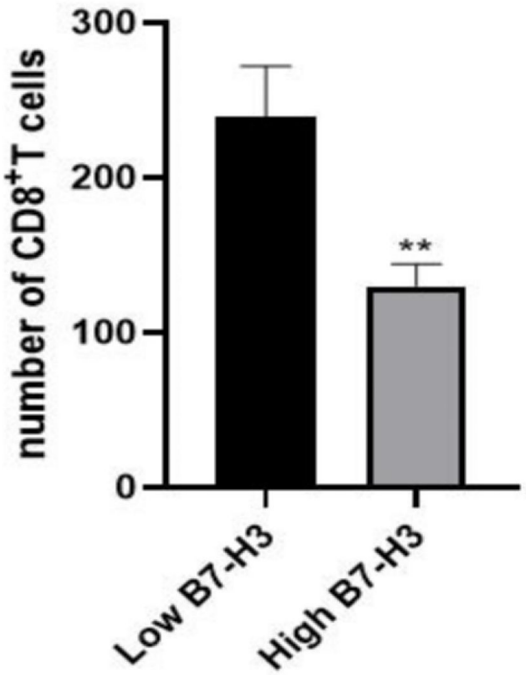

FIGURE 6 | The number of tumor-infiltrating $CD8^+$ T-cell was inversely correlated with B7-H3 expression in 24 patients with LSCC (**$p < 0.01$). This correlation was tested by Wilcoxon rank sum test.

$CD8^+$ T cells in tumor models (31). B7-H3 was also found to be an inhibitor of $CD4^+$T-cells, Th cells, Treg cells, and NK cells (32, 33). However, the receptor of B7-H3 is currently unknown. Some researchers have proposed that the triggering receptor expressed on myeloid cell (TREM)-like transcript 2 (TLT-2) may be a putative counter receptor for B7-H3 (34, 35). Therefore, further studies are advocated to identify the receptor of B7-H3, and elucidate the signaling mechanism of B7-H3. Immunotherapy has emerged as a promising treatment for malignancies. PD-L1/PD-1 blockade therapy has been approved for advanced head and neck cancer treatment, but a large fraction of patients do not respond to this therapy. Other studies have investigated the use of B7-H3 as an inhibitor of antibodies. For instance, 8H9, ^{131}I-monoclonal antibodies targeting B7-H3, was found to be an immunotherapeutic agent in neuroectodermal tumors, and has been tested in a phase I trial to treat patients with diffuse intrinsic pontine glioma (36, 37). Therefore, this study suggests that B7-H3 may be a promising target for LSCC immunotherapy.

CONCLUSIONS

Overall, this study demonstrates that B7-H3 is upregulated in LSCC, and the high expression level of B7-H3 was closely associated with clinicopathological features and poor prognosis of LSCC patients. Moreover, B7-H3 may inhibit $CD8^+$T-cell infiltration. These results suggest that B7-H3 may be a critical

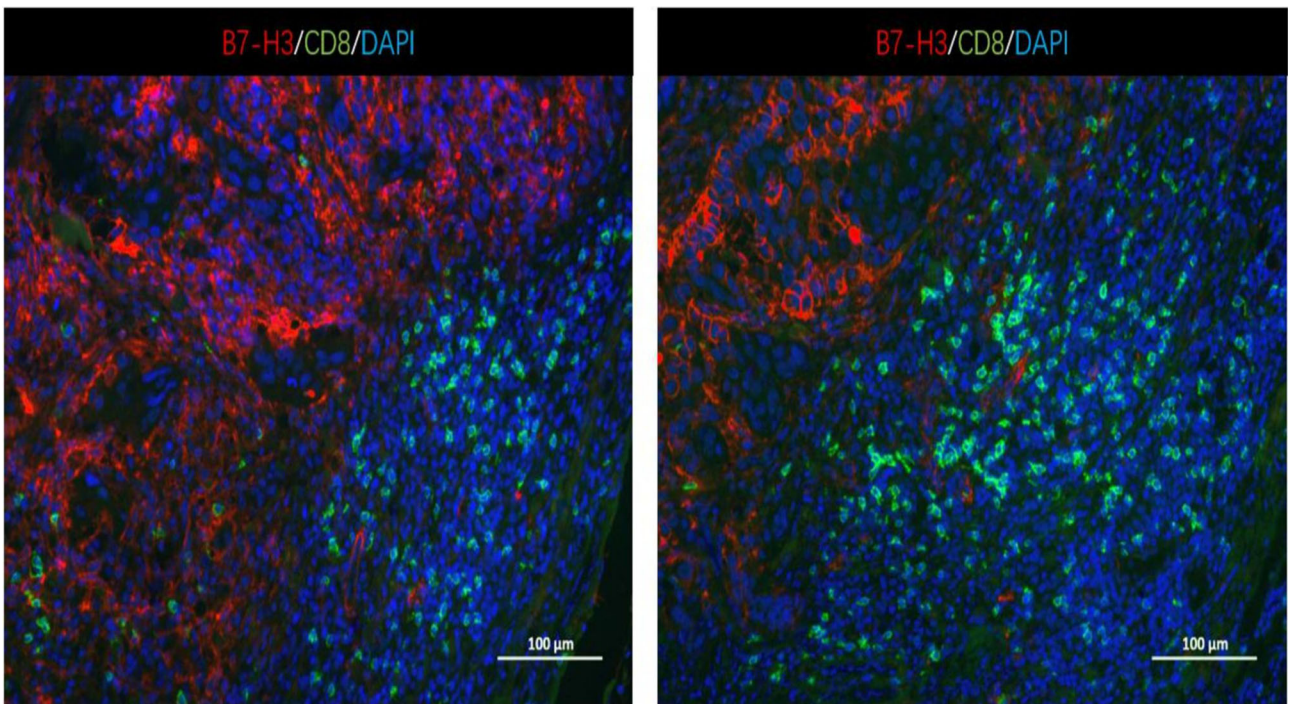

FIGURE 7 | Representative immunofluorescence images of B7-H3 and tumor-infiltrating $CD8^+$ T cells in LSCC tissues. Original magnification ×100; scale bar, 100 μm. No apparent colocalization of the B7-H3 (red) and CD8 (green) signal was found.

biomarker for predicting LSCC prognosis and a new target for LSCC immunotherapy.

DATA AVAILABILITY STATEMENT

The datasets presented in this study can be found in online repositories, further inquiries can be directed to the corresponding authors.

ETHICS STATEMENT

The studies involving human participants were reviewed and approved by Ethical Committee of Sun Yat-Sen University. The patients/participants provided their written informed consent to participate in this study.

AUTHOR CONTRIBUTIONS

YL performed the experiments and contributed to the writing of the manuscript. QC was as the cooperation teacher of the experiments and took charge of supplementary bioinformatic analysis; XS performed the experiments. XC took charge of the result analysis; ZG played a guiding role in conceiving and designing the study,and provided the overall writing guidance. All authors reviewed the manuscript. All authors contributed to the article and approved the submitted version.

FUNDING

This study was supported by the National Natural Science Foundation of China No. 81572648.

REFERENCES

1. Aupérin A. Epidemiology of Head and Neck Cancers: An Update. *Curr Opin Oncol* (2020) 32(3):178–86. doi: 10.1097/CCO.0000000000000629
2. Deng Y, Wang M, Zhou L, Zheng Y, Li N, Tian T, et al. Global Burden of Larynx Cancer, 1990-2017: Estimates From the Global Burden of Disease 2017 Study. *Aging (Albany NY)* (2020) 12(3):2545–83. doi: 10.18632/aging.102762
3. Chapoval AI, Ni J, Lau JS, Wilcox RA, Flies DB, Liu D, et al. B7-H3: A Costimulatory Molecule for T Cell Activation and IFN-Gamma Production. *Nat Immunol* (2001) 2(3):269–74. doi: 10.1038/85339
4. Katayama A, Takahara M, Kishibe K, Nagato T, Kunibe I, Katada A, et al. Expression of B7-H3 in Hypopharyngeal Squamous Cell Carcinoma as a Predictive Indicator for Tumor Metastasis and Prognosis. *Int J Oncol* (2011) 38(5):1219–26. doi: 10.3892/ijo.2011.949
5. Hu J, Jiang C, Zheng M, Guo Y, Tang X, Ren J, et al. Overexpression of B7-H3 as an Opportunity for Targeted Therapy in Head and Neck Cancers. *Am J Trans Res* (2019) 11(8):5183–96.
6. Altan M, Pelekanou V, Schalper KA, Toki M, Gaule P, Syrigos K, et al. B7-H3 Expression in NSCLC and Its Association With B7-H4, PD-L1 and Tumor-Infiltrating Lymphocytes. *Clin Cancer Res an Off J Am Assoc Cancer Res* (2017) 23(17):5202–9. doi: 10.1158/1078-0432.CCR-16-3107
7. Sun J, Guo Y-D, Li X-N, Zhang Y-Q, Gu L, Wu P-P, et al. B7-H3 Expression in Breast Cancer and Upregulation of VEGF Through Gene Silence. *OncoTargets Ther* (2014) 7:1979–86. doi: 10.2147/OTT.S63424
8. Zhang T, Jiang B, Zou ST, Liu F, Hua D. Overexpression of B7-H3 Augments Anti-Apoptosis of Colorectal Cancer Cells by Jak2-Stat3. *World J Gastroenterol* (2015) 21(6):1804–13. doi: 10.3748/wjg.v21.i6.1804
9. Shi T, Ma Y, Cao L, Zhan S, Xu Y, Fu F, et al. B7-H3 Promotes Aerobic Glycolysis and Chemoresistance in Colorectal Cancer Cells by Regulating HK2. *Cell Death Dis* (2019) 10(4):308. doi: 10.1038/s41419-019-1549-6
10. Wang R, Ma Y, Zhan S, Zhang G, Cao L, Zhang X, et al. B7-H3 Promotes Colorectal Cancer Angiogenesis Through Activating the NF-κb Pathway to Induce VEGFA Expression. *Cell Death Dis* (2020) 11(1):55. doi: 10.1038/s41419-020-2252-311
11. Liu H, Tekle C, Chen YW, Kristian A, Zhao Y, Zhou M, et al. B7-H3 Silencing Increases Paclitaxel Sensitivity by Abrogating Jak2/Stat3 Phosphorylation. *Mol Cancer Ther* (2011) 10(6):960–71. doi: 10.1158/1535-7163.MCT-11-0072
12. Janakiram M, Shah U, Liu W, Zhao A, Schoenberg M, Zang X. The Third Group of the B7-CD28 Immune Checkpoint Family: HHLA2, TMIGD2, B7x, and B7-H3. *Immunol Rev* (2017) 276(1):26–39. doi: 10.1111/imr.12521
13. Burugu S, Dancsok A, Nielsen T. Emerging Targets in Cancer Immunotherapy. *Semin Cancer Biol* (2018) 52:39–52. doi: 10.1016/j.semcancer.2017.10.001
14. Mao L, Fan T-F, Wu L, Yu G-T, Deng W-W, Chen L, et al. Selective Blockade of B7-H3 Enhances Antitumour Immune Activity by Reducing Immature Myeloid Cells in Head and Neck Squamous Cell Carcinoma. *J Cell Mol Med* (2017) 21(9):2199–210. doi: 10.1111/jcmm.13143
15. Wang J, Chong K, Nakamura Y, Nguyen L, Huang S, Kuo C, et al. B7-H3 Associated With Tumor Progression and Epigenetic Regulatory Activity in Cutaneous Melanoma. *J Invest Dermatol* (2013) 133(8):2050–8. doi: 10.1038/jid.2013.114
16. Li Z, Liu J, Que L, Tang X. The Immunoregulatory Protein B7-H3 Promotes Aerobic Glycolysis in Oral Squamous Carcinoma *via* PI3K/Akt/mTOR Pathway. *J Cancer* (2019) 10(23):5770–84. doi: 10.7150/jca.29838
17. Carvajal-Hausdorf D, Altan M, Velcheti V, Gettinger SN, Herbst RS, Rimm DL, et al. Expression and Clinical Significance of PD-L1, B7-H3, B7-H4 and TILs in Human Small Cell Lung Cancer (SCLC). *J immunotherapy Cancer* (2019) 7(1):65. doi: 10.1186/s40425-019-0540-1
18. Jiang B, Zhang T, Liu F, Sun Z, Shi H, Hua D, et al. The Co-Stimulatory Molecule B7-H3 Promotes the Epithelial-Mesenchymal Transition in Colorectal Cancer. *Oncotarget* (2016) 7(22):31755–71. doi: 10.18632/oncotarget.9035
19. Cai D, Li J, Liu D, Hong S, Qiao Q, Sun Q, et al. Tumor-Expressed B7-H3 Mediates the Inhibition of Antitumor T-Cell Functions in Ovarian Cancer Insensitive to PD-1 Blockade Therapy. *Cell Mol Immunol* (2019) 17(3):227–36. doi: 10.1038/s41423-019-0305-2
20. Liu CL, Zang XX, Huang H, Zhang H, Wang C, Kong YL, et al. The Expression of B7-H3 and B7-H4 in Human Gallbladder Carcinoma and Their Clinical Implications. *Eur Rev Med Pharmacol Sci* (2016) 20(21):4466–73.
21. Lupu CM, Eisenbach C, Lupu AD, Kuefner MA, Hoyler B, Stremmel W, et al. Adenoviral B7-H3 Therapy Induces Tumor Specific Immune Responses and Reduces Secondary Metastasis in a Murine Model of Colon Cancer. *Oncol Rep* (2007) 18(3):745–8.
22. Wu CP, Jiang JT, Tan M, Zhu YB, Ji M, Xu KF, et al. Relationship Between Co-Stimulatory Molecule B7-H3 Expression and Gastric Carcinoma Histology and Prognosis. *World J Gastroenterol* (2006) 12(3):457–9. doi: 10.3748/wjg.v12.i3.457
23. Digregorio M, Coppieters N, Lombard A, Lumapat P, Scholtes F, Rogister B. The Expression of B7-H3 Isoforms in Newly Diagnosed Glioblastoma and Recurrence and Their Functional Role. *Acta neuropathologica Commun* (2021) 9(1):59. doi: 10.1186/s40478-021-01167-w
24. Chen J-T, Chen C-H, Ku K-L, Hsiao M, Chiang C-P, Hsu T-L, et al. Glycoprotein B7-H3 Overexpression and Aberrant Glycosylation in Oral Cancer and Immune Response. *Proc Natl Acad Sci USA* (2015) 112(42):13057–62. doi: 10.1073/pnas.1516991112
25. Kim N, Park M, Lee J. Associations of B7-H3 and B7-H4 Expression in Ductal Carcinoma *In Situ* of the Breast With Clinicopathologic Features and T-Cell

Infiltration. *Appl immunohistochemistry Mol morphology AIMM* (2020) 28 (10):767–75. doi: 10.1097/PAI.0000000000000817
26. Ni L, Dong C. New B7 Family Checkpoints in Human Cancers. *Mol Cancer Ther* (2017) 16(7):1203–11. doi: 10.1158/1535-7163.MCT-16-0761
27. Mahnke K, Ring S, Johnson TS, Schallenberg S, Schönfeld K, Storn V, et al. Induction of Immunosuppressive Functions of Dendritic Cells *In Vivo* by CD4+CD25+ Regulatory T Cells: Role of B7-H3 Expression and Antigen Presentation. *Eur J Immunol* (2007) 37(8):2117–26. doi: 10.1002/eji.200636841
28. Suh WK, Gajewska BU, Okada H, Gronski MA, Bertram EM, Dawicki W, et al. The B7 Family Member B7-H3 Preferentially Down-Regulates T Helper Type 1-Mediated Immune Responses. *Nat Immunol* (2003) 4(9):899–906. doi: 10.1038/ni967
29. Wang C, Li Y, Jia L, Kim JK, Li J, Deng P, et al. CD276 Expression Enables Squamous Cell Carcinoma Stem Cells to Evade Immune Surveillance. *Cell Stem Cell* (2021) 28(9):1597–613.e7. doi: 10.1016/j.stem.2021.04.011
30. So Y, Byeon S, Ku B, Ko Y, Ahn M, Son Y, et al. An Increase of CD8 T Cell Infiltration Following Recurrence is a Good Prognosticator in HNSCC. *Sci Rep* (2020) 10(1):20059. doi: 10.1038/s41598-020-77036-8
31. You G, Lee Y, Kang Y, Park H, Park K, Kim H, et al. B7-H3×4-1BB Bispecific Antibody Augments Antitumor Immunity by Enhancing Terminally Differentiated CD8 Tumor-Infiltrating Lymphocytes. *Sci Adv* (2021) 7(3): eaax3160. doi: 10.1126/sciadv.aax3160
32. Kreymborg K, Haak S, Murali R, Wei J, Waitz R, Gasteiger G, et al. Ablation of B7-H3 But Not B7-H4 Results in Highly Increased Tumor Burden in a Murine Model of Spontaneous Prostate Cancer. *Cancer Immunol Res* (2015) 3(8):849–54. doi: 10.1158/2326-6066.CIR-15-0100
33. Castriconi R, Dondero A, Augugliaro R, Cantoni C, Carnemolla B, Sementa A, et al. Identification of 4Ig-B7-H3 as a Neuroblastoma-Associated Molecule That Exerts a Protective Role From an NK Cell-Mediated Lysis. *Proc Natl Acad Sci USA* (2004) 101(34):12640–5. doi: 10.1073/pnas.0405025101
34. Hashiguchi M, Kobori H, Ritprajak P, Kamimura Y, Kozono H, Azuma M. Triggering Receptor Expressed on Myeloid Cell-Like Transcript 2 (TLT-2) Is a Counter-Receptor for B7-H3 and Enhances T Cell Responses. *Proc Natl Acad Sci USA* (2008) 105(30):10495–500. doi: 10.1073/pnas.0802423105
35. Zhang SS, Tang J, Yu SY, Ma LI, Wang F, Xie SL, et al. Expression Levels of B7-H3 and TLT-2 in Human Oral Squamous Cell Carcinoma. *Oncol Lett* (2015) 10(2):1063–8. doi: 10.3892/ol.2015.3274
36. Kramer K, Kushner BH, Modak S, Pandit-Taskar N, Smith-Jones P, Zanzonico P, et al. Compartmental Intrathecal Radioimmunotherapy: Results for Treatment for Metastatic CNS Neuroblastoma. *J Neuro-Oncol* (2010) 97(3):409–18. doi: 10.1007/s11060-009-0038-7
37. Souweidane M, Kramer K, Pandit-Taskar N, Zhou Z, Haque S, Zanzonico P, et al. Convection-Enhanced Delivery for Diffuse Intrinsic Pontine Glioma: A Single-Centre, Dose-Escalation, Phase 1 Trial. *Lancet Oncol* (2018) 19 (8):1040–50. doi: 10.1016/S1470-2045(18)30322-X

Conflict of Interest: The authors declare that the research was conducted in the absence of any commercial or financial relationships that could be construed as a potential conflict of interest.

Publisher's Note: All claims expressed in this article are solely those of the authors and do not necessarily represent those of their affiliated organizations, or those of the publisher, the editors and the reviewers. Any product that may be evaluated in this article, or claim that may be made by its manufacturer, is not guaranteed or endorsed by the publisher.

frontiers in Oncology

ORIGINAL RESEARCH
published: 14 December 2021
doi: 10.3389/fonc.2021.783575

NK4 Regulates Laryngeal Squamous Cell Carcinoma Cell Properties and Inhibits Tumorigenicity by Modulating the DKK1/Wnt/β-Catenin Axis

Shoukai Zhang[1,2], *Hulai Wei*[3], *Xiaoqin Ha*[4], *Yueyu Zhang*[2] *and Yufen Guo*[1,5*]

[1] The Second School of Clinical Medicine, Lanzhou University, Lanzhou, China, [2] Otolaryngology-Head Neck Surgery, Gansu Provincial People's Hospital, Lanzhou, China, [3] School of Basic Medical Sciences, Lanzhou University, Lanzhou, China, [4] Laboratory, People's Liberation Army Joint Logistics Support Force 940th Hospital, Lanzhou, China, [5] Otolaryngology-Head Neck Surgery, Lanzhou University Second Hospital, Lanzhou, China

Objective: To investigate the effects of NK4 gene on the properties and tumorigenicity in laryngeal squamous cell carcinoma cell.

Methods: Here, we used the attenuated Salmonella carrying the NK4 gene to transfect the AMC-HN-8 cells and detected the expression of NK4 by the real-time quantitative polymerase chain reaction (q RT-PCR). The properties of NK4 gene was determined by MTT method, cell scratch test, and flow cytometry. A nude mouse tumorigenesis model was used to evaluate the effect of NK4 gene on the growth of AMC-HN-8 cells *in vivo*. While a western blot assay was used to assess the expression of DKK1, Wnt1 and β-Catenin in nude mouse tumors.

Results: qRT-PCR showed that the expression of NK4 in the transfection group was significantly higher than that in the control group ($P<0.01$), and the expression increased with the time of transfection. MTT results showed NK4 overexpression inhibited the proliferation of AMC-HN-8 cells, and the inhibitory activity no longer increased with increasing dose when 30% expression supernatant was added ($P<0.01$). Scratch experiment showed that NK4 overexpression decreased the cell migration ability ($P<0.01$). Annexin V/PI double staining experiment showed that NK4 gene induced AMC-HN-8 cell apoptosis ($P<0.01$), and cell cycle arrest in S phase ($P<0.01$). NK4 overexpression inhibited tumor formation ability of AMC-HN-8 cells *in vivo* ($P<0.05$). WB detection showed that the expression of DKK1 increased, Wnt1 and β-Catenin protein decreased after the high expression of NK4.

Conclusions: NK4 gene inhibit cell proliferation and migration, while promote cell apoptosis, and induce cell cycle arrest in S phase of laryngeal carcinoma AMC-HN-8 cells. NK4 overexpression inhibit the tumorigenesis ability of AMC-HN-8 cells, which may be related to the regulation of DKK1/Wnt1/β-Catenin signal axis.

Keywords: NK4, laryngeal carcinoma, proliferation, migration, apoptosis, tumorigenicity

OPEN ACCESS

Edited by:
Gary Goldberg,
Rowan University School of Osteopathic Medicine, United States

Reviewed by:
Harini Krishnan,
Stony Brook University, United States
Katarzyna Jachimowska,
Rowan University School of Osteopathic Medicine, United States

***Correspondence:**
Yufen Guo
gyflhmm@163.com

Specialty section:
This article was submitted to Head and Neck Cancer, a section of the journal Frontiers in Oncology

Received: *26 September 2021*
Accepted: *24 November 2021*
Published: *14 December 2021*

Citation:
Zhang S, Wei H, Ha X, Zhang Y and Guo Y (2021) NK4 Regulates Laryngeal Squamous Cell Carcinoma Cell Properties and Inhibits Tumorigenicity by Modulating the DKK1/Wnt/β-Catenin Axis. Front. Oncol. 11:783575. doi: 10.3389/fonc.2021.783575

INTRODUCTION

Laryngeal cancer is the most common malignancy in the head and neck, accounting for 1-5% of systemic malignancies, of which 96-98% are laryngeal squamous cell carcinoma (LSCC). A study in 2018 (1) estimated that 177,422 new cases of laryngeal cancer and 94,771 deaths. Surgery is still the most effective treatment. Adjuvant radiotherapy, chemotherapy and novel gene-targeted therapy have led to significant progress in the treatment of laryngeal cancer. In recent years, gene-targeted therapy has shown good development and application prospects in cancer treatment. Therefore, seeking new approaches to treat laryngeal cancer at the gene level has become a new challenge faced by otolaryngologists.

Hepatocyte growth factor (HGF) is a cytokine produced by many interstitial cells, such as fibroblasts and macrophages, and acts on the receptor tyrosine-protein kinase Met (c-Met) on the surface of tumor cells. As a splice variant of HGF, NK4 has a heavy chain consisting of an n-terminal domain and 4 kringle domains, which compete with HGF for the binding of c-Met, is a specific antagonist of HGF. NK4 inhibits not only the signal transduction of the HGF/c-Met system but also the formation, invasion and metastasis of tumors, and it also inhibits tumor angiogenesis independent of the HGF/c-Met pathway and promotes tumor cell apoptosis. Dickkopf-1 (DKK1) is a secreted protein of the DKK protein family and an inhibitor of the extracellular Wnt signal transduction pathway (2). The Wnt signal transduction pathway is related to the occurrence, development, metastasis and prognosis of a variety of tumors. The DKK protein family has a similar conserved cysteine domain, which inhibits the Wnt/β-catenin pathway by causing the degradation of proteasome β-catenin, inducing apoptosis and inhibiting cell proliferation (3). Research (4) showed that DKK1 gene is highly expressed in head and neck squamous cell carcinoma, and its high expression may be related to HPV status, age, pathological grade, and clinical stage.

Based on the dual antitumor properties of the NK4 gene and the high expression of Wnt1/β-Catenin signaling pathway in the head and neck, this study aims to explore the following issues: (1) NK4 expression in transfected LSCC AMC-HN-8 cells; (2) the effects of the NK4 gene on the proliferation, migration, apoptosis and cell cycle of LSCC AMC-HN-8 cells;(3) The effect of NK4 gene on the tumorigenesis ability of nude mice of laryngeal cancer cells, and to explore whether its DKK1/Wnt1/β-Catenin signaling pathway is involved in the effect of NK4 gene on laryngeal cancer. The exploration of these issues can provide a deeper understanding of the important role of the NK4 gene in the development and progression of LSCC and provide theoretical support for gene therapy for LSCC.

1 MATERIALS AND METHODS

1.1 Cells, Strains, and Main Reagents

The attenuated Salmonella strain carrying the NK4 gene was kindly provided by Professor Xiaoqin Ha from the 940 Hospital of Lanzhou People's Liberation Army Joint Logistics Support Force; the LSCC AMC-HN-8 cells were purchased from Beiner Biological Cell Bank; high-glucose Dulbecco's modified Eagle medium (H-DMEM) was purchased from HyClone Inc.; fetal bovine serum (FBS) was purchased from Hangzhou Sijiqing Bioengineering Materials Co., Ltd.; 0.25% trypsin-ethylenediaminetetraacetic acid (EDTA) was purchased from Gibco; penicillin and streptomycin were purchased from Biyuntian Biotechnology Co., Ltd.; methyl thiazolyl tetrazolium (MTT) was purchased from Beijing Solarbio Biotechnology Company; dimethyl sulfoxide (DMSO) was purchased from Wuhan BOSTER Biological Technology Co., Ltd.; total RNA extraction reagent, RNA reverse transcription kits, and real-time quantitative polymerase chain reaction (qRT-PCR) reagents were purchased from Takara Co., Ltd.; PCR primers were synthesized by Takara Biotechnology Co.; and annexin V fluorescein isothiocyanate (FITC)/propidium iodide (PI) double staining reagent kits and apoptosis kits were purchased from Invitrogen, USA. 4-6 weeks old, weighing 16-18g BALB/c nude mice were purchased from Beijing Weitong Lihua Laboratory Animal Technology Co., Ltd., license number SCXK (Beijing) 2016-0006; rabbit anti-human Wnt1 monoclonal antibody, rabbit anti-human β-Catenin and mouse anti-human DKK1 monoclonal antibody were purchased from Abcam, rabbit anti-human NK4 monoclonal antibody were purchased from Affinity.

1.2 Preparation of Attenuated Salmonella Carrying NK4 Gene

1.2.1 Acquisition of NK4 Gene

According to literature search, design NK4 mRNA sequence, design specific primers for amplification of NK4 cDNA (**Table 1**), extract total RNA from human placental tissue, reverse transcription into cDNA, amplify NK4 gene, and amplify NK4 gene by PCR The parameters are: 94°C 30 s, 54°C 30 s, 72°C 2 min, cycle 30 times; The amplified product was detected by 1.0% agarose gel electrophoresis, and the product size was 1460 bp.

1.2.2 Construction of the Eukaryotic Co-Expression Vector Carrying the NK4 Gene

After the PCR product of NK4 was recovered from the gel, it was digested with SalI and Not I. At the same time, the PIRES-SEQ plasmid was also digested with SalI and NotI; after 3 hours of digestion, it was digested with 1% Agarose gel electrophoresis respectively recovered NK4 gene fragment (about 1.5kb) and linearized PIRES-SEQ plasmid fragment (about 6.1kb); the recovered NK4 gene fragment and linearized pIRES-SEQ plasmid had a molar ratio of 5~ Mix at 10:1, add T4 ligase and

TABLE 1 | Primer list.

Gene name	Sequences 5'-3'	Size (bp)	Enzyme site
NK4	Forward: CTG GTCGAC ATG TGG GTG ACC AAA CTC Reverse: GCA GCGGCCGC TCAG ACT ATT GTA GGT GTG GT	1460	SalI NotI

connection Buffer, ligate at 4°C for 12 h; transform DH5a competent cells, spread on LB agar plates containing X-Gal IPTG Amp for culture.

1.2.3 Preparation of Attenuated Salmonella Ty21a Competent Cells

Attenuated Salmonella Ty21a (previously constructed by Professor Ha Xiaoqin of the 940th Hospital of the Joint Service Support Force of the Chinese People's Liberation Army) inoculate the attenuated Salmonella Ty21a strain in 50mL LB liquid medium, shake culture to A525nm of about 0.6, collect the bacteria by centrifugation at 4°C 4000 rpm/min, and use pre-chilled sterile Wash the bacteria twice with deionized water and suspend in 1 mL of ice-cold sterile deionized water.

1.2.4 Electrotransformation Process

Add 0.2 μg of plasmid pCMV-NK4-IRES to 200 μL of the above bacterial solution for electrotransformation, add 1 mL of SOC medium after electric shock, shake at 37°C for 45 minutes, and spread on an ampicillin-resistant LB plate. Incubate overnight at 37°C in an incubator.

1.2.5 Screening and Identification of Attenuated Salmonella Carrying NK4 Gene

Take out the LB plate the next day, pick 10 monoclonal colonies from the culture plate, and inoculate them in 3 mL of LB medium containing ampicillin resistance (selection positive only), 37 Incubate with shaking at °C overnight (not more than 16 h). Take 2 mL of the bacterial solution and mix with glycerol the next day, then freeze it (containing 15% glycerol). The remaining 1 mL of the bacterial solution was centrifuged to collect the bacteria, and the plasmid was extracted with a small plasmid extraction kit. The extracted plasmid was detected by 1% agarose electrophoresis and then identified by PCR and Sal 1/ NotIrestriction enzyme digestion.

1.3 Culture of LSCC AMC-HN-8 Cells

The cells were cultured in DMEM containing 10% FBS, 1% penicillin and streptomycin (100 U/mL penicillin and 100 μg/mL streptomycin) in a 37°C, 5% CO_2 incubator. Cells were digested with 0.25% trypsin and passaged once every 3 d. The culture medium was changed once every 2 d. Cells in logarithmic growth phase were used for subsequent experiments.

1.4 Transfection of LSCC AMC-HN-8 Cells

LSCC AMC-HN-8 cells were cultured in H-DMEM containing 10% FBS. After the cell confluence reached 90% or higher, the cells were digested with 0.25% trypsin and passaged. One day before transfection, the cells were inoculated on 6-well culture plates at 6×10^5 cells/well and were divided into a control group and NK4 group, with 3 wells for each group. The next day, attenuated Salmonella stains carrying NK4 were inoculated into 3 mL of Luria-Bertani (LB) broth. Cells were shaken at 37°C for 4 h. When the absorbance at 525 nm (A_{525nm}) was approximately 0.6, the bacteria were collected by centrifugation (4000 rpm/min) at 4°C. The bacteria were washed twice with precooled sterile deionized (DI) water and then suspended in sterile DI water at the bacterial concentration of 1×10^8/ml. Prior to transfection, cells in each group were washed with antibiotic-free DMEM twice. The prepared cells and bacteria were added into the culture wells of the transfection group at a ratio of 1:50 and incubated at 37°C for 1 h; then, the cells were washed with PBS twice and incubated in serum-free medium (containing 50 mg/L gentamicin) for 1 h, and last, complete medium with gentamicin (10 mg/L) was added for further culture.

1.5 NK4 Expression Detected by RT-PCR

At 24 h and 48 h after transfection, the LSCC AMC-HN-8 cells were harvested, and total RNA was extracted using Trizol according to the manufacturer's instructions. Reverse transcription of RNA was performed according to the manufacturer's instructions (Takara) to obtain complementary DNA (cDNA). Primer sequences for the NK4 gene (**Table 2**). The reverse transcription conditions were as follows: 42°C for 2 min, 37°C for 15 min, and 85°C for 5 s. The reverse transcription products were used as templates for PCR amplification; β-Actin was used as the internal reference. The PCR amplification conditions were as follows: step 1, 95°C for 30 s; step 2, 95°C for 5 s, 57°C for 35 s, and 72°C for 60 s, for a total of 45 cycles; and step 3, extension at 65°C for 5 min. The absorbance was read at each extension stage. Multiple wells were setup for each sample, and the average value was used for statistical analysis. Under the condition that the amplification efficiency was consistent, the $2^{-\Delta\Delta CT}$ method was used to obtain the relative quantitative results. Agarose gel electrophoresis was performed on PCR products to detect the expected NK4 gene fragment (163 bp). The expression of the target gene was detected by performing agarose gel electrophoresis with the PCR products.

1.6 Determination of Cell Proliferation Using the MTT Assay

The supernatant of laryngeal cancer AMC-HN-8 cells cultured 48h after transfection was collected according to the above 1.4 method, and the protein was extracted to identify the expression of NK4 protein. After the expression of NK4 protein was confirmed by Western blot, MTT was used to detect cell proliferation capacity on this basis: AMC-HN-8 cells in the logarithmic growth phase were inoculated into 96-well cell culture plates at 5×10^3 cells/well and divided into a control group and an NK4 group. After a 12-h culture, the original culture medium was aspirated and discarded. Serum-free DMEM (100 μl/well) and the cell culture supernatant after 48 h of transfection were added into the wells of the NK4 group, with percentages of expression supernatant accounting for 5%,

TABLE 2 | Primer sequences for the NK4 gene.

Primer name	Primer sequence 5′-3′	Product length
NK4	GTGAATACTGCAGACCAATGTGCTA GGTCAAATTCATGGCCAAATTC	163 bp
β-Actin	TGGCACCCAGCACAATGAA CTAAGTCATAGTCCGCCTAGAAGCA	186 bp

10%, 15%, 20%, 25%, 30%, and 35% of the total culture volume. The control group had 3 wells, and there were also 3 wells for each expression supernatant percentage in the NK4 group. In the control group, only serum-free DMEM (100 μl/well) was added. After incubating at 37°C for 48 h, 10 μl of MTT (5 mg/ml, prepared with PBS and then after filtered and sterilized) solution was added to each well, followed by incubation in a cell incubator for 4 h. Then, 100 μl of DMSO was added, and the cells were shaken for 15 min. The optical density (OD) at 570 nm was measured. A cell growth curve was plotted with OD as the vertical axis, and the inhibition rate of cell growth was calculated. Y = 1-A/B × 100%, where Y is the cell inhibition rate, A is the OD of the experimental group, and B is the OD of the control group. The experiment was repeated 3 times.

1.7 Cell Migration Measured by the Scratch Assay

Cells in logarithmic growth phase were inoculated into 6-well plates and divided into a control group and an NK4 group. After the cells reached more than 90% confluence, a 10-μL sterile tip was used to scratch the monolayer of the cells at the bottom of each well before transfection. The cells were transfected according to the method described in *Section 1.3.* At 0, 24, 48, and 72 h after transfection, healing was observed under a microscope and photographed. ImageJ software was used to measure the scratch area and calculate cell migration ability, as follows: migration ability = (scratch area at 0 h - scratch area at 24 h/48 h/72 h)/scratch area at 0 h × 100%. The experiment was repeated 3 times.

1.8 Cell Cycle Measured by Flow Cytometry

Cells in logarithmic growth phase were inoculated into 6-well plates at 6×10^5 cells/well and were divided into a control group and an NK4 group. The cells were transfected according to the method described in *Section 1.3.* A cell suspension was prepared after 48 h of culture. Cells were fixed in 75% ethanol overnight, washed with PBS once, and stained with PI. After incubation at 4°C in the dark for 30 min, flow cytometry was performed, and the percentage of cells in each cell cycle phase was calculated using Modifit software. The experiment was repeated 3 times.

1.9 Cell Apoptosis Measured by Flow Cytometry

Cells in logarithmic growth phase were inoculated into 6-well plates at 6×10^5 cells/well and were divided into a control group and an NK4 group. The cells were transfected according to the method described in *Section 1.3.* After 24 h, 48 h, and 72 h of culture, the cells were digested with trypsin and centrifuged, and the supernatant was discarded. Two hundred microliters of 1× binding buffer was added, and the cells were resuspended, followed by the addition of 5 μL of annexin V-FITC and 5 μL of PI. The reaction was carried out at room temperature for 15 min in the dark. Apoptosis was detected by flow cytometry. The experiment was repeated 3 times.

1.10 Establishment of Subcutaneous Laryngeal Carcinoma Xenograft Model in Nude Mice

Take 30 nude mice, inoculate the logarithmic growth phase of laryngeal cancer cells at a cell density of 1×10^7/ml on the skin of the right side of the axilla of the nude mice, and inoculate at a volume of 0.2 mL for each nude mouse. When a tumor nodule is visible to the naked eye, measure the longest diameter of the tumor (a) and the short diameter (b) perpendicular to it with a vernier caliper every 3 days. The final tumor volume is calculated according to the formula $V = 1/2ab^2$, when the tumor volume Reached about 100 mm3, they were randomly divided into a control group and a treatment group, with 15 animals in each group. Suspend the attenuated Salmonella carrying the NK4 gene in 10% NaHCO3, adjust the cell concentration to 1×10^9 cells/ml, and take the corresponding bacteria 0.1 ml with gastric tube feeding once a week for 4 times in total, the control group Take an equal volume of 0.1M PBS buffer solution. One week after the treatment, the nude mice were sacrificed by cervical vertebrae removal method, the subcutaneous tumor nodules were stripped, and the tumor weight was weighed after taking pictures. The tumor tissue was fixed with 10% neutral formalin for routine HE and immunohistochemical staining.

1.11 Western Blot Detection of DKK1, Wnt1, β-Catenin Protein

RIPA lyses the tumor to extract the protein. After the protein concentration is determined by the BCA method, the protein loading buffer is added and the protein is boiled in boiling water for 10 minutes to denature the protein. Equipped with 10% separation gel and 5% concentrated gel, the concentrated gel runs at a constant pressure of 80 V for 30 minutes, and the separation gel runs at a constant pressure of 110 V for 90 minutes. Cut out the glue of the corresponding molecular weight and transfer it for 30 to 90 min at a constant current of 200mA at 4° C. 5% milk blocking solution was sealed at room temperature for 1 h. Incubate the primary antibody overnight at 4°C. After washing the excess primary antibody with TBST the next day, incubate the secondary antibody at room temperature for 1 hour, add ECL luminescent reagent dropwise, and expose and image in the imager. Image J software analyzes the gray value of each band. The experiment was repeated 3 times.

1.12 Statistical Methods

All data were processed first using Excel, and statistical analysis was performed using SPSS 23.0 software. The data are expressed as the mean ± standard deviation ($\bar{x}+S$). The paired sample t test was used to compare the means between 2 groups. One-way analysis of variance (ANOVA) was used for comparisons among multiple groups. $P<0.05$ was considered statistically significant.

2 RESULTS

2.1 Morphological Changes in LSCC AMC-HN-8 Cells After Transfection

The growth state of cells was directly observed under a microscope. After transfection, the normal morphology of

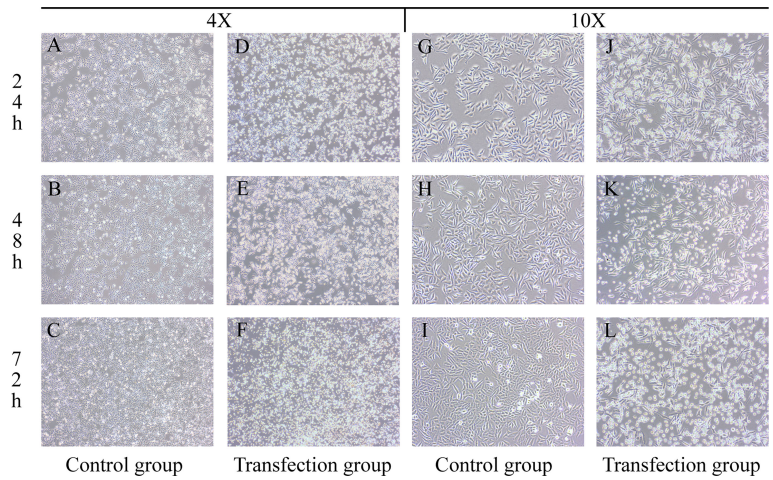

FIGURE 1 | Groups **(A–C, G–I)** are the control groups; Groups **(D–F, J–L)** are the transfection groups.

LSCC AMC-HN-8 cells was destroyed, and the proliferation and growth were inhibited. Microscopic observation showed that as the transfection time increased, apoptotic cells increased, and the cell morphology changed significantly. As shown in **Figure 1**, after the cells in the control group were cultured for 24 h, 48 h, and 72 h, the number of cells increased, adherent growth was vigorous, and the adjacent cells grew and fused together, with a full cytoplasm, clear cell profile, spindle or polygon shape, and well dispersed. After the transfected LSCC AMC-HN-8 cells were cultured for 24 h, 48 h, and 72 h, the number of visible cells gradually decreased, the cell morphology gradually became cord-like, the connection between cells was relaxed, the cells became nonadherent, granular substances increased, and the number of apoptotic cells increased.

2.2 Expression of the NK4 Gene in LSCC AMC-HN-8 Cells

The amplified NK4 gene and the β-actin fragment (the internal reference) were subjected to agarose gel electrophoresis. In the gel system, the NK4 fragment band (163 bp) and the β-actin fragment band (186 bp) were identified. The size of the NK4 fragment after PCR amplification was consistent with the theoretical size of the NK4 fragment, and the band intensity increased with the transfection time. The results are shown in **Figures 2A–C** (P<0.01). The relative expression level of NK4 in each group of cells was calculated using the $2^{-\Delta\Delta Ct}$ method. The RT-PCR results showed that NK4 expression was significantly increased in the transfection group; the difference was statistically significant (P<0.01, **Figure 2D**).

2.3 Effect of NK4 Gene Inhibition on the Proliferation of LSCC AMC-HN-8 Cells

After the expression of NK4 (26kD)protein was confirmed by Western blot, The results are shown in **Figure 3**. The MTT assay results showed that the expression products of the transfected cells significantly inhibited the proliferation activity of AMC-HN-8

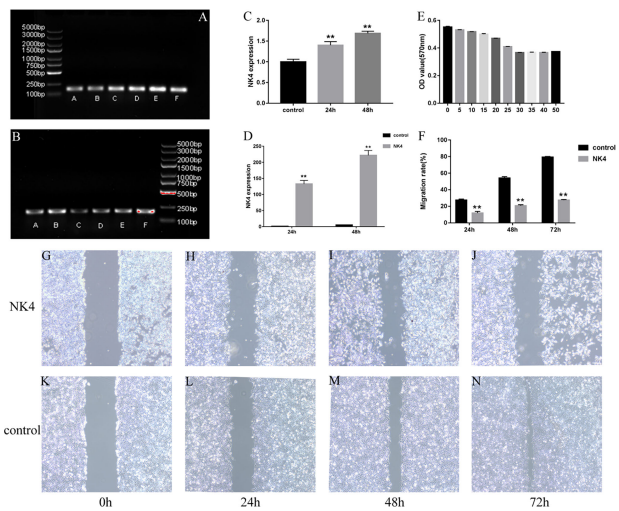

FIGURE 2 | **(A)** NK4 gene fragment; **(B)** β-actin gene (the internal reference); **(C)** Grayscale value analysis of electrophoretic gel images (after PCR); **(D)** NK4 gene expression; **(E)** NK4 inhibits the proliferation of laryngeal cancer cells; **(F)** the wound healing of cells in the control group and NK4 group at 24h, 48h, and 72h; **(G–N)** the wound healing of cells in the control group and NK4 group at 24h, 48h, and 72h. **P < 0.01.

cells in a percentage-dependent manner. After the percentage of expression supernatant reached 30%, the inhibitory effect no longer increased as the percentage increased, and the inhibition rate was 33.56% (**Figure 2E**, P<0.01).

2.4 Effects of NK4 Gene Inhibition on the Migration Ability of LSCC AMC-HN-8 Cells

The scratch assay was used to determine the effect of NK4 gene inhibition on the migration ability of LSCC AMC-HN-8 cells (**Figures 2F, G–N**). The scratch wound healing rates of transfected AMC-HN-8 cells at 24 h, 48 h, and 72 h after scratching were

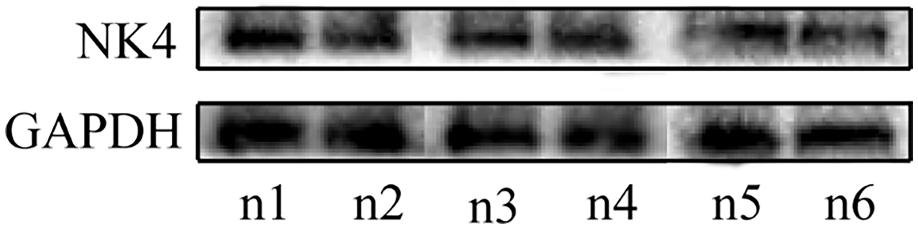

FIGURE 3 | n1-n6: the expression of NK4 protein.

11.97% ± 4.40%, 20.75% ± 3.55%, and 27.73% ± 2.56%, respectively, lower than those in the control group (24.82% ± 3.01%, 54.15% ± 5.11%, and 79.37% ± 2.45%, respectively); the differences were statistically significant (P<0.01). The scratch assay results showed that NK4 inhibited the migration of AMC-HN-8 cells.

2.5 Effect of the NK4 Gene on LSCC AMC-HN-8 Cell Apoptosis

Apoptosis of the cells in each group was detected by flow cytometry after annexin V-FITC and PI double staining. The results are shown in **Figures 4A–G**. The cell apoptosis rates in the NK4 group at 24 h, 48 h, and 72 h were 15.99% ± 2.83%, 37.37% ± 5.29%, and 69.21% ± 9.13%, respectively, which were all higher than those in the control group; the differences were statistically significant. The NK4 gene can promote AMC-HN-8 cell apoptosis.

2.6 Effect of the NK4 Gene on the Cell Cycle of LSCC AMC-HN-8 Cells

The flow cytometry results (**Figures 4H–J**) showed that the proportion of cells in G_1 phase in the NK4 group (65.78% ± 3.24%) was lower than that in the control group (74.98% ± 3.20%) and that the proportion of cells in S phase (29.77% ± 3.29%) was higher than that in the control group (21.41% ± 3.96%); the differences were statistically significant (P<0.01). The proportions of cells in G_2/M phases were 4.43% ± 0.72% and 3.58% ± 1.01%, respectively; the differences were not statistically significant

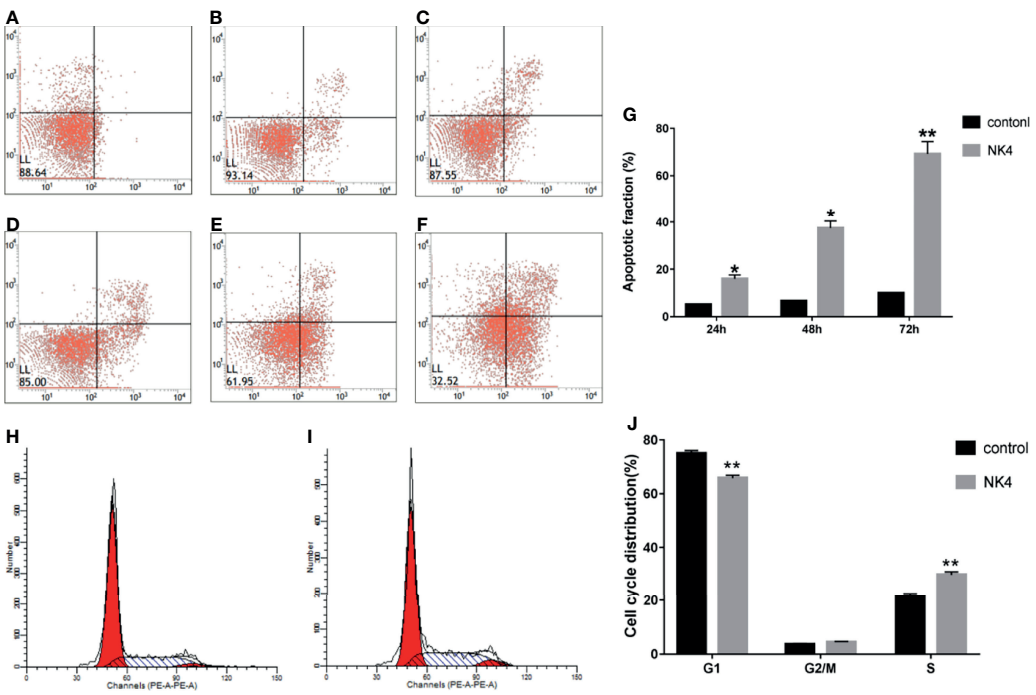

FIGURE 4 | **(A)** 24h control group; **(B)** 48h control group; **(C)** 72h control group; **(D)** 24h NK4 group; **(E)** 48h NK4 group; **(F)** 72h NK4 group; **(G)** Apoptosis rate of NK4 group at 24h, 48h, 72h; **(H)** Percentage of cells in each cell cycle phase (control group); **(I)** Percentage of cells in each cell cycle phase (NK4 group); **(J)** Percentage of cells in each cell cycle phase *P < 0.05 **P < 0.01.

(P>0.05). These results indicated that the NK4 gene induce S phase arrest.

2.7 Tumor Volume Growth Curve of Transplanted Tumor in Nude Mice

Subcutaneous nodules can be seen 5 days after inoculation. 1 animal in the control group died on the 20th day, and 14 mice remained; all 15 nude mice in the treatment group survived. The tumor volume was measured, recorded and calculated every 3 days, and the growth curve was drawn. The results showed that the subcutaneous tumor volume in the treatment group was smaller than that in the control group, and the difference between the two groups was significant (P<0.05), as shown in **Figure 5**.

2.8 Western Blot Method to Detect Protein Expression in Tumor Tissues of Nude Mice

Western blot method was used to detect the expression of various proteins in the tumors of the nude mice in the negative control group and the treatment group. The expressions of DKK1(35kD) increased, Wnt1(41kD) and β-Catenin(92kD) protein in the tumor tissues of the treatment group were significantly reduced, as shown in **Figure 6**.

3 DISCUSSION

At present, surgery is the major treatment strategy for laryngeal cancer. Most gene-targeted therapies for laryngeal cancer are at the experimental exploration stage. For patients with advanced laryngeal cancer, accompanying serious complications affect the prognosis; therefore, it is urgent to explore new auxiliary methods for treating laryngeal cancer. Gene-targeted therapy for tumors aims to limit the inhibitory effect of genes on specific target cells, tissues or organs, so as to increase gene sensitivity, improve curative effects and reduce side effects. The HGF/c-Met receptor pathway plays a role in tumor growth, metastasis, invasion, and angiogenesis (5). NK4 is a competitive antagonist isolated from HGF, consisting of an n-terminal domain and 4 kringle domains, and can counteract the association between HGF and c-Met. NK4 not only acts like an antagonist, inhibiting HGF/c-Met induced tumor growth, metastasis and invasion, but also inhibits vascular endothelial growth factor (VEGF) - and basic fibroblast growth factor (bFGF)-induced tumor angiogenesis, which is independent of the HGF/c-Met pathway, and ultimately causes the tumor cell apoptosis. NK4 gene therapy can inhibit growth, invasion, metastasis and angiogenesis in a variety of tumors, including breast cancer, prostate cancer, colon cancer, mesothelioma, lung cancer, pancreatic cancer and brain cancer (6). In experimental models of different cancers, NK4 gene therapy inhibited the activation of the Met receptor, which is related to the inhibition of tumor invasion and metastasis. Similarly, NK4 gene therapy inhibited tumor angiogenesis and thereby inhibited angiogenesis-dependent tumor growth. The NK4 gene deserves further research and attention as a potential cancer treatment target. Sawatsubashi et al. (7) used immunohistochemistry to study the pathological tissues of 82 cases of laryngeal cancer and found that HGF/c-Met was highly expressed in laryngeal squamous cell carcinoma, and the high expression of HGF/c-Met was positively correlated with the degree of lymph node metastasis. The research results of Haddad et al. (8) are consistent with their research results. Yucel et al. (9) found in a study of 60 cases of supraglottic carcinoma (including 30 cases of cervical lymph node metastasis) that 90% of tumors were High expression of c-Met; c-Met is highly expressed in 83% of metastatic lymph nodes. Choe J Y et al. (10) confirmed that the high expression of C-Met is related to the primary site of the tumor; the hypopharynx has the highest expression, followed by the oral cavity, pharynx and nasal cavity. Squamous cell carcinoma expresses c-Met more frequently than undifferentiated carcinoma. Jiang M et al. (11) used immunohistochemical methods to detect c-Met protein in 71 cases of primary laryngeal carcinoma. The expression rate of

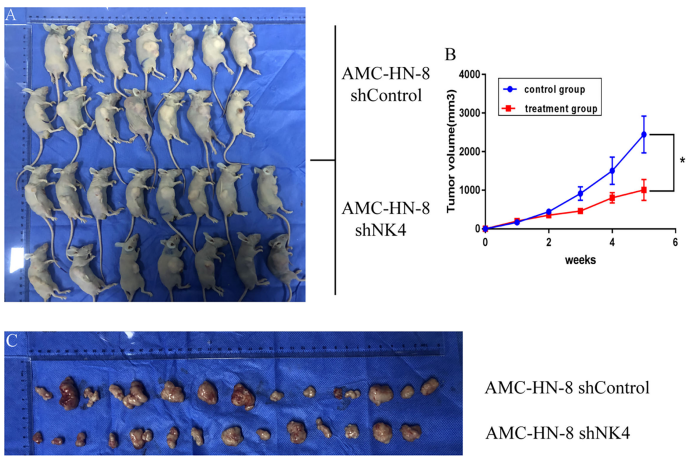

FIGURE 5 | **(A)** Tumor formation in nude mice; **(B)** Growth curve of transplanted tumor; **(C)** Change in volume and size of transplanted tumor. *P < 0.05.

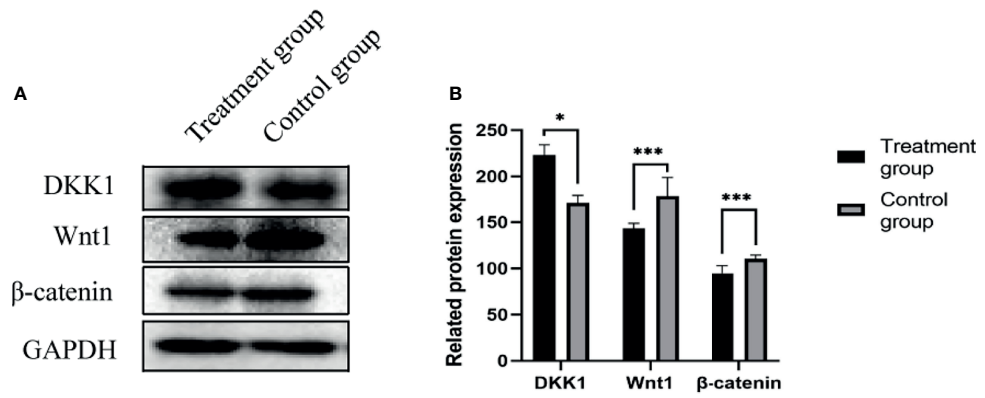

FIGURE 6 | **(A)** DKK1, Wnt1, β-Catenin protein expression band; **(B)** DKK1, Wnt1, β-Catenin protein expression level. *P < 0.05, ***P < 0.001.

c-Met in glottic squamous cell carcinoma of laryngeal carcinoma was 69.0%. There were patients with high c-Met expression. The tendency of the tumor to recur. In summary, the above studies have confirmed that the expression of HGF/c-Met in both serology and histology is an important factor affecting the occurrence and development of laryngeal squamous cell carcinoma, and is related to the pathological staging, disease prognosis, and survival rate of patients with laryngeal carcinoma. There is a correlation in such aspects. It can be inferred from this that NK4 antagonizes HGF/c-Met may inhibit the proliferation of laryngeal cancer cells and the formation of lymph vessels and microvessels in laryngeal cancer tissues, and block the occurrence, development and lymph node metastasis of laryngeal cancer.

This study used an attenuated Salmonella strain carrying the NK4 gene to transfect the LSCC cell line AMC-HN-8 to further investigate the effect of NK4 on the biological functions of AMC-HN-8 cells *in vitro*. NK4 gene delivery was mediated by the attenuated Salmonella vector. The attenuated Salmonella strain carrying the NK4 gene was successfully transfected into the LSCC AMC-HN-8 cells. Clinical common gene vectors include viral vectors, bacterial vectors and some non-bacterial vectors. Cai et al. (12) used bone marrow mesenchymal stem cells (BMSCs) as a vector for the NK4 gene and confirmed that NK4 gene-modified BMSCs can inhibit the growth, metastasis, and angiogenesis of liver cancer cells. BMSCs have the ability to migrate to tumor sites and integrate into the tumor vascular wall, with low immunogenicity. Adenovirus-mediated NK4 gene therapy can inhibit the mesothelioma cancer stem-like cells (13). Adenoviral NK4 (Ad-NK4) can effectively inhibit the activity, invasiveness and tumorigenicity of human multiple myeloma (MM) cells (14). NK4 expression can significantly decrease the activity of Met and AKT and inhibit the activity, invasiveness, and tumorigenicity of MM cells. These results are consistent with the previously reported effects of NK4. Currently, attenuated Salmonella strains are the most widely studied. Attenuated Salmonella strains are safe, invasive and tumor-targeting vectors for antitumor gene delivery (15), and the use of attenuated Salmonella strains carrying interleukin (IL)-2 (16), Fas ligand (FasL), IL-18 (17) and fms-like tyrosine kinase 3 (FLT3) ligand (18) led to great progress in antitumor research. In recent years, the attenuated Salmonella TPIN carrying NK4/IL-2, prepared by Professor Xiaoqin Ha, was shown to efficiently transfect tumor cells *in vitro* to express the target proteins IL-2 and NK4, and the expression products inhibited HepG2 cell proliferation and migration and inhibited the formation of vessels in chick chorioallantoic membrane. It was already used for the treatment of liver cancer (19) and its inhibitory effect was confirmed.

This study showed that an attenuated Salmonella strain carrying NK4 was successfully transfected into LSCC AMC-HN-8 cells. With increasing transfection time, the number of cells decreased, and the morphology of cells changed, indicating that the NK4 gene can affect the proliferation of AMC-HN-8 cells. QRT-PCR was used to detect the expression of the NK4 gene in AMC-HN-8 cells 24 and 48 h after transfection. The results showed that NK4 was highly expressed in AMC-HN-8 cells. MTT assay results confirmed that the NK4 gene affected cell proliferation. Given that in 24 hours the cells round up, cells die at 48 hours the inhibition of cell migration could be an indirect result of the cell death. In fact, in our experiment in order to shun the disturbing to cell migration caused by inhibited or dead cells, in the scratch assay the equal number of viable cells were used in Control group and NK4 group, respectively, and the viable cells were counted by typan blue exclusion. MTT test results showed that the expression products of the transfected cells significantly inhibited the proliferation activity of AMC-HN-8 cells in a percentage dependent manner with statistical difference. The NK4 gene is considered to inhibit cell proliferation. Studies have shown (20) that NK4 is used in the treatment of prostate cancer, The mechanism by which NK4 promotes apoptosis in DU145 cells maybe its inhibitory effect on HGF-induced proliferation, leading to increased apoptosis. The antitumor effect of NK4 on DU145cells was specific for the HGF signal. Activation of Ras/ERK/MAPK (mitogen-activated protein

kinase) changes the expression/activation of cell cycle regulators that affect cell proliferation. Activator that control cell migration and invasion, whereas PI3K/Akt activation by HGF mediates cell survival and resistance to apoptosis (21). NK4 gene is believed to inhibit the proliferation of laryngeal cancer cells. The possible mechanism is consistent with the above-mentioned studies, which promotes cell apoptosis and inhibits cell proliferation. The scratch assay results showed that at 72 h after transfection, the cells on either side of the scratch in the control group were close to each other, while the scratch in the transfection group was still wide, suggesting that the NK4 gene had an inhibitory effect on the migration of AMC-HN-8 cells. The inhibition of cell proliferation is known to be associated with the induction of apoptosis and cell cycle arrest. In this study, flow cytometry was used, and the results showed that the NK4 gene affected apoptosis and induced S phase arrest in AMC-HN-8 cells at 48 h after transfection. We found that NK4 inhibited the proliferation of AMC-HN-8 cells and induced apoptosis through S phase arrest. This is inconsistent with the results of previous studies showing that NK4 induces growth inhibition in other types of cells by causing G_1 phase arrest (14, 22). Preliminary *in vivo* experimental studies confirmed the effect of NK4 gene on the proliferation, migration and apoptosis of laryngeal cancer cells, and further *in vivo* experiments to explore its mechanism. We established a nude mouse model of laryngeal cancer and observed the tumor volume changes in nude mice after gavage treatment with attenuated Salmonella carrying the NK4 gene. The results showed that after treatment, the tumor volume in the treatment group was smaller than that in the control group. In this study, we used oral gavage to investigate whether Salmonella strains containing the NK4 gene can inhibit the growth of laryngeal cancer cells in nude mice. The main reason is that pre-tumor gene vaccine is the most effective biological treatment method at this stage. Attenuated Salmonella has the unique advantage of delivering therapeutic genes in tumor treatment and has become a hot spot for tumor gene vaccine research. The virulence gene mutations of Salmonella are induced through physical, chemical, genetic engineering and other techniques to obtain attenuated Salmonella that maintain invasiveness. Because its preparation method is mature, easy to expand, and stable in nature, oral administration does not affect the therapeutic effect, and it can be inoculated into tumor patients and animals on a large scale. Attenuated Salmonella mediated the target gene expression *in vivo* with high efficiency; specific aggregation in target tumor tissues and cells shows targeting; it can stimulate the body to quickly respond to the corresponding cells and humoral. Attenuated Salmonella can be used as a therapeutic gene carrier and its expression in tissues is highly targeted. Since this bacterium itself is an intestinal parasite, the amount of expression in the digestive tract can meet the needs of treatment. The experimental conclusion is consistent with the study of Theys, Sznol et al (19, 23, 24). By Western blot Method to detect the expression of DKK1 increased, Wnt1 and β-Catenin protein in tumor tissues are reduced, and previous studies have confirmed that the Wnt1/β-catenin signaling pathway is abnormally activated in a variety of human malignant tumors, and promotes tumor invasion and metastasis. The Wnt/β-catenin signaling pathway is involved in various key cell functions, such as stem cell regeneration and organogenesis (25). In various types of malignant tumors, including breast, lung, and hematopoietic system, Wnt activation has been found, and it has been proven to help tumor recurrence (26). When the Wnt ligand binds to the Frizzled (Frizzled, Fz)/low density lipoprotein-related receptor protein (LRP5/6) complex, the activity of destroying the complex is inhibited, and β-catenin in the cytoplasm is stabilized and continuously Accumulate, translocate to the nucleus after reaching a certain concentration and combine with the transcription factor T cytokine factor 4 (TCF4)/ lymphatic enhancer factor 1 (LEF1) to recruit different nuclear regulatory factors, thereby activating the expression of related genes downstream of the Wnt pathway to generate various types of Inflammatory mediators and fibrotic factors induce disease (27, 28). The activation of this pathway is related to a variety of chronic kidney disease, cancer, osteoporosis, degenerative diseases, etc. (29). It has also been confirmed in head and neck tumors that Wnt/β-catenin signaling can accelerate the tumor progression of nasopharyngeal carcinoma and esophageal squamous cell carcinoma (30). Therefore, inhibition of Wnt/β-catenin signaling pathway may be used as a kind of laryngeal cancer. In addition, DKK1 gene can be activated by competitively binding to LRP5/6 receptors to negatively regulate Wnt protein-mediated signal transduction. This experiment confirms that NK4 gene the anti-tumor effect may be related to the regulation of DKK1/Wnt/β-Catenin related pathways, but further experiments are needed to prove this conclusion.

In summary, NK4 can inhibit the proliferation and migration of AMC-HN-8 cells, induce the cell cycle S phase arrest, and has a significant impact on cell apoptosis. *In vivo* experiments have also confirmed that NK4 inhibits tumor formation in nude mice, and it may be related to the regulation of DKK1/Wnt1/β-Catenin related pathways. Therefore, the NK4 gene can be used as a new target for the treatment of laryngeal cancer. The limitation of this study is that the mechanism that the NK4 gene affects the occurrence and development of laryngeal cancer may be related to the regulation of the DKK1/Wnt1/β-Catenin related pathways, which needs to be demonstrated by further experiments. In follow-up experiments, we will further explore how the NK4 gene plays a specific role in laryngeal cancer, laying a solid theoretical foundation for the research and preparation of effective anti-tumor biologic drugs.

DATA AVAILABILITY STATEMENT

The original contributions presented in the study are included in the article/supplementary materials. Further inquiries can be directed to the corresponding author.

ETHICS STATEMENT

The animal study was reviewed and approved by the Ethics Committee of Gansu Provincial People's Hospital.

AUTHOR CONTRIBUTIONS

SZ is responsible for the conduct of the experiment and the writing of the paper, HW is responsible for guiding the conduct of the experiment and the writing of the thesis, XH is responsible for guiding the conduct of the experiment and the writing of the thesis, YZ is responsible for assisting in the conduct of the experiment and the writing of the paper, YG is responsible for guiding the conduct of the experiment and the writing of the thesis. All authors contributed to the article and approved the submitted version.

FUNDING

Science and Technology Plan Project of Gansu Province 20JRIORA367.

REFERENCES

1. Bray F, Ferlay J, Soerjomataram I, Siegel RL, Torre LA, Jemal A. Global Cancer Statistics 2018: GLOBOCAN Estimates of Incidence and Mortality Worldwide for 36 Cancers in 185 Countries. *CA: Cancer J Clin* (2018) 0:5–31. doi: 10.3322/caac.21492
2. Huang Y, Liu L, Liu A. Dickkopf-1: Current Knowledge and Related Diseases. *Life Sci* (2018) 209:249–54. doi: 10.1016/j.lfs.2018.08.019
3. Igbinigie E, Guo F, Jiang SW, Kelleya C, Jinping L. Dkk1 Involvement and Its Potential as a Biomarker in Pancreatic Ductal Adenocarcinoma. *Clinica Chimica Acta* (2019) 488:226–34. doi: 10.1016/j.cca.2018.11.023
4. Shoukai Z, Jian H, Xudong W, Danru L. The Clinical Value of DKK1 in Head and Neck Squamous Cell Carcinoma and Its Regulatory Factors Analysis. *Chin J Cancer Biother* (2020) 154(07):86–92. 27. doi: 10.3872/j.issn.1007-385x.2020.07.012
5. Takeuchi S, Wang W, Li Q, Yamada T, Kita K, Donev IS. Dual Inhibition of Met Kinase and Angiogenesis to Overcome HGF-Induced EGFR-TKI Resistance in EGFR Mutant Lung Cancer. *Am J Pathol* (2012) 181(3):1034–43. doi: 10.1016/j.ajpath.2012.05.023
6. Nakamura T, Sakai K, Matsumoto K. Anti-Cancer Approach With NK4: Bivalent Action and Mechanisms. *Anticancer Agents Med Chem* (2010) 10:36–46. doi: 10.2174/1871520611009010036
7. Sawatsubashi M, Sasatomi E, Mizokami H, Tokunaga O. Expression of C-Met in Laryngeal Carcinoma. *Virchows Arch* (1998) 432(4):331–5. doi: 10.1007/s004280050174
8. Haddad R, Lipson K E, Webb CP. Hepatocyte Growth Factor Expression in Human Cancer and Therapy With Specific Inhibitors. *Anticancer Res* (2001) 216:4243–52. doi; 10.1097/00001813-200111000-00011
9. Yucel O T, Sungur A, Kaya S. C-Met Overexpression in Supraglottic Laryngeal Squamouscell Carcinoma and Its Relation to Lymphnode Metastases. *Otloaryngol Head Neck Surg* (2004) 130(6):698–703. doi: 10.1016/j.otohns.2003.09.031
10. Choe JY, Yun JY, Nam S-J, Kim JE. Expression of C-Met is Different Along the Location and Associated With Lymph Node Metastasis of Head and Neck Carcinoma. *Korean J Pathol* (2012) 46:515–22. doi: 10.4132/KoreanJPathol.2012.46.6.515
11. Jiang M, Zhang H, Xiao He, Zhang Zm, Que D, Luo J, et al. High Expression of C-Met and EGFR Is Associated With Poor Survival of Patients With Glottic Laryngeal Squamous Cell Carcinoma. *Oncol Lett* (2018) 15(1 Pt.B):931–9. doi: 10.3892/ol.2017.7356
12. Chao C, Hou L, Zhang J, Zhao D, Wang Z, Hu H, et al. Author Correction: The Inhibitory Effect of Mesenchymal Stem Cells With Rad-NK4 on Liver Cancer. *Appl Biochem Biotechnol* (2018) 185(1):1–1. doi: 10.1007/s12010-018-2748-9
13. Deng XB, Xiao L, Wu Y, Jin F, Mossman B, Testa JR, et al. Inhibition of Mesothelioma Cancer Stem-Like Cells With Adenovirus-Mediated NK4 Gene Therapy. *Int J Cancer* (2015) 137(2):481–90. doi: 10.1002/ijc.29391
14. Que W, Liu H, Yang Q, Xu S. NK4 Inhibits the Proliferation and Induces Apoptosis of Human Rheumatoid Arthritis Synovial Cells. *Cell Biochem Funct* (2018) 36(5):1–7. doi: 10.1002/cbf.3339
15. Witherell G. Oral Typhoid Vaccine.Acambis/Berna. *Curr Opin Investig Drugs* (2003) 4(8):1010–8.
16. Sorenson BS, Banton KL, Frykman N L, Leonard AS, Saltzman DA. Attenuated Salmonella Typhimurium With IL-2 Gene Reduces Pulmonary Metastases in Murine Osteosarcoma. *Clin Orthop Relat Res* (2008) 466 (6):1285–91. doi: 10.1007/s11999-008-0243-2
17. Loeffler M, Le'Negrate G, Krajewska M, Reed JC. Attenuated Salmonella Engineered to Produce Human Cytokinelight Inhibit Tumor Growth. *Proc Natl Acad Sci* (2007) 104(31):12879–83. doi: 10.1073/pnas.0701959104
18. Yoon WS, Choi WC, Sin JI, Park YK. Antitumor Therapeutic Effects of Salmonella Typhimurium Containing Flt3 Ligand Expression Plasmids in Melanoma-Bearing Mouse. *Biotechnol Lett* (2007) 29(4):511–6. doi: 10.1007/s10529-006-9270-9
19. Hongyan F, Xiaoqin H, Shangdi Z, Zhihua Y, Yuejuan S, Xiaoyun L, et al. Effect of TPIN on the Biological Characteristics of Hepg2 Liver Cancer Cells. *Med J Chin People's Lib Army* (2014) 7):39–42. doi: 10.3969/j.issn.2095-140X.2014.07.010
20. Yue D, Wang Y, Ma P, Li Y-Y, Chen H, Wang P, et al. Effects of Transferred NK4 Gene on Proliferation, Migration, Invasion and Apoptosis of Human Prostate Cancer DU145 Cells. *Asian J Androl* (2010) 12(003):381–9. doi: 10.1038/aja.2010.22
21. Birchmeier C, Birchmeier W, Gherardi E, Vande Woude GF. Met, Metastasis, Motility and More. *Nat Rev Mol Cell Biol* (2003) 4:915–25. doi: 10.1038/nrm1261
22. Ge X, Wang Y, Wang Y, Li Q, Yu H, Miao L. NK4 Gene Therapy Inhibits HGF/Met-Induced Growth of Human Cholangiocarcinoma Cells. *Dig Dis Sci* (2013) 58(6):1636–43. doi: 10.1007/s10620-012-2523-7
23. Theys J, Barbé S, Landuyt W, Nuyts S, Mellaert L, Wouters B, et al. Tumor-Specificgene Delivery Using Genetically Engineered Bacteria. *Curr Gene Ther* (2003) 3(3):207–21. doi: 10.2174/1566523034578357
24. Sznol M, Lin SL, Bermudes D, et al. Use of Preferentially Replicating Bacteria for the Treatment of Cancer. *J Clin Invest* (2000) 105(8):1027–30. doi: 10.1172/JCI9818
25. Colozza G, Koo BK. Wnt/β-Catenin Signaling: Structure, Assembly and Endocytosis of the Signalosome. *Dev Growth Differ* (2021) 63(3):199–218. doi: 10.1111/dgd.12718
26. Krishnamurthy N, Kurzrock R. Targeting the Wnt/Beta-Catenin Pathway in Cancer: Update on Effectors and Inhibitors. *Cancer Treat Rev* (2018) 62:50–60. doi: 10.1016/j.ctrv.2017.11.002
27. Bian J, Dannappel M, Wan C, Firestein R. Transcriptional Regulation of Wnt/β-Cateninpathway in Colorectal Cancer. *Cells* (2020) 9(9):2125. doi: 10.3390/cells9092125
28. Huffstater T, Merryman WD, Gewin LS. Wnt/β-Catenin in Acute Kidney Injury and Progression to Chronic Kidney Disease. *Semin Nephrol* (2020) 40 (2):126–37. doi: 10.1016/j.semnephrol.2020.01.004
29. Nusse R, Clevers H. Wnt/β-Catenin Signaling, Disease, and Emerging Therapeutic Modalities. *Cell* (2017) 169(6):985–99. doi: 10.1016/j.cell.2017.05.016
30. Jiang R, Niu X, Huang Y, Wang X. β-Catenin Is Important for Cancer Stem Cell Generation and Tumorigenic Activity in Nasopharyngeal Carcinoma. *Acta Biochim Et Biophys Sin* (2016) 48(003):229–37. doi: 10.1093/abbs/gmv134

Conflict of Interest: The authors declare that the research was conducted in the absence of any commercial or financial relationships that could be construed as a potential conflict of interest.

this article, or claim that may be made by its manufacturer, is not guaranteed or endorsed by the publisher.

frontiers in Oncology

ORIGINAL RESEARCH
published: 27 January 2022
doi: 10.3389/fonc.2022.761428

A Retrospective Analysis of a Cohort of Patients Treated With Immune Checkpoint Blockade in Recurrent/ Metastatic Head and Neck Cancer

Michel Bila[1,2,3], Jeroen Van Dessel[1], Maximiliaan Smeets[1], Vincent Vander Poorten[4,5], Sandra Nuyts[6], Jeroen Meulemans[4,5] and Paul M. Clement[2,3]*

[1] Oral and Maxillofacial Surgery, University Hospitals Leuven and OMFS-IMPATH Research Group, Department of Imaging & Pathology, Faculty of Medicine, KU Leuven, Leuven, Belgium, [2] Department of Oncology, KU Leuven, Leuven, Belgium, [3] Department of General Medical Oncology, Leuven Cancer Institute, University Hospitals Leuven, Leuven, Belgium, [4] Otorhinolaryngology Head and Neck Surgery, University Hospitals Leuven, Leuven, Belgium, [5] Department of Oncology, Section Head and Neck Oncology, KU Leuven, Leuven, Belgium, [6] Radiation Oncology, Department of Oncology, Leuven Cancer Institute, University Hospitals Leuven, Leuven, Belgium

OPEN ACCESS

Edited by:
Pablo Parente-Arias, A Coruña University Hospital Complex (CHUAC), Spain

Reviewed by:
Khalil Saleh, Gustave Roussy Cancer Campus, France
Angeles Mercedes Oviedo Santos, University Hospital of Gran Canaria Dr. Negrin, Spain

***Correspondence:**
Michel Bila
michel.bila@uzleuven.be

Specialty section:
This article was submitted to Head and Neck Cancer, a section of the journal Frontiers in Oncology

Received: *19 August 2021*
Accepted: *03 January 2022*
Published: *27 January 2022*

Citation:
Bila M, Van Dessel J, Smeets M, Vander Poorten V, Nuyts S, Meulemans J and Clement PM (2022) A Retrospective Analysis of a Cohort of Patients Treated With Immune Checkpoint Blockade in Recurrent/ Metastatic Head and Neck Cancer. Front. Oncol. 12:761428. doi: 10.3389/fonc.2022.761428

Objective: The treatment approach of recurrent or metastatic head and neck squamous cell carcinoma (R/M HNSCC) has long been similar for all patients. Any difference in treatment strategy was only based on existing comorbidities and on preferences of the patient and the treating oncologist. The recent advance obtained with immune therapy and more specifically immune checkpoint blockade (ICB) has been a true game changer. Today, patients and physicians have a choice to omit chemotherapy. In a small subset of patients, ICB induces a very durable disease control. The subgroup of patients in which ICB without chemotherapy would be the preferential approach is still ill-defined. Yet, this evolution marks a major step towards a more personalized medicine in R/M HNSCC.

Materials and Methods: In this paper, we present a retrospective cohort study of a patient population that was treated with ICB in a single center and we analyze potential factors that are associated with outcome and may help to select patients for treatment with ICB.

Results: 137 consecutively treated patients were identified. Male gender and metastatic disease appeared to be associated with improved overall survival (OS). There was no correlation observed with age, number of previous treatment lines or immune target.

Conclusion: Along with PD-L1 status defined by Combined Positive Score (CPS), clinical parameters such as site of recurrence and gender may help to define the optimal treatment strategy in R/M HNSCC.

Keywords: mouth neoplasms, head and neck neoplasms, squamous cell carcinoma of head and neck (HNSCC), immunotherapy, immune checkpoint inhibitors, programmed cell death 1 (PD-1), Programmed death-ligand 1 (PD-L1), cytotoxic t-lymphocyte-associated protein 4 (CTLA-4)

INTRODUCTION

The treatment with curative intent of squamous cell carcinoma of the head and neck (HNSCC) has historically been based on surgery and radiation therapy. In recurrent or metastatic disease, platinum-based combination chemotherapy has long been the standard approach for treatment with palliative intent. In the absence of a proven survival benefit, the treatment choice was tailored mainly on comorbidity, costs and individual preferences. The first trial that showed an extra survival benefit in recurrent or metastatic squamous cell carcinoma of the head and neck (R/M HNSCC) introduced the addition of cetuximab to platinum-based chemotherapy (1). Although cetuximab, a monoclonal antibody against epidermal growth factor receptor (EGFR), is defined as a "targeted therapy", its use has not been restricted to tumors with proven expression of the target, because the vast majority of squamous cell carcinomas of the head and neck is characterized by EGFR amplification (2).

As a consequence, this so-called "EXTREME regimen" has emerged as the standard of care in R/M HNSCC for patients who could tolerate this treatment (3). More recently, immune checkpoint blockade (ICB) has also emerged as a valuable treatment option. The first solid evidence was provided by a randomized trial that showed superiority of the PD-1 antibody nivolumab over best investigator's choice, in a patient population that had been pretreated with cisplatin (4). Interestingly, the trial not only showed an improvement in median overall survival but was also associated with a better quality of life. Furthermore, it is important to highlight that the long-term survival rate in patients treated with nivolumab was substantially higher than in the control group. This observation is very important, because a substantial improvement in the chance to be alive after two years is clearly more relevant than an average two-month gain in survival probability. Subsequently, another PD-1 antibody, pembrolizumab, has shown similar survival statistics in platinum-pretreated R/M HNSCC, albeit without a statistically significant difference in overall survival compared to chemotherapy. The latter observation is probably due to a substantial subgroup that crossed over to immune therapy from the control group (5). Comparable findings have been reported with the PD-L1 antibody durvalumab, again without a proven benefit over standard of care (6). The addition of the CTLA4-antibody tremelimumab showed no extra added value in that trial.

Pembrolizumab was tested in first line R/M HNSCC, either as single agent or in combination with platinum/5FU, and compared to the standard of care, the EXTREME regimen (7). This trial showed a clearly superior outcome when pembrolizumab was combined with platinum/5FU compared to cetuximab combined with this chemotherapy doublet. Yet, this trial also showed that the chance of benefit was related with the PD-L1 status, calculated as a Combined Positive Score (CPS). Indeed, patients treated in both pembrolizumab-containing arms had a better survival compared to control, if CPS was greater than 1. Although an exact algorithm cannot be defined yet, the possibility to omit chemotherapy has risen, and with that, a giant step towards a more personalized approach in the treatment of this disease.

Next to PD-L1 status, other factors have been proposed that could influence the success of immunotherapy and may help tailoring our choice of treatment. A single-arm phase II study with durvalumab suggests a better prognosis in human papillomavirus-(HPV-) positive squamous cell carcinoma in a PD-1 positive cohort (8). It is hypothesized that HPV may induce a better antigen-presentation and thus enhance the ability of the immune system to target the tumor. Similarly, the cytotoxic effect of chemo- or radiotherapy may also induce more tumor epitopes. This idea has revived the concept of abscopal effects of radiation therapy. The combined use of radiotherapy and checkpoint inhibition is currently being explored in several trials (9).

In this manuscript we provide data that may help to select the best approach for patients presenting with R/M HNSCC. To this purpose we have retrospectively analyzed our own patient cohort with R/M HNSCC for significant factors that may influence treatment decisions or guide future research.

MATERIALS AND METHODS

Study Design and Patient Selection

A retrospective cohort study design was completed following the Strengthening the Reporting of Observational Studies in Epidemiology (STROBE) guidelines (10). The study was approved by the Medical Ethics Committee of the University Hospitals Leuven, Leuven, Belgium. The study sample was derived from a population who presented for immunotherapy of R/M HNSCC at the Department of General Medical Oncology of the University Hospitals Leuven from December 2013 to February 2020. Eligible patients were 18 years of age or older with histologically confirmed diagnosis of R/M HNSCC, not amenable to curative therapy. Patients received a single agent and fixed dose of either PD1, PDL-1 with or without CTLA-4 inhibitors. The number of prior treatments was not a limiting factor for inclusion. Performance status was not a formal selection criterion for ICB treatment in our standard of care practice. Patients who received concurrent chemotherapy or biological therapy were excluded.

Outcome Parameters

The primary endpoint was overall survival, defined as the time from start of immunotherapy to death due to any cause. Secondary endpoints included overall response rate, progression-free survival, duration and time of response. Tumor response [complete (CR), partial (PR), stable disease (SD) or progression of disease (PD)] was evaluated by Computed Tomography or Magnetic Resonance Imaging. These modalities were not standardized at predefined time points in this patient cohort, but patients had imaging at least every 3 months. Progression-free survival was defined as the time from therapy onset to first documented disease progression according to the Response Evaluation Criteria in Solid Tumors 1.1 (RECIST1.1) criteria (11), evident clinical progression or death due to any cause, whichever occurred first. Duration of response was defined as the time from the first RECIST response until disease progression in patients who achieved a partial or complete

response. Time to response was defined as the time from start of immunotherapy to CR or PR.

Statistical Analysis

The statistical analyses are based on a 24-month data cut-off. The distributions of overall survival and progression-free survival were estimated by the Kaplan-Meier method and compared by means of log-rank tests for therapeutic modality (PD-L1, PD1, CTLA-4 + PD-L1), gender (male, female), age (≤ 65, > 65 years), tumor type (metastatic, locoregional recurrence) and line of palliative treatment (first, second or more) for the entire patient group. The distribution of overall survival for subsequent salvage chemotherapy (yes, no) was calculated on the subgroup of patients with tumor progression after ICB treatment. Cox proportional-hazards models were used to univariately estimate HR and calculate corresponding 2-sided 95% CI's. Statistical analysis was performed in SPSS (IBM, New York, USA). The significance level α was 0.05 for all tests.

RESULTS

Patient Characteristics

The data cut-off date was 13 July 2020, 6 months after the last patient began treatment. The study sample included 137 patients in the final analysis. Twenty-six patients (19%) were still on treatment or were in follow-up at the time of analysis. Two patients (1%) were lost to follow-up. 76% of patients received a PD-1 inhibitor, 15% received a PD-L1 inhibitor and 9% received a PD-L1 inhibitor combined with CTLA-4 inhibitor. The median age was 64 years (range 31 – 84 years), and 78% of patients were male. The majority of patients were either current (56%) or former smokers (41%). Oral cavity was the primary location in most patients (45%), followed by pharynx (34%), larynx (16%) and other anatomical sites in the head and neck region (5%). Patterns of recurrence comprised exclusive locoregional recurrence in 66 patients (48%) and distant metastases with or without locoregional recurrence in 71 patients (52%). Ninety patients (66%) received two or more consecutive lines of systemic therapy for R/M HNSCC and thirty-nine patients (33%) received subsequent salvage chemotherapy after tumor progression under ICB treatment.

Efficacy

The Kaplan-Meier estimate of median overall survival was 9.0 months [95% Confidence Interval (CI) 6.9-11.0] in the entire patient group (**Figure 1A**). Patient survival at 6, 12 and 24 months was 64%, 39% and 16%, respectively. The median progression-free survival was 3.7 months (95% CI 2.9-4.4) for the whole patient group (**Figure 1B**). The proportion of patients with progression-free survival was 31% at 6 months, 10% at 12 months and 4% at 24 months. Median follow-up duration was 28 months (interquartile range (IQR) 17-37 months).

The median progression-free and overall survival for predefined demographic and clinical subgroups is shown in **Table 1**. Overall survival was significantly longer in men compared to women (HR = 0.59; 95% CI 0.38 – 0.91; p = 0.02) (**Figure 2B**), and in metastatic tumors compared to locoregionally recurrent HNSCC (HR = 0.68; 95% CI 0.46 – 0.99; p = 0.05) (**Figure 2E**). Patients who progressed under ICB treatment and subsequently received chemotherapy showed a significant longer overall survival (HR = 0.35; 95 CI 0.23 – 0.53; p = 0.001) compared to patients without administration of subsequent salvage therapy (**Figure 2F**).

No significant differences were observed with regard to the overall survival between the age groups at the cut-off of 65 years (HR = 0.89; 95% CI, 0.61 - 1.30; p = 0.55) (**Figure 2A**), between the targets PD-1 and PD-L1 + CTLA-4 (HR = 0.99; 95% CI, 0.54 - 1.81; p = 0.99), between the targets PD-1 and PD-L1 (HR = 1.11; 95% CI, 0.65 – 1.89; p = 0.71) (**Figure 2C**), and between first line of palliative treatment versus second line or more (HR =0.96; 95% CI, 0.65 - 1.43; p = 0.85) (**Figure 2D**).

Progression-free survival was significantly longer in men compared to women (HR = 0.63; 95% CI 0.40 - 0.98; p = 0.04) (**Figure 3B**). There were no significant differences found with regard to the progression-free survival between age groups below or above 65 (HR = 1.13; 95% CI, 0.78 - 1.63; p = 0.49) (**Figure 3A**),

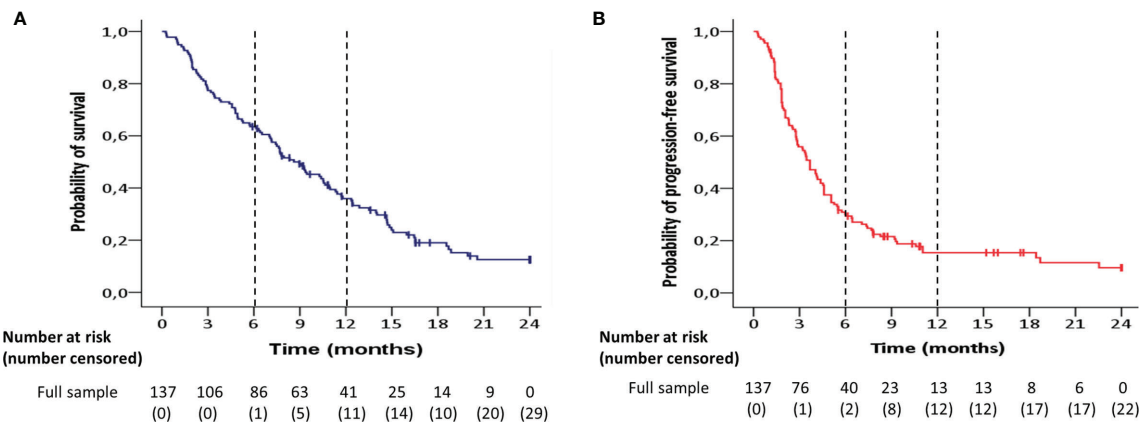

FIGURE 1 | Kaplan-Meier estimates of **(A)** overall survival and **(B)** progression-free survival for the entire patient group (n=137).

TABLE 1 | Overall survival (OS) and progression-free survival (PFS) according to predetermined demographic and clinical subgroups under immune checkpoint blockade treatment.

Variable		Patients	Median OS	Median PFS
		no. (%)	*months (95% CI)*	*months (95% CI)*
All patients		137 (100%)	9.0 (6.9 - 11.0)	3.7 (2.9 - 4.4)
Age	≤ 65 years old	59 (43%)	9.3 (6.8 - 11.8)	3.2 (2.3 - 4.1)
	> 65 years old	78 (57%)	7.7 (5.3 - 10.0)	4.6 (3.3 - 5.9)
Gender	Male	107 (78%)	10.3 (8.6 - 12.0)	4.0 (3.2 - 4.9)
	Female	30 (22%)	5.8 (3.8 - 7.7)	2.1 (1.3 - 2.9)
Drug	PD-1	104 (76%)	9.0 (6.7 - 11.1)	3.5 (2.5 - 4.4)
	PD-L1	20 (15%)	7.6 (2.2 - 13.1)	3.7 (2.9 - 4.5)
	CTLA-4 + PD-L1	13 (9%)	11.3 (0 - 22.8)	4.0 (1.6 - 4.4)
Consecutive line of treatment	First	47 (34%)	9.0 (6.9 - 11.1)	3.7 (2.5 - 4.9)
	Second or more	90 (66%)	8.3 (5.6 - 11.1)	3.4 (2.2 - 4.7)
Tumor type	Metastatic	73 (53%)	10.3 (7.0 - 13.5)	4.1 (2.8 - 5.4)
	Recurrent	64 (47%)	6.4 (3.8 - 9.0)	3.4 (2.6 - 4.2)
Salvage chemotherapy after progression	No	78 (67%)	4.8 (3.2 – 6.4)	
	Yes	39 (33%)	11.8 (9.6 – 14.0)	

between PD-1 and PD-L1 + CTLA-4 inhibitors (HR = 1.47; 95% CI, 0.82 - 2.63; p = 0.20) (**Figure 3C**), between PD-1 and PD-L1 inhibitors (HR = 1.09; 95% CI, 0.65 – 1.82; p = 0.75) (**Figure 3C**), between first line of treatment versus second line or more (HR = 0.90; 95% CI, 0.61 - 1.32; p = 0.59) (**Figure 3D**), or between metastatic or locoregionallly recurrent HNSCC (HR = 0.83; 95% CI, 0.58 - 1.20; p = 0.34) (**Figure 3E**).

The overall response rate in the entire patient cohort was 22% (95% CI, 16-37%). Twenty-eight patients (20%) had achieved a confirmed partial response (PR) and two patients (1%) achieved a complete response (CR). Median time to response was 3.6 months (IQR 2.0 - 5.2), while the median duration of response was 6.4 months (IQR 3.8 – 13.8) for all patients with R/M HNSCC receiving immunotherapy.

DISCUSSION

Treatment for R/M HNSCC has not changed dramatically over the last decades until the advent of immunotherapy started reshaping our treatment ability very quickly. Tumor profiling of HNSCC for a more targeted treatment approach was essentially absent, with the potential exception of p16 or HPV status in oropharyngeal SCC. Immunotherapy is challenging this "one size fits all" approach. Since the established efficacy of ICB treatment, multiple trials are on the way considering immunotherapy in an earlier stage in the disease process of HNSCC. The early identification of probable responders will be of vital importance for cost-effectiveness of these treatments.

Ferris and colleagues published a subgroup analysis in their trial according PD-1 and HPV status in which preliminary evidence suggested that patients with a tumor PD-L1 expression of 1% or more or p16 positive tumors may have greater effect from ICB, although the survival rate at two years was similar (12). Cohen et al. found – in the same line - that PD-L1 expression on tumor cells and associated immune cells did predict better outcomes for treatment with pembrolizumab (5). The landmark Keynote-048 study was subsequently published in which they reported profound overall survival benefit, particularly in PD-L1 positive tumors, defined by the combined positive score (CPS) (7). This is defined as the number of PD-L1–positive cells (tumor cells, lymphocytes, and macrophages) divided by the total number of tumor cells × 100; a minimum of 100 viable tumor cells must have been present for the specimen to be considered evaluable. Around 85% of HNSCC tumor cells express PD-L1 when measured with CPS (13). CPS has to be viewed as an "enrichment marker": a CPS score above 20 is associated with a higher chance of benefit from pembrolizumab, but a lower score does not exclude activity. Beyond analytical considerations, PD-1 and PD-L1 expression are known to express spatial and temporal heterogeneity within a tumor as well (14).

Looking at the results in our cohort, a median OS of 9 months is in keeping with the contemporary literature (OS 6.5 – 14.9 months) (7, 8, 12, 15). We did not observe significant differences in OS between three immune checkpoint inhibitors individually, with or without the addition of CTLA-4 inhibition, in this group of R/M HNSCC patients. Different from clinical trials, performance status was not used for inclusion in our clinical practice. Practically, the comparable survival curve in our unselected patient cohort suggests that the benefits observed in the pivotal trials can be extrapolated to patients seen in daily practice.

The significantly better OS in metastatic compared to recurrent HNSCC cases was unanticipated. Interestingly, also in the Keynote-048 trial, the OS benefit of pembrolizumab monotherapy over chemotherapy plus cetuximab seemed to be restricted to metastatic patients (7). This observation suggests a possible association based on biological differences.

A potential explanation lies in the "Tumor mutational burden" (TMB). TMB is a biomarker-based concept and a possible causal factor contributing to the prolonged OS in metastatic HNSCC as previous reports suggest that TMB in metastatic tissues is notably higher than in primary tissues (16). Lin and colleagues observed a correlation between PD-L1 expression and metastatic risk (17). Cold tumors are known to display lower levels of T-cell inflamed signature compared with healthy tissues in the same individual, from which it has been suggested that T-cell exhaustion is a locally active process of carcinogenesis (18). This process and the

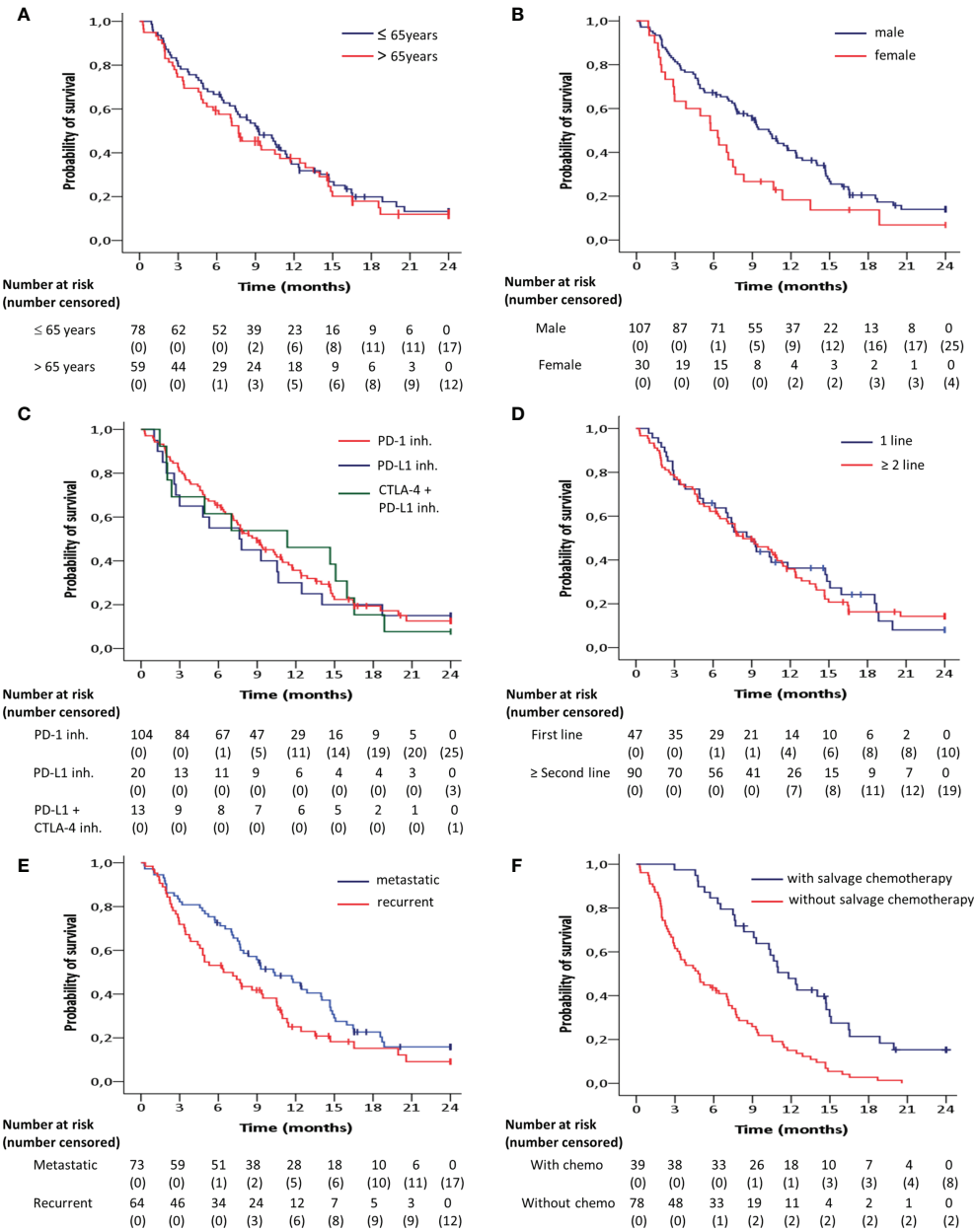

FIGURE 2 | Kaplan-Meier curves for overall survival according to **(A)** age, **(B)** gender, **(C)** target inhibitor, **(D)** line of treatment and **(E)** recurrence pattern, estimated for the entire patient group (n=137). **(F)** Overall survival for the subgroup of patients with tumor progression after immune checkpoint blockade treatment (n=117) depending on whether subsequent salvage chemotherapy was administered. Overall survival was significantly ($p<0.05$) longer in men compared to women, in metastatic tumors compared to locoregionally recurrent HNSCC and in patients who received subsequent salvage therapy compared to those without.

resulting T-cell exhaustion might hence be different in metastatic locations and it would be useful to assess any difference in tumor inflamed signature (TIS) in a local and metastatic recurrent tumor site. In colorectal cancer for instance, angiogenesis and inflammatory response are shown to be enriched in matched liver metastasis compared to the colorectal primary tumor (19). Furthermore, prior radiotherapy to the site of recurrence might influence the ICB response. Contrary to metastatic lesions, locoregional recurrence typically occurs in a previously irradiated area.

Further detailed subgroup analysis revealed a significantly better OS for male patients. This finding is in line with a meta-analysis reported by Conforti et al. (20) and with the subgroup analysis of the Keynote-048 (7). On the contrary, the earlier work of Lin et al. identified a higher likelihood of PD-L1 expression in female than in male patients (17). In the multivariate analysis,

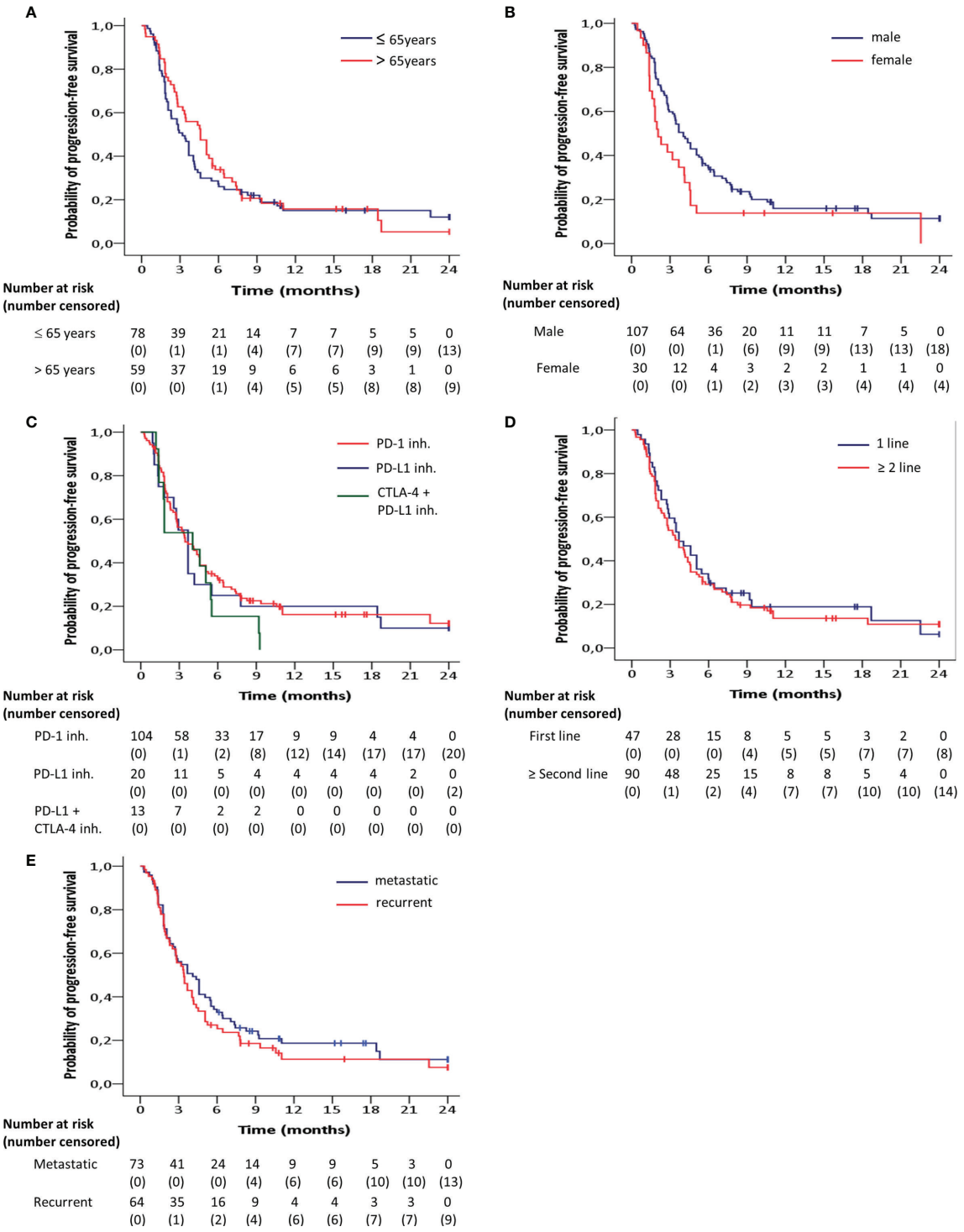

FIGURE 3 | Kaplan-Meier curves for progression-free survival according to **(A)** age, **(B)** gender, **(C)** target inhibitor, **(D)** line of treatment, **(E)** pattern of recurrence, estimated for the entire patient group (n=137). Progression-free survival was significantly ($p<0.05$) longer in men compared to women.

the PD-L1 status only correlated with worse prognosis in males and smokers, in an era when ICB was not available. Taken together, these data suggest that PD-L1 expression is associated with metastasis and poor prognosis, but that particularly male patients with metastatic PD-L1-positive disease may derive benefit from ICB.

Overall, the PFS of 31% at the six-month time point is comparable with results from the Keynote-048 (25-49%) and CheckMate-141 (19.7%) trials (7, 12). The median duration of response of 6.4 months is somewhat lower compared to the published trials (9.7 months in Checkmate-141 and 8 months in Keynote 055) (4, 21, 22). Interestingly, our data confirm the observation in another published cohort of patients treated with salvage chemotherapy after progression under ICB (23). Although the difference in OS compared to patients who did not receive salvage treatment is at least in part explained by selection bias, the observed median OS of 11,8 months is significantly better than what would be expected. This finding supports the use of ICB early in the treatment of HNSCC. Several trials are already exploring ICB treatment in high risk primary HNSCC.

In Europe, the indication of pembrolizumab in first line R/M HNSCC was registered in august 2020 in patients with a CPS score of 1 or higher. This new treatment option poses questions as clinicians have to make the choice whether or not to add chemotherapy to first line ICB in R/M HNSCC. CPS may guide this decision to some extent. Some suggest to use a score above 20 to select patients for single agent ICB, based on the analysis of Keynote-048. The platinum/5FU doublet adds a lot of toxicity, and the benefit in terms of long-term survival is questionable. The main downside of single agent pembrolizumab may be the possibility of fast progression. Therefore, we suggest to treat clinically fit patients with rapidly progressive disease with combined chemo- and immunotherapy. This way, the higher response rate of chemotherapy can be exploited. In frail patients or patients with a less threatening disease progression, we suggest single agent ICB in patients with CPS greater than 1, as it is much better tolerated and offers a better chance to obtain a durable response and disease control.

We report on a single-center, homogeneous population of patients that is treated with ICB without concurrent chemotherapy, with a mature follow-up. Nevertheless, there are some limitations that need to be taken in account when interpreting our findings. First, patients received different ICB treatments and different lines of previous palliative treatment. In current practice, ICB is commonly used as the treatment of choice. Therefore, these observations are representative for patients treated in daily practice. Second, data on HPV status and PD-L1 expression were not available for the entire patient population. Since the literature remains inconclusive on these matters, testing for p16 in other sites than oropharynx is not part of our standard of care routine. Assessment of PD-L1 expression by CPS has only recently become a standard procedure, with the registration of pembrolizumab as part of the first line treatment in R/M HNSCC.

In conclusion, ICB has profoundly changed our ability to treat R/M HNSCC and offers a small subgroup of patients a durable disease control without the need of chemotherapy. Selection of patients for the optimal treatment approach is challenging. Male patients and patients with metastatic disease appear to benefit more from ICB. Along with CPS, and comorbidity, site of recurrence may guide our treatment approach.

DATA AVAILABILITY STATEMENT

The data that support the findings of this study are available from the corresponding author upon reasonable request.

ETHICS STATEMENT

The studies involving human participants were reviewed and approved by Ethics Committee of the University Hospitals Leuven, Leuven, Belgium. Written informed consent for participation was not required for this study in accordance with the national legislation and the institutional requirements.

AUTHOR CONTRIBUTIONS

PC and MB contributed to conception and design of the study. MB and JVD acquired data. MB, JD, and MS performed data analysis. MB, JVD, and PC wrote the first draft of the manuscript. MS wrote sections of the manuscript. VVP, SN, and JM revised the work critically. All authors contributed to manuscript revision, read, and approved the submitted version.

REFERENCES

1. Vermorken JB, Mesia R, Rivera F, Remenar E, Kawecki A, Rottey S, et al. Platinum-Based Chemotherapy Plus Cetuximab in Head and Neck Cancer. *N Engl J Med* (2008) 359(11):1116–27. doi: 10.1056/NEJMoa0802656
2. Baselga J. The EGFR as a Target for Anticancer Therapy - Focus on Cetuximab. *Eur J Cancer* (2001) 37(SUPPL. 4):16–22. doi: 10.1016/S0959-8049(01)00233-7
3. Vermorken JB, Hitt R, Geoffrois L, Erfan J, Kawecki A, Zabolotnyy D, et al. 5501 ORAL Cetuximab Plus Platinum-Based Therapy First-Line in Recurrent and/or Metastatic (R/M) Squamous Cell Carcinoma of the Head and Neck (SCCHN): Efficacy and Safety Results of a Randomized Phase III Trial (EXTREME). *Eur J Cancer Suppl* (2007) 5(4):p324. doi: 10.1016/S1359-6349(07)71218-1
4. Ferris RL, Blumenschein G, Fayette J, Guigay J, Colevas AD, Licitra L, et al. Nivolumab vs Investigator's Choice in Recurrent or Metastatic Squamous Cell Carcinoma of the Head and Neck: 2-Year Long-Term Survival Update of CheckMate 141 With Analyses by Tumor PD-L1 Expression. *Oral Oncol* (2018) 81:45–51. doi: 10.1016/j.oraloncology.2018.04.008
5. Cohen EEW, Soulières D, Le Tourneau C, Dinis J, Licitra L, Ahn M-J, et al. Pembrolizumab Versus Methotrexate, Docetaxel, or Cetuximab for Recurrent or Metastatic Head-and-Neck Squamous Cell Carcinoma (KEYNOTE-040): A Randomised, Open-Label, Phase 3 Study. *Lancet* (2019) 393(10167):156–67. doi: 10.1016/S0140-6736(18)31999-8
6. Ferris RL, Haddad R, Even C, Tahara M, Dvorkin M, Ciuleanu TE, et al. Durvalumab With or Without Tremelimumab in Patients With Recurrent or Metastatic Head and Neck Squamous Cell Carcinoma: EAGLE, a Randomized,

Open-Label Phase III Study. *Ann Oncol* (2020) 31(7):942–50. doi: 10.1016/j.annonc.2020.04.001
7. Burtness B, Harrington KJ, Greil R, Soulières D, Tahara M, de Castro G, et al. Pembrolizumab Alone or With Chemotherapy Versus Cetuximab With Chemotherapy for Recurrent or Metastatic Squamous Cell Carcinoma of the Head and Neck (KEYNOTE-048): A Randomised, Open-Label, Phase 3 Study. *Lancet* (2019) 394(10212):1915–28. doi: 10.1016/S0140-6736(19)32591-7
8. Zandberg DP, Algazi AP, Jimeno A, Good JS, Fayette J, Bouganim N, et al. Durvalumab for Recurrent or Metastatic Head and Neck Squamous Cell Carcinoma: Results From a Single-Arm, Phase II Study in Patients With ≥25% Tumour Cell PD-L1 Expression Who Have Progressed on Platinum-Based Chemotherapy. *Eur J Cancer* (2019) 107:142–52. doi: 10.1016/j.ejca.2018.11.015
9. Qian JM, Schoenfeld JD. Radiotherapy and Immunotherapy for Head and Neck Cancer: Current Evidence and Challenges. *Front Oncol* (2020) 10:608772. doi: 10.3389/fonc.2020.608772
10. von Elm E, Altman DG, Egger M, Pocock SJ, GØtzsche PC, Vandenbroucke JP, et al. The Strengthening the Reporting of Observational Studies in Epidemiology (STROBE) Statement: Guidelines for Reporting Observational Studies. *J Clin Epidemiol* (2008) 61(4):344–9. doi: 10.1016/j.jclinepi.2007.11.008
11. Eisenhauer EA, Therasse P, Bogaerts J, Schwartz LH, Sargent D, Ford R, et al. New Response Evaluation Criteria in Solid Tumours: Revised RECIST Guideline (Version 1.1). *Eur J Cancer* (2009) 45(2):228–47. doi: 10.1016/j.ejca.2008.10.026
12. Ferris RL, Blumenschein G, Fayette J, Guigay J, Colevas AD, Licitra L, et al. Nivolumab for Recurrent Squamous-Cell Carcinoma of the Head and Neck. *N Engl J Med* (2016) 375(19):1856–67. doi: 10.1056/NEJMoa1602252
13. Rischin D, Harrington KJ, Greil R, Soulieres D, Tahara M, de Castro G, et al. Protocol-Specified Final Analysis of the Phase 3 KEYNOTE-048 Trial of Pembrolizumab (Pembro) as First-Line Therapy for Recurrent/Metastatic Head and Neck Squamous Cell Carcinoma (R/M HNSCC). *J Clin Oncol* (2019) 37(15_suppl):6000–0. doi: 10.1200/JCO.2019.37.15_suppl.6000
14. Bellesoeur A, Torossian N, Amigorena S, Romano E. Advances in Theranostic Biomarkers for Tumor Immunotherapy. *Curr Opin Chem Biol* (2020) 56:79–90. doi: 10.1016/j.cbpa.2020.02.005
15. Harrington KJ, Ferris RL, Blumenschein G, Colevas AD, Fayette J, Licitra L, et al. Nivolumab Versus Standard, Single-Agent Therapy of Investigator's Choice in Recurrent or Metastatic Squamous Cell Carcinoma of the Head and Neck (CheckMate 141): Health-Related Quality-of-Life Results From a Randomised, Phase 3 Trial. *Lancet Oncol* (2017) 18(8):1104–15. doi: 10.1016/S1470-2045(17)30421-7
16. Schnidrig D, Turajlic S, Litchfield K. Tumour Mutational Burden: Primary Versus Metastatic Tissue Creates Systematic Bias. *Immuno-Oncol Technol* (2019) 4:8–14. doi: 10.1016/j.iotech.2019.11.003
17. Lin Y-M, Sung W-W, Hsieh M-J, Tsai S-C, Lai H-W, Yang S-M, et al. High PD-L1 Expression Correlates With Metastasis and Poor Prognosis in Oral Squamous Cell Carcinoma. Suzuki H, Editor. *PloS One* (2015) 10(11):e0142656. doi: 10.1371/journal.pone.0142656
18. Dangaj D, Barras D, Coukos G. Tumor Landscapes: β-Catenin Drives Immune Desertification. *Clin Cancer Res* (2019) 25(10):2943–5. doi: 10.1158/1078-0432.CCR-19-0188
19. Liu J, Cho YB, Hong HK, Wu S, Ebert PJ, Bray SM, et al. Molecular Dissection of CRC Primary Tumors and Their Matched Liver Metastases Reveals Critical Role of Immune Microenvironment, EMT and Angiogenesis in Cancer Metastasis. *Sci Rep* (2020) 10(1):10725. doi: 10.1038/s41598-020-67842-5
20. Conforti F, Pala L. Sex-Based Heterogeneity of Efficacy of Anticancer Immunotherapy. *Ann Oncol* (2019) 30:v522–3. doi: 10.1093/annonc/mdz253.110
21. Bauml J, Seiwert TY, Pfister DG, Worden F, Liu SV, Gilbert J, et al. Pembrolizumab for Platinum- and Cetuximab-Refractory Head and Neck Cancer: Results From a Single-Arm, Phase II Study. *J Clin Oncol* (2017) 35(14):1542–9. doi: 10.1200/JCO.2016.70.1524
22. Colevas AD, Bahleda R, Braiteh F, Balmanoukian A, Brana I, Chau NG, et al. Safety and Clinical Activity of Atezolizumab in Head and Neck Cancer: Results From a Phase I Trial. *Ann Oncol* (2018) 29(11):2247–53. doi: 10.1093/annonc/mdy411
23. Saleh K, Daste A, Martin N, Pons-Tostivint E, Auperin A, Herrera-Gomez RG, et al. Response to Salvage Chemotherapy After Progression on Immune Checkpoint Inhibitors in Patients With Recurrent and/or Metastatic Squamous Cell Carcinoma of the Head and Neck. *Eur J Cancer* (2019) 121:123–9. doi: 10.1016/j.ejca.2019.08.026

Conflict of Interest: The authors declare that the research was conducted in the absence of any commercial or financial relationships that could be construed as a potential conflict of interest.

frontiers in Oncology

ORIGINAL RESEARCH
published: 28 January 2022
doi: 10.3389/fonc.2022.812044

Neutrophils Promote Tumor Progression in Oral Squamous Cell Carcinoma by Regulating EMT and JAK2/STAT3 Signaling Through Chemerin

Xiaoyuan Hu[1,2], *Fenggang Xiang*[1,3], *Yuanyong Feng*[1,4], *Fei Gao*[1], *Shengyou Ge*[1,4], *Chengqin Wang*[1,3], *Xuan Zhang*[1] *and Ning Wang*[1]*

[1] Department of Pathology, School of Basic Medicine, Medical College of Qingdao University, Qingdao, China, [2] Department of Pathology, Pingxiang People's Hospital, PingXiang, China, [3] Department of Pathology, the Affiliated Hospital of Qingdao University, Qingdao, China, [4] Department of Oral and Maxillofacial Surgery, School of Stomatology and The Affiliated Hospital of Qingdao University, Qingdao, China

OPEN ACCESS

Edited by:
Pablo Parente-Arias, A Coruña University Hospital Complex (CHUAC), Spain

Reviewed by:
Ahmed Al-Samadi, University of Helsinki, Finland
Juan Francisco Santibanez, University of Belgrade, Serbia

***Correspondence:**
Ning Wang
wangning7903@126.com

Specialty section:
This article was submitted to Head and Neck Cancer, a section of the journal Frontiers in Oncology

Received: *09 November 2021*
Accepted: *03 January 2022*
Published: *28 January 2022*

Citation:
Hu X, Xiang F, Feng Y, Gao F, Ge S, Wang C, Zhang X and Wang N (2022) Neutrophils Promote Tumor Progression in Oral Squamous Cell Carcinoma by Regulating EMT and JAK2/STAT3 Signaling Through Chemerin. Front. Oncol. 12:812044. doi: 10.3389/fonc.2022.812044

Oral squamous cell carcinoma (OSCC) is the most common malignancy of the oral cavity. In the tumor microenvironment, tumor-associated neutrophils (TANs) can promote tumor growth, invasion, and metastasis. The aim of our study was to explore the relationship between neutrophils infiltration and Chemerin expression in tumor cells, as well as their relationship with the clinicopathological parameters and clinical prognosis of 74 cases of OSCC. We also explored the role of the interaction between neutrophils and Chemerin in the functions of OSCC cells (Cal27, SCC9, and SCC15) *in vitro*. Our results showed that in OSCC, Chemerin over-expression may increase neutrophils infiltration in tumor tissues. Chemerin over-expression and neutrophils infiltration were the prognostic factors of poor clinical outcomes. Furthermore, we discovered that neutrophils promoted OSCC migration, invasion, and proliferation and EMT through Chemerin. Neutrophils activated JAK2/STAT3 signaling through Chemerin and then up-regulated its downstream signaling target genes, such as Phospho-Rb, E2F1, CyclinE1, and CyclinD1. Taken together, our results revealed that neutrophils and Chemerin are potentially involved in OSCC progression and metastasis. Neutrophils may promote the JAK2/STAT3 signaling pathway and EMT in OSCC cells through Chemerin.

Keywords: chemerin, oral squamous cell carcinoma, neutrophils, JAK2/STAT3, EMT, tumor progression

INTRODUCTION

Oral squamous cell carcinoma (OSCC) is the most common malignancy of the oral cavity (1). Although treatment methods, such as chemotherapy, radiotherapy, and surgical therapy, have advanced in recent years, the 5-year survival rate of patients with OSCC has remained less than 60% (2). The mechanisms of the occurrence and development of OSCC are still unclear. However, recent studies

have shown that the interaction between tumor cells and immune cells creates a favorable microenvironment for cancer initiation, progression, and metastasis (3, 4). The cross-talk between tumor cells and immune cells may promote tumor development (4).

Recent studies have revealed that in addition to tumor cells, inflammation and the immune system, as indispensable participants in tumor formation, provide an attractive environment for tumor growth and metastasis. Neutrophils are not only the most abundant circulating white blood cells, they are also one of the main infiltrating immune and inflammatory cells in OSCC (5). A growing body of research has demonstrated that tumor-associated neutrophils (TANs), a predominant component of the tumor microenvironment, participate in tumor initiation, growth, proliferation, and metastatic spread (6). In accordance with different tumor microenvironments and in addition to the contact mechanism, TANs can induce the paracrine release of cytokines and chemokines with tumor-promoting or antitumor functions to affect tumor progression (7). Evidence showing that increased TANs infiltration is associated with poor clinical outcomes in OSCC exists (8, 9).These novel aspects of neutrophils biology may contribute to OSCC progression and metastasis. However, only a few studies have been done on the specific signaling pathways and molecular mechanisms involved in the interaction between neutrophils and OSCC (10).

EMT is a key event where in epithelial cells lose their epithelial characteristics and acquire a mesenchymal phenotype (11). Its phenotypic transition is manifested as the loss of cell polarity and cell–cell connection and the acquisition of mesenchymal characteristics, such as motility and invasiveness, by epithelial cells (12). At the molecular level, it usually manifests as the decreased expression of E-cadherin and the increased expression of N-cadherin, mesenchymal markers (vimentin), and transcription factors (Slug and Snail) (12–14). Recent studies have illustrated that EMT plays a vital role in tumor progression and metastasis (15–17). Stromal cells in the tumor microenvironment can induce EMT. Neutrophils constitute an important part of tumor stroma, and they are mainly involved in regulating tumor progression (6, 18). However, studies on neutrophils function in EMT and its possible molecular mechanisms remain rare.

Chemerin, an effective chemoattractant protein encoded by retinoic acid receptor responder 2, was first discovered in psoriatic skin lesions (19, 20). Recent studies have revealed that the expression of Chemerin is dysregulated in several types of tumors. Chemerin expression is up-regulated in neuroblastoma, esophageal squamous cell carcinoma, and OSCC (20–22) but is down-regulated in hepatocellular carcinoma and adrenocortical carcinoma (23, 24). Weigert et al. (25) reported that Chemerin levels in the serum of patients with inflammatory bowel disease are elevated relative to those in the serum of healthy controls, indicating that Chemerin has a potential regulatory function in intestinal inflammation. In addition, Sotiropoulos et al. (8) reported that Chemerin,a biomarker of nonsmall cell lung cancer, is involved in tumor-promoting networks and inflammatory and cancer-related metabolic pathways.

Our previous studies demonstrated that Chemerin is over-expressed in OSCC (26), that TANs infiltration in tumor tissues is increased (9), and that both of these factors are correlated with the poor clinical outcomes of patients with OSCC (9, 22). Chemerin expression in tumor cells may play important roles in immune surveillance. However, the role of Chemerin and neutrophils in OSCC remains unknown. The JAK2/STAT3 pathway has been found to play a critical role in the progression of a variety of tumors (27–29). The expression levels of STAT3 and phosphorylated STAT3 in OSCC are increased compared with those in normal tissues (30). A number of previous findings strongly suggest that the persistent activation of STAT3 in head and neck squamous cell carcinomas, accompanied by increases in STAT3 tyrosine phosphorylation, is linked to cell proliferation, differentiation, and apoptosis (31, 32). The role of neutrophils, along with JAK2/STAT3 signaling and EMT,in OSCC has been poorly addressed. Therefore, the purpose of our work is to determine how neutrophils activate the JAK2/STAT3 pathway in OSCC and how Chemerin and neutrophils promote the migration, invasion, and proliferation of OSCC.

In the present study, we studied the relationship between TANs infiltration and Chemerin expression. We also investigated TANs infiltration and Chemerin expression in relation to clinicopathological parameters and clinical prognosis. Moreover, we explored the roles of neutrophils and Chemerin in EMT and JAK2/STAT3 signaling pathway regulation and identified the downstream targets phosphor-Rb, E2F1, CyclinD1, and CyclinE1. Our results indicated that neutrophils could regulate the JAK2/STAT3 signaling pathway and EMT through Chemerin to promote OSCC and provided support that neutrophils and Chemerin are potential therapeutic targets for the treatment of OSCC.

MATERIAL AND METHODS

Patients and Specimens

A total of 74 patients (51 males and 23 females) with primary tongue squamous cell carcinoma treated at the Affiliated Hospital of Qingdao University between 2005 and 2010 participated in this study. The clinical pathological data of all the patients were complete, and no radiotherapy or chemotherapy was performed before surgery. The clinicopathological information of the patients is presented in **Table 1**. The study protocol was approved by the ethics committee of the Affiliated Hospital of Qingdao University. Written informed consent was obtained from all of the patients and healthy controls. The studies were conducted in accordance with the Declaration of Helsinki.

Tissue Microarray and Double Staining Immunohistochemistry

The tissue microarray (TMA) used in this work was constructed as follows: First, representative areas located away from necrotic and hemorrhagic materials were premarked in paraffin-embedded wax blocks *via* H&E staining. Triplicates of 1-mm

diameter cylinders from the centers of the tumors of 74 cases and the peritumoral noncancerous squamous epithelial tissues of 17 cases (designated as tumor and peritumoral tissues, respectively) were included in the TMA. Thus, several different TMA blocks were constructed. The blocks then were sectioned to a thickness of 4 μm and placed on slides that were coated with 3-aminopropyltriethoxysilane for immunohistochemistry (IHC).

A polymer double-staining kit (Zhongshan Golden Bridge Biotech, China) was used for staining. After the deparaffinization and gradient ethanol hydration of the sections, endogenous enzymes were inactivated by using 3% H_2O_2 for 30 min. The sections were heated in a water bath for heat-induced epitope retrieval in EDTA buffer (95°C) and cooled naturally at room temperature. After washing with PBS, the sections were incubated with anti-Chemerin (dilution of 1:100, Proteintech, China) or anti-CD15 (dilution of 1:150) antibodies overnight at 4°C in a humidity chamber. The polymer horseradish peroxidase detection system (ZSGB, China) in this work used DAB and GBI for visualization and hematoxylin for nuclear counter staining. The results showed that DAB-stained CD15+ was brown, GBI-stained Chemerin was red, and hematoxylin-stained cell nuclei were blue.

Immunostaining

The evaluation criteria for the IHC results were as previously reported (6). Chemerin staining was evaluated on the basis of a semiquantitative scoring system. The intensity score represented the average intensity of the positive tumor cells (0, none; 1, weak; 2, intermediate; and 3, strong) (20). The proportion score represented the estimated proportion of positive tumor cells: 0: (<5%), 1: (5%–25%), 2: (26%–50%), 3: (51%–75%), and 4: (>75%). The proportion and intensity scores were then added to obtain a total score, which ranged from 0 to 7. All specimens were divided into two groups: weak expression, 0–3 points and strong expression, 4–7 points. For the CD15+ neutrophil count, positive cells in three cylinders with a diameter of 1 mm per patient were calculated and presented as the mean value of the triplicates (cells/core). The average value of CD15+ neutrophils in TMA was acquired, and the median of CD15+ neutrophils of the 74 samples was obtained as the cut-off value in subsequent analysis.

If the mean number of the triplicates was more than the median, the specimen was allocated into the high-density group and into the low-density group otherwise.

The specimens were divided into three groups to evaluate the expression of Chemerin and CD15+TANs density: the strong Chemerin expression+ high TANs density group (@1), the strong Chemerin expression+ low TANs density group/weak Chemerin expression+ high TANs density group (@2), and the weak Chemerin expression+ low TANs density group (@3).

Cell Culture

OSCC lines (Cal27, SCC9, and SCC15) were purchased from Shanghai Institutes for the Chinese Academy of Sciences and cultured at 37°C in a humidified atmosphere of 5% CO_2 in Dulbecco's modified Eagle's medium (DMEM) containing 10% FBS with 1% penicillin–streptomycin. For co-cultivation studies, 1×10^6 OSCC cells and neutrophils (1:3 ratio) seeded 24 h before co-cultivation were added to the upper chamber of a Transwell chamber with a 0.4-μm porous polycarbonate membrane (Corning, Union City, CA, USA) or to the lower chamber. The OSCC cells were collected after 24–48 h.

Extraction of Neutrophils From Peripheral Blood

Neutrophils were isolated from peripheral blood of healthy donors at the Affiliated Hospital of Qingdao University after written informed consent was obtained. In a 15 ml centrifuge tube, 5.0 ml of anticoagulated whole blood was layered on 5.0 ml of PolymorphPrep (Axis-Shield PoC AS, Norway).After centrifugation at 450 × *g* for 30 min, the mononuclear cell phase was discarded to isolate neutrophils. After centrifugation, two bands of white blood cells were obtained. The top band consisted of mononuclear cells, and the lower band consisted of polymorphonuclear neutrophils (PMNs). All the cell bands were collected, and the remaining RBCs were lysed with a hypotonic lysis program to obtain the pure PMNs population.

Transwell Chemotaxis Assay

The cell chemotaxis assay was performed in a 24-well Transwell chamber with a polycarbonate membrane with a 3 mm pore size (Corning, USA). A total of 2×10^5 neutrophils were suspended in 200 μl of serum-free medium in each upper compartment. Then, 600 μl of RPMI-1640 with 10% serum containing recombinant Chemerin (20, 50, 100, or 200 ng/ml) or 2×10^5 OSCC cells (Cal27, SCC9, and SCC15) was added to the lower compartment. RPMI-1640 with 10% serum was added to the lower compartment of the control group. After incubation at 37°C for 24 h, the suspended neutrophils in the lower compartment were counted by using a cell counting plate. The chemotactic index for each group was calculated as follows: neutrophils count of each experimental group/neutrophils count of the control group × 100%.

Enzyme-Linked Immunosorbent Assay

The concentration of Chemerin in the medium was measured *via* an enzyme-linked immunosorbent assay (ELISA, R&D Systems, USA) in accordance with the manufacturer's instructions.

Lentiviral Transduction

Lentiviruses were synthesized by GenePharma (Suzhou, China). The sequences of Chemerin-shRNA and scramble controls were as follows: Chemerin-shRNA1#, 5′-GCCCTTCCCAGCTGG AATATT-3′; Chemerin-shRNA2#, 5′-GCTTCTACTTCCCTG GACAGT-3′; negative control (Scr-shRNA), 5′-ACGUG ACACGUUCGGAGAADTDT-3′. Chemerin was over-expressed by using an over-expression vector plasmid (Chemerin). Empty plasmids were used as the negative control (NC). Plasmids were purchased from GenePharma (GenePharma, China).

Cell Viability Assay

For the cell co-culture, 3×10^3 OSCC cells were seeded into each well of 96-well plates in the presence or absence of neutrophils

(1:3 ratio). After 24 h, the neutrophils were removed from the co-culture system. Subsequently, methylthiazolyltetrazole (MTT) measurements were performed at different time points (0, 24, 48, 72, and 96 h). A total of 20 μl of MTT (5 mg/ml) was added into each well, and the cells were further incubated for 4 h. Then, the media were discarded, and 150 μl of DMSO was added. The plate was shaken at room temperature for 15 min, and absorbance was read at 490 nm on an automatic microplate reader (Bio-Tek Instruments, Winooski, VT, USA).

Colony Formation Assay

After 24–48 h of co-culture or non-co-culture with neutrophils, the OSCC cells were cultured in a six-well plate at the density of 3000 cells/well for 2 weeks. The colonies that formed were fixed with methanol for 30 min and sequentially stained with 0.5% crystal violet for half an hour.

Cell Cycle Analysis

After 24–48 h of co-culture or non-co-culture with neutrophils, the OSCC cells were washed with ice-cold PBS and harvested *via* trypsinization. After centrifugation for 5 min, the cells were washed with ice-cold PBS and fixed with 70% ethanol overnight at 4°C. RNaseA (20 μg/ml) was added to the cells for 30 min (at 37°C). Propidium iodine (50 μg/ml) was added to the cells in the dark. The cells were analyzed by using flow cytometry (BD Accuri C6).

Cell Migration and Invasion Assay

The cell migration/invasion assay was performed in a 24-well Transwell chamber with a polycarbonate membrane with an 8 mm pore size (Corning, Union City, CA, USA). A total of 50 μl of diluted Matrigel (Matrigel: serum-free medium=1:8) was added into the upper chamber of the Transwell plates for the invasion assay, whereas the plates without Matrigel in their upper chambers were used for the migration assay. The treated cells were incubated in serum-free medium for 24 h. A total of $1.25–2.5 \times 10^5$ neutrophils in 500 μl of RPMI-1640 containing 15% FBS were added to the lower chamber, and 5×10^4 OSCC cells in 500 μl of DMEM containing 15% FBS were added to the upper chamber. After 24–48 h of incubation at 37°C, the cells that had migrated to the medium containing 15% serum in the lower compartment were stained with 0.5% crystal violet. The number of cells in five random microscope fields (100×) was counted.

Quantitative Real-Time PCR

Total RNA extraction and quantitative real-time PCR (qRT-PCR)were performed as previously described (6). Primers were synthesized by the Shanghai Sangon Biological Engineering Technology & Services Co.

The primers used in this assay were:

Chemerin: 5′-AGACAAGCTGCCGGAAGAGG-3′(upper)

and 5′-TGGAGAAGGCGAACTGTCCA-3′(lower);

GAPDH: 5′-CGGAGTCAACGGATTTGGTCGTAT-3′(upper)

and 5′-AGCCTTCTCCATGGTGGTGAAGAC-3′(lower).

Western Blot Analysis

Protein preparation and Western blot analysis were performed as described previously (33). The antibodies used in the study were as follows: Chemerin (Abcam, dilution of 1:500), GAPDH, E-cadherin, N-cadherin, Vimentin, p-JAK2, JAK2, Phospho-Rb (Abcam, dilution of 1:1000), p-STAT3, STAT3, Phospho-Rb (Abcam, dilution of 1:2000), E2F1, Cyclin D1, Cyclin E1 (Abcam, dilution of 1:1000), Slug and Snail (ProteinTech, dilution of 1:1000), and β-actin (ProteinTech, dilution of 1:4000).

Statistical Analysis

All statistical analyses were performed by using SPSS 23.0 software. All values were presented as mean ± SD, and each experiment was performed at least three times. Mann–Whitney test was used for non-normally distributed data. Student's *t* test was used for data that were normally distributed. Differences were considered statistically significant at $P< 0.05$, $P< 0.01$, and $P< 0.001$.

RESULTS

Immunohistochemical Analysis of TANs Infiltration and Chemerin Expression and Their Correlation With Clinicopathological Parameters

Double IHC results revealed that Chemerin and CD15+ TANs co-localized in clinical OSCC specimens. The IHC results demonstrated that CD15+ TANs infiltration in OSCC tissues (**Figures 1B–D**) was greater than that in peritumoral tissues (**Figure 1A**). TANs were predominantly observed in the stroma around carcinoma nests (**Figure 1B**), within carcinoma nests (**Figure 1C**), and in the borderline of tumor invasion (**Figure 1D**). Tumors with negative or weak Chemerin expression had low TANs infiltration (**Figure 1E**), whereas those with strong Chemerin expression had high TANs infiltration (red arrow) (**Figure 1F**). The number of CD15+ TANs outside the blood vessels ranged from 1 to 1053.5 in each 1mm-diameter tissue sample. The median density was 59.5/core. If the mean number of the triplicates exceeded 59.5, the sample was allocated into the high-density group. Otherwise, it was allocated into the low-density group. In addition, the IHC results showed that in OSCC, Chemerin expression was heterogeneous. Among the 74 cases of OSCC, 25 (33.78%) had weak Chemerin expression and 49 (66.22%) had strong Chemerin expression.

In tumor tissues, strong Chemerin expression+ high TANs density was associated with high clinical stage ($P < 0.001$), lymph node metastasis ($P < 0.001$), and tumor recurrence ($P = 0.01$) (**Table 1**). As shown in **Table 2**, Spearman's rho coefficient revealed that Chemerin expression was positively correlated with CD15+ TANs infiltration in OSCC ($P = 0.017$).

Analysis of the Influence of TANs Infiltration and Chemerin Expression on the Survival of Patients With OSCC

We followed up all 74 patients to evaluate the effect of TAN infiltration and Chemerin expression on the survival of patients

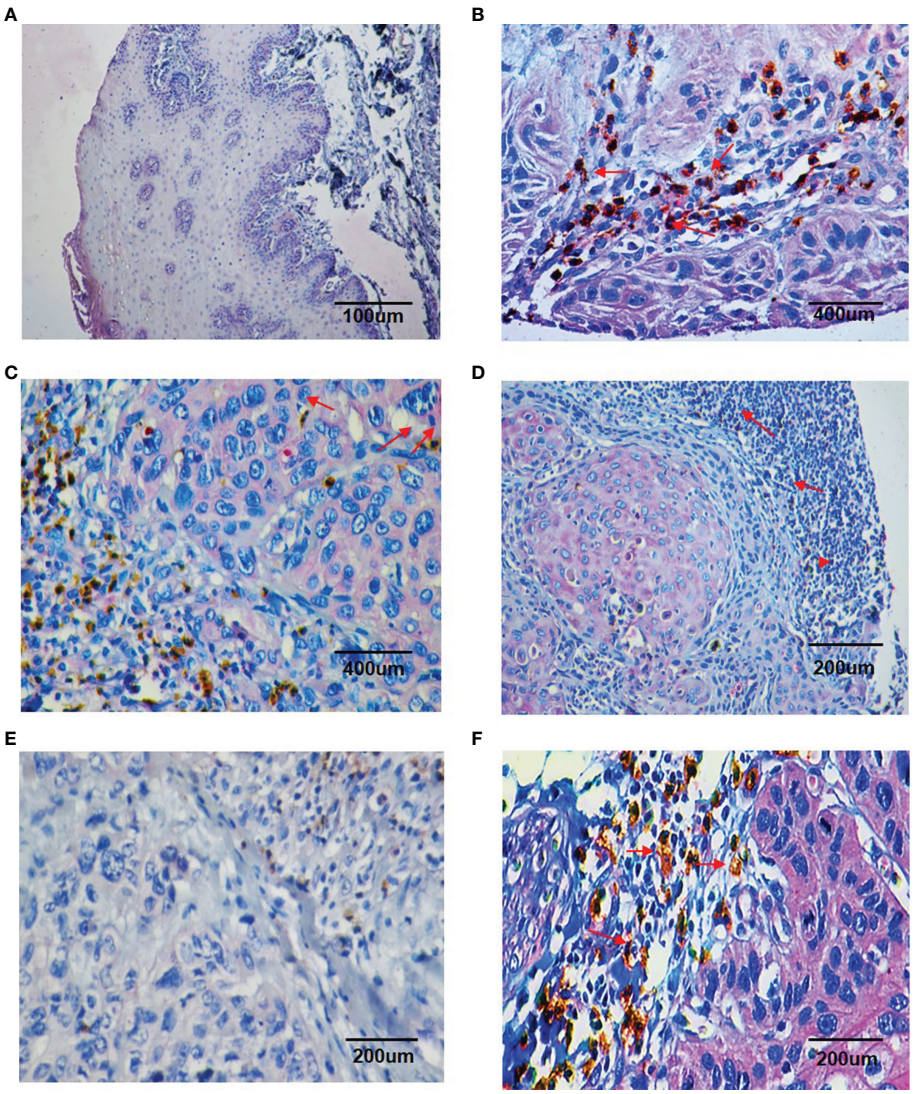

FIGURE 1 | Double staining immunohistochemistry results of CD15 + TANs and Chemerin. **(A–D)** The results showed more CD15 + TANs (red arrow) infiltrated in OSCC tissues **(B–D)** than in peritumoral tissues **(A)**, with TANs predominantly observed in stroma around the carcinoma nests **(B)**, within the carcinoma nests **(C)** and in the borderline of tumor invasion **(D)**. (A, 100×; B, C, 400×; D, 200×). Chemerin (pink color) was absent or weakly expressed in peritumoral non-neoplastic tissues **(A)**, whereas its expression was upregulated in cancer tissues compared with peritumoral tissues and located mainly in the cytoplasm of tumor cells **(B–D)**. **(E, F)** The relationship of Chemerin expression on tumor cells and infiltration of TANs. In negative or weak Chemerin expression tumors, there were relatively fewer TANs **(E)**; while in strong Chemerin expression tumors, there were more TANs (red arrow) **(F)**. (E, F, 200×). Brown: CD15 + (DAB staining), Pink: Chemerin (GBI staining).

with OSCC. The median follow-up time was 96 months. Within the observation period, 37 patients died from cancer.

Kaplan–Meier survival analysis revealed that strong Chemerin expression+ high neutrophil density (**Figures 2A, B**) and advanced clinical stage (**Figure 2C**) were associated with the short cancer-related survival of patients with OSCC. Tumor size ($P = 0.591$), tumor differentiation ($P = 0.312$), tumor recurrence ($P = 0.123$), patient gender ($P = 0.597$), and age ($P = 0.592$) had no effect on cancer-related survival. We performed multivariate survival analysis by using a Cox proportional hazards model to analyze whether the above parameters are independent prognostic factors for the survival of patients with OSCC. The results showed that strong Chemerin expression and high CD15+ TANs density were independent prognostic factors for patients with OSCC (**Tables 3** and **4**).

OSCC Cells Expressing Chemerin Attract Neutrophils *In Vitro*

On the basis of the IHC results, we explored whether Chemerin can attract neutrophils *in vitro via* Transwell assay. The results of ELISAs (**Figure 3A**) and qRT-PCR (**Figure 3B**) showed that all three cell lines had a certain level of Chemerin expression and

TABLE 1 | The relationship between the expression of Chemerin, CD15 + TANs density and clinicopathological parameters in OSCC (x / %).

Variables		n	@ 1	@ 2	@ 3	*Z*	*P value*
Sex	Male					-0.44	0.965
	Female	51	11 (21.57)	20 (39.22)	20 (39.22)		
		23	6 (26.09)	7 (30.43)	10 (43.48)		
Age						-1.225	0.221
	≤60 years	40	8 (20.00)	13 (32.50)	19 (47.50)		
	>60 years	34	9 (26.47)	14 (41.18)	11 (32.35)		
TNM stage						-4.293	0.000*
	I,II	37	14 (37.84)	17 (45.95)	7 (18.92)		
	III,IV	37	2 (5.41)	12 (32.43)	23 (62.16)		
Differentiation						-0.685	0.493
	G1,G2	34	8 (23.53)	10 (29.41)	16 (47.06)		
	G3	40	9 (22.50)	17 (42.50)	14 (35.00)		
Lymph node metastasis						-4.789	0.000*
	Yes	34	1 (2.94)	10 (29.41)	23 (67.65)		
	No	40	16 (40.00)	17 (42.50)	7 (17.50)		
Tumor size (d/cm)						-1.265	0.206
	<4cm	55	14 (25.45)	21 (38.18)	20 (36.36)		
	≥4cm	19	3 (15.79)	6 (31.58)	10 (52.63)		
Tumor recurrence						-2.578	0.010*
	Yes	27	3 (11.11)	8 (29.63)	16 (59.26)		
	No	47	14 (29.79)	19 (40.43)	14 (29.79)		

@ 1: strong Chemerin expression + high TANs density group (%).
@ 2: strong Chemerin expression + low TANs density group/weak Chemerin expression + high TANs density group (%).
@ 3: weak Chemerin expression + low TANs density group (%).
P value was estimated by the Mann–Whitney test.
**P < 0.05 was considered to be statistically significant.*

secretion. As depicted in **Figure 3C**, compared with the blank group, all three OSCC cells demonstrated improved chemotaxis to neutrophils ($P< 0.05$). Among the three cell lines, SCC15 demonstrated the most effective chemotaxis and the highest level of Chemerin (**Figures 3A–C**).The chemotactic effect of the SCC15-Chemerin-shRNA group of cells on neutrophils was weaker than that of the SCC15 group. By contrast, the chemotactic effect of the SCC9-Chemerin and Cal27-Chemerin groups was stronger than that of the SCC9 and Cal27 groups. After Chemerin knockdown, the chemotactic effect of SCC15 on neutrophils weakened, and after Chemerin over-expression, that of SCC9 and Cal27 on neutrophils strengthened (**Figure 3C**). R-Chemerin was also used to verify the chemotactic effect of Chemerin on neutrophils. The results showed that R-Chemerin improved the chemotaxis of neutrophils in a concentration-dependent manner (**Figure 3D**).

Lentiviral Transfection

Chemerin expression in the SCC9, SCC6, SCC15, and Cal27 cell lines was examined by using Western blot analyses (**Figure 4A**). SCC15 cells were selected for the knock-out of Chemerin with Chemerin-shRNA1# and 2# given their high Chemerin expression levels. The results showed that the Chemerin-shRNA2# was more effective than Chemerin-shRNA1# (**Figure 4B**). Therefore, Chemerin-shRNA 2# was chosen for the follow-up experiment. Meanwhile, given their low Chemerin expression levels, the Cal27 and SCC9 cell lines were transfected with the Chemerin over-expression lentivirus (**Figures 4C, D**).

Neutrophils Promote OSCC Cell Proliferation Through Chemerin

MTT and colony formation assays were performed to explore the effect of Chemerin and neutrophils on cell proliferation. OSCC cells were transfected with Chemerin-targeting knock-down (over-expression) and/or subjected to combined treatment with neutrophils. The results showed that the growth rate of the neutrophils group was significantly higher than that of the Scr-shRNA group (NC group). The growth rate of the Cal27 and SCC9 cells in the Chemerin over-expression group was significantly higher than that of the Cal27 and SCC9 cells in the NC group, and the growth rate of the Cal27 and SCC9 cells in the Chemerin+ neutrophils group was higher than that of the Cal27 and SCC9 cells in the neutrophils group (**Figure 5A**). Furthermore, the growth rate of the SCC15 cells in the

TABLE 2 | The relationship between Chemerin expression and TANs density in OSCC tissues.

Chemerin expression	CD15 + TANs density		Spearman's rho Coefficient test	
	Low	High	r	*P* value
Low	**16**	**9**	**0.309**	**0.017***
High	**20**	**29**		

**P < 0.05 was considered to be statistically significant.*

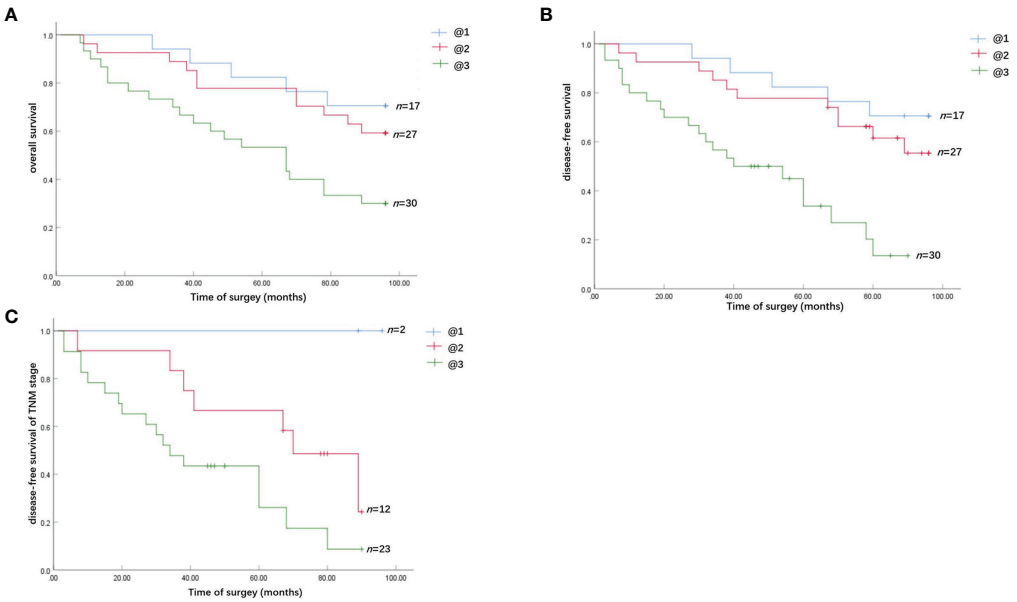

FIGURE 2 | Survival analysis of the effect of Chemerin expression and TANs infiltration on OSCC patients. **(A)** The overall cancer-related survival of OSCC patients in the strong Chemerin expression + high TANs density group was significantly reduced, compared with the weak Chemerin expression + low TANs density group (P = 0.008, log-rank test) and strong Chemerin expression + low TANs density group/weak Chemerin expression + high TANs density group (P = 0.017, log-rank test). **(B)** The OSCC patients in the strong Chemerin expression + high TANs density group also had significantly reduced disease-free survival related to cancer, compared with the weak Chemerin expression + low TANs density group (P = 0.000, log-rank test) and strong Chemerin expression + low TANs density group/ weak Chemerin expression + high TANs density group (P = 0.001, log-rank test). **(C)** In TNM stage III and IV OSCC patients, the cancer-related disease-free survival of OSCC patients in the strong Chemerin expression + high TANs density group was significantly reduced (P = 0.045, log-rank test).

Chemerin-shRNA (2#) group was significantly lower than that of the SCC15 cells in the Scr-shRNA group. The effect of neutrophils on cell proliferation was abolished after Chemerin knockdown (**Figure 5A**). The colony numbers of the Scr-shRNA, Scr-shRNA+ neutrophils, Chemerin-shRNA (2#), and Chemerin-shRNA (2#)+ neutrophils groups of the SCC15 cells were 304.29 ± 35.42, 459.66 ± 38.73,119.76± ± 32.91, and 154.15 ± 34.35, respectively (**Figure 5B**). The colony numbers of the Cal27 cells in the NC, NC+ neutrophils, Chemerin, and Chemerin+ neutrophils groups were 110.32 ± 31.41, 176.62 ± 35.53, 200.72 ± 38.91, and 301.35 ± 44.75, respectively, and those of the SCC9 cells in the Scr-shRNA, Scr-shRNA+ neutrophils, Chemerin-shRNA (2#), and Chemerin-shRNA (2#)+ neutrophils groups were 121.62 ± 35.39, 182.42 ± 31.59, 202.41 ± 42.21, and 331.18 ± 38.75, respectively (**Figure 5B**). These findings indicated that neutrophils promoted the proliferation of OSCC cells *via* Chemerin.

Flow cytometry was performed to further study the effects of Chemerin and neutrophils on the cell cycle. The cell phase distributions of the Scr-shRNA, Scr-shRNA+neutrophils,

TABLE 3 | Univariate and multivariate overall survival analysis in OSCC patients.

Variables	Regression coefficient	Univariate analysis		Regression coefficient	Multivariate analysis	
		Hazard ratio (95% CI)	*P* value		Hazard ratio (95% CI)	*P* value
Sex	-0.174	0.841 (0.415~1.702)	0.630			
Age	0.313	1.367 (0.716~2.612)	0.343			
TNM stage	0.934	2.544 (1.292~5.009)	0.007*	1.246	3.477 (0.76~15.894)	0.108
Differentiation	-0.218	0.804 (0.422~1.534)	0.508			
Lymph node metastasis	0.841	2.319 (1.2~4.482)	0.012*	-0.718	0.488 (0.101~2.349)	0.371
Tumor size	0.148	1.16 (0.561~2.396)	0.689			
Tumor recurrence	0.369	1.446 (0.753~2.775)	0.268			
The expression of Chemerin, CD15 + TANs density	0.691	1.995 (1.246~3.195)	0.004*	0.598	1.810 (1.056~3.133)	0.031*

CI, Confidence interval.
**P < 0.05 was considered to be statistically significant.*

TABLE 4 | Univariate and multivariate disease-free survival analysis in OSCC patients.

Variables	Regression coefficient	Univariate analysis		Regression coefficient	Multivariate analysis	
		Hazard ratio (95% CI)	*P* value		Hazard ratio (95% CI)	*P* value
Sex	-0.191	0.826 (0.408~1.674)	0.597			
Age	0.177	1.194 (0.624~2.285)	0.592			
TNM stage	1.907	2.996 (1.508~5.951)	0.002*	1.351	3.861 (0.838~17.79)	0.083
Differentiation	-0.335	0.716 (0.374~1.368)	0.312			
Lymph node metastasis	1.022	2.779 (1.423~5.427)	0.003*	-0.773	0.462 (0.095~2.236)	0.337
Tumor size	0.199	1.221 (0.591~2.523)	0.591			
Tumor recurrence	0.516	1.675 (0.87~3.225)	0.123			
The expression of Chemerin, CD15 + TANs density	0.968	2.634 (1.588~4.367)	<0.001*	0.877	2.405 (1.353~4.273)	0.003*

CI, Confidence interval.
**P < 0.05 was considered to be statistically significant.*

Chemerin-shRNA (2#), and Chemerin-shRNA (2#)+ neutrophils groups of SCC15 cells were as follows (**Figure 5C**): G1 phase: 55.13% ± 1.16%, 51.58% ± 2.71%, 58.34 ± 1.32% and 59.55% ± 2.15%; S phase: 21.67% ± 1.45%,26.11 ± 2.81%, 17.52% ± 1.74% and 17.81% ± 1.36%; and G2/M phase: 23.2% ± 2.19%, 22.31% ± 3.41%, 24.14% ± 2.08%, and 22.64% ± 1.95%. The proportion of the G1 phase was significantly decreased and the G2/M phase ratio was significantly increased in the Scr-shRNA group compared with those in the neutrophils group. Compared with the Scr-shRNA group, the Chemerin-shRNA (2#) group had a significant reduction in the proportion of cells in the G1 phase and a significant increase in the proportion of cells in the G2/M phase, indicating significant G2/M arrest. The effect of neutrophils on the cell cycle was abolished after Chemerin knock-down. The cell phase distributions of NC, NC+ neutrophils, Chemerin, and Chemerin+ neutrophils Cal27 cells were determined to further confirm these findings and were as follows (**Figure 4C**): G1 phase: 68.8% ± 2.96%,

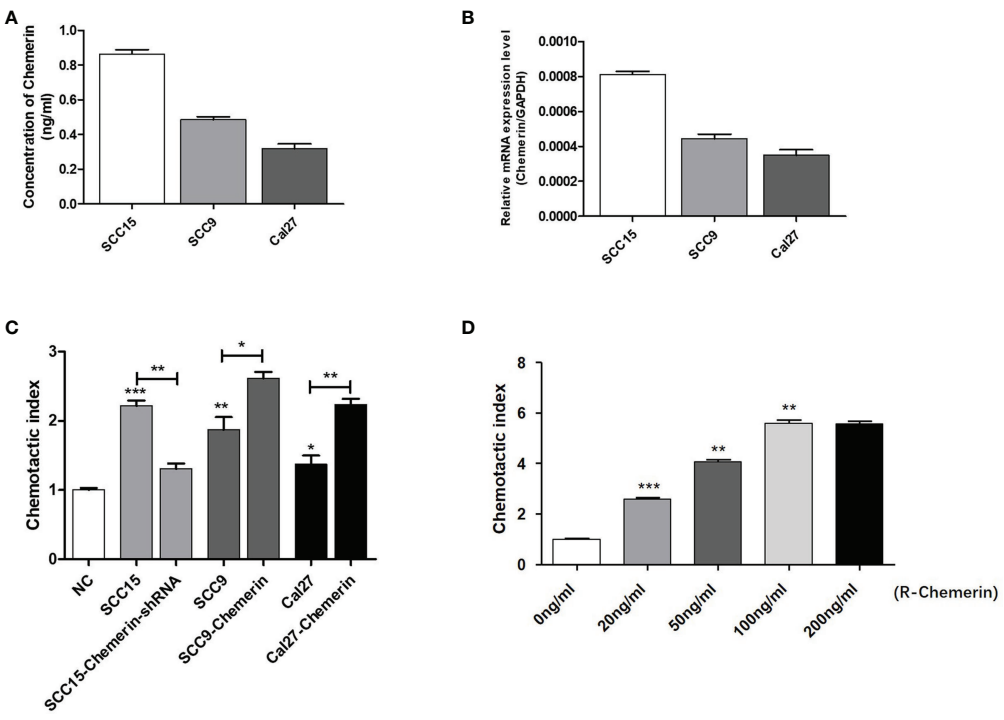

FIGURE 3 | OSCC cells expressing Chemerin attract neutrophils *in vitro*. **(A)** Supernatant Chemerin levels in OSCC cell lines were detected by ELISAs. **(B)** mRNA expression levels of Chemerin in OSCC cell lines were detected by qRT-PCR. **(C)** The effect of OSCC cells on neutrophils' chemotaxis was assayed using a transwell system. **(D)** The effect of R- Chemerin on neutrophils' chemotaxis was assayed using a transwell system at various concentrations (0-200 ng/ml). **P* < 0.05; ***P* < 0.01; ****P* < 0.001.

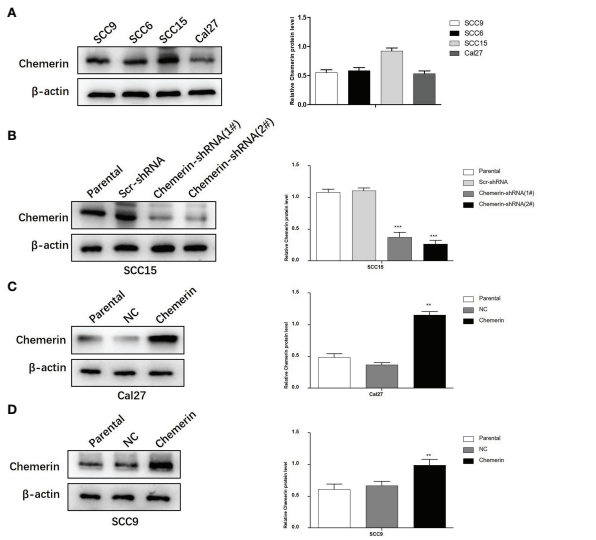

FIGURE 4 | The silencing and over-expression efficiency of Chemerin in OSCC cell lines. **(A)** Western blot analysis of Chemerin protein expression in SCC9, SCC6, SCC15 and Cal27 cells. β-actin was used as the control. **(B)** The knockdown efficiency of Chemerin-shRNA (1# and 2#) in SCC15 cell. In the following experiments, Chemerin-shRNA 2# was chosen because of its higher efficiency in silencing Chemerin. Scr-shRNA was used as a negative control. **(C, D)** SCC9 and Cal27 cells were used to over-express Chemerin by lentivirus, and Western blot analysis showed the expression of Chemerin increased after Chemerin transfection (*$P < 0.05$; **$P < 0.01$; ***$P < 0.001$). NC was used as a negative control. All data were presented as mean ± SD. All the experiments were repeated three times.

58.2% ± 2.01%, 57.5% ± 2.30%, and 49.5% ± 2.110%; S phase: 12.93% ± 2.29%,19.5% ± 1.87%, 20.3% ± 2.74%, and 27.3% ± 1.21%; and G2/M phase: 18.27% ± 2.01%, 22.3% ± 1.65%, 22.2% ± 2.35%, and 23.2% ± 2.25%. The cell phase distributions of the NC, NC+ neutrophils, Chemerin, and Chemerin+ neutrophils SCC9 cells were as follows (**Figure 5C**): G1 phase: 62.20% ± 1.26%, 56.70% ± 1.01%, 56.1% ± 1.30%, and 51.8% ± 1.45%; S phase: 18.40% ± 1.59%,27.10% ± 1.87%, 26.2% ± 1.74%, and 34.2% ± 2.71%; and G2/M phase: 19.1% ± 2.09%, 16.2% ± 3.05%, 17.7% ± 2.38%, and 14.0% ± 2.35%.

Neutrophils Promote the Migration, Invasion, and EMT of OSCC Cells Through Chemerin

Transwell assay was used to further investigate the migration and invasion of OSCC cells. The results showed that in the Scr-shRNA, Scr-shRNA+ neutrophils, Chemerin-shRNA (2#), and Chemerin-shRNA (2#)+ neutrophils groups, the numbers of migrated SCC15 cells were 188.67 ± 9.07, 295.67 ± 13.23, 107.67 ± 5.86, and 127.67 ± 10.02 (**Figure 6A**), respectively, and the numbers of invasive SCC15 cells were 173.56 ± 6.11, 255.00 ± 5.00, 103.47 ± 7.37 and 113.33 ± 6.65 (**Figure 6B**), respectively. These data suggested that neutrophils promoted cell migration and invasion and that the down-regulation of Chemerin significantly inhibited the migration and invasion of SCC15 cells. Furthermore, the effect of neutrophils on cell migration and invasion was abolished after Chemerin knockdown.

Transwell assays were performed on Chemerin-over-expressing Cal27 and SCC9 cells to further confirm these results. In the NC, NC + neutrophils, Chemerin, and Chemerin+ neutrophils groups, the numbers of migrated Cal27(SCC9) cells were 29.33 ± 4.14, 48.67 ± 7.12, 49.00 ± 5.62, and 88.67 ± 5.60 (105.32 ± 9.76, 189.67 ± 10.06, 200.32 ± 9.56, and 339.14 ± 7.02) (**Figure 6C**), respectively, and the numbers of invasive Cal27(SCC9) cells were 25.34 ± 6.13, 45.34 ± 5.51, 44.67 ± 6.66, and 81.52 ± 8.08(79.00 ± 6.56, 151.01 ± 9.07, 143.07 ± 7.94, and 301.67 ± 11.50), respectively (**Figure 6D**). Therefore, neutrophils may promote the migration and invasion of OSCC cells *via* Chemerin.

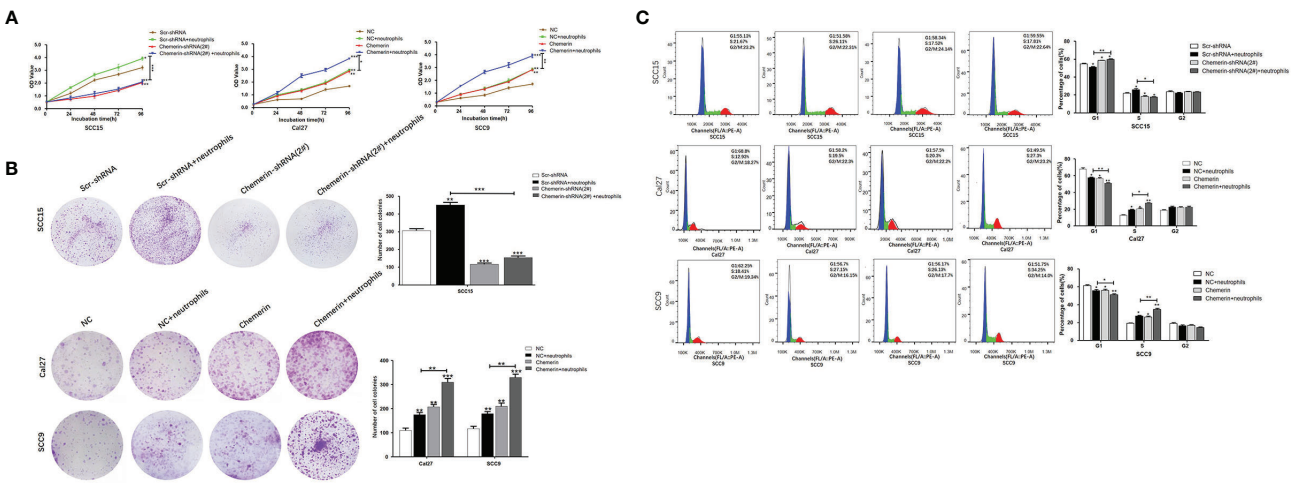

FIGURE 5 | Neutrophils promote cell proliferation through Chemerin. **(A)** Cell growth was analyzed using the MTT assay. Absorbance of 490 nm was measured. The data were presented as the means of six separated experiments, each performed in triplicate. **(B)** Colony formation in each group was photographed and colony numbers were illustrated in histogram. **(C)** Flow cytometry revealed the distribution of cell phases in the OSCC cell lines. Data were shown as mean ± SD from three independent experiments (*$P < 0.05$; **$P < 0.01$; ***$P < 0.001$).

EMT, a well-characterized embryological process, has been identified to play a critical role in tumor metastasis (34–36). We cultured OSCC cells with neutrophils in a previously described co-culture system to explore the role of neutrophils and Chemerin in mediating EMT in OSCC cells.

Chemerin, Slug, Snail, E-cadherin, N-cadherin, and Vimentin were detected in OSCC *via* Western blot analysis to further examine the effect of Chemerin and neutrophils on EMT. Neutrophils decreased the expression of E-cadherin and increased the expression levels of Chemerin, Slug, Snail, N-cadherin, and Vimentin in the three OSCC cell lines relative to in the control group. Compared with those in the Scr-shRNA group, the expression of E-cadherin increased and the expression levels of Chemerin, N-cadherin, Vimentin, Slug, and Snail decreased in the Chemerin-shRNA (2#) SCC15 cells. Moreover, the effects of neutrophils on Chemerin, E-cadherin, N-cadherin, Vimentin, Slug, and Snail significantly decreased after Chemerin knock-down (**Figure 6E**). This correlation was then confirmed in Cal27 and SCC9 cells (**Figures 6F, G**), in which Chemerin over-expression further promoted the expression of EMT-related proteins in the neutrophils group. Therefore, neutrophils promoted the EMT of OSCC cells and further promoted the migration and invasion of OSCC cells. This effect may be mediated by Chemerin.

Neutrophils Activate the JAK2/STAT3 Signaling Pathway in OSCC Cells Through Chemerin

We used using Western blot analysis to examine the expression levels of JAK2, p-JAK2, STAT3, p-STAT3, Phospho-Rb, E2F1, CyclinE1, and CyclinD1 in the Scr-shRNA, Scr-shRNA+ neutrophils, Chemerin-shRNA (2#), and Chemerin-shRNA (2#)+neutrophils groups of SCC15 cells and the NC, NC+ neutrophils, Chemerin, and Chemerin+ neutrophils groups of Cal27(SCC9) cells to investigate whether JAK2/STAT3 signaling is involved in the interaction between neutrophils and Chemerin in OSCC cells in the co-culture system. We found that neutrophils increased the expression levels of p-JAK2, p-STAT3, Phospho-Rb, E2F1, CyclinE1, and CyclinD1 in the three OSCC cells relative to those in the control group. p-JAK2, p-STAT3, Phospho-Rb, E2F1, CyclinE1, and CyclinD1 levels decreased in the Chemerin-shRNA (2#) SCC15 cells relative to those in the Scr-shRNA group. Moreover, the effects of neutrophils on p-JAK2, p-STAT3, Phospho-Rb, E2F1, CyclinE1, and CyclinD1 significantly decreased after Chemerin knockdown (**Figure 7A**). This correlation was then confirmed through Chemerin over-expression in Cal27 and SCC9 cells, in which Chemerin over-expression further promoted the expression of proteins in the neutrophils group (**Figures 7B, C**). All these data indicated that neutrophils may regulate the JAK2/STAT3 signaling pathway through Chemerin to promote the proliferation and invasion of OSCC cells.

DISCUSSION

Neutrophils are the most abundant subpopulation of leukocytes that provide the first line of defense against invading pathogens. Studies have found that TANs have multiple functions in the tumor microenvironment (6). Depending on the tumor microenvironment, TANs may affect tumor progression through cytokines and chemokines with tumor-promoting or antitumor functions (7). Chemerin is a chemoattractant and a novel multifunctional adipokine. It plays an important role in regulating inflammation, angiogenesis, fat metabolism, cell proliferation, migration, and chemotaxis (37–40). However, the possible roles of Chemerin expression and neutrophils in OSCC have not been experimentally verified.

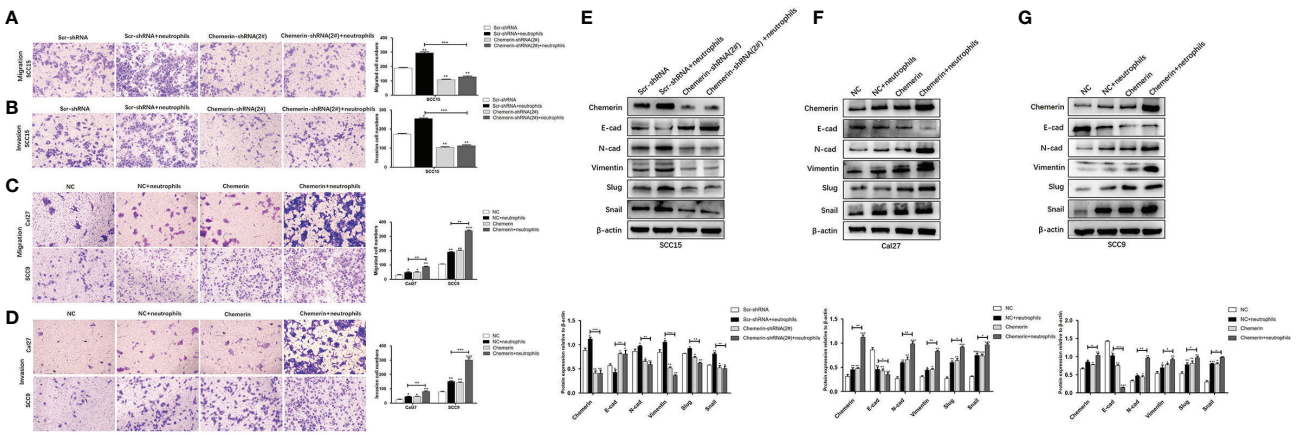

FIGURE 6 | Neutrophils promote migration, invasion and EMT of OSCC cells through Chemerin. **(A, B)** Transwell and invasion assays showed migration and invasion of SCC15 cells in the Scr-shRNA, Scr-shRNA + neutrophils, Chemerin-shRNA (2#), and Chemerin-shRNA (2#) +neutrophils groups. **(C, D)** Migration and invasion assay of Cal27 and SCC9 cells in NC, NC + neutrophils, Chemerin, and Chemerin + neutrophils groups. **(E–G)** Western blot of Chemerin, E-cadherin, N-cadherin, Vimentin, Slug and Snail. All data were presented as mean ± SD values from three independent experiments, each performed in triplicates (*$P < 0.05$; **$P < 0.01$; ***$P < 0.001$).

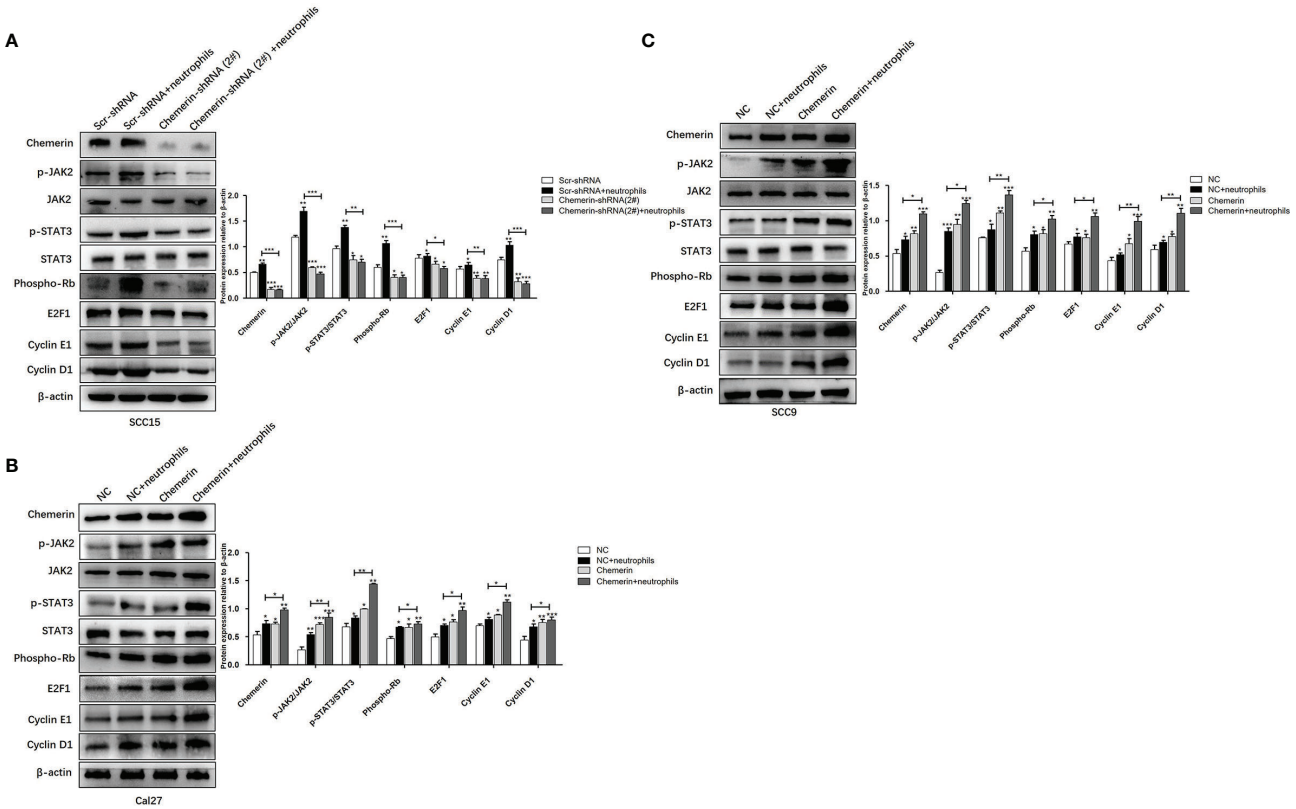

FIGURE 7 | Neutrophils activate the JAK2/STAT3 signaling pathway in OSCC cells through Chemerin. **(A)** The levels of JAK2, p-JAK2, STAT3, p-STAT3, Phospho-Rb, E2F1, CyclinE1, CyclinD1 protein of SCC15 in the Scr-shRNA, Scr-shRNA + neutrophils, Chemerin-shRNA (2#), and Chemerin-shRNA (2#) +neutrophils groups. **(B, C)** The levels of JAK2, p-JAK2, STAT3, p-STAT3, Phospho-Rb, E2F1, CyclinE1, CyclinD1 protein of Cal27 and SCC15 in NC, NC + neutrophils, Chemerin, and Chemerin + neutrophils groups. All data were presented as mean ± SD. All the experiments were repeated three times, each performed in triplicates (*$P < 0.05$; **$P < 0.01$; ***$P < 0.001$).

Chemokines are important components of cancer-related inflammatory conditions that promote tumor progression in many ways; these conditions include leukocyte recruitment and function, tumor cell proliferation, invasion, and metastasis (41–43). Previous research has demonstrated that Chemerin induces the chemotaxis of immune cells, such as immature dendritic cells, resident macrophages, and cytotoxic natural killer cells, to inflammatory sites (44). We used the Transwell assay to explore the possible chemotactic effects of Chemerin from tumor cells on neutrophils. Our results showed that all three OSCC cell lines exhibited enhanced chemotaxis to neutrophils, and SCC15, which had the highest Chemerin level, had the greatest chemotactic effect. R-Chemerin also improved chemotaxis to neutrophils in a concentration-dependent manner. Additionally, our double-staining IHC results revealed that Chemerin expression demonstrated great heterogeneity in OSCC tissues and that TANs infiltration was increased in areas with strong Chemerin expression. Spearman's rho coefficient test indicated that Chemerin expression was positively related to the density of CD15+ TANs in OSCC tissues. Strong Chemerin expression+ high TANs density was associated with lymph node metastasis, high clinical stage, and tumor recurrence. This association indicated that strong Chemerin expression+ high TANs density may predict poor clinical outcomes. Moreover, survival analysis illustrated that strong Chemerin expression+ high TANs density was related to shortened overall and disease-free survival and that each factor was an independent prognostic factor of patients with OSCC. These results implied that Chemerin over-expression in OSCC may attract additional neutrophils to tumor sites and promote neutrophil-mediated tumor progression.

EMT is a key step for tumor cells to obtain enhanced invasive and metastatic capabilities; this step is characterized by the loss of connections and the acquisition of mesenchymal properties, such as motility and invasiveness, by epithelial cells (45). Tumor cells use EMT as an intermediate phenotype to achieve self-renewal and adapt to their microenvironment (46, 47). Previous works have found that EMT can be induced not only by the loss of cell contact (for example, due to the degradation of the basement membrane or other changes in the microenvironment) but also by a variety of cytokines, such as TGF-β (48). Neutrophils can induce EMT in OSCC. However, the molecular mechanism of this effect is poorly understood. In the tumor microenvironment, a large number of cytokines and chemokines, such as IL-1β, IL-6, IL-8, and TNFα

(49), can also induce EMT in OSCC. However, the current mechanism of Chemerin+ neutrophils polarization and its role in the progression of OSCC remains unclear. In the present study, we showed that neutrophils induced EMT in OSCC cells through Chemerin; this process was characterized by the decreased expression of E-cadherin and the increased expression of Slug, Snail, N-cadherin, and Vimentin. These EMT changes may help enhance the capability of OSCC cells to move actively. This enhancement is demonstrated by the increase in migratory and invasion capabilities triggered by neutrophils.

Chemerin is positively correlated with the activation of the STAT3 signaling pathway (50). The JAK signaling pathway promotes the activation of STAT3 and Tyr705 phosphorylation (27, 50, 51). A growing body of evidence indicates that the activation of the JAK2/STAT3 signaling pathway by chemokines or cytokines plays a positive role in tumor growth and progression. However, the role of the JAK2/STAT3 signaling pathway in OSCC has been poorly addressed. Our study demonstrated that the knockdown of Chemerin significantly impaired neutrophils-induced migration, invasion, and proliferation, as well as the neutrophils-induced EMT of OSCC cells *in vitro*. We also found that neutrophils activated JAK2/STAT3 signaling through Chemerin and then up-regulated JAK2/STAT3 signaling target genes, including Phospho-Rb, E2F1, CyclinE1, and CyclinD1 (52–55), which are highly expressed in OSCC. At the same time, neutrophils affected the cell cycle through Chemerin. In this study, we discovered that that knockdown of Chemerin only partially inhibited JAK2 or STAT3 phosphorylation, indicating that Chemerin partially contributed to the tumor-promoting effect of neutrophils on OSCC cells. Although the involvement of other growth factors and/or cytokines cannot be ruled out, in general, Chemerin is an important mediator of the tumor-promoting effect of neutrophils. In OSCC, Chemerin may promote EMT, tumorigenesis, and development by activating the JAK2/STAT3 signaling pathway.

Collectively, our results provided support for the first time that Chemerin over-expression and neutrophils abundance are associated with the poor clinical outcomes of patients with OSCC. Chemerin over-expression and neutrophils infiltration were the prognostic factors of poor clinical outcomes. In addition, on the one hand, neutrophils/chemerin activated JAK2/STAT3 pathway and upregulated its down stream cycle-related proteins to promote tumor proliferation. On the other hand, neutrophils/chemerin induced EMT of OSCC also through the JAK2/STAT3 pathway and further promoted tumor migration and invasion *via* EMT. So we believe that neutrophils may promote tumor progression (proliferation and invasion) *via* regulating EMT and JAK2/STAT3 signaling through Chemerin in Oral squamous cell carcinoma.

DATA AVAILABILITY STATEMENT

The raw data supporting the conclusions of this article will be made available by the authors, without undue reservation.

ETHICS STATEMENT

This study was performed in line with the principles of the Declaration of Helsinki. Informed consent was obtained from all individual participants included in the study. Written informed consent for publication was obtained from the patients enrolled in the study. Approval was granted by the ethics committee of The Affiliated Hospital of Qingdao University (10.14.2020/QYFYWZLL25964). The patients/participants provided their written informed consent to participate in this study.

AUTHOR CONTRIBUTIONS

XH and NW conceived and designed the study. FX, YF, FG, SG and XZ collected clinical data. XH and NW wrote the manuscript. All authors have reviewed the final version of the manuscript and approved its submission for publishing.

FUNDING

This study was funded by NW (National Natural Science Foundation of China, Grant Number: 81702677) and CW (National Natural Science Foundation of China, grant 81602320).

ACKNOWLEDGMENTS

I would like to thank NW, FG, FX, etc. for their help in this research, as well as Qingdao University, Pingxiang People's Hospital and Affiliated Hospital of Qingdao University for their support to this research. The authors thank the patients and clinical staff for their assistance in this study.

REFERENCES

1. Coussens LM, Werb Z. Inflammation and Cancer. *Nature* (2002) 420 (6917):860–7. doi: 10.1038/nature01322
2. Forastiere AA, Goepfert H, Maor M, Pajak TF, Weber R, Morrison W, et al. Concurrent Chemotherapy and Radiotherapy for Organ Preservation in Advanced Laryngeal Cancer. *N Engl J Med* (2003) 349(22):2091–8. doi: 10.1056/NEJMoa031317
3. Hanahan D, Weinberg RA. Hallmarks of Cancer: The Next Generation. *Cell* (2011) 144(5):646–74. doi: 10.1016/j.cell.2011.02.013
4. Quail DF, Joyce JA. Microenvironmental Regulation of Tumor Progression and Metastasis. *Nat Med* (2013) 19(11):1423–37. doi: 10.1038/nm.3394
5. Magalhaes MA, Glogauer JE, Glogauer M. Neutrophils and Oral Squamous Cell Carcinoma: Lessons Learned and Future Directions. *J Leukoc Biol* (2014) 96(5):695–702. doi: 10.1189/jlb.4RU0614-294R
6. Galdiero MR, Garlanda C, Jaillon S, Marone G, Mantovani A. Tumor Associated Macrophages and Neutrophils in Tumor Progression. *J Cell Physiol* (2013) 228(7):1404–12. doi: 10.1002/jcp.24260
7. Tecchio C, Scapini P, Pizzolo G, Cassatella MA. On the Cytokines Produced by Human Neutrophils in Tumors. *Semin Cancer Biol* (2013) 23(3):159–70. doi: 10.1016/j.semcancer.2013.02.004
8. Li C, Zhao L, Wang Q, Ma S, Sun J, Ma C, et al. Neutrophils Infiltration and Its Correlation With Human Papillomavirus Status in the Oral Squamous Cell Carcinoma. *Cancer Manag Res* (2019) 11:5171–85. doi: 10.2147/CMAR.S202465

9. Wang N, Feng Y, Wang Q, Liu S, Xiang L, Sun M, et al. Neutrophils Infiltration in the Tongue Squamous Cell Carcinoma and Its Correlation With CEACAM1 Expression on Tumor Cells. *PloS One* (2014) 9(2):e89991. doi: 10.1371/journal.pone.0089991
10. Sotiropoulos GP, Dalamaga M, Antonakos G, Marinou I, Vogiatzakis E, Kotopouli M, et al. Chemerin as a Biomarker at the Intersection of Inflammation, Chemotaxis, Coagulation, Fibrinolysis and Metabolism in Resectable non-Small Cell Lung Cancer. *Lung Cancer* (2018) 125:291–9. doi: 10.1016/j.lungcan.2018.10.010
11. Nieto MA, Huang RY, Jackson RA, Thiery JP. EMT: 2016. *Cell* (2016) 166 (1):21–45. doi: 10.1016/j.cell.2016.06.028
12. Lamouille S, Xu J, Derynck R. Molecular Mechanisms of Epithelial-Mesenchymal Transition. *Nat Rev Mol Cell Biol* (2014) 15(3):178–96. doi: 10.1038/nrm3758
13. Singh R, Mandhani A, Agrawal V, Garg M. Positive Correlation Between Matrix Metalloproteinases and Epithelial-To-Mesenchymal Transition and its Association With Clinical Outcome in Bladder Cancer Patients. *Cancer Microenviron* (2018) 11(1):23–39. doi: 10.1007/s12307-017-0199-4
14. Puisieux A, Brabletz T, Caramel J. Oncogenic Roles of EMT-Inducing Transcription Factors. *Nat Cell Biol* (2014) 16(6):488–94. doi: 10.1038/ncb2976
15. Diepenbruck M, Christofori G. Epithelial-Mesenchymal Transition (EMT) and Metastasis: Yes, No, Maybe? *Curr Opin Cell Biol* (2016) 43:7–13. doi: 10.1016/j.ceb.2016.06.002
16. Mittal V. Epithelial Mesenchymal Transition in Aggressive Lung Cancers. *Adv Exp Med Biol* (2016) 890:37–56. doi: 10.1007/978-3-319-24932-2_3
17. Zheng X, Carstens JL, Kim J, Scheible M, Kaye J, Sugimoto H, et al. Epithelial-To-Mesenchymal Transition Is Dispensable for Metastasis But Induces Chemoresistance in Pancreatic Cancer. *Nature* (2015) 527(7579):525–30. doi: 10.1038/nature16064
18. Gabrilovich DI, Ostrand-Rosenberg S, Bronte V. Coordinated Regulation of Myeloid Cells by Tumours. *Nat Rev Immunol* (2012) 12(4):253–68. doi: 10.1038/nri3175
19. Ferland DJ, Watts SW. Chemerin: A Comprehensive Review Elucidating the Need for Cardiovascular Research. *Pharmacol Res* (2015) 99:351–61. doi: 10.1016/j.phrs.2015.07.018
20. Bondue B, Wittamer V, Parmentier M. Chemerin and its Receptors in Leukocyte Trafficking, Inflammation and Metabolism. *Cytokine Growth Factor Rev* (2011) 22(5-6):331–8. doi: 10.1016/j.cytogfr.2011.11.004
21. Tummler C, Snapkov I, Wickstrom M, Moens U, Ljungblad L, Maria Elfman LH, et al. Inhibition of Chemerin/CMKLR1 Axis in Neuroblastoma Cells Reduces Clonogenicity and Cell Viability *In Vitro* and Impairs Tumor Growth In Vivo. *Oncotarget* (2017) 8(56):95135–51. doi: 10.18632/oncotarget.19619
22. Wang N, Wang QJ, Feng YY, Shang W, Cai M. Overexpression of Chemerin was Associated With Tumor Angiogenesis and Poor Clinical Outcome in Squamous Cell Carcinoma of the Oral Tongue. *Clin Oral Invest* (2014) 18 (3):997–1004. doi: 10.1007/s00784-013-1046-8
23. Liu-Chittenden Y, Patel D, Gaskins K, Giordano TJ, Assie G, Bertherat J, et al. Serum RARRES2 Is a Prognostic Marker in Patients With Adrenocortical Carcinoma. *J Clin Endocrinol Metab* (2016) 101(9):3345–52. doi: 10.1210/jc.2016-1781
24. Lin W, Chen YL, Jiang L, Chen JK. Reduced Expression of Chemerin is Associated With a Poor Prognosis and a Lowed Infiltration of Both Dendritic Cells and Natural Killer Cells in Human Hepatocellular Carcinoma. *Clin Lab* (2011) 57(11-12):879–85.
25. Weigert J, Obermeier F, Neumeier M, Wanninger J, Filarsky M, Bauer S, et al. Circulating Levels of Chemerin and Adiponectin Are Higher in Ulcerative Colitis and Chemerin is Elevated in Crohn's Disease. *Inflamm Bowel Dis* (2010) 16(4):630–7. doi: 10.1002/ibd.21091
26. Kumar JD, Kandola S, Tiszlavicz L, Reisz Z, Dockray GJ, Varro A. The Role of Chemerin and ChemR23 in Stimulating the Invasion of Squamous Oesophageal Cancer Cells. *Br J Cancer* (2016) 114(10):1152–9. doi: 10.1038/bjc.2016.93
27. Loncle C, Bonjoch L, Folch-Puy E, Lopez-Millan MB, Lac S, Molejon MI, et al. IL17 Functions Through the Novel Reg3β-JAK2-STAT3 Inflammatory Pathway to Promote the Transition From Chronic Pancreatitis to Pancreatic Cancer. *Cancer Res* (2015) 75(22):4852–62. doi: 10.1158/0008-5472.CAN-15-0896
28. Yuan K, Ye J, Liu Z, Ren Y, He W, Xu J, et al. Complement C3 Overexpression Activates JAK2/STAT3 Pathway and Correlates With Gastric Cancer Progression. *J Exp Clin Cancer Res* (2020) 39(1):9. doi: 10.1186/s13046-019-1514-3
29. Wu X, Tao P, Zhou Q, Li J, Yu Z, Wang X, et al. IL-6 Secreted by Cancer-Associated Fibroblasts Promotes Epithelial-Mesenchymal Transition and Metastasis of Gastric Cancer *via* JAK2/STAT3 Signaling Pathway. *Oncotarget* (2017) 8(13):20741–50. doi: 10.18632/oncotarget.15119
30. Zheng M, Cao MX, Yu XH, Li L, Wang K, Wang SS, et al. STAT3 Promotes Invasion and Aerobic Glycolysis of Human Oral Squamous Cell Carcinoma *via* Inhibiting Foxo1. *Front Oncol* (2019) 9:1175. doi: 10.3389/fonc.2019.01175
31. Kijima T, Niwa H, Steinman RA, Drenning SD, Gooding WE, Wentzel AL, et al. STAT3 Activation Abrogates Growth Factor Dependence and Contributes to Head and Neck Squamous Cell Carcinoma Tumor Growth In Vivo. *Cell Growth Differ* (2002) 13(8):355–62.
32. Leeman RJ, Lui VW, Grandis JR. STAT3 as a Therapeutic Target in Head and Neck Cancer. *Expert Opin Biol Ther* (2006) 6(3):231–41. doi: 10.1517/14712598.6.3.231
33. Wang N, Wang Q, Chi J, Xiang F, Lin M, Wang W, et al. Carcinoembryonic Antigen Cell Adhesion Molecule 1 Inhibits the Antitumor Effect of Neutrophils in Tongue Squamous Cell Carcinoma. *Cancer Sci* (2019) 110 (2):519–29. doi: 10.1111/cas.13909
34. Hao Y, Baker D, Ten Dijke P. TGF-β-Mediated Epithelial-Mesenchymal Transition and Cancer Metastasis. *Int J Mol Sci* (2019) 20(11):2767. doi: 10.3390/ijms20112767
35. Chaffer CL, San Juan BP, Lim E, Weinberg RA. EMTCell Plasticity and Metastasis. *Cancer Metastasis Rev* (2016) 35(4):645–54. doi: 10.1007/s10555-016-9648-7
36. Bakir B, Chiarella AM, Pitarresi JR, Rustgi AK. EMT, MET, Plasticity, and Tumor Metastasis. *Trends Cell Biol* (2020) 30(10):764–76. doi: 10.1016/j.tcb.2020.07.003
37. Sell H, Laurencikiene J, Taube A, Eckardt K, Cramer A, Horrighs A, et al. Chemerin is a Novel Adipocyte-Derived Factor Inducing Insulin Resistance in Primary Human Skeletal Muscle Cells. *Diabetes* (2009) 58(12):2731–40. doi: 10.2337/db09-0277
38. Mariani F, Roncucci L. Chemerin/chemR23 Axis in Inflammation Onset and Resolution. *Inflamm Res Off J Eur Histamine Res Soc* (2015) 64(2):85–95. doi: 10.1007/s00011-014-0792-7
39. Kaur J, Adya R, Tan BK, Chen J, Randeva HS. Identification of Chemerin Receptor (ChemR23) in Human Endothelial Cells: Chemerin-Induced Endothelial Angiogenesis. *Biochem Biophys Res Commun* (2010) 391 (4):1762–8. doi: 10.1016/j.bbrc.2009.12.150
40. Erdogan S, Yilmaz FM, Yazici O, Yozgat A, Sezer S, Ozdemir N, et al. Inflammation and Chemerin in Colorectal Cancer. *Tumour Biol* (2016) 37 (5):6337–42. doi: 10.1007/s13277-015-4483-y
41. Nishida J, Momoi Y, Miyakuni K, Tamura Y, Takahashi K, Koinuma D, et al. Epigenetic Remodelling Shapes Inflammatory Renal Cancer and Neutrophil-Dependent Metastasis. *Nat Cell Biol* (2020) 22(4):465–75. doi: 10.1038/s41556-020-0491-2
42. Mantovani A, Savino B, Locati M, Zammataro L, Allavena P, Bonecchi R. The Chemokine System in Cancer Biology and Therapy. *Cytokine Growth Factor Rev* (2010) 21(1):27–39. doi: 10.1016/j.cytogfr.2009.11.007
43. Nagarsheth N, Wicha MS, Zou W. Chemokines in the Cancer Microenvironment and Their Relevance in Cancer Immunotherapy. *Nat Rev Immunol* (2017) 17(9):559–72. doi: 10.1038/nri.2017.49
44. Wittamer V, Franssen JD, Vulcano M, Mirjolet JF, Le Poul E, Migeotte I, et al. Specific Recruitment of Antigen-Presenting Cells by Chemerin, a Novel Processed Ligand From Human Inflammatory Fluids. *J Exp Med* (2003) 198 (7):977–85. doi: 10.1084/jem.20030382
45. Thiery JP, Acloque H, Huang RY, Nieto MA. Epithelial-Mesenchymal Transitions in Development and Disease. *Cell* (2009) 139(5):871–90. doi: 10.1016/j.cell.2009.11.007
46. Klymkowsky MW, Savagner P. Epithelial-Mesenchymal Transition: A Cancer Researcher's Conceptual Friend and Foe. *Am J Pathol* (2009) 174(5):1588–93. doi: 10.2353/ajpath.2009.080545
47. Savagner P. The Epithelial-Mesenchymal Transition (EMT) Phenomenon. *Ann Oncol* (2010) 21(Suppl 7):vii89–92. doi: 10.1093/annonc/mdq292

48. Kalluri R, Weinberg RA. The Basics of Epithelial-Mesenchymal Transition. *J Clin Invest* (2009) 119(6):1420–8. doi: 10.1172/JCI39104
49. Zhang W, Gu J, Chen J, Zhang P, Ji R, Qian H, et al. Interaction With Neutrophils Promotes Gastric Cancer Cell Migration and Invasion by Inducing Epithelial-Mesenchymal Transition. *Oncol Rep* (2017) 38(5):2959–66. doi: 10.3892/or.2017.5942
50. An X, Liu J, Li Y, Dou Z, Li N, Suo Y, et al. Chemerin/CMKLR1 Ameliorates Nonalcoholic Steatohepatitis by Promoting Autophagy and Alleviating Oxidative Stress Through the JAK2-STAT3 Pathway. *Peptides* (2021) 135:170422. doi: 10.1016/j.peptides.2020.170422
51. Bromberg J, Wang TC. Inflammation and Cancer: IL-6 and STAT3 Complete the Link. *Cancer Cell* (2009) 15(2):79–80. doi: 10.1016/j.ccr.2009.01.009
52. Kuo YY, Lin HP, Huo C, Su LC, Yang J, Hsiao PH, et al. Caffeic Acid Phenethyl Ester Suppresses Proliferation and Survival of TW2.6 Human Oral Cancer Cells *via* Inhibition of Akt Signaling. *Int J Mol Sci* (2013) 14(5):8801–17.
53. Yin Y, Tan Y, Yao Y, Lu N, Zhang F. SNHG12/miR-326/E2F1 Feedback Loop Facilitates the Progression of Oral Squamous Cell Carcinoma. *Oral Dis* (2020) 26(8):1631–9. doi: 10.1111/odi.13458
54. Li Y, Wang Y, Li J, Ling Z, Chen W, Zhang L, et al. Tacrolimus Inhibits Oral Carcinogenesis Through Cell Cycle Control. *BioMed Pharmacother* (2021) 139:111545. doi: 10.1016/j.biopha.2021.111545
55. Jiang Q, Cao Y, Qiu Y, Li C, Liu L, Xu G. Progression of Squamous Cell Carcinoma Is Regulated by miR-139-5p/CXCR4. *Front Biosci (Landmark Ed)* (2020) 25:1732–45. doi: 10.2741/4875

Conflict of Interest: The authors declare that the research was conducted in the absence of any commercial or financial relationships that could be construed as a potential conflict of interest.

Publisher's Note: All claims expressed in this article are solely those of the authors and do not necessarily represent those of their affiliated organizations, or those of the publisher, the editors and the reviewers. Any product that may be evaluated in this article, or claim that may be made by its manufacturer, is not guaranteed or endorsed by the publisher.

frontiers in Oncology

ORIGINAL RESEARCH
published: 24 February 2022
doi: 10.3389/fonc.2022.781348

Anti–PD-1 Monoclonal Antibody Combined With Anti-VEGF Agent Is Safe and Effective in Patients With Recurrent/Metastatic Head and Neck Squamous Cancer as Second-Line or Beyond Treatment

Yonghong Hua[1*], *Ruizeng Dong*[2], *Ting Jin*[1], *Qifeng Jin*[1] *and Xiaozhong Chen*[1*]

[1] Key Laboratory of Radiation Oncology, Zhejiang Cancer Hospital, University of Chinese Academy of Sciences, Hangzhou, China, [2] Department of Abdominal Medical Oncology, Zhejiang Cancer Hospital, University of Chinese Academy of Sciences, Hangzhou, China

OPEN ACCESS

Edited by:
Pablo Parente-Arias,
A Coruña University Hospital Complex (CHUAC), Spain

Reviewed by:
Vito Carlo Alberto Caponio,
University of Foggia, Italy
Gary Goldberg,
Rowan University School of Osteopathic Medicine, United States

***Correspondence:**
Yonghong Hua
yonghonghua@163.com
Xiaozhong Chen
cxzfyun@sina.com

Specialty section:
This article was submitted to Head and Neck Cancer, a section of the journal Frontiers in Oncology

Received: 22 September 2021
Accepted: 27 January 2022
Published: 24 February 2022

Citation:
Hua Y, Dong R, Jin T, Jin Q and Chen X (2022) Anti–PD-1 Monoclonal Antibody Combined With Anti-VEGF Agent Is Safe and Effective in Patients With Recurrent/Metastatic Head and Neck Squamous Cancer as Second-Line or Beyond Treatment. Front. Oncol. 12:781348. doi: 10.3389/fonc.2022.781348

Background: Numerous preclinical studies have revealed the complex regulatory mechanisms between anti-angiogenesis and immune inhibition in the tumor immune microenvironment and have proposed the efficacy of combined immunotherapy and anti-angiogenic treatment. Moreover, the combination strategy had been confirmed in a number of clinical trials. In this study, we aimed to evaluate the safety and efficacy of this combination strategy in recurrent/metastatic head and neck squamous cell carcinoma.

Methods: In this real-world study, 43 patients who received the combination of programmed cell death protein 1 (PD-1) inhibitors and anti-vascular endothelial growth factor (VEGF) agents in Zhejiang cancer hospitals between March 2019 and December 2020 were reviewed. Clinical characteristics and follow-up data were collected, and the preliminary efficacy and safety of the combination therapy were assessed.

Results: The median follow-up time was 12.4 months (range, 3.7-25.3 months), and the follow-up rate was 100%. The median duration of exposure was 9.5 months. Thirty-seven patients (86.0%) reported treatment-related adverse events (TRAEs) of any grade. The most frequently reported events were fatigue, decreased appetite, and hypertension. Grade 3 TRAEs occurred in 8 patients (18.6%), and no grade 4 or 5 TRAEs occurred. Twenty-four patients (55.9%) had an overall response to treatment: 6 (14.0%) had a complete response and 18 (41.9%) had a partial response. In addition, 5 (11.6%) patients had stable disease, and the disease control rate 12 was 67.4%. The median time to response was 1.6 months (range, 1.1-2.8 months). The median progression-free survival (PFS) was not reached, and the 1-year PFS rate was 69.1%. The 1-year overall survival (OS) rate was 87.7%. Patients with primary tumors located in the nasopharynx had better OS than those with tumors outside the nasopharynx. ECOG PS were related to PFS; patients with an ECOG PS of 0 had a slight survival advantage.

Conclusion: The combination strategy of anti–PD-1 monoclonal antibodies and anti-VEGF agents was tolerable in patients with recurrent/metastatic head and neck cancer. This treatment exhibited antitumor potential despite the heavily pretreated population.

Keywords: head and neck squamous cell carcinoma, anti–PD-1 monoclonal antibodies, anti-VEGF agents, safety, efficacy

INTRODUCTION

Head and neck squamous cell carcinoma (HNSCC) include a variety of malignancies in the oral cavity, nasal cavity, oropharynx, nasopharynx, and laryngopharynx. In 2020, more than 870,000 new cases of HNSCC were diagnosed globally, accounting for 4.5% of all newly diagnosed malignant cancers worldwide (1). More than 50% of diagnosed HNSCC cases are at locally advanced stages. Despite the use of multimodal treatment for locally advanced HNSCC, more than 50% of these patients will experience recurrence or metastasis within 3 years (2). EXTREME regimen (cetuximab + cisplatin/carboplatin + fluorouracil) is often used to treat recurrent and/or metastatic (R/M) disease, which has been approved as the first-line choice for R/M HNSCC in many countries (3). However there is no standard treatment for R/M HNSCC that fails to respond to first-line platinum-containing systemic chemotherapy. Single-drug chemotherapy or cetuximab is usually recommended, but the median overall survival (OS) is 7 or fewer months (4).

Immunotherapy has revolutionized the treatment dilemma, enabling durable control of some previously incurable R/M HNSCC (5). Programmed cell death protein 1 (PD-1) is a transmembrane immune checkpoint receptor that is expressed on activated T cells, B cells, natural killer cells, and some myeloid cells; it can recognize PD-1 ligands (PD-L1 and PD-L2) and limit the cytotoxic T cell effect within tissues (6, 7). Overexpression of PD-L1 has been found to block the antitumor immune response in some tumor cells (8). Zandberg et al. reported that PD-L1 was expressed in 50%-60% of HNSCC (9). Anti–PD-1 antibodies can improve survival in some patients with R/M HNSCC by blocking the recognition of PD-1 and PD-L1. The pivotal phase III Checkmate 141 trial and Keynote 040 trial confirmed respectively the efficacy of nivolumab and pembrolizumab in pretreated R/M HNSCC compared with the investigator's choice of treatment (10, 11). The same benefit was observed in R/M nasopharyngeal carcinoma in the POLARIS-02 study of Toripalimab (12).

On the basis of above clinical researches, PD-1 inhibitors as monotherapy have been approved by the US Food and Drug Administration and the European Medicines Agency to treat some pretreated R/M HNSCC. However, two key problems remain: First, the overall response rate (ORR) remains relatively low—the ORR ranges from 14% to 43% in pretreated R/M HNSCC (including nasopharyngeal cancer)—so the majority of patients with R/M HNSCC do not benefit from this monotherapy (10–12). Second, the therapeutic effect differs significantly across patients. A durable response could last a long time in some patients, whereas some patients could experience hyperprogression (13). No robust mechanistic data has explained the unpredictable clinical response to anti–PD-1 antibodies. Given the problems with immunotherapy as monotherapy, many clinical studies have explored the combination of different immune checkpoint inhibitors or immune checkpoint inhibitors with chemotherapy, radiotherapy, and targeted therapy (14–16).

Anti-angiogenic agents have opened a new window for immunotherapy combinations. Initially, anti-angiogenic agents appeared to play an antitumor role by blocking neovascularization (17). Subsequently, it was found that anti-angiogenic agents could also regulate immune cells and the tumor immune microenvironment (18). Some exploratory studies have verified the value of anti-angiogenic agents combined with immunotherapy in lung cancer, liver cancer, and renal cell cancer (19–22). Keynote-146 (NCT02501096) is an open-label, one-arm phase Ib/II clinical study to evaluate the efficacy of Pembrolizumab combined with Lenvatinib in a variety of solid tumors. 22 patients with R/M HNSCC were included in the cohort. The data showed that the ORR of the combined regimen was 46%, and the median duration of remission was 8.2 months (95% CI:2.2-12.6). The median PFS was 4.7 months (95% CI:4.0-9.8). Based on the good results, we tried to use the both drugs to posterior line treat R/M HNSCC in clinical practices. Most of patients had received multiple systemic chemotherapy. In this real-world study, we collected and analyzed the data about these patients' characteristics, treatment experience, toxicity and tumor control, and the safety and preliminary efficacy were assessed.

METHODS

Patient Selection

This real-world study enrolled patients who were diagnosed as R/M HNSCC (including nasopharyngeal cancer) and treated with the combination of PD-1 inhibitors and anti-VEGF agents in Zhejiang cancer hospitals between March 2019 and December 2020. PD-1 inhibitors included camrelizumab (Jiangsu Hengrui Medicine, Lianyungang, China), toripalimab (Junshi Bioscience, Shanghai, China), tislelizumab (Beigene, Guangzhou, China), sintilimab (Innovent Biologics, Suzhou, China), nivolumab (Bristol-Myers Squibb, Newyork, USA), and pembrolizumab (Merck & Co., Kenilworth, USA). Anti-VEGF agents included anlotinib (Chia Tai Tianqing Pharmaceutical, Lianyungang, China), apatinib (Jiangsu Hengrui Medicine, Lianyungang, China), and bevacizumab (Roche Group, Basel, Switzerland). The study was approved by the Ethics Committee of Zhejiang

Cancer Hospital, and the informed consent for this retrospective analysis was waived.

Data Collection

Treatment related adverse events (TRAEs) were one of observation factors, which were documented according to patient chief complaints and abnormal laboratory measures, including blood chemistry, hematology, coagulation, and urinalysis, at baseline and during the treatment period. National Cancer Institute Common Terminology Criteria for Adverse Events, version 4.0 was used to evaluate the severity of TRAEs. Efficacy was another observation factor. ORR, which was defined as a complete or partial response, was assessed during treatment and for 3 months after treatment discontinuation. Disease control rate at 12 weeks (DCR12), which was defined as complete or partial response or stable disease for more than 12 weeks, and duration of response (DOR), which was defined as the time from the first documentation of objective tumor response until the first documentation of objective tumor progression or death from any cause, whichever occurred first. Magnetic resonance imaging scan of the head and neck as well as chest, abdominal, and pelvic computed tomography scans were performed to assess the response to treatment. Measurable and nonmeasurable diseases were evaluated according to the modified RECIST 1.1 for immune-based therapeutics (iRECIST). Observation factors about efficacy also included OS and progression-free survival (PFS). Patients who discontinued treatment because of toxicity without evidence of disease progression had their PFS censored at the time of cutoff.

Statistical Analysis

Statistical comparisons were performed using chi-squared or Fisher's exact tests for categorical data and t tests for continuous variables. ORR and DCR12 were estimated using the exact binomial method. OS and PFS were estimated and presented graphically using the Kaplan-Meier method. DOR12 was estimated using the Kaplan-Meier method. Patients were censored at the time of death or last follow-up. All statistical analyses were performed with a 5% alpha risk or 95% confidence interval using SPSS software (version 20.0, Chicago, IL, USA).

RESULTS

Patient Population

From March 2019 to December 2020, 43 patients with R/M HNSCC received the combination regimens. At the data cutoff on March 31, 2021, the median follow-up time was 12.4 months (range, 3.7-25.3 months), and the follow-up rate was 100%. All patients received anti–PD-1 immune checkpoint inhibitors, namely camrelizumab (n=17), toripalimab (n=13), tislelizumab (n=8), sintilimab (n=2), nivolumab (n=1), and pembrolizumab (n=2). Patients received the following anti-VEGF agents: anlotinib (n=25), apatinib (n=17), and bevacizumab (n=1). All 43 patients were included in the safety analysis and evaluated for response. Most patients (90.7%) were men, and the median age was 55.0 years (range, 30-80 years). All patients had an ECOG PS of 0-1. Most patients (86.0%) had metastatic disease, of which 31 (72.0%) had metastatic disease alone and 4 (14.0%) had metastatic and recurrent disease. Most patients (76.7%) had received 2or more prior lines of systemic therapy for R/M disease, and 30.2% had received 3or more previous lines of systemic therapy. The reason for changing the treatment included disease progression within 6 months (n=21; 48.8%), progression after 6 months (n=12; 27.9%), and intolerance to the previous line of treatment (n=10; 23.3%). Overall, 46.5% of patients had previously received 1or 2 targeted therapies, including anti-EGFR monoclonal antibodies (n=15) and endostatin (n=5). No patient had received PD-1 inhibitors in previous treatment. Two patients (4.7%) received local radiotherapy to the R/M disease. All patient characteristics are shown in **Table 1**.

Treatment Delivery and Compliance

A total of 43 patients enrolled in the real-world study. As of March 31, 2021, 21 patients (48.8%) were off treatment; of these, 17 (80.9%) discontinued both study drugs. The reasons for discontinuing both agents were disease progression (n=9), adverse events (n=1), and patient refusal(n=7). One patient experienced bleeding from the larynx, which was relieved through symptomatic treatment; then, this patient discontinued entire treatment. One patient with complete response terminated both agents when the entire treatment lasted for 2 years. Six patients interrupted therapy because of economic reasons, of which, 5 patients received fewer than 3 cycles of combination regimens. Four patients (25.0%) discontinued anti–PD-1 antibodies (n=3; 18.8%) or anti-VEGF agents (n=1; 6.2%). Two patients experienced adverse events (reactive capillary hyperplasia in 1 patient and increased blood creatinine concentration in 1 patient) before discontinuing the PD-1 inhibitors, although these adverse events were reversible with drug discontinuation and/or corticosteroid therapy. One patient with a continuous complete response stopped the PD-1 inhibitor but maintained treatment with apatinib when the entire treatment lasted for 1 year. One patient discontinued anlotinib because of grade 3 throat pain. During the therapy, no patient underwent dose reduction of the anti–PD-1 inhibitors or anti-VEGF agents.

Safety

Of the 43 patients for safety analysis, the median duration of exposure to combination therapy was 9.5 months (range, 0.5-24.8 months). Thirty-seven patients (86.0%) reported TRAEs of any grade. The most frequently reported events were fatigue, decreased appetite, and hypertension. The majority of the TRAEs were low grade. Grade 3 TRAEs occurred in 8 patients (18.6%). One patient developed grade 3 oropharyngeal pain, which was considered to be related to the small molecular anti-VEGF agent anlotinib. This patient discontinued anti-VEGF treatment for 1 month, and the pain stopped; thereafter, the patient refused to continue anlotinib, so only the immune checkpoint inhibitor was continued. One patient with treatment-related grade 3 increases in blood creatinine concentrations discontinued the anti–PD-1

TABLE 1 | Baseline characteristics of study patients.

Characteristic, n (%)	All patients (n = 43)
Median age (range, year)	55.0 (30-80)
Age (year), n (%)	
≤60	28 (65.1)
>60	15 (34.9)
Sex, n(%)	
Male	39 (90.7)
Female	4 (9.3)
ECOG PS, n (%)	
0	22 (51.2)
1	21 (48.8)
No. of prior systemic regimens, n (%)	
1	10 (23.3)
2	20 (46.5)
≥3	13 (30.2)
Reasons for change the previous-line, n (%)	
Progression within 6 months	21 (48.8)
Progression after 6 months	12 (27.9)
Intolerance to pervious line	10 (23.3)
Primary tumor, n (%)	
Nasopharynx	29 (67.4)
Larynx	5 (11.6)
Hypopharynx	6 (14.0)
Oral cavity	2 (4.7)
Oropharynx	1 (2.3)
Previous target therapy, n (%)	
No	23 (53.5)
Yes	20 (46.5)
Radiotherapy to R/M disease, n (%)	
No	41 (95.3)
Yes	2 (4.7)
R/M at baseline, n (%)	
Recurrence	6 (14.0)
Metastasis	31 (72.0)
Recurrence and metastasis	6 (14.0)
PD-L1 CPS status, n (%)	
≥20	6 (14.0)
1-19	5 (11.6)
<1	3 (7.0)
Unknown	29 (67.4)
EGFR status, n (%)	
Positive	37 (86.1%)
Negative	1 (2.3%)
Unknown	5 (11.6%)

ECOG PS, Eastern Cooperative Oncology Group performance status; R/M, recurrence/metastasis; PD-L1, Programmed cell death-Ligand 1; CPS, Combined positive score; EGFR, epidermal growth factor receptor.

TABLE 2 | Treatment-Related Adverse Events in all patients (n = 43).

Adverse events	Any grade	Grade 3*
Any	37 (86.0)	8 (18.6)
Fatigue	25 (58.1)	1 (2.3)
Decreased appetite	21 (48.8)	0
Hypertension	16 (37.2)	1 (2.3)
Hypothyroidism	14 (32.6))	1 (2.3)
Nausea	13 (30.2)	0
Increased blood glucose concentration	7 (16.3)	0
Oropharyngeal pain	7 (16.3)	2 (4.7)
Increased aminotransferase concentration	6 (14.0)	0
Pruritus	6 (14.0)	0
Anemia	5 (11.6)	0
Increased blood creatinine concentration	4 (9.3)	1 (2.3)
Bleeding	3 (7.0)	0
Reactive capillary hyperplasia	3 (7.0)	1 (2.3)
Infusion-related reaction	3 (7.0)	0
Hand-foot syndrome	2 (4.7)	1 (2.3)

Data are n (%) of all 43 participants. The table lists maximum grade adverse events reported at grades 1–2 in at least 5% patients and grade 3 events.
There were no grade 4 or 5 TRAEs.

monoclonal antibody toripalimab for 3.5 months; the abnormal creatinine concentration was relieved to grade 1 with corticosteroid treatment. There was no grade 4 or 5 TRAEs. Four patients discontinued treatment for TRAEs. All adverse events are shown in **Table 2**.

Efficacy

During follow-up, 24 patients (55.9%) had an ORR to treatment, and the DCR12 was 67.4%. The efficacy evaluation for all patients is shown in **Table 3**. According to the maximum percent change in target lesion size from the baseline, 25 patients experienced a response to the combination therapy; the corresponding waterfall plot is presented in **Figure 1**. The median time to response was 1.6 months (range, 1.1-2.8 months). Among these 25 responding patients, 24(96.0%) had an ongoing response at the last follow-up. Only 1 responding patient had subsequent disease progression. This patient had multiple hepatic metastasis but achieved an initial response after 1.7 months and then maintained treatment for 8.7 months; standard follow-up scans demonstrated a radiographic enlargement of hepatic disease, and the evaluation of curative effect was revised to progressive disease. At the data cutoff on March 31, 2021, the median DOR in responding patients was 10.5 months (range, 1.9-23.7 months).

Throughout the treatment period, 10 patients developed disease progression, of which 3 tumors were at the site of the original focus, 4 were new lesions, and 3 were at both original and new sites. 4 patients developed disease progression after interrupting treatment for poor economic conditions. The median PFS was not reached, and the 1-year PFS was 69.1% (**Figure 2**). Five patients died from the disease during the observation period; the median OS was not reached, and 1-year OS was 87.7% (**Figure 3**). Univariate Cox analysis was performed to determine whether any clinical features were associated with PFS and OS. The ECOG PS score was related to PFS; patients with a PS score of 0 had a PFS advantage compared with patients with a PS score of 1 (p=0.005) (**Figure 4**). Patients with primary tumors located in the nasopharynx had better OS than those with tumors outside the nasopharynx, and the preponderance was significant (p=0.001) (**Figure 5**). Multivariate Cox analysis wasn't performed because of the small sample size of the study. Details of the univariate analysis are shown in **Table 4**.

DISCUSSION

Anti-angiogenic agents have the advantage of regulating the tumor immune microenvironment, so they are suitable to combine with immune checkpoint inhibitors. To date, VEGF is the most studied

TABLE 3 | Clinical therapeutic evaluation for study patients.

All patients (n = 43)	
Response-evaluable patients	43 (100)
Overall response	
Complete response	6 (14.0)
Partial response	18 (41.9)
Stable disease	5 (11.6)
Progressive disease	14 (32.6)
ORR	24 (55.9)
DCR12	29 (67.4)

DCR 12, disease control rate 12; ORR, overall response rate.

angiogenesis factor. Its immunosuppressive function manifests prominently as inhibition of immune effector cell differentiation and maturation (18). Many studies have observed that anti-VEGF agents promote the accumulation of CD8+ and CD4+ T lymphocytes in tumors, decrease PD-1 expression of tumor-infiltrating T lymphocytes and inhibit regulatory T cells as well

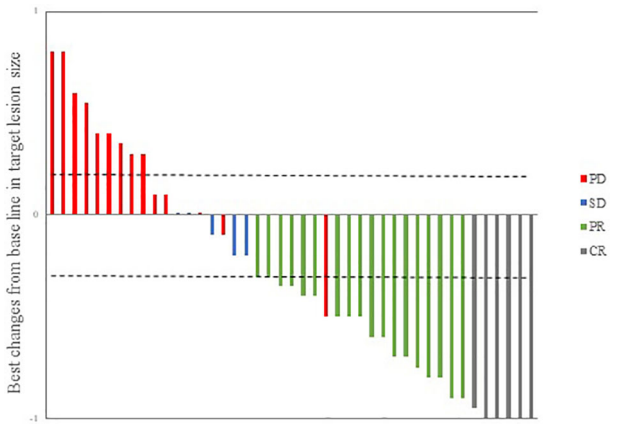

FIGURE 1 | Waterfall plot illustrating maximum changes in target lesions size (n = 43). CR, complete response; PR, partial response; SD, stable disease; PD, progressive disease.

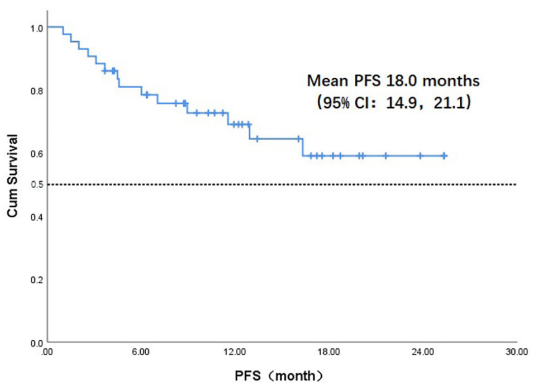

FIGURE 2 | Kaplan-Meier survival curve of progression-free survival in 43 head and neck cancer patients. PFS, progression-free survival;CI, confidence interval.

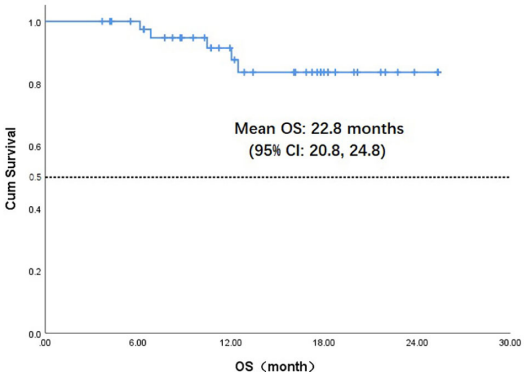

FIGURE 3 | Kaplan-Meier survival curve of overall survival in 43 head and neck cancer patients. OS,overall survival;CI, confidence interval.

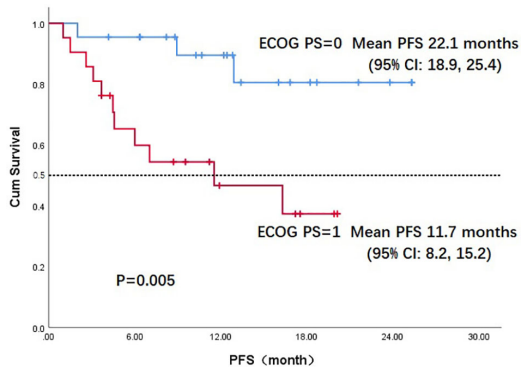

FIGURE 4 | Kaplan-Meier survival curve of progression-free survival in ECOG PS 0 and PS 1 patients. PFS, progression-free survival;ECOG PS, Eastern Cooperative Oncology Group performance status; CI, confidence interval.

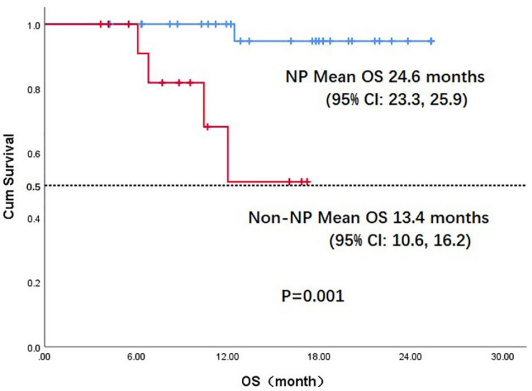

FIGURE 5 | Kaplan-Meier survival curve of overall survival in NP and non-NP patients. OS, overall survival;NP, nasopharyngeal cancer; CI, confidence interval.

TABLE 4 | Univariate analysis of factors associated with PFS and OS.

	PFS			OS		
	Mean ± SD (months)	χ^2	p value	Mean ± SD (months)	χ^2	p value
Age (years)						
≤60	19.6 ± 1.8	2.483	0.115	23.7 ± 1.0	2.149	0.143
>60	14.5 ± 2.9			20.6 ± 2.3		
Gender						
Male	17.9 ± 1.7	0.062	0.803	23.1 ± 1.0	1.078	0.299
Female	20.5 ± 4.2			18.6 ± 4.7		
ECOG PS						
0	22.2 ± 1.7	7.933	0.005	24.4 ± 0.9	2.917	0.088
1	11.7 ± 1.8			18.5 ± 1.0		
No. of prior systemic regimens						
1	NR			NR		
≥2	16.0 ± 1.8			22.2 ± 1.2		
Reasons for changed line						
Progression within 6 months	15.1 ± 2.6	0.139	0.669	23.1 ± 1.5	0.329	0.848
Progression after 6 months	17.3 ± 2.5			22.1 ± 1.6		
Intolerance	15.9 ± 2.6			19.9 ± 1.8		
Primary tumor						
Nasopharynx	19.5 ± 1.7	2.311	0.128	24.6 ± 0.7	10.422	0.001
Non-nasopharynx	10.9 ± 1.9			13.4 ± 1.4		
R/M at baseline						
Recurrence ± metastasis	12.2 ± 2.3	2.403	0.121	17.8 ± 1.5	0.434	0.510
Metastasis only	19.4 ± 1.7			23.2 ± 1.1		

ECOG PS, Eastern Cooperative Oncology Group performance status; NR, not reached (no event occurred); OS, overall survival; PFS, progression-free survival; R/M, recurrence and/or metastasis; SD, standard deviation.

as myeloid-derived suppressor cells and their immunosuppressive functions (23–25). However, angiogenic factors prevent immune cells from infiltrating into the tumor immune microenvironment through the tumor vessels. Overexpression of angiogenesis could promote expression of adhesion molecules and chemokines, and abnormal vascular structure could form a selective immune-cell barrier (26). Anti-angiogenic activity could promote the infiltration of different immune cells and upregulate the effectiveness of immunotherapy (27). Based on this mechanism, anti-VEGR agents in combination with anti–PD-1 monoclonal antibodies have been applied to lung cancer, hepatic cell cancer, and renal cell carcinoma; the combination was considered effective and tolerable, and no unexpected toxicities were observed.

In this study, we reviewed patients with R/M HNSCC who had experienced failure with or intolerance to frontline therapy to receive the combination strategy. In all, grade 3 TRAEs occurred in 18.6% of patients, and no grade 4 or 5 TRAEs occurred. Compared with monotherapy using PD-1 inhibitors or anti-VEGF agents, the combination strategy didn't increase the incidence and severity of TRAEs, and no new TRAEs were observed. Moreover, the combination was associated with decreases in some specific adverse responses. The unique toxicity caused by camrelizumab was reactive capillary hyperplasia, which occurred at rates up to 74.1% in clinical studies of camrelizumab alone (28). In this study, 18 patients (41.7%) were treated with camrelizumab, but only 4 patients developed reactive capillary hyperplasia, accounting for 22% of patients taking camrelizumab. Zhou used camrelizumab and apatinib to treat patients with advanced *EGFR* and *ALK* wild-type non–small cell lung cancer; he found that the combination regimen significantly reduced reactive capillarity to 15.6%—a rate similar to that in our study (29). We speculate that anti-VEGF agents normalized the vascular malformation in skin and sodecreased the incidence and severity of reactive capillary hyperplasia.

Because of overlapping toxicities with combination therapy, it was difficult to determine whether the adverse events resulted from anti-VEGF agents or anti–PD-1 monoclonal antibodies. We can only classify them roughly according to our experience, which can help us deal with various adverse reactions. The 3 most common adverse events reported in this study, fatigue, decreased appetite, and hypertension, seemed related to antiangiogenic agents; however, some potentially immune-related adverse events, including hypothyroidism and increased blood glucose concentrations, were reported. The safety profile of the combination regimen was generally consistent with the known safety data of anti–PD-1 antibodies and antiangiogenic agents. No unique adverse events were reported in the HNSCC population. For 8 patients with grade 3 TRAEs, all were manageable by standard guidelines.

Twenty-four patients (55.9%) achieved overall responses in the study; this rate was less than the rates in the CAPTAIN-1st and JUPITER studies but more than the rate in Keynote048 (14, 30, 31). These 3 studies were designed to combine PD-1 inhibitors with systemic chemotherapy to treat first-line R/M HNSCC (including NPC). The ORR of our study was notable, because three quarters of patients had already received at least 2 lines of prior systemic therapy. At the data cutoff on March 31, 2021, the median DOR in responding patients was 10.5 months (range, 1.9-23.7 months); moreover, only 1 patient of the 25 experienced disease progression, which suggests that the DOR

can be maintained for a long time after patients are in remission. Similar results have been observed with other combination strategies using PD-1 inhibitors and anti-angiogenic agents (e.g., in lung cancer, renal cancer). The success of combination strategies suggests that the immune checkpoint inhibitors combined with anti-angiogenesis agents might improve survival, not merely postpone treatment failure.

In our study, 22 patients (51.2%) had a PS score of 0. In univariate analysis, the PS score was associated with PFS; patients with a PS score of 0 had an advantage in PFS compared with those with a PS score of 1 (mean, 22.2 vs. 11.7 months, p=0.005). OS differed according to the location of primary tumor: the OS in patients with nasopharyngeal carcinoma was much better than in those with non-nasopharyngeal carcinoma (mean, 24.6 vs. 14.9months, p=0.027); the difference was attributed to the prognosis difference between the tumor types. The combination of PD-1 inhibitors and anti-angiogenic agents has increased the 1-year OS from a range of 36%-60% to 92% according to data from Checkmate-141 and BGB-A317-102, which used anti–PD-1 monotherapy in later treatment lines for R/M HNSCC and nasopharyngeal carcinoma (10, 32). These results suggest that the antitumor efficacy of a combination strategy is at least additive and possibly synergistic. In our study, the antitumor activity of the combination regimen was superior to that expected from anti–PD-1 monotherapy.

However, this study had some limitations. First, this study was retrospective, so its intrinsic selection bias may be responsible for the observed differences in outcome. Randomized comparisons between PD-1 inhibitors alone and PD-1 inhibitors in combination are warranted to avoid imbalances and selection biases. Second, the relatively small sample size of the patient cohort might weaken the effectiveness of the statistical analysis. Last, 6 PD-1 inhibitors and 3 VEGF inhibitors were utilized. As different agents had different molecular targets and toxicity profiles, which would make the analysis of efficacy and safety more difficult.

CONCLUSION

This case-series study shows that the combination of anti–PD-1 monoclonal antibodies and anti-VEGF agents is tolerable in patients with R/M HNSCC and that the treatment exhibits antitumor potential despite the heavily pretreated status of many enrolled patients. The path from laboratory to clinic remains long; in-depth research should be investigated according to different primary tumors, and the mechanism of the synergistic effects of anti–PD-1 and anti-VEGF agents must be explored.

DATA AVAILABILITY STATEMENT

The raw data supporting the conclusions of this article will be made available by the authors, without undue reservation.

ETHICS STATEMENT

The studies involving human participants were reviewed and approved by Ethics Committee of Zhejiang Cancer Hospital. The ethics committee waived the requirement of written informed consent for participation.

AUTHOR CONTRIBUTIONS

Conception and design: YH and XC. Collection and assembly of data: YH, QJ, and TJ. Data analysis and interpretation: YH and RD. Manuscript writing and final approval of manuscript: all authors. All authors contributed to the article and approved the submitted version.

FUNDING

This work was supported by the Zhejiang Natural Science Foundation (LY17H160042), and the Medical Science and Technology Project of Zhejiang province (2016ZB021).

ACKNOWLEDGMENTS

We appreciate the patients who participated in this study.

REFERENCES

1. Ferlay J, Colombet M, Soerjomataram I, Parkin DM, Piñeros M, Znaor A, et al. Cancer Statistics for the Year 2020: An Overview. *Int J Cancer* (2021). doi: 10.1002/ijc.33588
2. Blanchard P, Baujat B, Holostenco V, Bourredjem A, Baey C, Bourhis J, et al. Meta-Analysis of Chemotherapy in Head and Neck Cancer (MACH-NC): A Comprehensive Analysis by Tumour Site. *Radiother Oncol* (2011) 100(1):33–40. doi: 10.1016/j.radonc.2011.05.036
3. Vermorken JB, Mesia R, Rivera F, Remenar E, Kawecki A, Rottey S, et al. Platinum-Based Chemotherapy Plus Cetuximab in Head and Neck Cancer. *N Engl J Med* (2008) 359(11):1116–27. doi: 10.1056/NEJMoa0802656
4. National Comprehensive Cancer Network. *NCCN Clinical Practice Guidelines (NCCN Guidelines®) in Oncology: Head and Neck Cancers. Version 1.2018.* Available at: https://www.nccn.org/professionals/physician_gls/pdf/head-and-neck.pdf.
5. Mehra R, Seiwert TY, Gupta S, Weiss J, Gluck I, Eder JP, et al. Efficacy and Safety of Pembrolizumab in Recurrent/Metastatic Head and Neck Squamous Cell Carcinoma: Pooled Analyses After Long-Term Follow-Up in KEYNOTE-012. *Br J Cancer* (2018) 119(2):153–59. doi: 10.1038/s41416-018-0131-9
6. Blank C, Brown I, Peterson AC, Spiotto M, Iwai Y, Honjo T, et al. PD-L1/B7H-1 Inhibits the Effector Phase of Tumor Rejection by T Cell Receptor (TCR) Transgenic CD8+ T Cells. *Cancer Res* (2004) 64(3):1140–5. doi: 10.1158/0008-5472.can-03-3259
7. Latchman Y, Wood CR, Chernova T, Chaudhary D, Borde M, Chernova I, et al. PD-L2 is a Second Ligand for PD-1 and Inhibits T Cell Activation. *Nat Immunol* (2001) 2(3):261–8. doi: 10.1038/85330

8. Iwai Y, Ishida M, Tanaka Y, Okazaki T, Honjo T, Minato N. Involvement of PD-L1 on Tumor Cells in the Escape From Host Immune System and Tumor Immunotherapy by PD-L1 Blockade. *Proc Natl Acad Sci U.S.A.* (2002) 99 (19):12293–7. doi: 10.1073/pnas.192461099
9. Zandberg DP, Strome SE. The Role of the PD-L1:PD-1 Pathway in Squamous Cell Carcinoma of the Head and Neck. *Oral Oncol* (2014) 50(7):627–32. doi: 10.1016/j.oraloncology.2014.04.003
10. Ferris RL, Blumenschein GJr, Fayette J, Guigay J, Colevas AD, Licitra L, et al. Nivolumab for Recurrent Squamous-Cell Carcinoma of the Head and Neck. *N Engl J Med* (2016) 375(19):1856–67. doi: 10.1056/NEJMoa1602252
11. Cohen EEW, Soulieres D, Le Tourneau C, Dinis J, Licitra L, Ahn MJ, et al. Pembrolizumab Versus Methotrexate, Docetaxel, or Cetuximab for Recurrent or Metastatic Head and Neck Squamous Cell Carcinoma (KEYNOTE-040): A Randomised Open-Labe, Phase 3 Study. *Lancet* (2019) 393(10167):156–67. doi: 10.1016/S0140-6736(19)32591-7
12. Wang FH, Wei XL, Feng J, Li Q, Xu N, Hu XC, et al. Efficacy, Safety, and Correlative Biomarkers of Toripalimab in Previously Treated Recurrent or Metastatic Nasopharyngeal Carcinoma: A Phase II Clinical Trial (POLARIS-02). *J Clin Oncol* (2021) 39(7):704–12. doi: 10.1200/JCO.20.02712
13. Saâda-Bouzid E, Defaucheux C, Karabajakian A, Coloma VP, Servois V, Paoletti X, et al. Hyperprogression During Anti-PD-1/PD-L1 Therapy in Patients With Recurrent and/or Metastatic Head and Neck Squamous Cell Carcinoma. *Ann Oncol* (2017) 28(7):1605–11. doi: 10.1093/annonc/mdx178
14. Burtness B, Harrington KJ, Greil R, Soulières D, Tahara M, de Castro GJr, et al. Pembrolizumab Alone or With Chemotherapy Versus Cetuximab With Chemotherapy for Recurrent or Metastatic Squamous Cell Carcinoma of the Head and Neck (KEYNOTE-048): A Randomised, Open-Label, Phase 3 Study. *Lancet* (2019) 394(10212):1915–28. doi: 10.1016/S0140-6736(19)32591-7
15. Lien MY, Wang TH, Hsieh CY, Tsai MH, Hua CH, Cheng FM, et al. Both Combined or Sequential Use With Immune Checkpoint Inhibitors on Cetuximab-Treated Patients With Recurrent or Metastatic Head and Neck Squamous Cell Carcinoma Improve the Overall Survival. *Oral Oncol* (2021) 119:105380. doi: 10.1016/j.oraloncology.2021.105380
16. Qian JM, Schoenfeld JD. Radiotherapy and Immunotherapy for Head and Neck Cancer: Current Evidence and Challenges. *Front Oncol* (2021) 10:608772:608772. doi: 10.3389/fonc.2020.608772
17. Hicklin DJ, Ellis LM. Role of the Vascular Endothelial Growth Factor Pathway in Tumor Growth and Angiogenesis. *J Clin Oncol* (2005) 23(5):1011–27. doi: 10.1200/JCO.2005.06.081
18. Rahma OE, Hodi FS. The Intersection Between Tumor Angiogenesis and Immune Suppression. *Clin Cancer Res* (2019) 25(18):5449–57. doi: 10.1158/1078-0432.CCR-18-1543
19. Song Y, Fu Y, Xie Q, Zhu B, Wang J, Zhang B. Anti-Angiogenic Agents in Combination With Immune Checkpoint Inhibitors: A Promising Strategy for Cancer Treatment. *Front Immunol* (2020) 11:1956:1956. doi: 10.3389/fimmu.2020.01956
20. Damato A, Iachetta F, Antonuzzo L, Nasti G, Bergamo F, Bordonaro R, et al. Phase II Study on First-Line Treatment of Nivolumab in Combination With Folfoxiri/Bevacizumab in Patients With Advanced ColoRectal Cancer RAS or BRAF Mutated - NIVACOR Trial (GOIRC-03-2018). *BMC Cancer* (2020) 20 (1):822. doi: 10.1186/s12885-020-07268-4
21. Wang P, Fang X, Yin T, Tian H, Yu J, Teng F. Efficacy and Safety of Anti-PD-1 Plus Anlotinib in Patients With Advanced Non-Small-Cell Lung Cancer After Previous Systemic Treatment Failure-A Retrospective Study. *Front Oncol* (2021) 11:628124:628124. doi: 10.3389/fonc.2021.628124
22. Rini BI, Plimack ER, Stus V, Gafanov R, Hawkins R, Nosov D, et al. Pembrolizumab Plus Axitinib Versus Sunitinib for Advanced Renal-Cell Carcinoma. *N Engl J Med* (2019) 380(12):1116–27. doi: 10.1056/NEJMoa1816714
23. Bourhis M, Palle J, Galy-Fauroux I, Terme M. Direct and Indirect Modulation of T Cells by VEGF-A Counteracted by Anti-Angiogenic Treatment. *Front Immunol* (2021) 12:616837. doi: 10.3389/fimmu.2021.616837
24. Lapeyre-Prost A, Terme M, Pernot S, Pointet AL, Voron T, Tartour E, et al. Immunomodulatory Activity of VEGF in Cancer. *Int Rev Cell Mol Biol* (2017) 330:295–42. doi: 10.1016/bs.ircmb.2016.09.007
25. Voron T, Colussi O, Marcheteau E, Pernot S, Nizard M, Pointet AL, et al. VEGF-A Modulates Expression of Inhibitory Checkpoints on CD8+ T Cells in Tumors. *J Exp Med* (2015) 212(2):139–48. doi: 10.1084/jem.20140559
26. Hendry SA, Farnsworth RH, Solomon B, Achen MG, Stacker SA, Fox SB. The Role of the Tumor Vasculature in the Host Immune Response: Implications for Therapeutic Strategies Targeting the Tumor Microenvironment. *Front Immunol* (2016) 7:621:621. doi: 10.3389/fimmu.2016.00621
27. Motz GT, Santoro SP, Wang LP, Garrabrant T, Lastra RR, Hagemann IS, et al. Share Tumor Endothelium FasL Establishes a Selective Immune Barrier Promoting Tolerance in Tumors. *Nat Med* (2014) 20(6):607–15. doi: 10.1038/nm.3541
28. Wang F, Qin S, Sun X, Ren Z, Meng Z, Chen Z, et al. Reactive Cutaneous Capillary Endothelial Proliferation in Advanced Hepatocellular Carcinoma Patients Treated With Camrelizumab: Data Derived From a Multicenter Phase 2 Trial. *J Hematol Oncol* (2020) 13(1):47. doi: 10.1186/s13045-020-00886-2
29. Zhou C, Wang Y, Zhao J, Chen G, Liu Z, Gu K, et al. Efficacy and Biomarker Analysis of Camrelizumab in Combination With Apatinib in Patients With Advanced Nonsquamous NSCLC Previously Treated With Chemotherapy. *Clin Cancer Res* (2021) 27(5):1296–04. doi: 10.1158/1078-0432.CCR-20-3136
30. Yang Y, Qu S, Li J, Hu C, Xu M, Li W, et al. Camrelizumab Versus Placebo in Combination With Gemcitabine and Cisplatin as First-Line Treatment for Recurrent or Metastatic Nasopharyngeal Carcinoma (CAPTAIN-1st): A Multicentre, Randomised, Double-Blind, Phase 3 Trial. *Lancet Oncol* (2021) 22(8):1162–74. doi: 10.1016/S1470-2045(21)00302-8
31. Mai HQ, Chen QY, Chen D, Hu C, Yang K, Wen J, et al. Toripalimab or Placebo Plus Chemotherapy as First-Line Treatment in Advanced Nasopharyngeal Carcinoma: A Multicenter Randomized Phase 3 Trial. *Nat Med* (2021) 27(9):1536–43. doi: 10.1038/s41591-021-01444-0
32. Shen L, Guo J, Zhang QY, Pan HM, Yuan Y, Bai YX, et al. Tislelizumab in Chinese Patients With Advanced Solid Tumors: An Open-Label, non-Comparative, Phase 1/2 Study. *J Immunother Cancer* (2020) 8(1):e000437. doi: 10.1136/jitc-2019-000437

Conflict of Interest: The authors declare that the research was conducted in the absence of any commercial or financial relationships that could be construed as a potential conflict of interest.

frontiers in Oncology

ORIGINAL RESEARCH
published: 01 March 2022
doi: 10.3389/fonc.2022.809589

Upregulation of IGF2BP2 Promotes Oral Squamous Cell Carcinoma Progression That Is Related to Cell Proliferation, Metastasis and Tumor-Infiltrating Immune Cells

Lijie Zhou[1†], Hongyu Li[2,3†], Hongshi Cai[2,3†], Wenhui Liu[1], Enjiu Pan[1], Dongsheng Yu[3,4] and Shuai He[1*]*

[1] Department of Stomatology, The Second Affiliated Hospital and Yuying Children's Hospital of Wenzhou Medical University, Wenzhou, China, [2] Department of Oral and Maxillofacial Surgery, Hospital of Stomatology, Guanghua School of Stomatology, Sun Yat-sen University, Guangzhou, China, [3] Guangdong Provincial Key Laboratory of Stomatology, Sun Yat-sen University, Guangzhou, China, [4] Department of Oral Emergency, Hospital of Stomatology, Guanghua School of Stomatology, Sun Yat-sen University, Guangzhou, China

OPEN ACCESS

Edited by:
Song Fan,
Sun Yat-sen Memorial Hospital, China

Reviewed by:
Xi Jin,
Fudan University, China
Liang Ding,
Nanjing University, China

***Correspondence:**
Shuai He
capitall@163.com
Dongsheng Yu
yudsh@mail.sysu.edu.cn

[†]These authors have contributed equally to this work

Specialty section:
This article was submitted to Head and Neck Cancer, a section of the journal Frontiers in Oncology

Received: *05 November 2021*
Accepted: *31 January 2022*
Published: *01 March 2022*

Citation:
Zhou L, Li H, Cai H, Liu W, Pan E, Yu D and He S (2022) Upregulation of IGF2BP2 Promotes Oral Squamous Cell Carcinoma Progression That Is Related to Cell Proliferation, Metastasis and Tumor-Infiltrating Immune Cells. Front. Oncol. 12:809589. doi: 10.3389/fonc.2022.809589

The strong invasive and metastatic abilities of oral squamous cell carcinoma (OSCC) cells in the early stage are the main reason for its poor prognosis. The early diagnosis and treatment of OSCC may reduce the metastasis rate and improve the survival rate. The aim of this study was to explore candidate biomarkers related to the prognosis and progression of OSCC. We performed weighted gene coexpression network analysis to identify key modules and genes associated with OSCC and intersected the differentially expressed genes (DEGs) in The Cancer Genome Atlas (TCGA)-OSCC and GSE30784 datasets. Next, we performed survival analysis and immunohistochemistry to screen and validate the hub gene insulin-like growth factor 2 (IGF2) mRNA binding protein 2 IGF2BP2. We also used TCGA pan-cancer data to verify that IGF2BP2 was expressed at high levels in a variety of cancers and was related to a poor prognosis in patients. Furthermore, we divided patients with OSCC into high and low expression groups based on the median expression level of IGF2BP2. Gene set enrichment analysis (GSEA) showed that IGF2BP2 led to a poor prognosis in OSCC by affecting cancer-related (epithelial-mesenchymal transition, glycolysis, cell cycle, etc.) and immune-related biological functions and pathways. Single-sample GSEA (ssGSEA), CIBERSORT, and xCell algorithms helped reveal that high IGF2BP2 expression was accompanied by a significant reduction in the immune score, stromal score, and microenvironment score and a decrease in the number of infiltrating CD8+ T cells in OSCC. In addition, silencing IGF2BP2 suppressed the proliferation, migration, and invasion of OSCC cells. In general, IGF2BP2 is a potential biomarker for the progression, immunotherapy response, and prognosis of OSCC.

Keywords: IGF2BP2, oral squamous cell carcinoma, prognosis, WGCNA, GSEA, immunity

INTRODUCTION

Oral squamous cell carcinoma (OSCC) accounts for approximately 90% of oral cancers and has a high degree of malignancy; it can rapidly invade tissues and readily form metastases in the cervical lymph nodes and distant sites (1, 2). According to global cancer statistics in 2020, more than 370,000 cases of OSCC were diagnosed, and more than 170,000 patients died due to the disease (3). Despite the existence of mature diagnosis and comprehensive treatment methods, the 5-year overall survival (OS) rate of patients with OSCC has not been significantly improved in the past few decades and is still at approximately 50% (3, 4). Therefore, it is essential to clarify the causes and mechanisms of OSCC malignant progression and to explore more effective treatment strategies.

In recent years, with the rise of high-throughput sequencing technology, a large number of omics datasets [such as those in The Cancer Genome Atlas (TCGA) database (https://www.cancer.gov/tcga)] have been generated, and the Gene Expression Omnibus (GEO) database (https://www.ncbi.nlm.nih.gov/geo/), which stores high-throughput sequencing data, emerged. Due to the rapid development of bioinformatics, key pathways and genes involved in cancer have been identified based on a biomolecular network analysis. Weighted gene coexpression network analysis (WGCNA) is a systems biology method suitable for complex multisample data analysis. It can assess the expression relationship between genes, construct a coexpression network, identify gene modules consisting of highly coexpression genes, and combine gene modules. Correlation analysis of the phenotype of the sample can reveal the module related to the phenotype (5). WGCNA can identify gene modules that are highly related to the malignant progression of OSCC to explore the genes and biological processes that have changed in OSCC patients and normal controls.

Human insulin-like growth factor 2 (IGF2) mRNA binding protein 2 (IGF2BP2/IMP2) has a molecular mass of 66 kDa, with two N-terminal RNA recognition motifs and four C-terminal human heterogeneous ribonucleoprotein-K homologous structures (6, 7). Previously, IGF2BP2 was considered to be a gene related to type 2 diabetes (T2D) (6, 8). In fact, IGF2BP2, as an RNA-binding protein, regulates cell metabolism in human metabolic diseases such as diabetes, obesity and fatty liver through the posttranscriptional regulation of many genes in a variety of cell types (9). New evidence shows that IGF2BP2 is an m6A-binding protein that promotes mRNA (for example, MYC) stability and translation in an m6A-dependent manner and participates in the development and progression of several malignant cancers (10, 11). The expression of IGF2BP2 is significantly upregulated in head and neck squamous cell carcinoma (HNSC) tissue and predicts a poor prognosis (12). In addition, IGF2BP2 polymorphisms are associated with adverse clinical features and the development of oral cancers (13).

In this study, we performed WGCNA to identify key modules and genes associated with OSCC. Next, we assessed the prognostic value of the differentially expressed genes (DEGs) to screen out the hub gene IGF2BP2. Furthermore, we divided patients with OSCC into high- and low-expression groups based on the median expression value of IGF2BP2. Gene set enrichment analysis (GSEA) was preformed to explore the biological functions related to the expression of IGF2BP2 in OSCC. Single-sample GSEA (ssGSEA), CIBERSORT, and xCell were applied to evaluate the effect of IGF2BP2 expression on immune cell infiltration and the microenvironment in OSCC. Finally, we conducted a series of functional experiments *in vitro* to investigate the impact of IGF2BP2 on cell proliferation, migration, and invasion.

MATERIALS AND METHODS

OSCC Samples and Cell Culture

Ten OSCC tissues and their corresponding adjacent noncancerous normal tissues were collected from the Stomatology Hospital of Sun Yat-sen University with approval from the Stomatology Hospital Research Ethics Committee. All patients signed an informed consent form for participation in this study. The human OSCC cell lines SCC25 and CAL27 were obtained from the American Type Culture Collection (ATCC). SCC25 cells were cultured in Dulbecco's modified Eagle's medium/Ham's F12 (DMEM/F12, Gibco, USA) supplemented with 10% fetal bovine serum (FBS, WISENT, Canada) and 400 ng/mL hydrocortisone (H811182, MACKLIN, China). CAL27 cells were grown in Dulbecco's modified Eagle's medium (DMEM, Gibco, USA) containing 10% FBS. Cells were cultured in a humidified incubator at 37°C and 5% CO_2.

Data Collection and Processing and Identification of DEGs

The mRNA expression [log2(FPKM+1)] and corresponding clinical data of the OSCC patients (providing 306 OSCC samples and 30 matched normal samples) in the TCGA were downloaded from the UCSC Xena browser (https://xenabrowser.net) (14). The mRNA expression data were converted to log2 (TPM+1) values and used for further analysis. The gene expression matrix and corresponding clinical data from the GSE30784 and GSE42743 datasets were downloaded from the GEO database. The GSE30784 dataset contains data on 167 OSCC samples and 45 normal samples. The GSE42743 dataset includes information on 74 OSCC samples and 29 normal samples. We used the R package "limma" to analyze and filter DEGs with $|\log2(\text{fold change})| > 1$ and false discovery rate (FDR) <0.05 (15).

WGCNA

Genes with a standard deviation (SD) > 1 were used to construct a weighted gene coexpression network with the WGCNA package (5). First, we applied the goodSamplesGenes function to detect the quality of samples and genes and performed hierarchical clustering analysis on the samples through the average linkage method of the hclust function to screen and eliminate outliers. Second, after obtaining the best soft threshold power (β) according to the powerEstimate function, we selected a

β value of 5 for TCGA-OSCC dataset and 11 for the GSE30784 dataset to construct a weighted gene coexpression network based on scale-free topology. Next, we converted the expression matrix into an adjacency matrix using the adjacency function, and then implemented the TOMsimilarity function to convert the adjacency matrix into a topological overlap matrix, and calculated the degree of dissimilarity between genes. Third, based on the degree of dissimilarity between genes derived from the topological overlap matrix, we applied the dynamic shear tree method to hierarchically cluster the genes and set the minimum number of genes in the module to 30. The gene modules with dissimilarity less than 0.2 (correlation greater than 0.8) were merged using the mergeCloseModules function. Finally, we obtained the correlation coefficients and P values of each module eigengene and trait. The module eigengene with the largest correlation coefficient and smallest P value was the hub module.

Identification and Validation of the Hub Gene

We took the intersection of DEGs and genes in the modules most relevant to OSCC, all of which were obtained from TCGA-OSCC and GSE30784 datasets. The Venn diagram drawn with jvenn shows the intersection of these 4 gene sets and identified 12 overlapping genes (16). Univariate Cox analysis was performed to determine the correlation of the expression of these 12 genes with OS in TCGA-OSCC and GSE42743 datasets. The P value, hazard ratio (HR), and 95% confidence interval (CI) of each gene are presented in a forest plot. With a P value < 0.05 serving as the threshold, the two genes ANO1 and IGF2BP2 were finally screened out. In addition, univariate Cox analysis was applied to analyze the relationship of ANO1 expression and IGF2BP2 expression to recurrence-free survival (RFS) from TCGA-OSCC dataset. To verify the relationship between ANO1 and IGF2BP2 and the OS of HNSC patients in TCGA database using the Gene Expression Profiling Interactive Analysis 2 (GEPIA2) (http://gepia2.cancer-pku.cn/) web server.

Pan-Cancer Expression and Prognostic Value of ANO1 and IGF2BP2

GEPIA2 is an online website containing RNA-seq and clinical data of tumor tissues and normal tissues from the TCGA and GTEx databases. The TCGA pan-cancer database has 33 cancer subtypes. The included subtypes are abbreviated as follows: ACC, adrenocortical carcinoma; BLCA, bladder urothelial carcinoma; BRCA, breast invasive carcinoma; CESC, cervical squamous cell carcinoma and endocervical adenocarcinoma; CHOL, cholangiocarcinoma; COAD, colon adenocarcinoma; DLBC, lymphoid neoplasm diffuse large B-cell lymphoma; ESCA, esophageal carcinoma; GBM, glioblastoma multiforme; HNSC, head and neck squamous cell carcinoma; KICH, kidney chromophobe; KIRC, kidney renal clear cell carcinoma; KIRP, kidney renal papillary cell carcinoma; LAML, acute myeloid leukemia; LGG, brain lower grade glioma; LIHC, liver hepatocellular carcinoma; LUAD, lung adenocarcinoma; LUSC, lung squamous cell carcinoma; MESO, mesothelioma; OV, ovarian serous cystadenocarcinoma; PAAD, pancreatic adenocarcinoma; PCPG, pheochromocytoma and paraganglioma; PRAD, prostate adenocarcinoma; READ, rectum adenocarcinoma; SARC, sarcoma; SKCM, skin cutaneous melanoma; STAD, STOMACH adenocarcinoma; TGCT, testicular germ cell tumor; THCA, thyroid carcinoma; THYM, thymoma; UCEC, uterine corpus endometrial carcinoma; UCS, uterine carcinosarcoma; and UVM, uveal melanoma. We carried out differential expression analysis and OS analysis of ANO1 and IGF2BP2 in TCGA pan-cancer datasets by using GEPIA2.

GSEA

GSEA can be applied to analyze the enrichment of gene expression in biological functions and pathways (17). We performed GSEA between the high- and low- IGF2BP2 expression groups in TCGA-OSCC and GSE30784 datasets. The analysis of enriched biological functions and pathways according to IGF2BP2 expression was analyzed using hallmark gene sets and Kyoto Encyclopedia of Genes and Genomes (KEGG) gene sets. Gene sets with an adjusted P value < 0.05 and FDR <0.05 were considered significantly enriched.

IGF2BP2 Expression and Immune Cell Infiltration in OSCC

We used the CIBERSORT algorithm to analyze the RNA-seq data from the OSCC samples in TCGA-OSCC and GSE30784 datasets and determined the relative proportions of 22 tumor-infiltrating immune cells in each sample (18). ssGSEA was performed using the R package "GSVA" to quantify the enrichment scores of 28 immune cells in OSCC samples in TCGA-OSCC and GSE30784 datasets (19). In addition, we employed xCell (20), a method for cell type enrichment analysis based on ssGSEA, to infer the immune score, stromal score, and microenvironment score.

Immunohistochemistry, Western Blotting and Quantitative Real-Time PCR

The methods for IHC staining, IHC scoring, western blotting and qRT-PCR were described in previous studies (21). Primary antibodies against IGF2BP2 (1:250, D4R2F, Cell Signaling Technology, USA) were utilized for IHC staining, and those against β-actin (1:1,000, D6A8, Cell Signaling Technology, USA) and IGF2BP2 (1:1000, D4R2F, Cell Signaling Technology, USA) were used for western blotting. The primer sequences used were as follow: IGF2BP2-forward: 5′-AGTGGAATTGCATGGGAAAATCA-3′; IGF2BP2- reverse: 5′-CAACGGCGGTTTCTGTGTC-3′; MYC-forward: 5′-TCCCTCCACTCGGAAGGAC-3′; MYC-reverse: 5′-CTGGTGCATTTTCGGTTGTTG-3′; CD8A-forward: 5′-TCCTCCTATACCTCTCCCAAAAC-3′; CD8A-reverse: 5′-GGAAGACCGGCACGAAGTG-3′; β-actin-forward: 5′-CTACCTCATGAAGATCCTCACCGA-3′; and β-actin-reverse: 5′-TTCTCCTTAATGTCACGCACGATT-3′.

SiRNA Transfection

SCC25 and CAL27 cells were seeded into a 6-well plate and cultured for 24 h, and then PepMute Transfection Reagent

(SL100566, Signagen, USA) was applied to transfect 30 nM negative control (siNC) or IGF2BP2 siRNAs (si-IGF2BP2-1: GGGUAGAUAUCCAUAGAAA; si-IGF2BP2-2: AGAUAGA GAUUAUGAAGAA; si-IGF2BP2-3: GUUGAUUACUC AGUCUCUA) per well according to the manufacturer's instructions. Cells were collected 48 h after transfection.

Cell Proliferation

SCC25 and CAL27 cells were transfected with siRNA and seeded into 96-well plates at 2,000 cells per well. The time of 0 h was defined as the point were fully attached and Cell Counting Kit-8 (CCK-8, 40203ES80, Yeasen, China) reagent was used to detect cell proliferation at 5 time points (0, 24, 48, 72 and 96 h). One hundred microliters of 10% CCK-8 reagent (10 μL of CCK-8 and 90 μL of serum-free media) were added to each well after aspirating the old media, and the mixture was incubated at 37°C for 1 h. We used a microplate reader (Bio-Rad, USA) to measure the absorbance values at 450 nm and drew a growth curve based on the absorbance values and time.

The colony formation assay was performed by inoculating 500 SCC25 cells or 10,000 CAL 27 cells transfected with siRNA in 6-well plates. After 7-14 days of culture, the cells were stained and fixed. The number of SCC25 cell colonies was directly counted, while the colony number of CAL27 cells was counted in three random fields under a microscope at 5× magnification.

Migration and Invasion Assays

OSCC cell migration and invasion were estimated by Transwell assays. In short, 200 μL of FBS-free media containing 1.5×10^5 SCC25 cells or 2×10^5 CAL27 cells was plated on the upper chambers of Transwell inserts (for the migration assay, 8-μm pore size, Corning, USA), and Transwell inserts coated with 1 mg/mL Matrigel (for the invasion assay, 354234, Corning, USA), while 800 μL of complete media were added to the lower chambers. After culture for 48 h, cells in the upper chamber were removed, while the cells in the lower chamber were fixed, stained, and counted under a microscope at 100× magnification according to the number of nuclei.

Statistical Analysis

All statistical analyses were performed using R software (R version 4.1.0, https://www.r-project.org/) or GraphPad Prism 9.0 software. Each *in vitro* experiment was repeated at least three times, and all data are presented as the mean and SD. The normality of the distribution of the data was assessed by the Shapiro-Wilk test. Two-tailed unpaired or paired Student's t test was used to analyze the significance of differences between the two groups in accordance with the normal distribution, while the Mann-Whitney U test was performed for data with a nonnormal distribution. For the comparisons of three or more groups, one-way or two-way ANOVA was used for parametric analysis, and Kruskal-Wallis tests were performed for nonparametric analysis. The correlation between genes was analyzed using Pearson's correlation. Differences were considered to be statistically significant at a P value < 0.05.

RESULTS

Construction of a Weighted Gene Coexpression Network and Identification of Hub Modules

Figure 1 We used TCGA-OSCC and GSE30784 datasets to construct a weighted gene coexpression network and screened the hub module related to the progression of OSCC. First, we filtered and eliminated outliers with the hclust function and drew clustering dendrograms for the remaining samples with a sample type heatmap (**Supplementary Figures 1A, B**). Next, we selected a soft threshold power of 5 for TCGA-OSCC dataset and 11 for the GSE30784 dataset to construct a weighted gene coexpression network based on a scale-free topology fit index reaching 0.85 (**Supplementary Figures 1C, D**). We further assessed the scale-free topology fit index and found that the correlation coefficients (R-squared) were 0.97 and 0.84, respectively, indicating that the selected β values established scale-free networks (**Supplementary Figures 1E, F**). After determining the soft threshold powers, the degree of dissimilarity between genes was calculated by obtaining the adjacency matrix and the topological overlap matrix (TOM). The hierarchical clustering tree was divided into multiple modules (12 modules for TCGA-OSCC dataset and 13 modules for the GSE30784 dataset) using the dynamic tree cut method, and the modules with dissimilarity of <0.2 were merged (**Supplementary Figures 1G, H** and **Figures 2A, B**). We identified 11 modules in TCGA-OSCC dataset, and the module most significantly related to OSCC was the green module (**Figure 2C**), which contained 257 genes (**Supplementary Data Sheet 1**). We identified 12 modules in the GSE30784 dataset, and the module most significantly associated with OSCC was the turquoise module (**Figure 2D**), which contained 346 genes (**Supplementary Data Sheet 2**).

IGF2BP2 Was Selected as a Hub Gene Through a Prognostic Analysis

By comparing the expression profiles of OSCC and normal samples, we identified2,393 DEGs in TCGA-OSCC dataset and 2,217 DEGs in the GSE30784 dataset (**Figures 3A, B** and **Supplementary Data Sheets 3**, **4**). In this study, we intersected the genes in the modules most relevant to OSCC and DEGs to intersect and obtained 12 candidate genes between the two datasets (**Figure 3C**). The 12 candidate genes were ANO1, DNMT3B, FSCN1, FST, HMGA2, HOXD10, IGF2BP2, NETO2, PROCR, WDR54, WDR66, and ZNF144. We divided patients into high- and low-expression groups based on the median expression levels of these 12 candidate genes to verify their effects on the prognosis of patients with OSCC. Three candidate genes were found to be significantly associated with the OS of the patients in TCGA-OSCC dataset by applying univariate Cox regression analysis (**Figure 3D**). Seven candidate genes were identified to be significantly related to the OS of the patients in the GSE42743 dataset (**Figure 3E**). Among them, only ANO1 and IGF2BP2 had statistically significantly associated with the OS of patients with OSCC in both datasets. However,

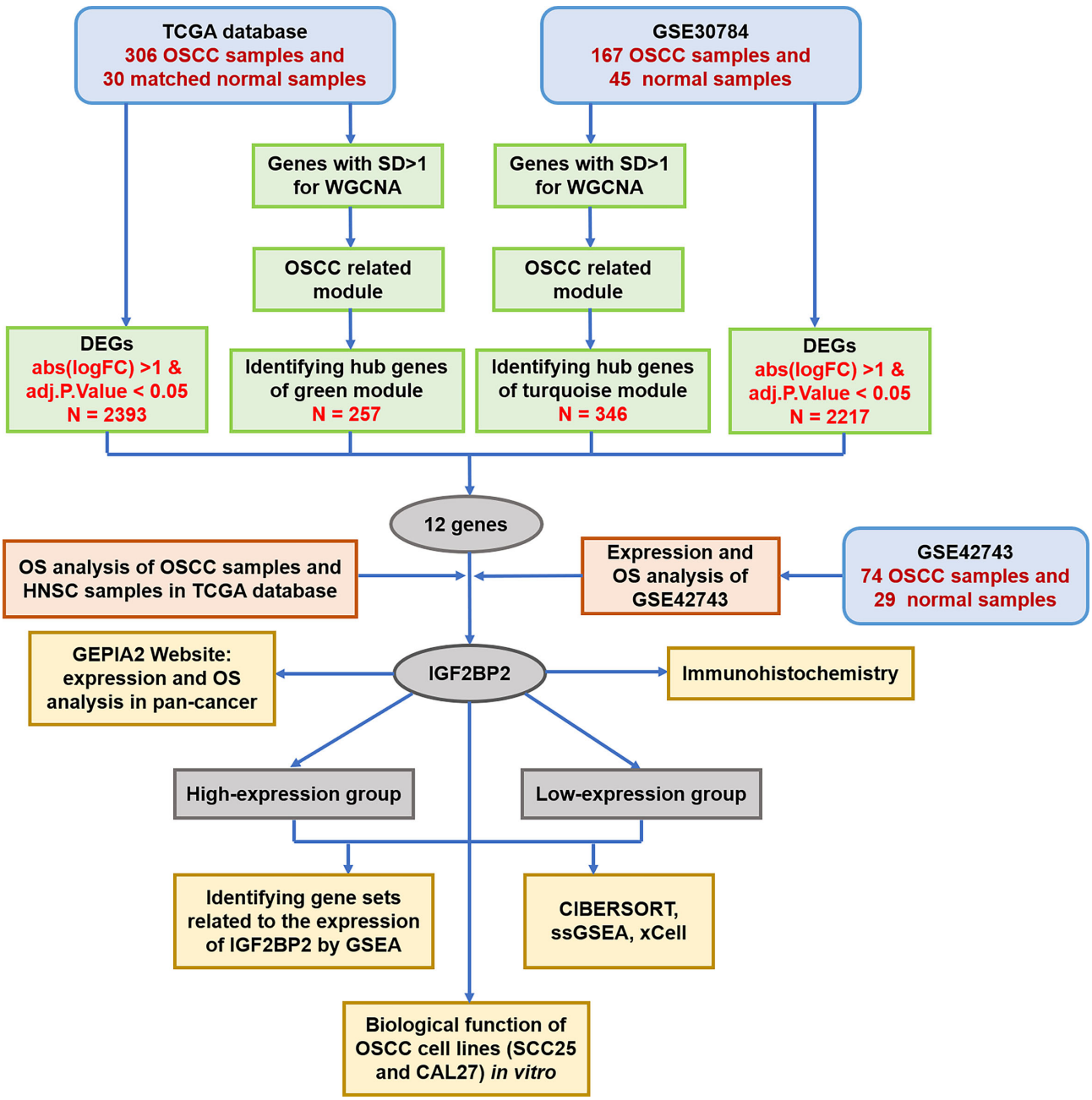

FIGURE 1 | Flowchart of the data preparation, screening, analysis and validation. TCGA, The Cancer Genome Atlas; OSCC, oral squamous cell carcinoma; SD, standard deviation; WGCNA, weighted gene coexpression network analysis; DEGs, differentially expressed genes; OS, overall survival; HNSC, head and neck squamous cell carcinoma; IGF2BP2, insulin-like growth factor 2 mRNA binding protein 2; GEPIA, gene expression profiling interactive analysis; GSEA, gene set enrichment analysis; ssGSEA, single-sample gene set enrichment analysis.

ANO1 and IGF2BP2 were not statistically significant with the RFS of patients in the TCGA-OSCC dataset (**Supplementary Figures 2A, B**). We further analyzed the differences in the expression of ANO1 and IGF2BP2 between OSCC samples and normal samples and found higher expression of both ANO1 and IGF2BP2 in OSCC samples than in normal samples in TCGA-OSCC dataset (**Supplementary Figures 2C, D**). The same results were obtained from the GSE30784 and GSE42743 datasets, and but the difference in IGF2BP2 expression was greater than that of ANO1 (**Supplementary Figures 2E–H**). Next, the effects of ANO1 and IGF2BP2 on the prognosis of HNSC patients were evaluated. The GEPIA2 results showed that HNSC

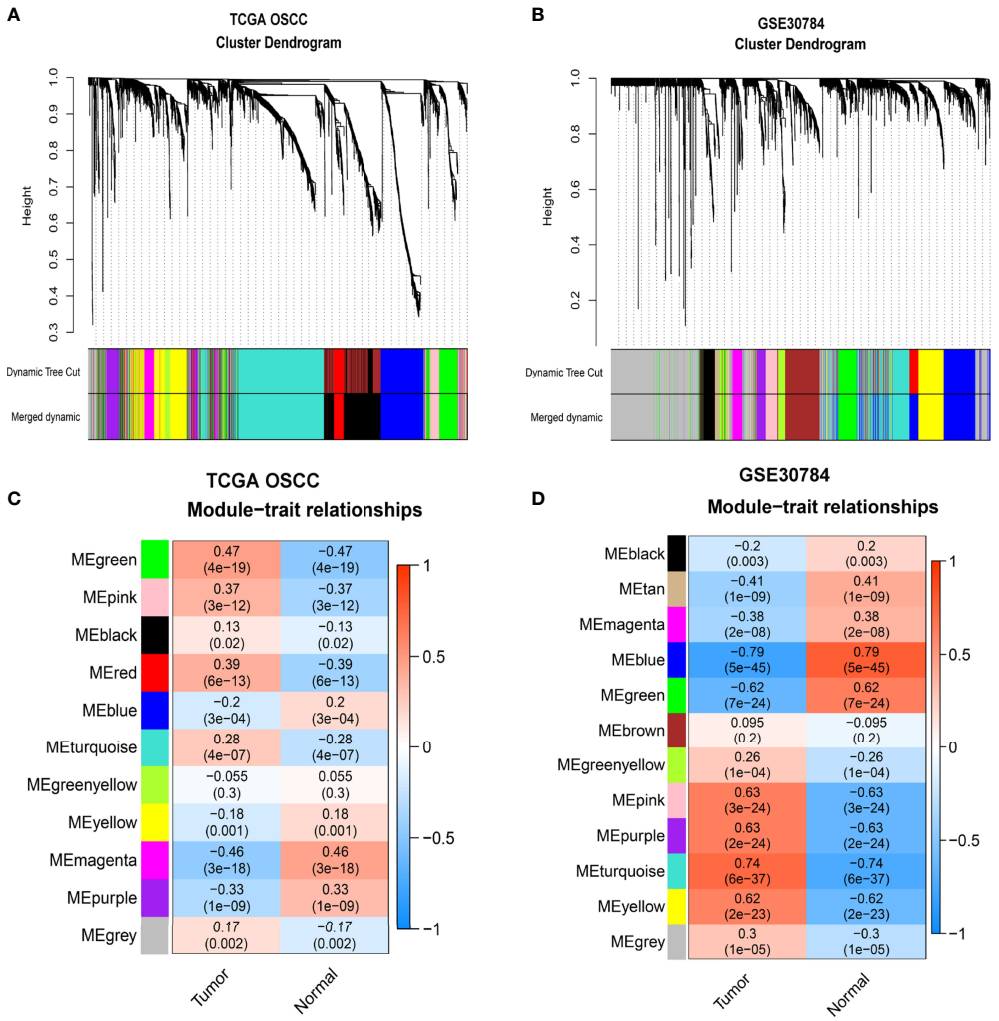

FIGURE 2 | Identification of modules related to OSCC. **(A, B)** Hierarchical clustering tree developed by gene dissimilarity based on topological overlap for TCGA-OSCC **(A)** and GSE30784 datasets **(B)**. Each color represents a module (gray represents unassigned genes). **(C, D)** The correlation coefficients and p-values of module-trait relationships for TCGA-OSCC **(C)** and GSE30784 datasets **(D)**. Each row corresponds to a module eigengene, and each column corresponds to a trait.

patients with high IGF2BP2 expression had a worse OS rate than those with low IGF2BP2 expression, but this pattern was not observed for ANO1 (**Figure 3F**). To understand the expression and prognosis of ANO1 and IGF2BP2 across cancers, we used the GEPIA2 web server to analyze data containing 33 cancer subtypes derived from TCGA and GTEx databases. Compared with that in normal samples, ANO1 expression was significantly reduced in KIRP, PRAD, SKCM, TGCT, UCEC and UCS cancer samples, while it was significantly upregulated in ESCA, HNSC, KIRC, OV, PAAD, STAD and THYM cancer samples (**Supplementary Figure 2I**). IGF2BP2 expression was significantly reduced in ACC, BRCA and KIRC cancer samples, while it was significantly upregulated in COAD, ESCA, GBM, HNSC, LIHC, LUSC, OV, PAAD, READ, SKCM, STAD, TGCT and UCS cancer samples (**Figure 3G**). For the OS analysis, the Kaplan–Meier curves revealed that high ANO1 expression predicted worse prognosis for patients with LIRP, PAAD and UVM (**Supplementary Figure 2J**). While high IGF2BP2 expression predicted worse prognosis for patients with BLCA, HNSC, KIRC, LGG, LUAD, PAAD, SARC, and UVM (**Figure 3H**). Based on the above results, IGF2BP2 was selected as the hub gene for further analysis. We performed IHC staining on 10 pairs of OSCC tissues and adjacent noncancerous normal tissues, and found that the level of the IGF2BP2 protein was also significantly upregulated in OSCC tissues (**Figures 3I–K**).

Functional Annotation of IGF2BP2 in OSCC

We used the R package "clusterProfiler" to perform GSEA between the high and low IGF2BP2 expression groups in TCGA-OSCC and GSE30784 datasets, respectively (22). Twenty-three enriched gene sets with statistically significant differences (adjusted P value < 0.05, FDR < 0.05) for TCGA-

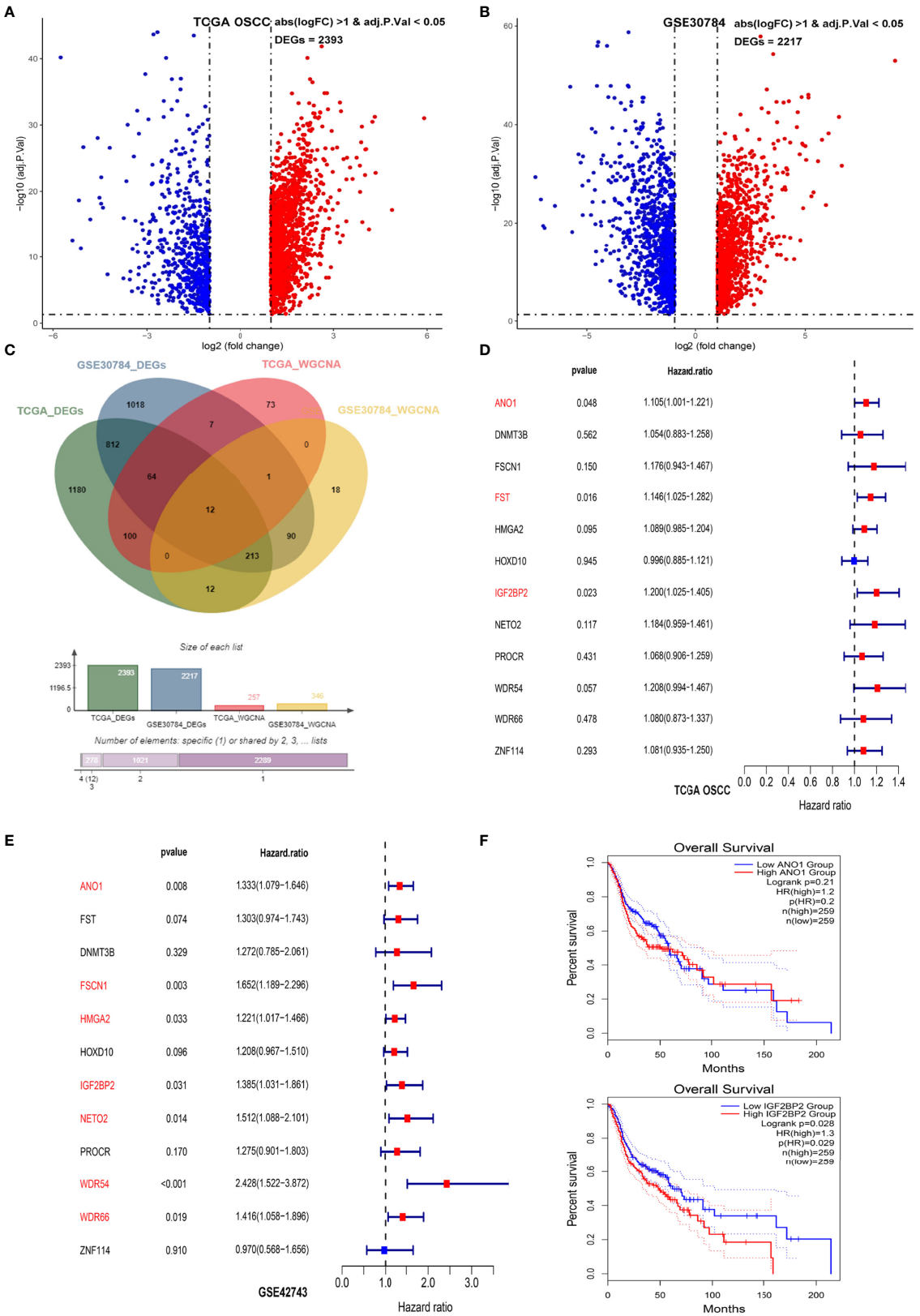

FIGURE 3 | Continued

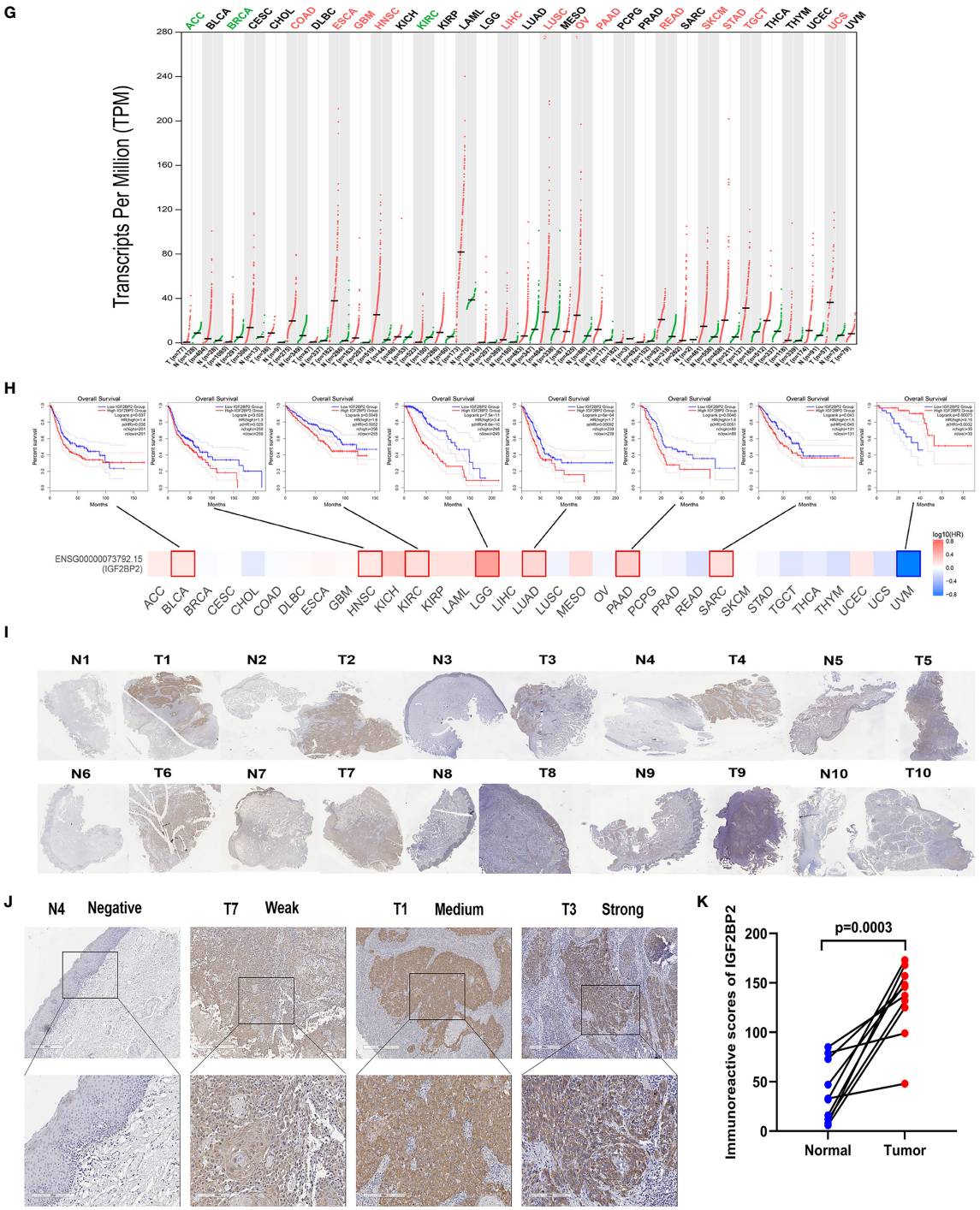

FIGURE 3 | IGF2BP2 was selected as a hub gene through prognostic analysis. **(A)** Volcano plot of 2,393 DEGs between normal (N=30) and OSCC (N=306) tissues from the TCGA database. **(B)** Volcano plot of 2,217 DEGs between OSCC and normal tissues from the GSE30784 dataset. **(C)** The Venn diagram shows 12 common genes of DEGs and hub genes from WGCNA between OSCC tissues and normal tissues in the TCGA and GSE30784 datasets. **(D, E)** The forest plots show the hazard ratios and 95% confidence intervals of 12 hub genes associated with OS in TCGA-OSCC **(D)** and GSE42743 datasets **(E)** according to univariate Cox regression analysis. **(F)** Kaplan–Meier curves of OS based on HNSC patients in the TCGA database with high and low ANO1 and IGF2BP2 expression. **(G)** Differential expression of IGF2BP2 in 33 different tumor tissues and paired normal tissues from the TCGA and GTEx databases. Each dot represents the expression of samples. **(H)** The prognostic impact of IGF2BP2 expression level based on the survival heatmap, showing significance in BLCA, HNSC, KIRC, LGG, LUAD, PAAD, SARC, and UVM. **(I)** Images of IHC staining for IGF2BP2 in 10 pairs of OSCC tissues (T) and adjacent noncancerous normal tissues (N). Magnification at 50× **(J)** Representative images of IHC staining for IGF2BP2 in adjacent noncancerous normal tissues and OSCC tissues. Magnification at 200× **(K)** Histological scoring of IGF2BP2 in 10 pairs of OSCC tissues and adjacent noncancerous normal tissues.

OSCC dataset and 26 enriched gene sets for the GSE30784 dataset in the hallmark gene sets (**Supplementary Data Sheets 5**, **7**) (23). In these two datasets, the hallmark gene sets enriched in the IGF2BP2 high-expression group were mainly "E2F targets", "epithelial-mesenchymal transition" (EMT), "G2M checkpoint", "glycolysis", and "myc targets v1" (**Figures 4A, C**). Thirty-eight enriched gene sets with statistically significant differences from TCGA-OSCC dataset and 39 enriched gene sets from the GSE30784 dataset in the KEGG analysis (**Supplementary Data Sheets 6**, **8**). "Cell cycle", "ECM receptor interaction", "focal adhesion", and "pathways in cancer" were the enriched KEGG gene sets in the high IGF2BP2 expression group, whereas "primary immunodeficiency" was enriched in the low IGF2BP2 expression group (**Figures 4B, D**). Based on the GSEA results, IGF2BP2 might promote the malignant progression of OSCC by affecting cancer-related and immune-related biological functions and pathways.

Correlation Between Immune Cell Infiltrates and IGF2BP2 Expression in OSCC

Immune cell infiltration in the tumor microenvironment (TME) has been shown to play a key role in tumor development and will affect the prognosis of patients with cancer (24). Therefore, we analyzed the correlations between IGF2BP2 expression and infiltrating immune cells in OSCC. The results estimated with the CIBERSORT algorithm showed lower levels of infiltrating plasma cells, CD8 T cells, gamma delta T cells, resting dendritic cells, and resting mast cells ($P < 0.05$) in the high IGF2BP2 expression group of TCGA-OSCC and GSE30784 cohorts, while resting NK cells, M0 macrophages, and eosinophils ($P < 0.05$) exhibited higher levels of infiltration (**Figures 5A, B**). Furthermore, ssGSEA revealed that activated CD8 T cells, effector memory CD4 cells, effector memory CD4 cells, type 1 T helper cells, MDSCs, activated B cells, immature B cells,

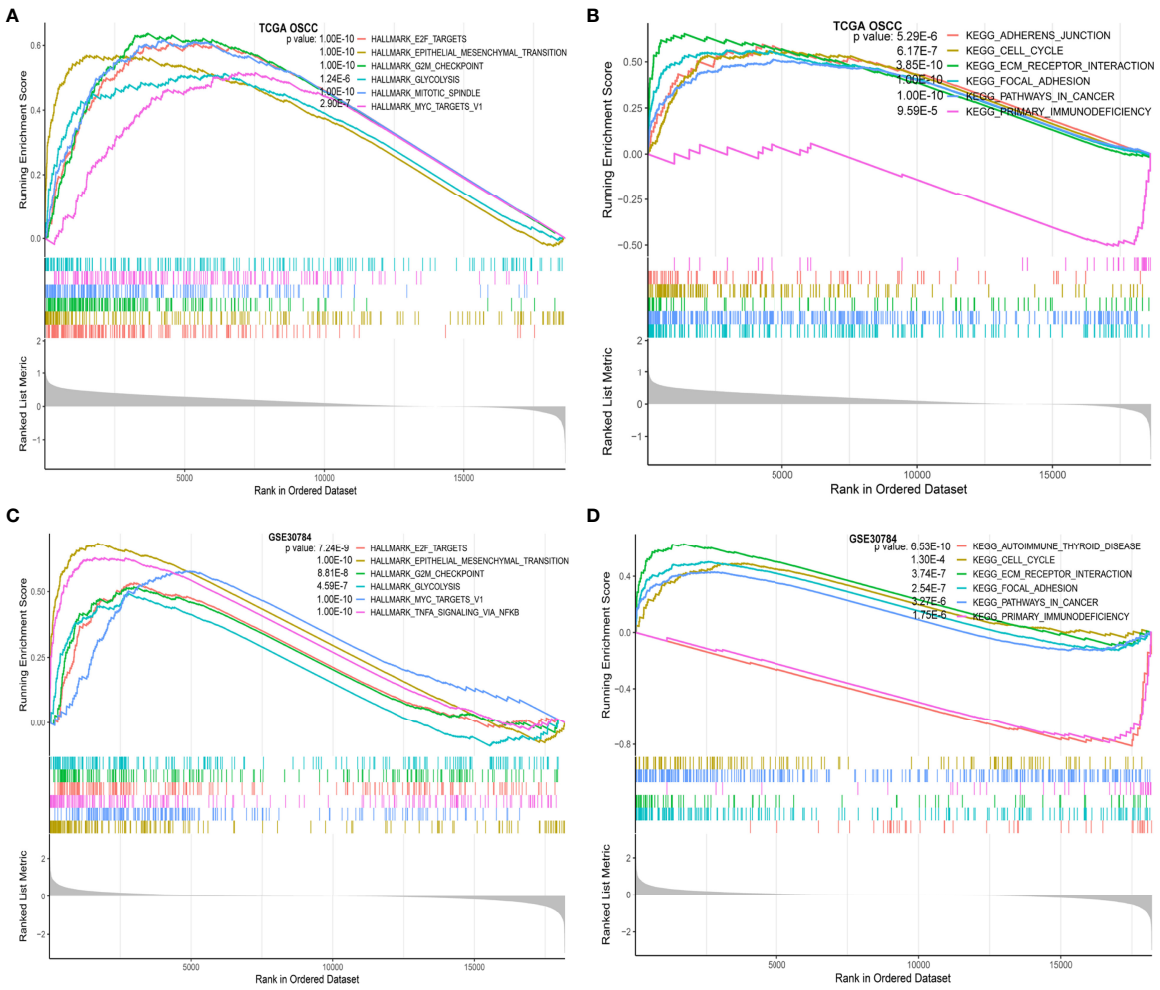

FIGURE 4 | Functional annotation of IGF2BP2 in OSCC. **(A)** The GSEA results show the functional enrichment of hallmark gene sets based on IGF2BP2 expression in TCGA-OSCC dataset; **(B)** GSEA results show the functional enrichment of KEGG gene sets based on IGF2BP2 expression in TCGA-OSCC dataset; **(C)** GSEA results show the functional enrichment of hallmark gene sets based on IGF2BP2 expression in the GSE30784 dataset; **(D)** GSEA results show the functional enrichment of KEGG gene sets based on IGF2BP2 expression in the GSE30784 dataset.

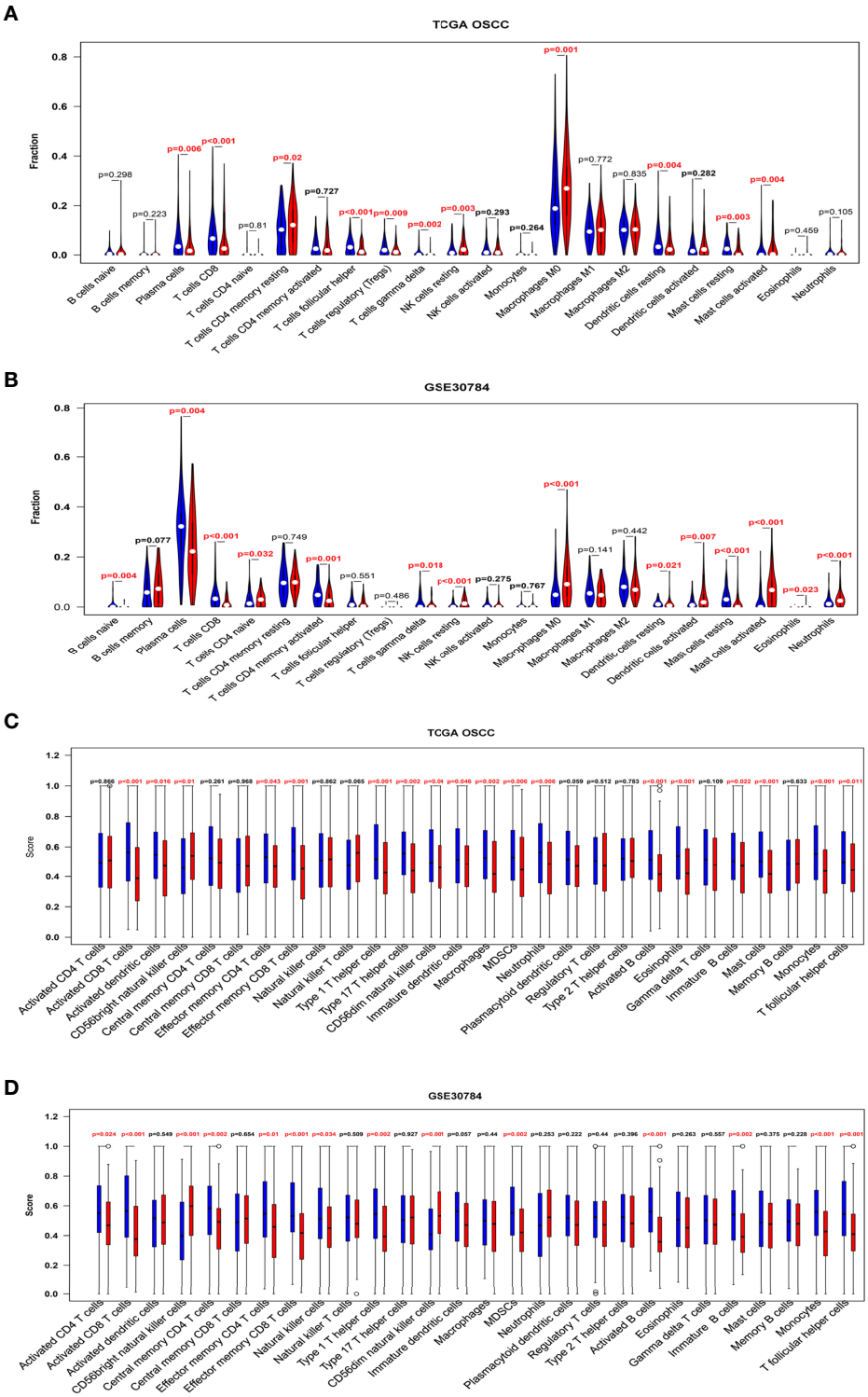

FIGURE 5 | Continued

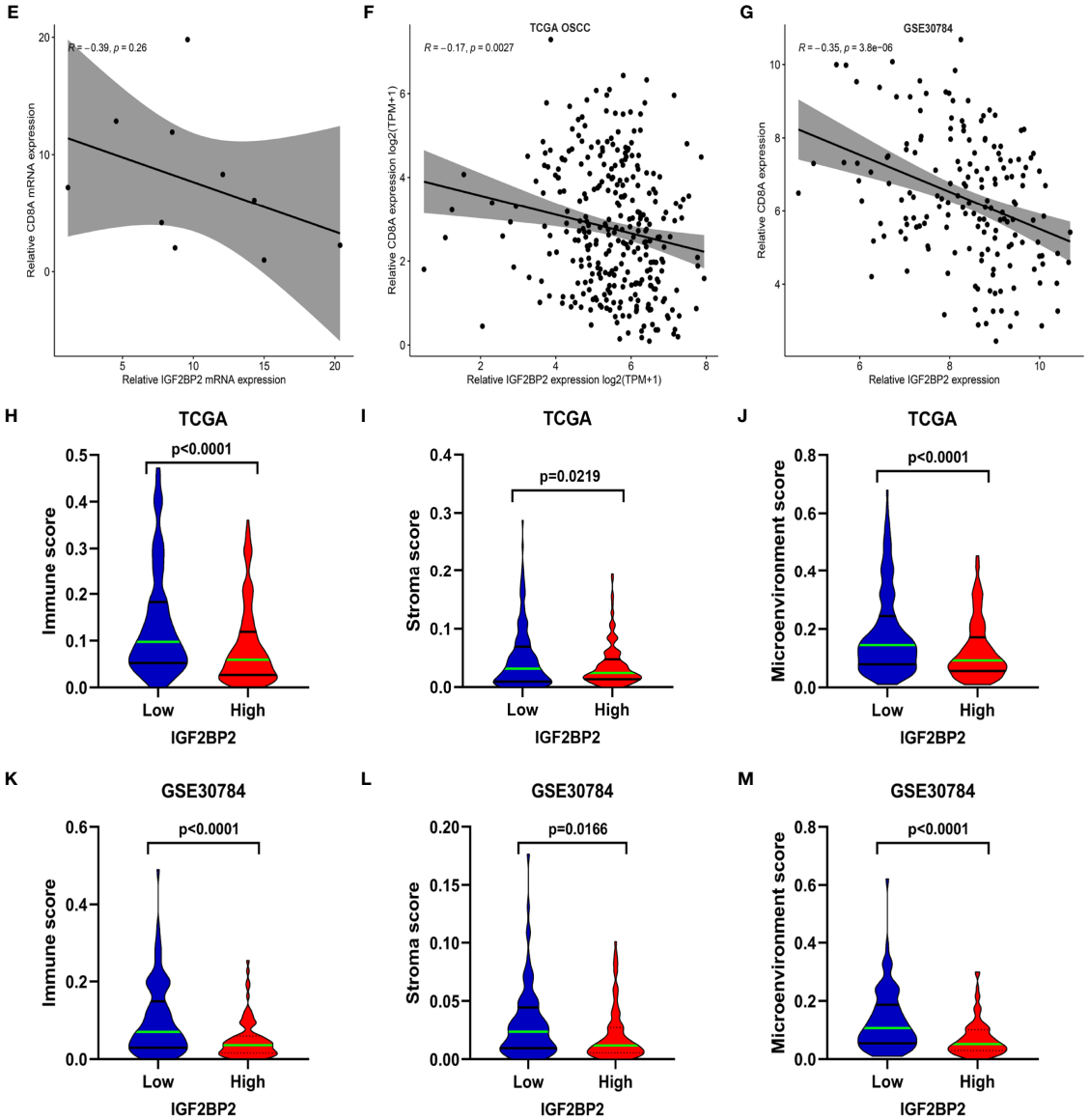

FIGURE 5 | Correlation between immune infiltrates and IGF2BP2 expression in OSCC. **(A, B)** Infiltration fraction between IGF2BP2 expression and 22 immune cells in the OSCC in TCGA-OSCC **(A)** and GSE30784 datasets **(B)** according to the CIBERSORT algorism. **(C, D)** Boxplots show IGF2BP2 expression and the score of 28 immune cells in the OSCC in TCGA-OSCC **(C)** and the GSE30784 datasets **(D)** with ssGSEA algorism. **(E)** Correlation between IGF2BP2 and CD8A expression in TCGA-OSCC dataset. **(F)** Correlation between IGF2BP2 and CD8A expression in GSE30784 dataset. **(G)** Correlation between the mRNA levels of IGF2BP2 and CD8A in 10 OSCC tissues. **(H–J)** The immune score **(H)**, stromal score **(I)**, and microenvironment score **(J)** of the IGF2BP2 high- and low-expression groups in the OSCC in the TCGA database according to the xCell algorithm. **(K–M)** The immune score **(K)**, stromal score **(L)**, and microenvironment score **(M)** of IGF2BP2 high- and low-expression groups in the OSCC in the GSE30784 dataset according to the xCell algorithm.

monocytes, and T follicular helper cells ($P < 0.05$) were significantly less enriched in the high IGF2BP2 expression group of TCGA-OSCC and GSE30784 cohorts. However, the infiltration of CD56 bright natural killer cells ($P < 0.05$) was positively correlated with IGF2BP2 expression (**Figures 5C, D**). Based on the results obtained from CIBERSORT and ssGSEA, we found that the expression of IGF2BP2 was significantly negatively correlated with the infiltration of immune cells, especially CD8+ T cells. The same results were obtained in from TCGA-OSCC and GSE30784 datasets that IGF2BP2 expression was significantly negatively correlated with the CD8A (A marker gene for CD8+ T cells) (**Figures 5E, F**). RT-qPCR analysis of mRNA levels in 10 OSCC tumor tissues revealed that the mRNA levels of IGF2BP2 was also negatively correlated with that of CD8A (**Figure 5G**). Similarly, the immune score ($P < 0.0001$), stromal score ($P < 0.05$), and microenvironment score ($P < 0.0001$) of the high IGF2BP2 expression group in these two datasets were significantly lower

than those of the low IGF2BP2 expression group according to the xCell algorithm (**Figures 5H–M**).

Silencing IGF2BP2 Inhibits the Proliferation, Migration, and Invasion of OSCC Cells *In Vitro*

This study revealed that IGF2BP2 is upregulated in OSCC and is associated with a poor prognosis in patients. The biological function of IGF2BP2 in OSCC cells is still unclear, and we then knocked down IGF2BP2 in SCC25 and CAL27 cells to explore its effects on cell proliferation, migration and invasion *in vitro* (**Figures 6A, B**). We chose two sequences with higher silencing efficiency, si-IGF2BP2-1 and si-IGF2BP2-3, for the subsequent experiments. Given that MYC is a well-defined oncogene, and IGF2BP2 can increase its stability in a m6A-dependent manner. We hypothesized that IGF2BP2 might play an oncogenic role in OSCC. In fact, knockdown of IGF2BP2 in SCC25 and CAL27 cells significantly suppressed MYC expression (**Figure 6C**). The results of correlation analysis also showed that the expressions of IGF2BP2 and MYC were significantly positively correlated in TCGA-OSCC and GSE30784 datasets (**Supplementary Figures 2A, B**). Furthermore, as shown in **Figures 6D–F**, compared with the si-NC group, the IGF2BP2 silencing group showed inhibited proliferation of SCC25 and CAL27 cells according to CCK-8 and colony formation assays. Moreover, the Transwell assay showed that silencing IGF2BP2 suppressed the migration and invasion of SCC25 and CAL27 cells (**Figures 6G, H**). The above results indicated that IGF2BP2 may play an important role in regulating the proliferation, migration and invasion of OSCC cells *in vitro*.

DISCUSSION

The occurrence and development of OSCC is a complex, multistep, and multifactorial process that mainly includes the dysregulation of oncogenes or tumor suppressor genes, the accumulation of epigenetic changes, and the interaction between tumor cells and the microenvironment (25). OSCC is a severely teratogenic and fatal disease. It is often invasive and accompanied by cervical lymph node metastasis and distant metastasis, which indicates a poor prognosis (26). Therefore, exploring the biological markers of OSCC plays an important role in early diagnosis and improvement of prognosis. We performed WGCNA to screen the key modules in TCGA-OSCC and GSE30784 gene sets, intersected the genes in the modules with DEGs, and then performed hub gene selection and survival analysis. Finally, IGF2BP2 was selected as the hub gene and as a biomarker that affects the prognosis of OSCC. The results of GSEA and tumor-infiltrating immune cell analysis indicated that IGF2BP2 might promote the malignant progression of OSCC by affecting cancer-related and immune-related biological functions and pathways. Moreover, silencing IGF2BP2 inhibited the proliferation, migration and invasion of SCC25 and CAL27 cells *in vitro*. The present study revealed that IGF2BP2 may act as a prognostic and immune biomarker by promoting the proliferation, migration and invasion of OSCC cells.

Several independent datasets indicated that IGF2BP2 was expressed at high levels in OSCC tissues and that high expression predicts a worse prognosis than low expression, consistent with studies on acute myelocytic leukemia (27), hepatocellular carcinoma (11), and pancreatic cancer (28). The results of the pan-cancer analysis also showed that IGF2BP2 was upregulated in a variety of cancers and was negatively correlated with the OS rate. In addition, our IHC results also showed that IGF2BP2 was expressed at high levels in OSCC tissues, indicating that IGF2BP2 functions as an oncogene in OSCC.

We conducted a GSEA to identify gene sets related to IGF2BP2 expression and to explore the molecular mechanism by which IGF2BP2 expression contributes to the malignant progression of OSCC using OSCC expression data provided by TCGA-OSCC and GSE30784 datasets. According to the GSEA results, high expression of IGF2BP2 mainly activates the EMT, glycolysis, and cell cycle three cancer-related pathways that affect cancer cell proliferation, migration, and invasion. The regulatory effect of IGF2BP2 on cancer cell proliferation, migration, and invasion is an important factor contributing to prognosis. Recently, LINC01559 was found to recruit IGF2BP2 to stabilize ZEB1 expression and accelerate gastric cancer cell proliferation, migration and EMT (29). A study on GBM found that by activating the IGF2BP2/PI3K/Akt axis, IGF2BP2 can significantly promote cell proliferation, migration, invasion, and EMT (30). Additionally, long noncoding RNA (LncRNA) CASC9 and IGF2BP2 synergistically increases the stability of HK2 mRNA, thereby promoting aerobic glycolysis in GBM (31). Similarly, IGF2BP2 stabilizes the HK2 and SLC2A1 mRNAs, and accelerates glycolytic metabolism and cell proliferation in colorectal cancer (32). This evidence indicates that IGF2BP2 promotes the proliferation, migration and invasion of cancer cells. Consistently, the results of this study also demonstrate that IGF2BP2 knockdown inhibits the proliferation, migration and invasion of OSCC cells *in vitro*. In summary, IGF2BP2 may facilitate the malignant progression of OSCC by enhancing glycolysis, inducing EMT, and promoting the cell cycle.

Antitumor immunotherapy is based on the principle that immune monitoring and the adaptability of the TME allow immune escape (33). Immune cells are the cellular basis of antitumor immunotherapy. A comprehensive analysis of tumor-infiltrating immune cells will help clarify the mechanism of tumor immune evasion, which is the key to improving the response rate of immunotherapy and developing new treatment strategies (24, 34). The imbalance of the TME may also be an important reason IGF2BP2 affects the progression and confers a poor prognosis in OSCC. As shown in the present study, high IGF2BP2 expression was accompanied by a significant reduction in the immune score, stromal score, and microenvironment score and a decrease in infiltrating CD8+ T cells. CD8+ T cells play a central role in tumor immunity and can specifically kill tumor cells. Reduced infiltration or impaired function of CD8+ T cells in the TME can lead to a poor prognosis

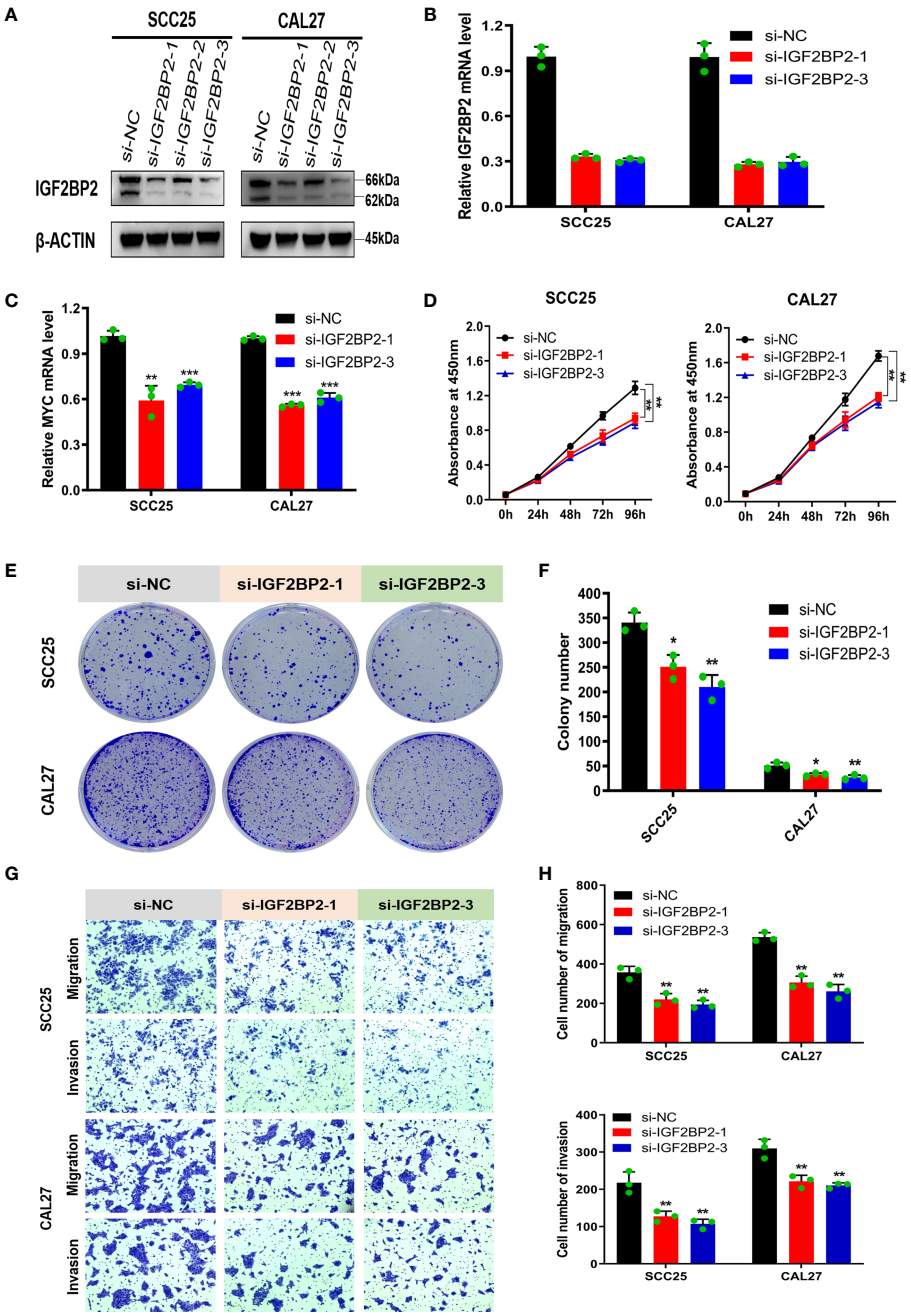

FIGURE 6 | Silencing IGF2BP2 inhibits the proliferation, migration, and invasion of OSCC cells *in vitro*. **(A, B)** Western blotting and qRT-PCR were performed to detect IGF2BP2 expression after transfection of siRNA. **(C)** The mRNA levels of MYC was detected by qRT-PCR in IGF2BP2-knockdown SCC25 and CAL27 cells. **(D–F)** The proliferation of NC and IGF2BP2-silenced SCC25 and CAL27 cells was detected using CCK-8 **(D)** and colony formation assays **(E, F)**. **(G, H)** Transwell assays were performed to assess migration and invasion in NC and IGF2BP2 knockdown SCC25 and CAL27 cells, which were photographed **(G)** and assessed **(H)**; Magnification at 100×. The experiment was repeated three times; error bars indicate standard deviation. $^{*}p < 0.05$, $^{**}p < 0.01$, $^{***}p < 0.001$.

for many cancers (35). Shimizu et al. showed that in the invading edge and peripheral stroma of OSCC, an increase in tumor infiltrating CD8+ T cells was associated with an improvement in OS and disease-specific survival (36). Tabachnyk et al. found that the increase in tumor-infiltrating CD8+ T cells in OSCC patients significantly increased disease-free survival after concurrent radiotherapy and chemotherapy (36). However, programmed cell death-ligand 1 (PD-L1) on the surface of tumor cells binds to the activated CD8+ T cell receptor programmed cell death-1 (PD-1), which significantly inhibits the ability of CD8+ T cells to

kill tumor cells. The effect of anti-PD-1 monoclonal antibody treatment can be reflected in the density of tumor-infiltrating CD8+ T cells in solid tumors (37). A recent study suggested that IGF2BP2 can combine with PD-L1 to promote the proliferation and inhibit the apoptosis of hypopharyngeal carcinoma cells through the PD-1/PD-L1 axis (38). Taken together, these data indicate that IGF2BP2 may affect the infiltration of CD8+ T cells in OSCC and is related to the efficacy of antitumor immunotherapy response and the prognosis, but these findings require further confirmation.

Multiple mechanisms may account for the role of IGF2BP2 in tumor progression. IGF2BP2 is a posttranscriptional regulator of mRNA localization, stabilization and translation and is related to the regulation of the expression of miRNAs, lncRNAs and m6A-related genes (39). Target binding of miRNAs to IGF2BP2 inhibits its expression and malignant tumor progression. For example, miR-1193 activates ERK and PI3K/Akt signaling pathways by binding to the 3' UTR of the IGF2BP2 mRNA to inhibit the proliferation and invasion of breast cancer cells (40). In addition, miR-138 inhibitsIGF2BP2 expression by targeting its 3′-UTR, thereby inhibiting the EMT and reducing the proliferation and invasion of low-grade glioma cells (41). IGF2BP2 interacts with lncRNAs to maintain multiple malignant biological behaviors of tumors. For instance, the lncRNA LINRIS blocks the ubiquitination of K139 in IGF2BP2 and prevents its degradation through the autophagy-lysosomal pathway, thus maintaining MYC-mediated glycolysis and promoting the proliferation of colorectal cancer cells (42). Moreover, linc01305 increases the stability of HTR3A mRNA by interacting with IGF2BP2, thereby promoting the metastasis and proliferation of esophageal squamous cell carcinoma (43). A recent study found that IGF2BP2 is an m6A-binding protein that enhances the stability of m6A-related genes/mRNAs and promotes translation (10). Li et al. proved that METTL3 upregulates SOX2 expression through IGF2BP2 to recognize and increase the stability of SOX2 mRNA and promote colorectal carcinoma cell self-renewal, increase stem cell frequency and promote migration in a m6A-dependent manner (44). In hepatocellular carcinoma, IGF2BP2 directly recognizes and binds to the m6A site of the FEN1 mRNA, increased the stability of FEN1 mRNA, and promotes the proliferation of hepatocellular carcinoma cells (11). At present, the mechanisms by which IGF2BP2 promotes the proliferation and metastasis of OSCC cells are still unclear. However, the mechanisms may involve the EMT, glycolysis, and tumor infiltrating immune cells, and further research is needed.

In summary, we conducted WGCNA to identify the key modules and genes related to OSCC that intersect with DEGs and performed an analysis of the survival prognosis and IHC to screen and validate the hub gene IGF2BP2. The GSEA results showed that IGF2BP2 promotes the malignant progression of OSCC by affecting cancer-related processes (EMT, glycolysis, cell cycle, etc.) and immune-related biological functions and pathways. Our study also revealed that IGF2BP2 is closely associated with remodeling immune microenvironment and that high IGF2BP2 expression is accompanied by a decrease in the number of tumor-infiltrating CD8+ T cells. In addition, we demonstrated that IGF2BP2 knockdown inhibits the proliferation, migration and invasion of OSCC cells *in vitro*. However, these findings must be verified *in vivo* in our future studies. Moreover, the molecular mechanism of IGF2BP2 in the progression of OSCC should be further systematically elucidated and investigated in depth.

DATA AVAILABILITY STATEMENT

The original contributions presented in the study are included in the article/**Supplementary Material**. Further inquiries can be directed to the corresponding authors.

ETHICS STATEMENT

The studies involving human participants were reviewed and approved by the Stomatology Hospital Research Ethics Committee of Sun Yat-sen University. The patients/participants provided their written informed consent to participate in this study.

AUTHOR CONTRIBUTIONS

LZ, DY, and SH conceived and designed the study. LZ, WL, and EP performed the data acquisition and analysis. LZ, HL, HC, WL, and EP prepared the figures and supplementary materials. HL and HC performed the experiments. LZ, HL, and HC wrote the original manuscript. DY and SH reviewed and revised the manuscript. All authors read and approved the final manuscript.

FUNDING

This study was supported by the National Natural Science Foundation of China (82073378), Natural Science Foundation of Guangdong province (2021A1515012399), and Science and Technology Plan Project of Wenzhou (Y20190446).

ACKNOWLEDGMENTS

The authors would like to thank all reviewers for their valuable comments.

SUPPLEMENTARY MATERIAL

The Supplementary Material for this article can be found online at: https://www.frontiersin.org/articles/10.3389/fonc.2022.809589/full#supplementary-material

Supplementary Data Sheet 1 | Genes in the green module for TCGA-OSCC dataset.

Supplementary Data Sheet 2 | Genes in the turquoise module for the GSE30784 dataset.

Supplementary Data Sheet 3 | DEGs between OSCC and normal samples in TCGA-OSCC dataset.

Supplementary Data Sheet 4 | DEGs between OSCC and normal samples in the GSE30784 dataset.

Supplementary Data Sheet 5 | Enriched Hallmark gene sets based on IGF2BP2 expression in TCGA-OSCC dataset.

Supplementary Data Sheet 6 | Enriched KEGG gene sets based on IGF2BP2 expression in TCGA-OSCC dataset.

Supplementary Data Sheet 7 | Enriched Hallmark gene sets based on IGF2BP2 expression in the GSE30784 dataset.

Supplementary Data Sheet 8 | Enriched KEGG gene sets based on IGF2BP2 expression in the GSE30784 dataset.

REFERENCES

1. Bosetti C, Carioli G, Santucci C, Bertuccio P, Gallus S, Garavello W, et al. Global Trends in Oral and Pharyngeal Cancer Incidence and Mortality. *Int J Cancer* (2020) 147(4):1040– x9. doi: 10.1002/ijc.32871
2. Mupparapu M, Shanti RM. Evaluation and Staging of Oral Cancer. *Dental Clinics North Am* (2018) 62(1):47–58. doi: 10.1016/j.cden.2017.08.003
3. Sung H, Ferlay J, Siegel RL, Laversanne M, Soerjomataram I, Jemal A, et al. Global Cancer Statistics 2020: GLOBOCAN Estimates of Incidence and Mortality Worldwide for 36 Cancers in 185 Countries. *CA Cancer J Clin* (2021) 71(3):209–49. doi: 10.3322/caac.21660
4. Zeng H, Chen W, Zheng R, Zhang S, Ji JS, Zou X, et al. Changing Cancer Survival in China During 2003–15: A Pooled Analysis of 17 Population-Based Cancer Registries. *Lancet Global Health* (2018) 6(5):e555–67. doi: 10.1016/s2214-109x(18)30127-x
5. Langfelder P, Horvath S. WGCNA: An R Package for Weighted Correlation Network Analysis. *BMC Bioinf* (2008) 9:559. doi: 10.1186/1471-2105-9-559
6. Christiansen J, Kolte AM, Hansen TVO, Nielsen FC. IGF2 mRNA-Binding Protein 2: Biological Function and Putative Role in Type 2 Diabetes. *J Mol Endocrinol* (2009) 43(5-6):187–95. doi: 10.1677/JME-09-0016
7. Nielsen J, Christiansen J, Lykke-Andersen J, Johnsen AH, Wewer UM, Nielsen FC. A Family of Insulin-Like Growth Factor II mRNA-Binding Proteins Represses Translation in Late Development. *Mol Cell Biol* (1999) 19(2):1262–70. doi: 10.1128/MCB.19.2.1262
8. Zhao Y, Ma Y-S, Fang Y, Liu L, Wu S-D, Fu D, et al. IGF2BP2 Genetic Variation and Type 2 Diabetes: A Global Meta-Analysis. *DNA Cell Biol* (2012) 31(5):713–20. doi: 10.1089/dna.2011.1400
9. Dai N. The Diverse Functions of IMP2/IGF2BP2 in Metabolism. *Trends Endocrinol Metab* (2020) 31(9):670–9. doi: 10.1016/j.tem.2020.05.007
10. Huang H, Weng H, Sun W, Qin X, Shi H, Wu H, et al. Recognition of RNA N (6)-Methyladenosine by IGF2BP Proteins Enhances mRNA Stability and Translation. *Nat Cell Biol* (2018) 20(3):285–95. doi: 10.1038/s41556-018-0045-z
11. Pu J, Wang J, Qin Z, Wang A, Zhang Y, Wu X, et al. IGF2BP2 Promotes Liver Cancer Growth Through an M6a-FEN1-Dependent Mechanism. *Front Oncol* (2020) 10:578816. doi: 10.3389/fonc.2020.578816
12. Deng X, Jiang Q, Liu Z, Chen W. Clinical Significance of an M6a Reader Gene, IGF2BP2, in Head and Neck Squamous Cell Carcinoma. *Front Mol Biosci* (2020) 7:68. doi: 10.3389/fmolb.2020.00068
13. Chou CH, Chang CY, Lu HJ, Hsin MC, Chen MK, Huang HC, et al. IGF2BP2 Polymorphisms Are Associated With Clinical Characteristics and Development of Oral Cancer. *Int J Mol Sci* (2020) 21(16):5662. doi: 10.3390/ijms21165662
14. Goldman M, Craft B, Hastie M, Repečka K, Kamath A, McDade F, et al. The UCSC Xena Platform for Cancer Genomics Data Visualization and Interpretation. *bioRxiv* (2018). doi: 10.1101/326470
15. Ritchie ME, Phipson B, Wu D, Hu Y, Law CW, Shi W, et al. Limma Powers Differential Expression Analyses for RNA-Sequencing and Microarray Studies. *Nucleic Acids Res* (2015) 43(7):e47. doi: 10.1093/nar/gkv007
16. Bardou P, Mariette J, Escudie F, Djemiel C, Klopp C. Jvenn: An Interactive Venn Diagram Viewer. *BMC Bioinf* (2014) 15:293. doi: 10.1186/1471-2105-15-293
17. Subramanian A, Tamayo P, Mootha VK, Mukherjee S, Ebert BL, Gillette MA, et al. Gene Set Enrichment Analysis: A Knowledge-Based Approach for Interpreting Genome-Wide Expression Profiles. *Proc Natl Acad Sci USA* (2005) 102(43):15545–50. doi: 10.1073/pnas.0506580102
18. Chen B, Khodadoust MS, Liu CL, Newman AM, Alizadeh AA. Profiling Tumor Infiltrating Immune Cells With CIBERSORT. *Methods Mol Biol* (2018) 1711:243–59. doi: 10.1007/978-1-4939-7493-1_12
19. Hanzelmann S, Castelo R, Guinney J. GSVA: Gene Set Variation Analysis for Microarray and RNA-Seq Data. *BMC Bioinf* (2013) 14:7. doi: 10.1186/1471-2105-14-7
20. Aran D, Hu Z, Butte AJ. Xcell: Digitally Portraying the Tissue Cellular Heterogeneity Landscape. *Genome Biol* (2017) 18(1):220. doi: 10.1186/s13059-017-1349-1
21. Cai H, Li J, Zhang Y, Liao Y, Zhu Y, Wang C, et al. LDHA Promotes Oral Squamous Cell Carcinoma Progression Through Facilitating Glycolysis and Epithelial-Mesenchymal Transition. *Front Oncol* (2019) 9:1446. doi: 10.3389/fonc.2019.01446
22. Wu T, Hu E, Xu S, Chen M, Guo P, Dai Z, et al. Clusterprofiler 4.0: A Universal Enrichment Tool for Interpreting Omics Data. *Innovation (N Y)* (2021) 2(3):100141. doi: 10.1016/j.xinn.2021.100141
23. Liberzon A, Birger C, Thorvaldsdottir H, Ghandi M, Mesirov JP, Tamayo P. The Molecular Signatures Database (MSigDB) Hallmark Gene Set Collection. *Cell Syst* (2015) 1(6):417–25. doi: 10.1016/j.cels.2015.12.004
24. Zhang Y, Zhang Z. The History and Advances in Cancer Immunotherapy: Understanding the Characteristics of Tumor-Infiltrating Immune Cells and Their Therapeutic Implications. *Cell Mol Immunol* (2020) 17(8):807–21. doi: 10.1038/s41423-020-0488-6
25. Li CC, Shen Z, Bavarian R, Yang F, Bhattacharya A. Oral Cancer: Genetics and the Role of Precision Medicine. *Surg Oncol Clinics North Am* (2020) 29 (1):127–44. doi: 10.1016/j.soc.2019.08.010
26. Bagan J, Sarrion G, Jimenez Y. Oral Cancer: Clinical Features. *Oral Oncol* (2010) 46(6):414–7. doi: 10.1016/j.oraloncology.2010.03.009
27. He X, Li W, Liang X, Zhu X, Zhang L, Huang Y, et al. IGF2BP2 Overexpression Indicates Poor Survival in Patients With Acute Myelocytic Leukemia. *Cell Physiol Biochem* (2018) 51(4):1945–56. doi: 10.1159/000495719
28. Dahlem C, Barghash A, Puchas P, Haybaeck J, Kessler SM. The Insulin-Like Growth Factor 2 mRNA Binding Protein IMP2/IGF2BP2 Is Overexpressed and Correlates With Poor Survival in Pancreatic Cancer. *Int J Mol Sci* (2019) 20(13):3204. doi: 10.3390/ijms20133204
29. Shen H, Zhu H, Chen Y, Shen Z, Qiu W, Qian C, et al. ZEB1-Induced LINC01559 Expedites Cell Proliferation, Migration and EMT Process in Gastric Cancer Through Recruiting IGF2BP2 to Stabilize ZEB1 Expression. *Cell Death Dis* (2021) 12(4):349. doi: 10.1038/s41419-021-03571-5
30. Mu Q, Wang L, Yu F, Gao H, Lei T, Li P, et al. Imp2 Regulates GBM Progression by Activating IGF2/PI3K/Akt Pathway. *Cancer Biol Ther* (2015) 16(4):623–33. doi: 10.1080/15384047.2015.1019185
31. Liu H, Qin S, Liu C, Jiang L, Li C, Yang J, et al. M(6)A Reader IGF2BP2-Stabilized CASC9 Accelerates Glioblastoma Aerobic Glycolysis by Enhancing HK2 mRNA Stability. *Cell Death Discov* (2021) 7(1):292. doi: 10.1038/s41420-021-00674-y
32. Shen C, Xuan B, Yan T, Ma Y, Xu P, Tian X, et al. M(6)A-Dependent Glycolysis Enhances Colorectal Cancer Progression. *Mol Cancer* (2020) 19 (1):72. doi: 10.1186/s12943-020-01190-w
33. Kraehenbuehl L, Weng CH, Eghbali S, Wolchok JD, Merghoub T. Enhancing Immunotherapy in Cancer by Targeting Emerging Immunomodulatory Pathways. *Nat Rev Clin Oncol* (2021) 19(1):37–50. doi: 10.1038/s41571-021-00552-7

34. Cramer JD, Burtness B, Ferris RL. Immunotherapy for Head and Neck Cancer: Recent Advances and Future Directions. *Oral Oncol* (2019) 99:104460. doi: 10.1016/j.oraloncology.2019.104460
35. Ock CY, Keam B, Kim S, Lee JS, Kim M, Kim TM, et al. Pan-Cancer Immunogenomic Perspective on the Tumor Microenvironment Based on PD-L1 and CD8 T-Cell Infiltration. *Clin Cancer Res: Off J Am Assoc Cancer Res* (2016) 22(9):2261–70. doi: 10.1158/1078-0432.CCR-15-2834
36. Shimizu S, Hiratsuka H, Koike K, Tsuchihashi K, Sonoda T, Ogi K, et al. Tumor-Infiltrating CD8(+) T-Cell Density Is an Independent Prognostic Marker for Oral Squamous Cell Carcinoma. *Cancer Med* (2019) 8(1):80–93. doi: 10.1002/cam4.1889
37. Doroshow DB, Bhalla S, Beasley MB, Sholl LM, Kerr KM, Gnjatic S, et al. PD-L1 as a Biomarker of Response to Immune-Checkpoint Inhibitors. *Nat Rev Clin Oncol* (2021) 18(6):345–62. doi: 10.1038/s41571-021-00473-5
38. Yang X, Liu J. Targeting PD-L1 (Programmed Death-Ligand 1) and Inhibiting the Expression of IGF2BP2 (Insulin-Like Growth Factor 2 mRNA-Binding Protein 2) Affect the Proliferation and Apoptosis of Hypopharyngeal Carcinoma Cells. *Bioengineered* (2021) 12(1):7755–64. doi: 10.1080/21655979.2021.1983278
39. Wang J, Chen L, Qiang P. The Role of IGF2BP2, an M6a Reader Gene, in Human Metabolic Diseases and Cancers. *Cancer Cell Int* (2021) 21(1):99. doi: 10.1186/s12935-021-01799-x
40. Li X, Li Y, Lu H. miR-1193 Suppresses Proliferation and Invasion of Human Breast Cancer Cells Through Directly Targeting Igf2bp2. *Oncol Res* (2017) 25 (4):579–85. doi: 10.3727/97818823455816X14760504645779
41. Yang Y, Liu X, Cheng L, Li L, Wei Z, Wang Z, et al. Tumor Suppressor microRNA-138 Suppresses Low-Grade Glioma Development and Metastasis *via* Regulating Igf2bp2. *OncoTargets Ther* (2020) 13:2247–60. doi: 10.2147/OTT.S232795
42. Wang Y, Lu JH, Wu QN, Jin Y, Wang DS, Chen YX, et al. LncRNA LINRIS Stabilizes IGF2BP2 and Promotes the Aerobic Glycolysis in Colorectal Cancer. *Mol Cancer* (2019) 18(1):174. doi: 10.1186/s12943-019-1105-0
43. Huang GW, Chen QQ, Ma CC, Xie LH, Gu J. Linc01305 Promotes Metastasis and Proliferation of Esophageal Squamous Cell Carcinoma Through Interacting With IGF2BP2 and IGF2BP3 to Stabilize HTR3A mRNA. *Int J Biochem Cell Biol* (2021) 136:106015. doi: 10.1016/j.biocel.2021.106015
44. Li T, Hu PS, Zuo Z, Lin JF, Li X, Wu QN, et al. METTL3 Facilitates Tumor Progression *via* an M(6)A-IGF2BP2-Dependent Mechanism in Colorectal Carcinoma. *Mol Cancer* (2019) 18(1):112. doi: 10.1186/s12943-019-1038-7

Conflict of Interest: The authors declare that the research was conducted in the absence of any commercial or financial relationships that could be construed as a potential conflict of interest.

Publisher's Note: All claims expressed in this article are solely those of the authors and do not necessarily represent those of their affiliated organizations, or those of the publisher, the editors and the reviewers. Any product that may be evaluated in this article, or claim that may be made by its manufacturer, is not guaranteed or endorsed by the publisher.

frontiers in Oncology

ORIGINAL RESEARCH
published: 04 March 2022
doi: 10.3389/fonc.2022.815437

TGF-β1-Mediated PD-L1 Glycosylation Contributes to Immune Escape *via* c-Jun/STT3A Pathway in Nasopharyngeal Carcinoma

Xue-Min Ma[1], *Yun-Fan Luo*[2], *Fang-Fang Zeng*[1], *Chang Su*[1], *Xiong Liu*[1], *Xiang-Ping Li*[1]* *and Juan Lu*[1]*

[1] Department of Otolaryngology-Head and Neck Surgery, Nanfang Hospital, Southern Medical University, Guangzhou, China, [2] Department of Otolaryngology-Head and Neck Surgery, Shenzhen Second People's Hospital, The First Affiliated Hospital of Shenzhen University, Shenzhen, China

Immunotherapy targeting programmed death ligand-1/programmed cell death protein-1 (PD-L1/PD-1) has achieved great success in multiple cancers, but only a small subset of patients showed clinical responses. Recent evidences have shown that post-translational modification of PD-L1 protein could regulate its protein stability and interaction with cognate receptor PD-1, thereby affecting anticancer immunotherapy in several solid tumors. However, the molecular mechanisms underlying how PD-1/PD-L1 expression is regulated still remain unclear in nasopharyngeal carcinoma (NPC). Here, we found N-glycosylation of PD-L1 in NPC cells and tissues. Mechanistically, we showed that STT3A transferred N-linked glycans to PD-L1, and TGF-β1 could positively regulate STT3A expression through activating c-Jun to bind to STT3A promoter. Functional assays showed that inhibition of TGF-β1 resulted in a decrease of glycosylated PD-L1 and enhanced cytotoxic T-cell function against NPC cells. Analysis of clinical specimens revealed that the expression of STT3A was positively correlated with TGF-β1 and c-Jun, and high STT3A expression was positively correlated with a more advanced clinical stage. Altogether, TGF-β1 activated c-Jun/STT3A signaling pathway to promote N-glycosylation of PD-L1, thus further facilitating immune evasion and reducing the efficacy of cancer immunotherapy. As such, all these data suggested that targeting TGF-β1 pathway might be a promising approach to enhance immune checkpoint blockade, and simultaneous blockade of PD-L1 and TGF-β1 pathways might elicit potent and superior antitumor activity relative to monotherapies.

Keywords: TGF-β1, PD-L1, glycosylation, nasopharyngeal carcinoma, immunotherapy

OPEN ACCESS

Edited by:
Song Fan,
Sun Yat-sen Memorial Hospital, China

Reviewed by:
Jung-Mao Hsu,
China Medical University, Taiwan
Zhiwei Wang,
Wenzhou Medical University, China

***Correspondence:**
Xiang-Ping Li
li321162@qq.com
Juan Lu
lujuanqz@163.com

Specialty section:
This article was submitted to Head and Neck Cancer, a section of the journal Frontiers in Oncology

Received: *15 November 2021*
Accepted: *14 February 2022*
Published: *04 March 2022*

Citation:
Ma X-M, Luo Y-F, Zeng F-F, Su C, Liu X, Li X-P and Lu J (2022) TGF-β1-Mediated PD-L1 Glycosylation Contributes to Immune Escape via c-Jun/STT3A Pathway in Nasopharyngeal Carcinoma. Front. Oncol. 12:815437. doi: 10.3389/fonc.2022.815437

INTRODUCTION

Nasopharyngeal carcinoma (NPC) is a kind of epithelial squamous cell carcinoma that originates from the nasopharyngeal mucosa with a high incidence in South China and Southeast Asia. NPC is characterized by prevailing Epstein-Barr virus (EBV) infection and a heavy infiltration of immune cells in tumor microenvironment (1). At present, metastasis and recurrence are the main cause of

death in NPC (1). Immunotherapy involving blocking programmed death ligand-1/programmed cell death protein-1 (PD-L1/PD-1) immune checkpoints has achieved great success in many solid tumors (2–6). Due to the efficacy of improving immunosuppressive microenvironment, anti-PD-1/PD-L1 treatment is suggested to be a promising therapeutic method for recurrent or metastatic NPC patients. Although PD-L1 is extremely highly expressed in NPC tissues (7), the response rate of PD-L1/PD-1 blocking therapy in NPC is only 20-30% (8–10). Moreover, an inconsistency occurs between the expression level of PD-L1 and the therapeutic effect (11). Therefore, a better understanding of the molecular mechanisms underlying how PD-1/PD-L1 expression is regulated will provide new insights to improve anti-PD-1/PD-L1 efficacy in NPC.

PD-L1, also known as CD274 or B7-H1, is a transmembrane glycoprotein expressed by tumor cells, macrophages and T cells. PD-L1 inhibits T cells activity and promotes immune evasion through binding to its receptor PD-1 on T cells (12). Recent studies have found that post-translational modifications (PTMs) of PD-L1 have played significant roles in modulating immunosuppression in cancers. PTMs of PD-L1, such as phosphorylation, N-glycosylation, acetylation and poly-ubiquitination, are known to emerge as important mechanisms in regulating its stability, translocation, and interactions with other proteins and directly affect PD-L1-mediated immune tolerance (13–15). A recent report indicated that glycosylation of PD-L1 led to the block of recognition of PD-L1/PD-1 by monoclonal antibodies and a low response rate of anti-PD-L1/PD-1 therapy in breast cancer (11).

TGF-β is a multifunctional cytokine with an important role in both physiologic and pathologic processes, including cancer. The aberrantly upregulated production of TGF-β has been strongly implicated in tumor progression, angiogenesis, and metastasis, as well as immune escape. TGF-β has been regarded as a critical immunosuppressive cytokine, which suppresses the antitumor activity of effector cells, including CD8+ T cells, natural killer (NK) cells, and macrophages (16). Several studies have indicated that TGF-β-mediated inhibitory immune microenvironment weakens the ability of PD-L1/PD-1 inhibitors to rebuild anti-tumor immune response, and ultimately leads to the resistance to PD-1/PD-L1 inhibitors (17–19). A recent report found that epithelial-mesenchymal transition (EMT) driven by TGF-β caused PD-L1 glycosylation by activating β-catenin to transcriptionally upregulate the expression of N-glycosyltransferase STT3, and eventually promoted immune escape in cancer stem cells (CSCs) (20). Furthermore, our previous study has revealed that enrichment of TGF-β1 in NPC microenvironment promotes immune escape by inducing chemotactic migration of Regulatory T (Treg) cells to remodel the inhibitory immune microenvironment *via* the TGF-β1-SMAD3-PI3K-AKT-c-JUN-miR-200a-CXCL12-CXCR4 axis (21, 22). Based on these previous results, we wonder whether TGF-β1 exerts synergistic effects on the PD-L1 induction and attenuates tumor response to PD-L1 blockade in NPC.

In this study, we verified the N-glycosylation of PD-L1 in NPC and further investigated whether TGF-β1 induced glycosylation of PD-L1 to promote immune escape, which may contribute to develop more effective immunotherapy strategies and improve the survival rate of NPC patients.

METHODS AND MATERIALS

Cell Culture

All the NPC cell lines including 5-8F, CNE1, CNE2, SUNE1, HONE1, and HNE1 were obtained from the Cancer Research Center of Southern Medical University. Cells were cultured in RPMI 1640 medium (11875176, Gibco, USA) with supplement of 10% fetal bovine serum (2053264, BI, Israel), 100 mg/ml streptomycin and 100 U/ml penicillin(C125C5, NCM Biotech, China) in an incubator at 5% CO2, 37°C. The PD-L1-knockdowned cells and c-Jun-overexpressed cells were cultured with antibiotic [puromycin (1μg/ml) (P8230, Solarbio, China)] while the Flag-PD-L1 cells and c-Jun- and STT3A-knockdowned cells were cultured with neomycin (400μg/ml) (G8160, Solarbio, China).

Western Blotting

The radio immunoprecipitation assay lysis buffer (RIPA) (P0013B, Beyotime, China) containing a protease-inhibitor cocktail (HY-K0010, MCE, USA) were used to extract proteins from cells. The proteins were lysed in SDS-loading buffer (FD006, Fdbio, China), then 20μg proteins were resolved on a 10% sodium dodecyl sulphate–polyacrylamide gel electrophoresis and transferred to polyvinylidene fluoride (PVDF) membrane (IPVH00010, Millipore, USA). The membrane was incubated with primary antibodies against PD-L1(13684, Cell Signaling Technology, USA), FLAG (80010-1-RR, Proteintech, USA), STT3A (12034-1-AP, Proteintech, USA), c-Jun (AF6089, Affinity, USA), HA (51064-2-AP, Proteintech, USA) and GAPDH (60004-1-Ig, Proteintech, USA) at a dilution of 1:1000, followed by incubation with species-specific (rabbit or mouse) HRP-conjugated secondary antibodies at a dilution of 1:5000. The immunoreactive bands were visualized by Omni ECL reagent (SQ101, EpiZyme, China).

Protein Deglycosylation

The protein lysate exacted from samples using RIPA was undergo glycoprotein denaturation at 100°C for 10minwith 1μl 10X Glycoprotein Denaturing Buffer and ddH_2O, and then incubated with PNGase F (P0704, NEB, USA) or O-glycosidase (P0733, NEB, USA) for 16h with 2μl 10X GlycoBuffer, 2μl 10% NP-40 and 5ul ddH_2O or 2μl neuraminidase and 3ul ddH_2O. The extent of deglycosylation was assessed by mobility shifts on SDS-PAGE gels.

Generation of Stable Cells Using Lentiviral Infection

The lentiviral –based short-hairpin RNA (shRNA) (Genechem, China) was used to knock down PD-L1, c-Jun and STT3A of 5-8F and CNE1 cells. Based on the knockdown of endogenous PD-L1, a pCMV-Flag-PD-L1 overexpressing plasmid was generated

to reconstitute Flag-PD-L1. A pCMV-HA-c-Jun overexpressing plasmid was used to culture stable overexpressing c-Jun cell lines.

RNA Extraction, Reverse Transcription and qRT-PCR

Total RNA of cells was extracted RNA isolation Kit (RC112-01, Vazyme, China) and reversely transcribed to cDNA using a reverse transcription kit (R323-01, Vazyme, China). ChamQ SYBR RT-qPCR Master Mix (Low ROX Premixed) (Q331-02, Vazyme, China) was used to used make a 20μL reaction amplification system to perform reverse transcription quantitative polymerase chain reaction (RT-qPCR) on an ABI QuantStudio6 System. All samples were normalized to the internal control GAPDH mRNA, and the relative expression levels were calculated based on the $2^{-\triangle\triangle CT}$ method. The primer sequences for RT-qPCR are shown in **Supplementary Table 2**.

ConA Lectin Binding Assay

Immunoprecipitated PD-L1 proteins were subjected to SDS-PAGE gels, transferred onto PVDF (IPVH00010, Millipore, USA), blocked with RIPA buffer for 1h at room temperature, and then incubate by peroxidase-conjugated ConA lectin (dilute to 0.1 μg/ml with RIPA buffer) (L6397, Sigma-Aldrich, USA) for 2h. Wash the membrane with RIPA buffer and detection using a chemiluminescent substrate.

Dual-Luciferase Assay

For the preparation of the 293T cells for transfection, they (1 × 105 cells) were grown by incubation on a 24-well plate for 24 hours. The control pcDNA3.1 plasmid (4.0 μg/ml) or the c-Jun plasmid (4.0 μg/ml), together with the control vector, pGL3-basic (4.0 μg/ml) or the STT3A plasmid (4.0 μg ml) were added into the medium with Lipofectamine 2000 (116680119, Invitrogen, USA). Cell lysates were collected after 36h incubation and firefly/renilla luciferase values were measured by the Dual-Luciferase Reporter Assay System (E1910, Promega, USA).

CHIP-PCR

The EZ-Magna ChIP™ A/G (17-10086, Millipore, USA) was used to perform CHIP experiment according to the manufacturer's instruction. Anti-c-Jun antibodies (AB40766, Abcam, USA) were used for immunoprecipitation and two primer sets (**Supplementary Table 3**) designed against human STT3A promoter were used to detect the bound DNA.

Co-Culture Experiment

Jurkat T cells were activated by Dynabeads Human T-Activator CD3/CD28(11161D, Gibco, USA), and were then co-cultured with 5-8F or CNE1 cells pretreated with SB431542 (20μM) (HY-431542, MCE, USA) or tunicamycin (15μg/ml) (T8480, Solarbio, China) for 48h at 3:1 (Jurkat: 5-8F/CNE1) ratio for 6h. The death rate of tumor cells was detected by CFSE/PI Double Stain Kit (BB4214, Bestbio, China). The medium supernatant of the co-culture system was collected for detecting the level of IL-2 by the ELISA kit (70-EK102, MultiSciences, China) according to manufacturer's instructions.

Clinical Samples and Immunohistochemistry

The NPC tissue specimens (n=36) were collected from the Nanfang Hospital of Southern Medical University (Guangzhou, China). These tissue specimens were from biopsy samples of NPC patients (pathologically confirmed) in 2021. The TNM classification was performed according to the 8th edition of the UICC/AJCC staging criteria. The clinical characteristics of these 36 patients with NPC are shown in **Supplementary Table 3**. This study was approved by the Ethics Committee of Nanfang Hospital of Southern Medical University. Formalin-fixed, and paraffin-embedded tissues were sectioned at 4 mm thickness, then harvested and fixed in 4% paraformaldehyde overnight at 4° C. The antigen blocking was performed using 10% goat serum (SP-9000, Zsbio, China). The sections were probed overnight at 4°C with primary anti-TGF-β1 (PA5-40772, Invitrogen, USA), anti-c-Jun (AF6089, Affinity, USA) and anti-STT3A (sc-100796, Santa Cruz, USA) antibodies. DAB color reagent kit (ZLI-9018, Zsbio, China) was used for staining. The numbers of positive cells were measured by two independent pathologists through five randomly selected fields at ×400 magnification.

Statistical Analysis

The SPSS 20.0 software was used for statistical analyses. All data were from at least three independent experiments. The comparison between two independent groups of data following a normal distribution is analyzed by two-tailed student's t-test. The relationship between STT3A and TGF-β1 or c-Jun was analyzed by the Spearman's correlation analysis. The data are shown as the mean ± SEM unless otherwise. *p*-values of <0.05 were considered statistically significant.

RESULTS

PD-L1 Was N-glycosylated in Nasopharyngeal Carcinoma

We analyzed PD-L1 expression in human NPC tissues and six different NPC cell lines by western blot, and found that most of PD-L1 expression was presented as two kinds of molecular weight size, which were distributed at around 50kDa and ~ 40kDa respectively (**Figures 1A, B**). These findings were consistent with previous results in breast cancer (23), suggesting that the 50-kDa form in NPC might be glycosylated PD-L1, and the ~40-kDa form might be non-glycosylated PD-L1. To further confirm the glycosylation of PD-L1 in NPC, we treated 5-8F and CNE1 cells with recombinant glycosidase (peptide-N-glycosidase F; PNGase F) or O-glycosidase. Compared with O-glycosidase-treated groups, virtually all PD-L1 migrated from 50 kDa to around 40 kDa upon PNGase F treatment in 5-8F and CNE1 cells (**Figure 1C**). The 50-kDa PD-L1 in 5-8F and CNE1 cells was also restrained by the N-glycosylation inhibitor tunicamycin (TM) (**Figure 1D**). Taken together, the results suggested that PD-L1 in NPC was N-glycosylated, and 50-kDa PD-L1 was glycosylated form and ~40-kDa PD-L1 was un-glycosylated form.

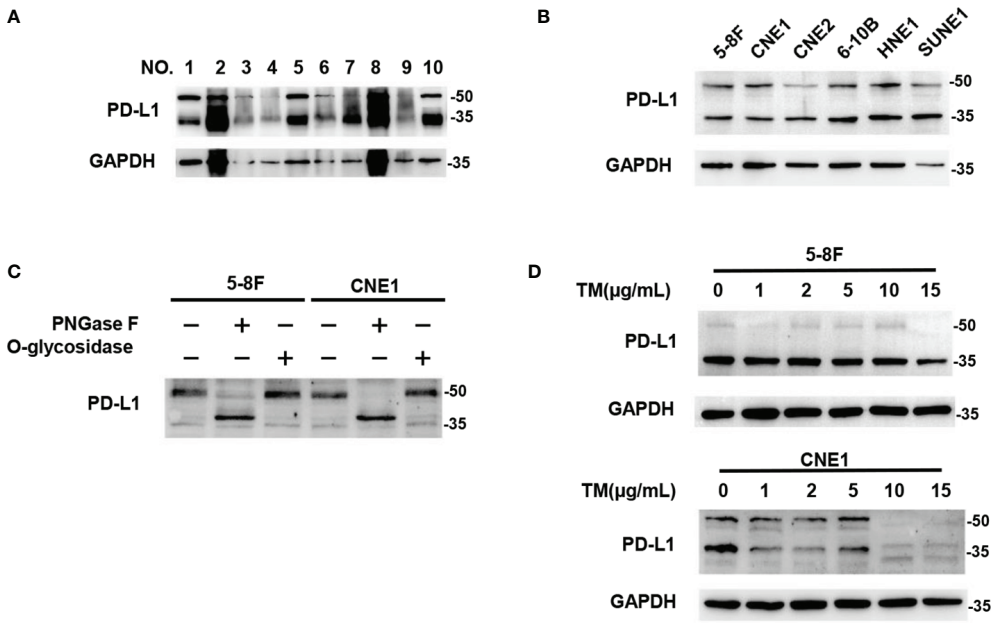

FIGURE 1 | PD-L1 was N-glycosylated in Nasopharyngeal Carcinoma. **(A)** Western blot analysis of PD-L1 in NPC patient samples. **(B)** Western blot analysis of PD-L1 in 6 NPC cells including 5-8F, CNE1, CNE2, 6-10B, HNE1, SUNE1. **(C)** Glycosylation pattern of PD-L1 protein in 5-8F and CNE1 cells. Cell lysates were treated with PNGase F or O-glycosidase and analyzed by western blot analysis. **(D)** Western blot analysis of PD-L1 in 5-8F and CNE1 cells treated by Tunicamycin (TM) with increasing concentrations.

Inhibition of TGF-β1 by SB431542 Reduced PD-L1 Glycosylation *In Vitro*

To explore the relationship between TGF-β1 and PD-L1 glycosylation, SB431542, a TGF-β type I receptor inhibitor, was used to block the effect of TGF-β1 in 5-8F and CNE1 cells. The results showed that inhibition of TGF-β1 by SB431542 reduced PD-L1 expression (**Figure 2A**). Then, 5-8F and CNE1 cells stably overexpressing exogenous Flag-tagged-PD-L1 were constructed, in which the expression of PD-L1 was independently of the transcriptional regulation of endogenous PD-L1. If PD-L1 protein expression was upregulated or downregulated by any cytokines in those cells, it likely occurred through post-translational modifications. The results showed that the exogenous PD-L1 in Flag-PD-L1 5-8F and CNE1 cells could be reduced by SB431542 (**Figure 2B**). Moreover, PD-L1 lost its binding ability to ConA lectin after the treatment of SB431542 (**Figure 2C**). In summary, these results demonstrated that blocking the effect of TGF-β1 by SB431542 suppressed PD-L1 glycosylation *in vitro*.

SB431542 Downregulated Glycosylation of PD-L1 *via* C-Jun/STT3A Pathway *In Vitro*

Although SB431542 reduced PD-L1 glycosylation, the exact mechanism was still unclear. We verified that SB431542 also downregulated c-Jun expression in Flag-PD-L1 5-8F and CNE1 cells (**Figure 2B**). In our previous study, we also found that EBV-EBNA1 promoted the chemoattraction of Treg cells by governing the protein-protein interactions of the SMAD3/c-JUN complex in a TGF-β1-dependent manner in NPC (21). Furthermore, we detected the expression of 15 glycosyltransferases related to PD-L1 glycosylation in 5-8F cells after the treatment of TGF-β1, and found that STT3A had the most significant increase in transcription levels (**Figure S1**). We assumed that SB431542 could downregulate PD-L1 glycosylation by blocking TGF-β1 receptor to inhibit c-Jun and STT3A. In order to explore the exact mechanism, we knocked down c-Jun expression in 5-8F and CNE1 cells with shRNA, and the results showed that silencing c-Jun inhibited STT3A expression and PD-L1 glycosylation (**Figure 3A**). Next, after knockdown of STT3A, glycosylated PD-L1 in 5-8F and CNE1 cells were also downregulated (**Figure 3B**). Furthermore, we overexpressed c-Jun and then knocked down STT3A in 5-8F and CNE1 cells. The data demonstrated that upregulation of PD-L1 glycosylation caused by c-Jun overexpression was reversed by knockdown of STT3A (**Figure 3C**). Altogether, these results demonstrated that SB431542 reduced PD-L1 glycosylation through c-Jun/STT3A pathway, and c-Jun was an upstream regulator of STT3A (**Figure 3D**).

C-Jun Was a Direct Transcriptional Regulator of STT3A

C-Jun is a major component of the dimeric transcription factor activator protein-1 (AP-1) (24), which regulates the expression of target genes at transcriptional level by binding to their promoters. Therefore, we speculated that c-Jun might regulate the expression of STT3A at the transcription level. We used UCSC and JASPAR databases to predict c-Jun-binding sites in the STT3A promoter (**Figure 3E**). A chromatin immunoprecipitation (CHIP) assay was performed to validate the interaction between c-Jun and

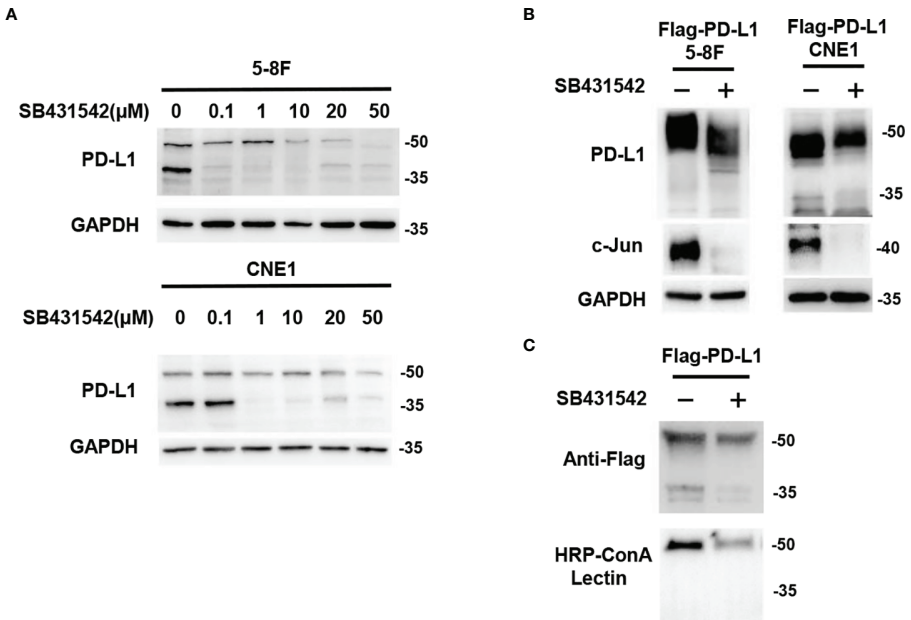

FIGURE 2 | Inhibition of TGF-β1 by SB431542 Reduced PD-L1 Glycosylation *in Vitro*. **(A)** Western blot analysis of PD-L1 in 5-8F and CNE1 cells treated by SB431542 with increasing concentrations. **(B)** Western blot analysis of PD-L1 and c-Jun in exogenous Flag-PD-L1 expressing 5-8F and CNE1 cells with the treatment of 20μM SB431542. **(C)** The glycosylation status of PD-L1 protein purified from SB431542 treating cells was analyzed by ConA lectin binding assay.

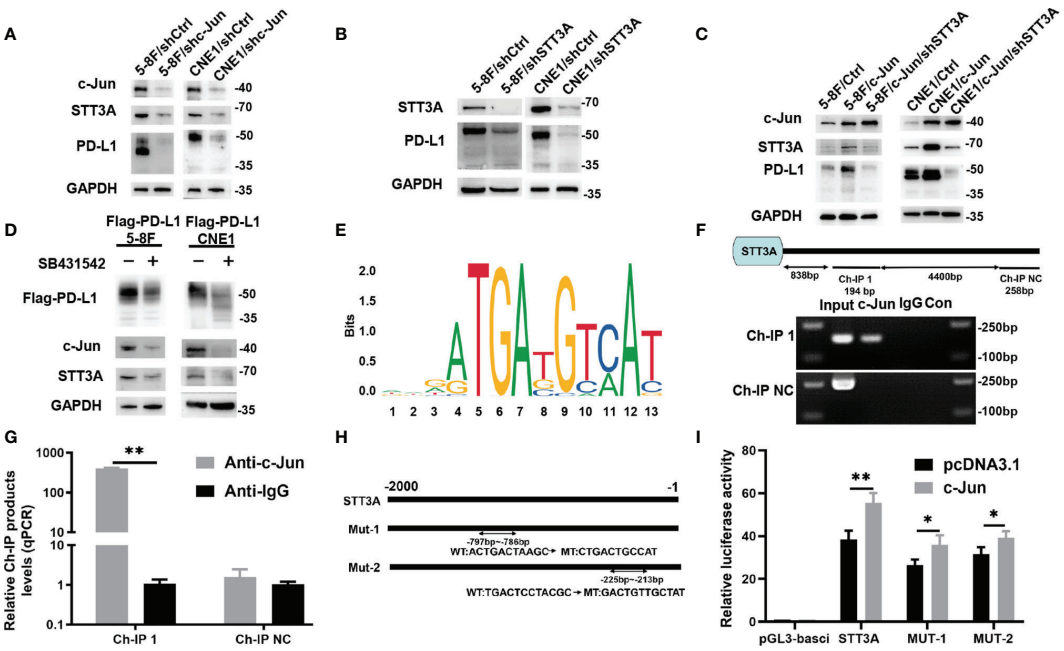

FIGURE 3 | SB431542 Downregulated Glycosylation of PD-L1 *via* C-Jun/STT3A Pathway *in Vitro* and C-Jun was a Direct Transcriptional Regulator of STT3A. **(A)** Western blot analysis of c-Jun, STT3A and PD-L1 after silencing c-Jun in 5-8F and CNE1 cells. **(B)** Western blot analysis of STT3A and PD-L1 after silencing STT3A in 5-8F and CNE1 cells. **(C)** Western blot analysis of c-Jun, STT3A and PD-L1 after overexpressing c-Jun with(out) silencing STT3A in 5-8F and CNE1 cells. **(D)** Western blot analysis of PD-L1, c-Jun and STT3A in exogenous Flag-PD-L1 expressing 5-8F and CNE1 cells with the treatment of 20μM SB431542. **(E)** The binding motif of c-Jun from JASPAR database. **(F)** The CHIP-PCR assay was used to assess the binding of STT3A promoter region. **(G)** Anti-c-Jun-pulled down chromatins were analyzed by qRT-PCR. **(H)** A diagram showing the relationship of full-length and mutant STT3A promoters. **(I)** Dual-luciferase reporter gene assay was performed to indicate the interaction between c-Jun and STT3A. Bars, mean ± SD, *p<0.5, **p<0.01.

STT3A promoter. The data of CHIP-PCR showed that the predicted STT3A binding sequence was successfully pulled down by anti-c-Jun group (**Figure 3F**). And RT-qPCR analysis of the pulled down chromatins demonstrated that c-Jun could bind to STT3A promoter through the putative binding site in the anti-c-Jun group but not in the IgG group (**Figure 3G**). Then, we constructed a series of luciferase reporter vectors containing the full-length of the wild type (WT) or mutant (Mut) c-Jun promoter. The mutant STT3A promoters contained two degenerate c-Jun-binding elements, including Mut-1 (CTGACTGCCAT) and Mut-2 (GACTGTTGCTAT) (**Figure 3H**). Luciferase reporter assays displayed that c-Jun promoted the luciferase activity of STT3A promoter but not the control vector. Furthermore, Mut-1 and Mut-2 reduced the STT3A transactivation, indicating that Mut-1 and Mut-2 were the effective binding sites (**Figure 3I**). The above results revealed that c-Jun regulated the expression of STT3A at transcriptional level by binding to its promoter.

STT3A Expression Was Positively Correlated With TGF-β1 and C-Jun in NPC Tissues, and High STT3A Expression Was Associated With a Advanced Stage in NPC

To further investigate the relationship among TGF-β1, c-Jun and STT3A in human NPC tissues, we analyzed the correlations among them in NPC tissues. As expected, STT3A expression was respectively positively correlated with TGF-β1 (r=0.412, p=0.013) and c-Jun (r=0.5859, p=0.0002) expression (**Figures 4A–C**). Meanwhile, the NPC patients with early-stage tumors (clinical stage I and II) had significantly downregulated expression of STT3A compared to those with a more advanced stage (clinical stage III and IV) (p<0.01) (**Figure 4D**), indicating that high STT3A expression was associated with a more advanced stage in NPC.

Inhibition of TGF-β1 by SB431542 Increased T Cells Activity by Inhibiting PD-L1 Glycosylation *In Vitro*

The above results have confirmed that TGF-β1 promoted PD-L1 glycosylation in NPC through c-Jun/STT3A pathway, and we wondered whether TGF-β1 induced immunosuppression by mediating PD-L1 glycosylation. A co-culture system containing NPC cells and Jurkat T cells was conducted to detect the effect of STT3A-knockdown, SB431542 and tunicamycin (TM) on T cells. The results showed that compared with control group, STT3A-knockdown group had greatly increased tumor cell death rate but lower than SB431542 or TM-treated groups (**Figures 5A, B**). We also detected IL-2 level in the supernatant of the co-culture system, and found that in SB431542 and TM pretreated groups, the secretion of IL-2 by T cells was highest, and IL-2 level of STT3A-knockdown group also had a significant increase compared with control group (**Figures 5C, D**).

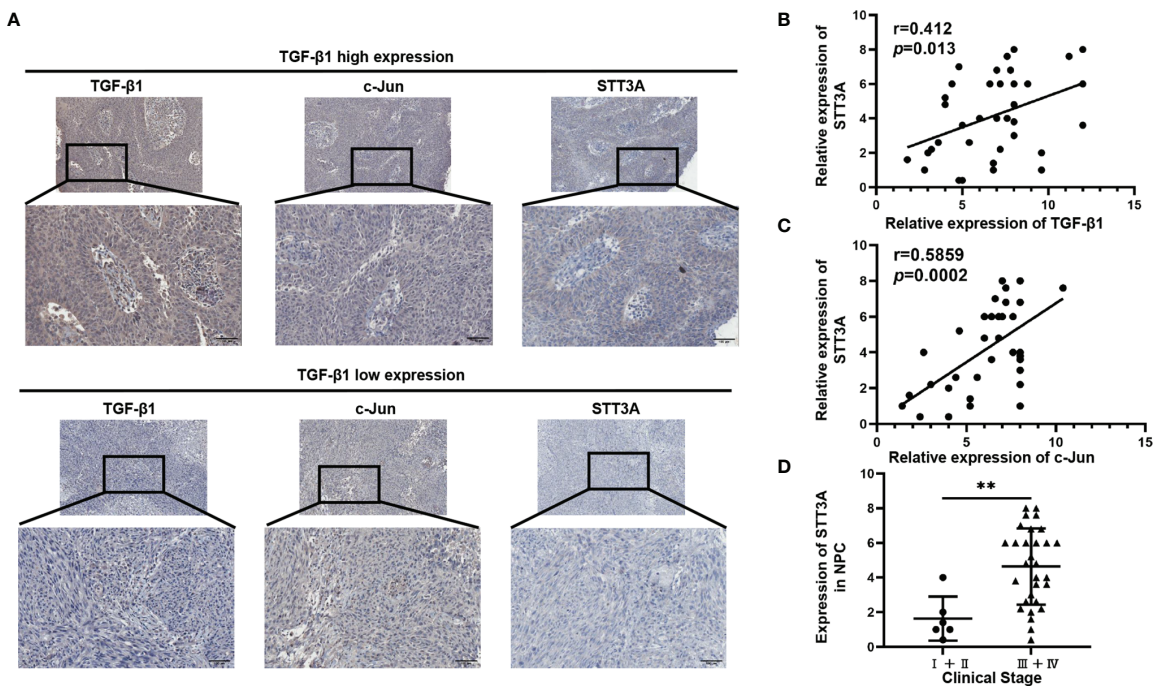

FIGURE 4 | STT3A Expression was Positively Correlated with TGF-β1 and C-Jun in NPC Tissues, and High STT3A Expression was Associated with a more advanced stage in NPC. **(A)** Representative pictures of c-Jun and STT3A expression in NPC patients in TGF-β1-low and high expression groups. Scale bars represented 100μm. **(B, C)** Pearson correlation analysis of the association between TGF-β1 and STT3A (r=0.412; p=0.013) and between c-Jun and STT3A (r=0.5859; p=0.0002) in NPC tissues. **(D)** Comparison of STT3A levels in 36 NPC patients with different clinical stages. **p<0.01.

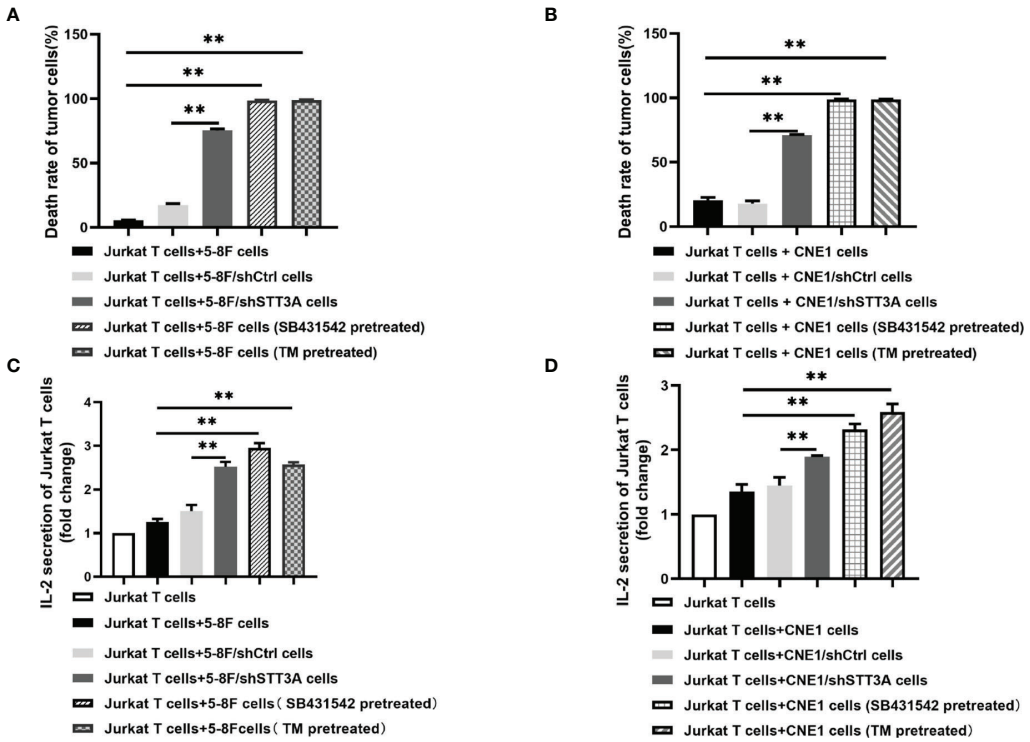

FIGURE 5 | Inhibition of TGF-β1 by SB431542 suppressed T cells activity by inhibiting PD-L1 glycosylation in Vitro. **(A, B)** The death rate of 5-8F or CNE1 cells co-cultured with Jurkat T cells for 6h. The tumor cells were STT3A-kncokdowned by shRNA or pretreated with SB431542 (20μM) or TM (10μg/ml) for 48h. **(C, D)** IL-2 production by activated Jurkat T cells co-cultured with 5-8F or CNE1 cells with shSTT3A or pretreated with SB431542 (20μM) or TM (15μg/ml) for 48h. IL-2 secretion was measured by ELISA. Bars, mean ± SD, $^{**}p<0.01$.

The above results suggested that immunosuppression in NPC induced by inhibition of TGF-β1 was largely dependent on STT3A-regulated PD-L1 glycosylation.

DISCUSSION

Immunotherapy is one of the most encouraging treatment for cancer patients, and the most common immunotherapy strategy includes the interruption of the interaction between immune checkpoints expressed on tumor and immune cells, especially targeting PD-L1/PD-1 (25). PD-L1 is an important immunosuppressive contributor to trigger immune escape by binding to its receptor PD-1 (26). Recent evidence has shown that the expression status of PD-L1, as detected by immunohistochemistry (IHC) has exhibited a significant correlation with response to immunotherapy, and patients whose tumors overexpress PD-L1 by IHC have improved clinical outcomes with anti-PD-1-directed therapy (27). Emerging studies have reported that NPC tumor cells highly express PD-L1, with a positive expression rate from 89% to 100% (28), however, only 20%-30% of NPC patients respond well to anti-PD-L1/PD-1 therapy (8–10). Therefore, understanding the regulation of PD-L1 expression are urgently needed to further improve response to immunotherapy.

Increasing studies have revealed that the expression and function of PD-L1 are regulated by PTMs (29). Among them, N-glycosylation is important in PD-L1/PD-1-mediated tumor immunosuppressive function and influences the efficacy of immunotherapy (30). Li CW et al. reported that glycosylation on N192/200/219 of PD-L1 inhibited the degradation of itself through suppressing GSK3β-β-Trcp-induced PD-L1 polyubiquitination (23). Moreover, PD-L1 glycosylation promoted its interaction with PD-1 and further suppressed T cells activity in triple-negative breast cancer (TNBC) (31). In addition, many studies suggested that targeting glycosylation of PD-L1 was an effective strategy to improve anti-tumor activity. In breast cancer, STT3 upregulated PD-L1 *via* increasing PD-L1 glycosylation in CSCs. Etoposide, which could inhibit EMT-mediated STT3 expression, enhanced the therapeutic outcomes of T cell immunoglobulin mucin-3 (TIM-3) blockade therapy (20). It was later reported that targeting PD-L1 glycosylation by 2-deoxy-D-glucose (2-DG) combined with EGFR inhibitors reduced tumor size and enhanced anti-tumor immunity mediated by 4-1BB, a glycoprotein receptor belonging to the tumor necrosis factor receptor superfamily, in syngeneic mouse models of TNBC (32). However, it remains unknown whether glycosylation of PD-L1 contributes to immune escape in NPC.

In our study, we confirmed that PD-L1 was heavily glycosylated in NPC, and found that TGF-β1 played an important role in N-

glycosylation of PD-L1 by regulating glycotransferase STT3A in NPC. We also revealed that TGF-β1 could upregulate PD-L1 glycosylation and exert immunosuppressive effect *via* activating c-Jun/STT3A signaling pathway. Compared with the studies which reported that TGF-β1-induced EMT increased PD-L1 expression in NSCLC and TNBC, our data identified a novel pathway about TGF-β1-mediated PD-L1 glycosylation, further expanding the understanding of the regulatory mechanisms and cellular functions underlying PD-L1 glycosylation. Additionally, our data will also lead to the development of potentially effective therapeutics targeting PD-L1 glycosylation for clinical application.

As a driving factor of tumor progression, TGF-β can induce tumor cell plasticity by inhibiting the anti-tumor immune response, making epithelial tumor cells more mesenchymal, stem-like and resistant to immunotherapy. TGF-β also produces additional stromal modifiers that promote tumor progression and metastasis and shapes an immunosuppressive tumor microenvironment (16). Bintrafusp alfa is a dual-target inhibitor that can capture TGF-β while binding to PD-L1. This dual-target combination therapy can block the tumor-driving effect of TGF-β1 and overcome the immune escape induced by TGF-β1 (33), which provides more suitable conditions for the binding of monoclonal antibodies and PD-L1. It has been carried out in clinical trials of various tumors such as breast cancer, non-small cell lung cancer, prostate cancer, pancreatic cancer, bile duct cancer and cervical cancer and has achieved remarkable effects (34). In this study, we demonstrated that TGF-β1-mediated PD-L1 glycosylation promoted immune escape *via* c-Jun/STT3A pathway in NPC, which provided a theoretical basis for the clinical practice of bintrafusp alfa in NPC.

In summary, our study verified that TGF-β1 induced PD-L1 glycosylation and exerted immunosuppressive effect *via* c-Jun/STT3A signaling pathway in NPC. These results will provide a new understanding of the resistance mechanisms of anti-PD-1/PD-L1 therapy in NPC, and suggest that targeting TGF-β1 pathway might be a promising approach to enhance immune checkpoint blockade in NPC.

DATA AVAILABILITY STATEMENT

The original contributions presented in the study are included in the article/**Supplementary Material**. Further inquiries can be directed to the corresponding author.

ETHICS STATEMENT

The studies involving human participants were reviewed and approved by Ethics Committee of Nanfang hospital. The patients/participants provided their written informed consent to participate in this study.

AUTHOR CONTRIBUTIONS

X-PL and JL conceived the study and drafted the manuscript. X-MM, Y-FL, FZ, and CS performed the experiments. XL contributed to the quality. All authors contributed to the article and approved the submitted version.

FUNDING

This work was supported by National Natural Science Foundation of China (81472535) and Natural Science Foundation of Guangdong Province, China (2019A1515010968).

SUPPLEMENTARY MATERIAL

The Supplementary Material for this article can be found online at: https://www.frontiersin.org/articles/10.3389/fonc.2022.815437/full#supplementary-material

REFERENCES

1. Chen Y-P, Chan ATC, Le Q-T, Blanchard P, Sun Y, Ma J. Nasopharyngeal Carcinoma. *Lancet* (2019) 394(10192):64–80. doi: 10.1016/S0140-6736(19)30956-0
2. Dong H, Strome SE, Salomao DR, Tamura H, Hirano F, Flies DB, et al. Tumor-Associated B7-H1 Promotes T-Cell Apoptosis: A Potential Mechanism of Immune Evasion. *Nat Med* (2002) 8(8):793–800. doi: 10.1038/nm730
3. Muro K, Chung HC, Shankaran V, Geva R, Catenacci D, Gupta S, et al. Pembrolizumab for Patients With PD-L1-Positive Advanced Gastric Cancer (KEYNOTE-012): A Multicentre, Open-Label, Phase 1b Trial. *Lancet Oncol* (2016) 17(6):717–26. doi: 10.1016/S1470-2045(16)00175-3
4. Sznol M, Chen L. Antagonist Antibodies to PD-1 and B7-H1 (PD-L1) in the Treatment of Advanced Human Cancer. *Clin Cancer Res* (2013) 19(5):1021–34. doi: 10.1158/1078-0432.CCR-12-2063
5. Velcheti V, Schalper KA, Carvajal DE, Anagnostou VK, Syrigos KN, Sznol M, et al. Programmed Death Ligand-1 Expression in Non-Small Cell Lung Cancer. *Lab Invest* (2014) 94(1):107–16. doi: 10.1038/labinvest.2013.130
6. Xu F, Jin T, Zhu Y, Dai C. Immune Checkpoint Therapy in Liver Cancer. *J Exp Clin Cancer Res* (2018) 37(1):110. doi: 10.1186/s13046-018-0777-4
7. Liu X, Shan C, Song Y, Du J. Prognostic Value of Programmed Cell Death Ligand-1 Expression in Nasopharyngeal Carcinoma: A Meta-Analysis of 1,315 Patients. *Front Oncol* (2019) 9:1111. doi: 10.3389/fonc.2019.01111
8. Fang W, Yang Y, Ma Y, Hong S, Lin L, He X, et al. Camrelizumab (SHR-1210) Alone or in Combination With Gemcitabine Plus Cisplatin for Nasopharyngeal Carcinoma: Results From Two Single-Arm, Phase 1 Trials. *Lancet Oncol* (2018) 19(10):1338–50. doi: 10.1016/S1470-2045(18)30495-9
9. Hsu C, Lee S-H, Ejadi S, Even C, Cohen RB, Le Tourneau C, et al. Safety and Antitumor Activity of Pembrolizumab in Patients With Programmed Death-Ligand 1-Positive Nasopharyngeal Carcinoma: Results of the KEYNOTE-028 Study. *J Clin Oncol* (2017) 35(36):4050–6. doi: 10.1200/JCO.2017.73.3675
10. Ma BBY, Lim W-T, Goh B-C, Hui EP, Lo K-W, Pettinger A, et al. Antitumor Activity of Nivolumab in Recurrent and Metastatic Nasopharyngeal Carcinoma: An International, Multicenter Study of the Mayo Clinic Phase 2 Consortium (NCI-9742). *J Clin Oncol* (2018) 36(14):1412–8. doi: 10.1200/JCO.2017.77.0388
11. Lee H-H, Wang Y-N, Xia W, Chen C-H, Rau K-M, Ye L, et al. Removal of N-Linked Glycosylation Enhances PD-L1 Detection and Predicts Anti-PD-1/PD-L1 Therapeutic Efficacy. *Cancer Cell* (2019) 36(2):168–78. doi: 10.1016/j.ccell.2019.06.008
12. Han Y, Liu D, Li L. PD-1/PD-L1 Pathway: Current Researches in Cancer. *Am J Cancer Res* (2020) 10(3):727–42.

13. Dai X, Gao Y, Wei W. Post-Translational Regulations of PD-L1 and PD-1: Mechanisms and Opportunities for Combined Immunotherapy. *Semin Cancer Biol* (2021) S1044-579X(21):00103–6. doi: 10.1016/j.semcancer.2021.04.002
14. Hu X, Lin Z, Wang Z, Zhou Q. Emerging Role of PD-L1 Modification in Cancer Immunotherapy. *Am J Cancer Res* (2021) 11(8):3832–40.
15. Hu X, Wang J, Chu M, Liu Y, Wang Z-W, Zhu X. Emerging Role of Ubiquitination in the Regulation of PD-1/PD-L1 in Cancer Immunotherapy. *Mol Ther* (2021) 29(3):908–19. doi: 10.1016/j.ymthe.2020.12.032
16. Batlle E, Massagué J. Transforming Growth Factor-β Signaling in Immunity and Cancer. *Immunity* (2019) 50(4):924–40. doi: 10.1016/j.immuni.2019.03.024
17. Hugo W, Zaretsky JM, Sun L, Song C, Moreno BH, Hu-Lieskovan S, et al. Genomic and Transcriptomic Features of Response to Anti-PD-1 Therapy in Metastatic Melanoma. *Cell* (2016) 165(1):35–44. doi: 10.1016/j.cell.2016.02.065
18. Mariathasan S, Turley SJ, Nickles D, Castiglioni A, Yuen K, Wang Y, et al. Tgfβ Attenuates Tumour Response to PD-L1 Blockade by Contributing to Exclusion of T Cells. *Nature* (2018) 554(7693):544–8. doi: 10.1038/nature25501
19. Tauriello DVF, Palomo-Ponce S, Stork D, Berenguer-Llergo A, Badia-Ramentol J, Iglesias M, et al. Tgfβ Drives Immune Evasion in Genetically Reconstituted Colon Cancer Metastasis. *Nature* (2018) 554(7693):538–43. doi: 10.1038/nature25492
20. Hsu J-M, Xia W, Hsu Y-H, Chan L-C, Yu W-H, Cha J-H, et al. STT3-Dependent PD-L1 Accumulation on Cancer Stem Cells Promotes Immune Evasion. *Nat Commun* (2018) 9(1):1908. doi: 10.1038/s41467-018-04313-6
21. Huo S, Luo Y, Deng R, Liu X, Wang J, Wang L, et al. EBV-EBNA1 Constructs an Immunosuppressive Microenvironment for Nasopharyngeal Carcinoma by Promoting the Chemoattraction of Treg Cells. *J Immunother Cancer* (2020) 8(2):e001588. doi: 10.1136/jitc-2020-001588
22. Wang J, Luo Y, Bi P, Lu J, Wang F, Liu X, et al. Mechanisms of Epstein-Barr Virus Nuclear Antigen 1 Favor Tregs Accumulation in Nasopharyngeal Carcinoma. *Cancer Med* (2020) 9(15):5598–608. doi: 10.1002/cam4.3213
23. Li C-W, Lim S-O, Xia W, Lee H-H, Chan L-C, Kuo C-W, et al. Glycosylation and Stabilization of Programmed Death Ligand-1 Suppresses T-Cell Activity. *Nat Commun* (2016) 7:12632. doi: 10.1038/ncomms12632
24. Papavassiliou AG, Musti AM. The Multifaceted Output of C-Jun Biological Activity: Focus at the Junction of CD8 T Cell Activation and Exhaustion. *Cells* (2020) 9(11):2470. doi: 10.3390/cells9112470
25. Pardoll DM. The Blockade of Immune Checkpoints in Cancer Immunotherapy. *Nat Rev Cancer* (2012) 12(4):252–64. doi: 10.1038/nrc3239
26. Ostrand-Rosenberg S, Horn LA, Haile ST. The Programmed Death-1 Immune-Suppressive Pathway: Barrier to Antitumor Immunity. *J Immunol* (2014) 193(8):3835–41. doi: 10.4049/jimmunol.1401572
27. Bodor JN, Boumber Y, Borghaei H. Biomarkers for Immune Checkpoint Inhibition in non-Small Cell Lung Cancer (NSCLC). *Cancer* (2020) 126 (2):260–70. doi: 10.1002/cncr.32468
28. Wotman M, Herman SW, Costantino P, Tham T. The Prognostic Role of Programmed Death-Ligand 1 in Nasopharyngeal Carcinoma. *Laryngoscope* (2020) 130(11):2598–606. doi: 10.1002/lary.28523
29. Hsu J-M, Li C-W, Lai Y-J, Hung M-C. Posttranslational Modifications of PD-L1 and Their Applications in Cancer Therapy. *Cancer Res* (2018) 78 (22):6349–53. doi: 10.1158/0008-5472.CAN-18-1892
30. Wang Y-N, Lee H-H, Hsu JL, Yu D, Hung M-C. The Impact of PD-L1 N-Linked Glycosylation on Cancer Therapy and Clinical Diagnosis. *J BioMed Sci* (2020) 27(1):77. doi: 10.1186/s12929-020-00670-x
31. Li C-W, Lim S-O, Chung EM, Kim Y-S, Park AH, Yao J, et al. Eradication of Triple-Negative Breast Cancer Cells by Targeting Glycosylated PD-L1. *Cancer Cell* (2018) 33(2):187–201. doi: 10.1016/j.ccell.2018.01.009
32. Shao B, Li C-W, Lim S-O, Sun L, Lai Y-J, Hou J, et al. Deglycosylation of PD-L1 by 2-Deoxyglucose Reverses PARP Inhibitor-Induced Immunosuppression in Triple-Negative Breast Cancer. *Am J Cancer Res* (2018) 8(9):1837–46.
33. Kim B-G, Malek E, Choi SH, Ignatz-Hoover JJ, Driscoll JJ. Novel Therapies Emerging in Oncology to Target the TGF-β Pathway. *J Hematol Oncol* (2021) 14(1):55. doi: 10.1186/s13045-021-01053-x
34. Lind H, Gameiro SR, Jochems C, Donahue RN, Strauss J, Gulley JL, et al. Dual Targeting of TGF-β and PD-L1 *via* a Bifunctional Anti-PD-L1/TGF-βrii Agent: Status of Preclinical and Clinical Advances. *J Immunother Cancer* (2020) 8(1):e000433. doi: 10.1136/jitc-2019-000433

Conflict of Interest: The authors declare that the research was conducted in the absence of any commercial or financial relationships that could be construed as a potential conflict of interest.

Publisher's Note: All claims expressed in this article are solely those of the authors and do not necessarily represent those of their affiliated organizations, or those of the publisher, the editors and the reviewers. Any product that may be evaluated in this article, or claim that may be made by its manufacturer, is not guaranteed or endorsed by the publisher.

frontiers in Oncology

ORIGINAL RESEARCH
published: 08 March 2022
doi: 10.3389/fonc.2022.782058

Correlation Between TCF7$^+$ T Cells and Prognosis of Patients With Oral Squamous Cell Carcinoma

Haixu Rong[1,2†], Tingting Cai[1,2†], Yu Peng[1,3†], Xiaojuan Wang[1], Tianjun Lan[1], Zhanpeng Ou[2], Ling Qiu[2], Qunxing Li[2], Lizao Zhang[1,2], Fan Wu[2], Hsinyu Lin[2], Siqi Ren[1], Zitian Li[4], Song Fan[1,2] and Jinsong Li[1,2*]*

[1] Guangdong Provincial Key Laboratory of Malignant Tumor Epigenetics and Gene Regulation of Sun Yat-sen Memorial Hospital, Guangzhou, China, [2] Department of Oral and Maxillofacial Surgery, Sun Yat-sen Memorial Hospital of Sun Yat-sen University, Guangzhou, China, [3] The Stomatology Department of The First Affiliated Hospital, Medical College of Shantou University, Shantou, China, [4] School of Stomatology, Jilin University, Changchun, China

OPEN ACCESS

Edited by:
Nerina Denaro,
Azienda Sanitaria Ospedaliera S.Croce e Carle Cuneo, Italy

Reviewed by:
Sebastiaan De Visscher,
University Medical Center Groningen, Netherlands
Wen-Wei Sung,
Chung Shan Medical University Hospital, Taiwan

***Correspondence:**
Jinsong Li
lijins@mail.sysu.edu.cn
Song Fan
fansong8888@163.com

[†]These authors have contributed equally to this work and share first authorship

Specialty section:
This article was submitted to Head and Neck Cancer, a section of the journal Frontiers in Oncology

Received: 23 September 2021
Accepted: 14 February 2022
Published: 08 March 2022

Citation:
Rong H, Cai T, Peng Y, Wang X, Lan T, Ou Z, Qiu L, Li Q, Zhang L, Wu F, Lin H, Ren S, Li Z, Fan S and Li J (2022) Correlation Between TCF7$^+$ T Cells and Prognosis of Patients With Oral Squamous Cell Carcinoma. Front. Oncol. 12:782058. doi: 10.3389/fonc.2022.782058

Objective: To investigate whether TCF7$^+$ T cells constitute an important factor to improve the existing postoperative prediction model for patients with oral squamous cell carcinoma.

Method: TCF7$^+$ T cells were detected in the tissues of 167 OSCC patients by multiplex immunofluorescence. The percentage of TCF7$^+$ T cells was transformed into a dichotomous variable, combined with the clinicopathological data for the OSCC patients, and then subjected to univariate and multivariate analyses. The derived independent predictors were then incorporated into risk models to analyze their relationship with the prognosis of patients.

Results: The high TCF7$^+$ group had a better prognosis than the low TCF7$^+$ group (OS: p<0.001; RFS: p<0.001). Univariate and multivariate analyses showed that TCF7$^+$ T cells serve as an independent predictor of OSCC (univariate/multivariate analysis: p<0.001). In Cox risk progression models, inclusion of the TCF7$^+$ T cell percentage improved the predictive accuracy of Grade and TNM stage (Grade-OS/RFS: p<0.001; TNM-OS/RFS: p<0.001; TNM+Grade-OS: p<0.001, TNM+Grade-RFS: p=0.004). Inclusion of the TCF7$^+$ T cell percentage improved the clinical utility.

Conclusions: TCF7$^+$ T cells can act as an independent predictor for postoperative OSCC patients. The inclusion of TCF7$^+$ T cells improved the predictive accuracy and clinical utility of the nomograms to different degrees.

Keywords: oral squamous cell carcinoma, TCF7/TCF1, survival analysis, Cox regression, prognosis, nomogram

INTRODUCTION

Oral squamous cell carcinoma (OSCC) is a common tumor worldwide. In 2020, an estimated 377,713 cases of oral cancer occurred, with an estimated 177,757 deaths and male dominance, making it the 8th most common tumor in men (1). Despite progress in the treatment of solid tumors with emerging immunotherapies (2), significant therapeutic effects are lacking in

nonresponders (3, 4), and immune-related adverse events may occur (5, 6). Therefore, to expand the therapeutic population of immunotherapy, improve the response rates and increase the duration of enduring remission, the search for new markers has become urgent.

Studies have shown a stronger antitumor response when more self-renewing, expanding and persistent T cells are present within the tumor (7, 8). T cell factor 1 (TCF1) is a transcription factor of the typical Wnt signaling pathway encoded by the TCF7 gene (9). The critical role of TCF1 in T cell differentiation and memory formation is widely recognized. For example, Moshe et al. (10) reported high expression of markers such as PLAC8, LTB, LY9, SELL, TCF7, and CCR7 in T cells in response to anti-PD-1 treatment. Additionally, $TCF7^+$ ($TCF1^+$) T cells (hereafter referred to as $TCF7^+$ T cells) amplify immune responses and improve the response to immunotherapy in cancer. The reason may be that T cells appear to have a stem cell-like ability to expand, differentiate and self-renew by expressing large amounts of TCF7 (11). Therefore, Moshe et al. suggested that $TCF7^+$ T cells may improve the prognosis of immune checkpoint inhibitor therapy for melanoma. However, the prognosis of $TCF7^+$ T cells in OSCC is unclear.

In this study, multiplex immunofluorescence was used to detect the expression of $TCF7^+$ T cells in OSCC, combined with the clinicopathological data for 167 OSCC patients. After univariate analysis and multivariate analysis, the variables with statistical significance were transformed into a Cox risk prediction model to elucidate the potential of $TCF7^+$ T cells as a new marker valuable reference for predicting OSCC patient prognosis.

MATERIALS AND METHODS

TCGA and Survival Data

The transcriptomic data and clinical information shown in the **Supplemental Figures** were obtained from the TCGA repository at GDC (https://portal.gdc.cancer.gov/). mRNA expression screening of OSCC patients was performed according to NCCN Guidelines Version 2.2021. The expression of CD3 and TCF7 transcripts, survival time and survival status were included in the downloaded survival data. To obtain reliable and ideal grouping, each gene was divided into high- and low-expression groups using the R packages "survminer" and "maxstat"; *p value*s were calculated using the log-rank test.

Data Collection and Patient Information

The sample size followed the principle of 20 EPV (Event Per Variable) (12), and 167 paraffin tissue specimens from surgical resection at the Department of Oral and Maxillofacial Surgery, Sun Yat-sen Memorial Hospital, Sun Yat-sen University were collected from January 2015 to December 2019. All the patients met the following criteria: (a) a first pathologic diagnosis of OSCC; (b) no radiotherapy or chemotherapy before surgery; (c) preserved postoperative wax blocks; (d) available complete electronic medical records, histological pathology reports and follow-up records. Clinicopathological factors, including age, sex, alcohol consumption, tobacco factor, primary site location, T stage, lymph node metastasis, TNM stage, histological grade, $CD3^+$ T cell expression, and $CD3^+TCF7^+$ T cell expression, were collected. The clinical stages and differentiation degrees of the tumor were classified based on TNM classification of the AJCC 7th edition and WHO grade classification, respectively. The 167 patients were followed up postoperatively every 3 months for 1 year and every 6 months from the second year for 5 years. Written informed consent was obtained from each patient participating in the study.

Multiplexed Immunofluorescence and Evaluation

All the paraffin tissue specimens were fixed with 4% formaldehyde, embedded in conventional paraffin, serially sectioned at approximately 4 μm thickness, and dewaxed. EDTA alkaline antigen retrieval was performed, and the samples were blocked with goat serum. After incubation with the primary antibody, the slides were washed with TBST for 3 min, incubated with the secondary antibody (goat anti-mouse HRB, 10 min), washed with TBST for 3 min and incubated with a fluorescent dye (Panovue). The above process was repeated for additional markers, after which DAPI was added dropwise; after staining, an anti-quenching agent was added dropwise, and coverslips were sealed. The incubation conditions were as follows: TCF7 (cst, rabbit monoclonal antibody, 1:200, first cycle), CD3 (Abcam, rabbit monoclonal antibody, 1:100, second cycle), and DAPI (1:200). The tissue sections were scanned using the Akoya Vectra Polaris system (1.0.10; PerkinElmer, Inc), and images were analyzed using inForm software (2.4.6; PerkinElmer, Inc). The results were evaluated as follows: four fields of view were selected arbitrarily for each patient's section, the percentage of $CD3^+$ $TCF7^+$ T cells among total $CD3^+$ T cells in each field of view was obtained, and the sum was averaged as the percentage of $TCF7^+$ T cells in the tumor. The optimal cutoff percentage values of $TCF7^+$ T cells were divided in X-tile 3.6.1 (Yale University, New Haven, Connecticut, USA) software (13) based on OS and RFS.

Statistical Analysis

Statistical analysis was performed using SPSS 25.0 (SPSS, Inc., Chicago, IL, USA) and R (R Foundation for Statistical Computing, Beijing, China). In the baseline table, the measures were expressed as means ± standard deviation, and χ^2 test was used for comparisons between groups. Cox regression was employed for both univariate and multivariate analyses. The *p value* was determined by the *Benjamini & Hochberg* (BH) method for multiple testing correction. $p<0.05$ was considered a statistically significant difference. The statistically significant variables in univariate analysis were subjected to multivariate analysis, and the variables ultimately selected were used as variables in the nomogram. Nomograms and calibration curves were plotted using R software (rms package, survivor package). Regarding the performance of the predictive model, the C-index was applied to evaluate the discrimination of different models,

where the C-index was compared using the *compareC* function. Calibration curves were used to assess calibration of the model under 1000 resamplings (B=1000). We used decision curve analysis to compare clinical utility among the models at 1, 3 and 5 years.

RESULTS

Expression of TCF7$^+$ T Cells in OSCC Tissues and Its Correlation With Clinicopathological Features

We first estimated the prognostic value of CD3$^+$TCF7$^+$ T cells in OSCC patients at the transcriptional level. The transcriptome data for 212 OSCC patients and their survival information were downloaded from TCGA. The patients were divided into a CD3^{hi} TCF7^{hi} (DH) group, CD3^{low} TCF7^{low} (DL) group, CD3^{hi} TCF7^{low} (CD3^{hi}) group, and CD3^{low} TCF7^{hi} (TCF7^{hi}) group based on transcript levels. No significant difference (p=0.160) was found in the OS rates among the four groups (**Supplementary Figure 1A**). However, statistical significance (p=0.041) was shown for the DH group and DL group (**Supplementary Figure 1B**), indicating that the DH group had a better prognosis based on transcriptional data.

To test whether TCF7$^+$ T cells also influence the prognosis of OSCC patients, the number of TCF7$^+$ T cells was assessed by multiplex immunofluorescence analysis in 167 OSCC patients (**Figure 1**). The proportion of TCF7$^+$ T cells to CD3+ T cells was used as a continuous variable. The 167 patients were divided into a TCF7$^+$ T cell low expression group (hereafter referred to as the TCF7^{low} group) (**Figures 1E, F**) and a TCF7$^+$ T cell^{hi} expression group (hereafter referred to as the TCF7^{hi} group) according to the results calculated by X-tile software (**Figures 1A–D, G, H**). The cutoff value in the OS cohort was 0.39, with 81 patients assigned to the TCF7^{low} group (**Figure 1B**); the cutoff value in the RFS cohort was 0.41, with 88 patients assigned to the TCF7^{low} group (**Figure 1D**). Based on both OS and RFS survival curves, the TCF7^{hi} group had a more favorable prognosis than the TCF7^{low} group (**Figures 1A, C**). Associations between the TCF7^{hi} and TCF7^{low} groups in the OS cohort and RFS cohort and clinicopathological characteristics are summarized in **Table 1**. TCF7$^+$ T cells were associated with T stage, lymph node metastasis and TNM stage, with statistically significant differences (p<0.05), but not with sex, age, tobacco, alcohol, histological grade,

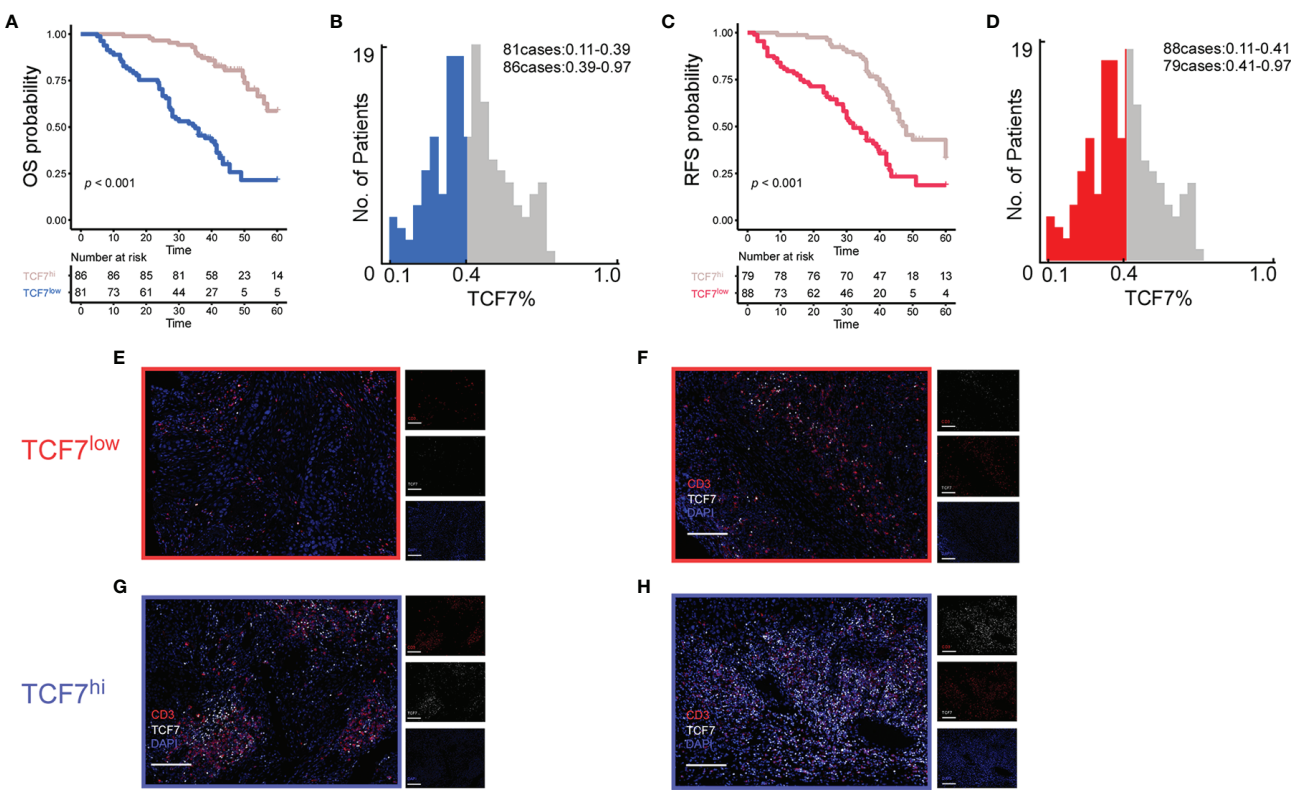

FIGURE 1 | A total of 167 patients were classified into the TCF7$^+$ T cell low expression group and TCF7$^+$ T cell high expression group based on optimal cutoff values of 0.39 **(B)** and 0.41 **(D)** for OS **(A)** and RFS **(C)**, respectively, using X-tile software. Representative multiplex immunofluorescence results plots were selected in each of the two groups to demonstrate the expression of TCF7$^+$ T cells in the low expression group **(E, F)** and high expression group **(G, H)**. The markers of fluorescence used were CD3 (red), TCF7 (white), and DAPI (blue). Magnification, 20×; white scale bar, 100 μm; OS, overall survival; RFS, recurrence-free survival.

TABLE 1 | Clinicopathological characteristics of OSCC patients according to TCF7 expression.

Characteristic	Overall (n=167)	OS			RFS		
		$TCF7^{hi}$ (n=86)	$TCF7^{low}$ (n=81)	*p value*[b]	$TCF7^{hi}$ (n=79)	$TCF7^{low}$ (n=88)	*p value*[b]
Age, y (mean ± SD)	53.71 ± 12.71	53.86 ± 12.08	53.54 ± 13.41	0.161	54.16 ± 11.80	53.30 ± 13.53	0.660
Sex							
Male	98 (58.68%)	51 (59.30%)	47 (58.02%)		46 (58.23%)	52 (59.09%)	
Female	69 (41.32%)	35 (40.70%)	34 (41.98%)	0.992	33 (41.77%)	36 (40.91%)	0.999
Alcohol							
No	97 (58.08%)	52 (60.47%)	45 (55.56%)		47 (59.49%)	50 (56.82%)	
Yes	70 (41.92%)	34 (39.53%)	36 (44.44%)	0.627	32 (40.51%)	38 (43.18%)	0.847
Tobacco							
No	104 (62.28%)	52 (60.47%)	52 (64.20%)		48 (60.76%)	56 (63.64%)	
Yes	63 (37.72%)	34 (39.53%)	29 (35.80%)	0.736	31 (39.24%)	32 (36.36%)	0.823
Primary tumor site							
Oral tongue	133 (79.64%)	70 (81.40%)	63 (77.78%)		65 (82.28%)	68 (77.27%)	
Gingiva	12 (7.19%)	8 (9.30%)	4 (4.94%)		8 (10.13%)	4 (4.55%)	
Buccal mucosa	7 (4.19%)	1 (1.16%)	6 (7.41%)		1 (1.27%)	6 (6.82%)	
Hard palate	5 (2.99%)	2 (2.33%)	3 (3.70%)		1 (1.27%)	4 (4.55%)	
Floor of mouth	10 (5.99%)	5 (5.81%)	5 (6.17%)	0.262	4 (5.06%)	6 (6.82%)	0.167
T-stage[a]							
T1	50 (29.94%)	35 (40.70%)	15 (18.52%)		34 (43.04%)	16 (18.18%)	
T2	42 (25.15%)	22 (25.58%)	20 (24.69%)		21 (26.58%)	21 (23.86%)	
T3	75 (44.91%)	29 (33.72%)	46 (56.79%)		24 (30.38%)	51 (57.95%)	
T4	0	0	0	0.003	0	0	<0.001
N-stage[a]							
N0	73 (43.71%)	51 (59.30%)	22 (27.16%)		49 (62.03%)	24 (27.27%)	
N1	30 (17.96%)	14 (16.28%)	16 (19.75%)		13 (16.64%)	17 (19.32%)	
N2a	6 (3.59%)	3 (3.49%)	3 (3.7%)		3 (3.80%)	3 (3.41%)	
N2b	57 (34.13%)	18 (20.93%)	39 (48.15%)		14 (17.72%)	43 (48.86%)	
N2c	1 (0.60%)	0	1 (1.23%)	<0.001	0	1 (1.14%)	<0.001
TNM stage[a]							
I	40 (23.95%)	31 (36.05%)	9 (11.11%)		29 (36.71%)	11 (12.50%)	
II	29 (17.37%)	18 (20.93%)	11 (13.28%)		18 (22.78%)	11 (12.50%)	
III	31 (18.56%)	15 (17.44%)	16 (19.75%)		14 (17.72%)	17 (19.32%)	
IV	67 (40.12%)	22 (25.58%)	45 (55.56%)	<0.001	18 (22.78%)	49 (55.68%)	<0.001
Histologic grade							
Well	72 (43.11%)	40 (46.51%)	32 (39.51%)		36 (45.57%)	36 (40.91%)	
Poor	95 (56.89%)	46 (53.49%)	49 (60.49%)	0.449	43 (54.43%)	52 (59.09%)	0.652
CD3	1311 ± 946	1219 ± 837	1408 ± 1047	0.197	1177 ± 818	1431 ± 1038	0.084

[a]*American Joint Committee on Cancer, 7th Edition staging.*

[b]*Fisher's exact test or chi-squared test was used to examine the correlation between TCF7 expression and clinicopathological characteristics in 167 patients with OSCC.*

or CD3 density ($p > 0.05$). Clinicopathological baseline tables for the $TCF7^{hi}$ and $TCF7^{low}$ groups were established (**Table 1**).

$TCF7^{hi}$ Predicts a Good Prognosis for OSCC Patients Regarding OS and RFS

We performed univariate and multivariate analyses to further assess whether the $TCF7^{+}$ T cell proportion is an independent predictor of OS and RFS. Univariate analysis showed (**Table 2**) that the $TCF7^{+}$ T cell percentage as a continuous variable was a risk factor for OS and RFS (OS: HR=0.013, 95% CI=0.002 to 0.074, $p<0.001$; RFS: HR=0.041, 95% CI=0.009 to 0.185, $p<0.001$) and that T stage (T2-OS: HR=2.187, 95% CI=0.814 to 5.872, $p=0.185$; T2-RFS: HR=1.056, 95% CI=0.572 to 1.950, $p=0.919$; T3-OS: HR=8.621, 95% CI=3.709 to 20.039, $p<0.001$; T3-RFS: HR=2.645, 95% CI=1.592 to 4.397), lymph node metastasis (N1-OS: HR=4.510, 95% CI=2.077 to 9.792, $p<0.001$; N1-RFS: HR=3.548, 95% CI=1.972 to 6.382, $p<0.001$; N2a-OS: HR=7.789, 95% CI=2.718 to 22.327, $p<0.001$; N2a-RFS: HR=5.077, 95% CI=2.064 to 12.490, $p<0.001$; N2b-OS: HR=7.770, 95% CI=4.065 to 14.854, $p< 0.001$; N2b-RFS: HR=4.770, 95% CI=2.881 to 7.900, $p<0.001$; N2c-OS: HR=9.796, 95% CI=1.261 to 76.104, $p=0.0517$, N2c-RFS: HR<0.001, 95% CI=0 to infinity, $p=0.996$), TNM stage (II-OS: HR=1.695, 95% CI=0.401 to 7.155, $p=0.541$; II-RFS: HR=0.822, 95% CI=0.364 to 1.857, $p=0.113$), histological grade (OS: HR=0.471, 95% CI=0.286 to 0.776, $p=0.006$; RFS: HR=0.564, 95% CI=0.367 to 0.868, $p=0.018$) were also risk factors for OS and RFS. Additionally, the percentage of $TCF7^{+}$ T cells was transformed into a dichotomous variable and then included in multivariate analysis (**Table 3**). Thus, the $TCF7^{+}$ T cell expression level was a risk factor for OS and RFS (OS: HR=0.235, 95% CI=0.133 to 0.414, $p<0.001$; RFS: HR=2.661, 95% CI=1.675 to 4.227, $p<0.001$). In multivariate analysis, TNM stage (OS: HR=8.539, 95% CI=2.144 to 34.013, $p=0.004$; RFS: HR=4.992, 95% CI=1.054 to 23.649, $p=0.086$) and histological grade (OS: HR=0.408, 95% CI=0.246 to 0.679, $p=0.002$; RFS: HR=0.469, 95% CI=0.303 to 0.724, $p=0.001$) were risk factors for OS and RFS.

TABLE 2 | Univariate analysis of factors associated with overall survival.

Univariate analysis	OS (n=167)		RFS (n=158)	
Variable	**HR (95% CI)**	***p value****	**HR (95% CI)**	***p value****
Sex				
Male vs. Female	1.032 (0.649-1.643)	0.893	1.058 (0.702-1.594)	0.900
Age				
<50 vs. >50	1.285 (0.809-2.041)	0.354	1.232 (0.818-1.855)	0.424
Tobacco				
Yes vs. No	0.726 (0.449-1.178)	0.260	0.799 (0.526-1.214)	0.424
Alcohol				
Yes vs. No	1.127 (0.712-1.78)	0.651	1.279 (0.854-1.915)	0.371
T stage				
T1	Ref.		Ref.	
T2	2.187 (0.814-5.872)	0.185	1.056 (0.572-1.950)	0.919
T3	8.621 (3.709-20.039)	<0.001	2.645 (1.592-4.397)	<0.001
Node metastasis				
N0	Ref.		Ref.	
N1	4.510 (2/077-9.792)	<0.001	3.548 (1.972-6.382)	<0.001
N2a	7.789 (2.718-22.327)	<0.001	5.077 (2.064-12.490)	<0.001
N2b	7.770 (4.065-14.854)	<0.001	4.770 (2.881-7.900)	<0.001
N2c	9.796 (1.261-76.104)	0.0517	<0.001 (-)	0.996
TNM stage				
I	Ref.		Ref.	
II	1.695 (0.401-7.155)	0.541	0.822 (0.364-1.857)	0.113
III	9.079 (1.626-31.380)	0.001	3.289 (1.632-6.624)	0.002
IV	15.450 (4.815-49.573)	<0.001	4.645 (2.510-8.609)	<0.001
Histologic Grade				
Well vs. Poor	0.471 (0.286-0.776)	0.006	0.564 (0.367-0.868)	0.018
CD3	1.000 (1.000-1.000)	0.185	1.000 (0.999-1.000)	0.897
TCF7	0.013 (0.002-0.074)	<0.001	0.041 (0.009-0.185)	<0.001

HR, hazard ratio; CI, confidence interval.
p value: Multiple test correction by the "Benjamini & Hochberg" (BH) method.*

Survival Analysis of TCF7$^+$ T Cell Expression in OSCC Patients With Different Risk Levels

Patients were divided into two clinical risk levels by TNM stage: TNM (I+II) and TNM (III+IV) (**Figure 2**). Differences in the percentage of TCF7$^+$ T cells regarding OS and RFS were analyzed separately. Although differences in TNM (I+II) between the TCF7^{hi} group and TCF7^{low} group were not statistically significant for OS or RFS (OS: p=0.130, **Figure 2A**; RFS: p=0.780, **Figure 2B**), differences between the TCF7^{hi} group and TCF7^{low} group for TNM (III+IV) were statistically significant (OS: p<0.001, **Figure 2A**; RFS: p<0.001, **Figure 2B**). Similarly, histological grade classified patients into two pathological risk levels: a well-differentiated group (well) and a poorly differentiated group (poor). In the well-differentiated group, differences in OS and RFS between the TCF7^{hi} and

TABLE 3 | Multivariate analysis of factors associated with overall survival.

Multivariate analysis	OS (n=167)		RFS (n=167)	
Variable	**HR (95% CI)**	***p value****	**HR (95% CI)**	***p value****
T stage				
T1	Ref.		Ref.	
T2	2.037 (0.740-5.604)	0.202	1.009 (0.534-1.908)	0.977
T3	2.597 (1.070-6.303)	0.053	0.773 (0.432-1.384)	0.581
Node metastasis				
N0 vs. N+	1.284 (0.458-3.596)	0.635	0.924 (0.223-3.837)	0.977
TNM stage				
I +II vs. III+IV	8.539 (2.144-34.013)	0.004	4.992 (1.054-23.649)	0.086
Histologic Grade				
Well vs. Poor-	0.408 (0.246-0.679)	0.002	0.469 (0.303-0.724)	0.001
TCF7				
Low vs. High	0.235 (0.133-0.414)	<0.001	2.661 (1.675-4.227)	<0.001

HR, hazard ratio; CI, confidence interval.
p value: Multiple test correction by the "Benjamini & Hochberg" (BH) method.*

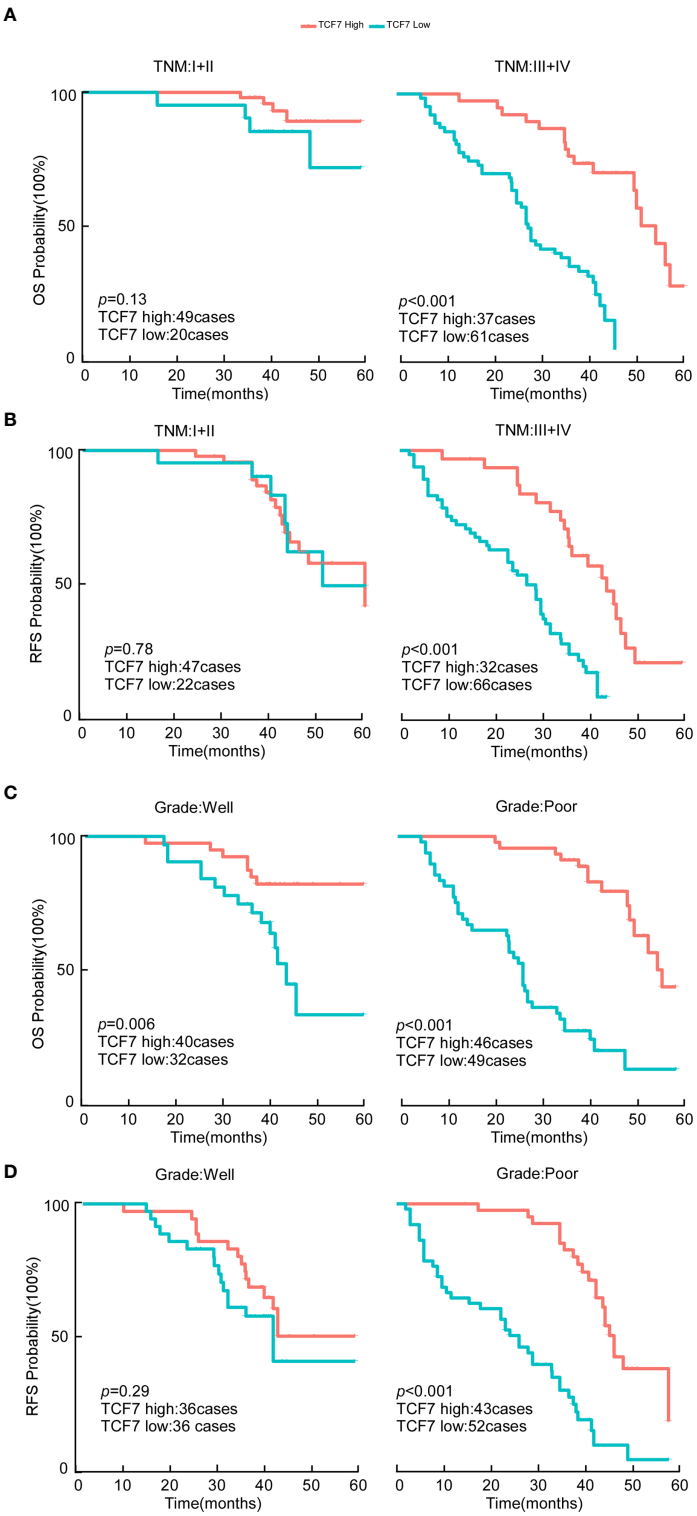

FIGURE 2 | OS and RFS analysis of OSCC patients in the TCF7$^+$ T cell high expression group versus the TCF7$^+$ T cell low expression group. **(A)** Kaplan–Meier analysis of OS in the TNM low-risk group (n=69) and high-risk group (n=98). **(B)** Kaplan–Meier analysis of RFS in the TNM low-risk group (n=69) and high-risk group (n=98). **(C)** Kaplan–Meier analysis of OS in the histological grade low-risk group (n=72) and high-risk group (n=95). **(D)** Kaplan–Meier analysis of RFS in the histological grade low-risk group (n=72) and high-risk group (n=95). The *p* values of survival curves were calculated by the log-rank test. $p<0.05$ was considered to indicate significance. OS, overall survival; RFS, recurrence-free survival.

$TCF7^{low}$ groups were not statistically significant (Well-OS: p=0.006, **Figure 2C**; Well-RFS: p=0.290, **Figure 2D**). However, in the poorly differentiated group, differences in OS and RFS were both statistically significant (Poor-OS: p<0.001, **Figure 2C**; Poor-RFS: p<0.001, **Figure 2D**).

$TCF7^+$ T Cell Expression Improves the Predictive Accuracy of Existing Models

In a previous analysis, $TCF7^+$ T cell expression could be used as an independent predictor of postoperative OSCC; this variable alone was included in the Cox risk regression model, which calculated a C-index=0.701 (95% CI=0.654 to 0.748) for $TCF7^+$ T cell expression for OS and a C-index=0.654 (95% CI=0.610 to 0.698) for RFS, (**Table 4**), suggesting that the model has good predictive accuracy. Next, significantly different variables (TNM stage, histological grade, and $TCF7^+$ T-cell expression) were obtained from the results of multivariate analysis. Different Cox risk regression models using the C-index as a measure were established to investigate whether inclusion of the $TCF7^+$ T cell percentage enhances the predictive accuracy of the TNM stage and histological grade. Inclusion of the $TCF7^+$ T cell percentage improved the prediction accuracy of the TNM stage and histological grade (**Table 4**). The variable grade also improved the C-index from 0.594 (0.539–0.649) to 0.746 (0.690–0.802) for OS (p<0.001) and from 0.564 (0.511–0.617) to 0.686 (0.631–0.740) for RFS (p<0.001) after including the $TCF7^+$ T cell percentage (p<0.001). The variable TNM stage increased the C-index from 0.732 (0.685–0.779) to 0.798 (0.752–0.838) for OS (p<0.001) and from 0.690 (0.646–0.734) to 0.740 (0.695–0.785) (p<0.001) for PFS. In TNM+Grade multivariate analysis, the C-index increased from 0.765 (0.715–0.815) to 0.820 (0.778–0.862) for OS (p<0.001) and from 0.728 (0.678–0.777) to 0.758 (0.711–0.805) for RFS after including the $TCF7^+$ T cell percentage (p = 0.004).

Prognostic Nomogram of OSCC and Its Calibration Curve

We incorporated the TNM stage, histological grade, and $TCF7^+$ T cell percentage status into the Cox risk regression model to construct two nomograms to predict OS and RFS in OSCC patients at 1, 3, and 5 years after surgery (**Figures 3A, E**). The C-index displayed good predictive accuracy for both the OS and RFS nomograms (OS: C-index=0.728, 95% CI=0.678 to 0.777); C-index=0.758, 95% CI=0.711 to 0.858) (**Table 4**). We also constructed calibration curves for predicting OS and RFS at 1, 3 and 5 years by internal resampling 1000 times (**Figures 3B–D**, **F–H**), and the calibration curves showed good consistency in predicting and the actual event occurrence of patients.

$TCF7^+$ T Cell Expression Improves the Clinical Utility of Existing Models

We further compared the clinical utility of models ("TNM+Grade+TCF7" vs. "TNM+Grade") using decision curves within 1, 3 and 5 years (**Figure 4**). First, for both the "TNM+Grade+TCF7" and "TNM+Grade" prediction models, the DCA showed that the net benefit range was greater than that of the prediction model with all variables included ("All"). Second, the area under the decision curve of "TNM+Grade+TCF7" was larger than that of "TNM+Grade" at 1, 3, and 5 years for OS (**Figures 4A–C**) and RFS (**Figures 4D, E**) but smaller than the area under the decision curve at year 5 (**Figure 4F**). This finding also indicated that adding the $TCF7^+$ T cell expression level improved the clinical utility of the existing model, suggesting that $TCF7^+$ T cells warrant further research.

DISCUSSION

OSCC is a prevalent tumor of the head and neck cancer (HNSCC) type, and immunotherapy characterized by immune checkpoint inhibitors (ICIs) has emerged as therapy for OSCC in recent years. Because of the high tumor heterogeneity of OSCC, ICIs such as nivolumab are only beneficial for a small number of patients; indeed, ICIs generally have low response rates, with short remission durations in HNSCC (14). Hence, identifying new markers to improve existing treatment strategies is urgent.

T cell factor 1 (TCF1), encoded by TCF7, is a transcription factor of the classical Wnt/β-catenin signaling pathway (15, 16) that maintains the stem cell-like state of T cells (17) and their lymphatic recirculation and self-renewal potential (18). Kurtulus et al. (19) stated that an effective antitumor response requires TCF7/TCF1 expression; in the absence of TCF7 expression, memory precursor cells show little resistance. Plesca et al. (20) showed that an elevated frequency of $TCF7^+$ T cells in melanoma

TABLE 4 | Comparison of the predictive accuracy of the prognostic models.

Model	OS (n=167)		RFS (n=167)	
	C-index (95% CI)	*p value*	C-index (95% CI)	*p value*
TCF7	0.701 (0.654-0.748)		0.654 (0.610-0.698)	
Grade	0.594 (0.539-0.649)		0.564 (0.511-0.617)	
Grade+TCF7	0.746 (0.690-0.802)	<0.001	0.686 (0.631-0.740)	<0.001
TNM	0.732 (0.685-0.779)		0.690 (0.646-0.734)	
TNM+TCF7	0.795 (0.752-0.838)	<0.001	0.740 (0.695-0.785)	<0.001
TNM+Grade	0.765 (0.715-0.815)		0.728 (0.678-0.777)	
Nomogram	0.820 (0.778-0.862)	<0.001	0.758 (0.711-0.805)	0.004

OS, overall survival; RFS, recurrence-free survival; C-index, concordance index; CI, confidence interval.
A higher c-index indicates better discrimination.

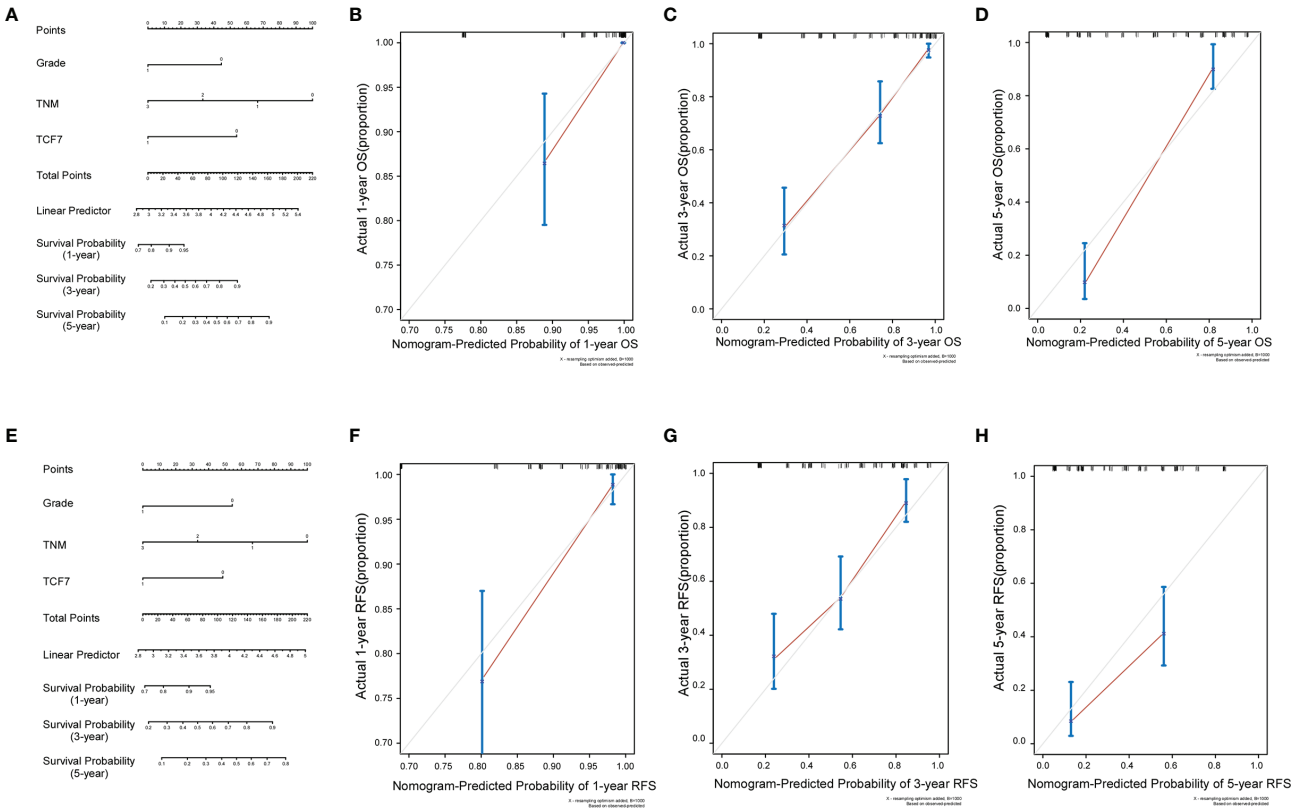

FIGURE 3 | Nomograms and calibration curves of OS versus RFS. Three independent predictors, including TCF7$^+$ T cells, TNM stage, and histological grouping, were incorporated into the nomogram for OS **(A)** and RFS **(E)**. Calibration curves were established for predicting OS at 1 year **(B)**, 3 years **(C)** and 5 years **(D)** for OSCC patients and RFS at 1 year **(F)**, 3 years **(G)** and 5 years **(H)** for OSCC patients. OS, overall survival; RFS, recurrence-free survival.

infiltrates is associated with beneficial clinical outcomes in patients treated with anti-PD-1 therapy.

In the present study, we found that high TCF7 expression was associated with a better prognosis in OSCC. Additionally, high TCF7 expression was an independent predictor for both OS and RFS. We also found that TCF7$^+$ T cell expression levels were strong predictors of TNM stage III+IV and a histological grade of poor differentiation. Concerning current models such as the TNM model, adding pathological grading and TCF7$^+$ T cell expression levels improved the predictive power. We also generated two nomograms with a good C-index to predict OS and RFS in OSCC patients. Finally, comparison of the range of net benefits by DCA suggests that the nomogram has good clinical utility.

One of the novelties of our study is that the TCGA data were used for prediction and screening to identify target immune subgroups. We first investigated the effect of CD3 and TCF7 on the prognosis of OSCC patients starting at the transcriptional level, and four groups of patients were obtained based on high and low expression of CD3 and TCF7. Although no significant difference was found in OS among the four groups, we detected a trend that the magnitude of the probability of survival was DH group > CD3^{hi} group, TCF7^{hi} group > DL group. Therefore, we excluded the CD3^{hi} and TCF7^{hi} groups, divided the remaining 129 patients into DH and DL groups, and then performed survival analysis. We found that OSCC patients in the DH group had a better prognosis than OSCC patients in the DL group after excluding the effect of the background level (not a single CD3^{hi} expression or a single TCF7^{hi} expression effect). Thus, TCF7$^+$ T cells with high expression of both CD3 and TCF7 may affect the prognosis of OSCC patients.

Additionally, the algorithm of clinical information to obtain cutoff values was applied, making the statistical results closer to clinical reality. For more convenient statistics, we converted the proportion of TCF7$^+$ T cells (continuous variable) to the TCF7$^+$ T cell expression level (dichotomous variable) to classify all patients into two groups. We used X-tile to calculate the optimal cutoff value of TCF7$^+$ T cell expression based on survival data, and this method is convincing for use in various diseases (21–23).

To avoid the effect of X-tile grouping, we performed univariate analysis using tumor-infiltrating CD3$^+$ T lymphocyte (TIL) expression and TCF7$^+$ T cell expression as continuous variables. We determined no significant difference in the prognosis based on tumor-infiltrating CD3$^+$ T lymphocyte (TIL) expression, which excluded the effect of the entire tumor-

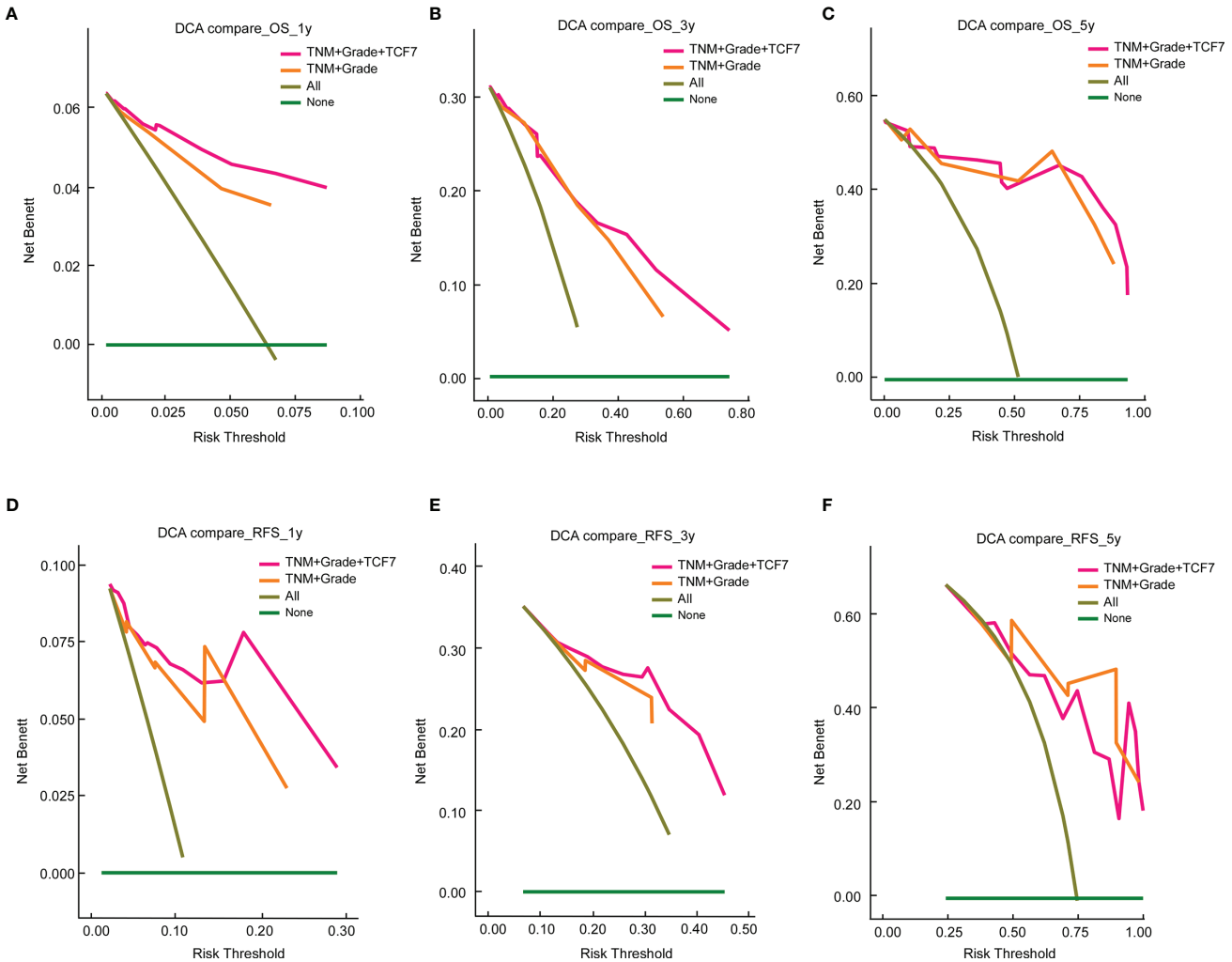

FIGURE 4 | Decision curve analysis comparison of the nomogram and "TNM+Grade" models at 1 year **(A)**, 3 years **(B)**, and 5 years **(C)** for OS and 1 year **(D)**, 3 years **(E)**, and 5 years **(F)** for RFS. DCA, decision curve analysis. OS, overall survival; RFS, recurrence-free survival.

infiltrating $CD3^+$ T lymphocyte (TIL) background, and then investigated a subpopulation of $TCF7^+$ T cells. We determined that the difference in $TCF7^+$ T cell expression (continuous variable) was strongly significant for prognosis in univariate analysis and then transformed $TCF7^+$ T cell expression into $TCF7^+$ T cell expression (dichotomous variable) for multivariate analysis and nomogram production.

Survival analysis further suggested that at two different clinicopathological risk levels,the $TCF7^{hi}$ group at high clinical and pathological risk levels predicted a good prognosis for OSCC patients, suggesting that immune infiltration of $TCF7^+$ T cells in advanced OSCC or poorly differentiated OSCC may improve patient survival. This finding may be related to precursor exhausted T cells. Exhausted T cells can be classified into precursor exhausted T cells and terminally differentiated exhausted T cells according to their phenotype (24). Precursor exhausted T cells have low expression of exhaust surface markers (25–27), and TCF1/TCF7 is a key regulator of precursor exhausted T cells (25). Compared with terminally differentiated exhausted T cells, precursor exhausted T cells have stronger proliferative capacity (17) and differentiation potential (28) and longer longevity (29). Precursor exhausted T cells also exhibit antitumor effects in patients with melanoma (10), pancreatic cancer (30) and colorectal cancer (31).

To better evaluate the prediction accuracy of the model, we used the index of concordance (C-index). In the multivariate Cox risk regression model, we clarified that the inclusion of the $TCF7^+$ T cell percentage improved the prediction accuracy of existing accepted models by comparing the difference in the C-index. To improve the clinical usefulness of the prediction model, we transformed the modified model into a nomogram. The nomograms were resampled 1000 times for internal validation, yielding calibration curves with good agreement. To assess clinical utility, we used DCA to compare the area under

the curve (net benefit range), and the inclusion of the $TCF7^+$ T cell percentage improved the clinical utility of the existing model.

However, this study has limitations. The specific mechanism by which $TCF7^+$ T cells affect tumor prognosis is currently unclear, warranting further investigation in combination with single-cell sequencing and other technologies to explore the specific mechanism of TCF7. Additionally, support is needed from external validation sets in the risk Cox regression model. Therefore, further studies are needed to investigate the role of $TCF7^+$ T cells in OSCC.

CONCLUSION

The current study showed that the $TCF7^+$ T cell expression level can be used as an independent predictor for OSCC patients and that the nomogram incorporating the $TCF7^+$ T cell expression level has good discrimination, calibration and clinical utility; however, it should be externally validated. $TCF7^+$ T cells are expected to serve as new immunotherapeutic markers and should be further validated by basic experiments.

DATA AVAILABILITY STATEMENT

The original contributions presented in the study are included in the article/**Supplementary Material**, further inquiries can be directed to the corresponding authors.

ETHICS STATEMENT

The studies involving human participants were reviewed and approved by Institutional Review Board of the Sun Yat-Sen Memorial Hospital, Sun Yat-sen University. The patients/participants provided their written informed consent to participate in this study.

AUTHOR CONTRIBUTIONS

HR: Data curation; Formal analysis; Methodology; Writing original draft; Writing-review & editing. TC and XW: Data curation; Formal analysis; Methodology, Writing-original draft. YP: Data curation; Formal analysis; Project administration. TL: Resources; Validation. ZO: Supervision, Resources. LQ: Methodology, Formal analysis. QL and LZ: Supervision. HL: Resources. FW: Project administration. SR and ZL: Methodology. SF: Conceptualization; Supervision; Writing-original draft; Writing-review & editing. JL: Conceptualization; Funding acquisition; Supervision; Writing original draft; Writing-review & editing. All authors contributed to the article and approved the submitted version.

FUNDING

This study was supported by the Natural Science Foundation of China (Grant Nos. 82072990, 81872194 and 81772890), grants from Guangzhou Science and Technology Bureau (2021A1515012355), Science and Technology Program of Guangzhou Grant numbers: 2021020104207, and Open Project Contract (2020B1212060018OF003) from Guangdong Provincial Key Laboratory of Malignant Tumor Epigenetics and Gene Regulation. The funders had no role in the study design, data collection and analysis, decision to publish, or manuscript preparation.

ACKNOWLEDGMENTS

The authors gratefully acknowledge all the study participants and study staff for their help and cooperation during this study. We thank Bowen Li for contributions to our data curation, formal analysis.

SUPPLEMENTARY MATERIAL

The Supplementary Material for this article can be found online at: https://www.frontiersin.org/articles/10.3389/fonc.2022.782058/full#supplementary-material

Supplementary Figure 1 | (A) A total of 212 patients were divided into four groups for Kaplan–Meier analysis. **(B)** A total of 129 patients were divided into two groups for Kaplan–Meier analysis. Green=$CD3^{hi}$ $TCF7^{hi}$ (DH). Red=$CD3^{low}$ $TCF7^{low}$ (DL). Blue=$CD3^{hi}$ $TCF7^{low}$. Purple=$CD3^{low}$ $TCF7^{hi}$. Survival curves were compared by the log-rank test. $p<0.05$ was considered to indicate significance.

REFERENCES

1. Siegel RL, Miller KD, Jemal A. Cancer Statistics, 2020. *CA Cancer J Clin* (2020) 70:7–30. doi: 10.3322/caac.21590
2. Tang J, Yu JX, Hubbard-Lucey VM, Neftelinov ST, Hodge JP, Lin Y. Trial Watch: The Clinical Trial Landscape for PD1/PDL1 Immune Checkpoint Inhibitors. *Nat Rev Drug Discov* (2018) 17:854–5. doi: 10.1038/nrd.2018.210
3. Gstalder C, Liu D, Miao D, Lutterbach B, DeVine AL, Lin C, et al. Inactivation of Fbxw7 Impairs dsRNA Sensing and Confers Resistance to PD-1 Blockade. *Cancer Discov* (2020) 10:1296–311. doi: 10.1158/2159-8290.CD-19-1416
4. Kumar S, Zeng Z, Bagati A, Tay RE, Sanz LA, Hartono SR, et al. CARM1 Inhibition Enables Immunotherapy of Resistant Tumors by Dual Action on Tumor Cells and T Cells. *Cancer Discov* (2021) 8:2050–71. doi: 10.1158/2159-8290.CD-20-1144
5. Pollack R, Ashash A, Cahn A, Rottenberg Y, Stern H, Dresner-Pollak R. Immune Checkpoint Inhibitor-Induced Thyroid Dysfunction Is Associated With Higher Body Mass Index. *J Clin Endocrinol Metab* (2020) 105:dgaa458. doi: 10.1210/clinem/dgaa458
6. Yanai S, Nakamura S, Kawasaki K, Toya Y, Akasaka R, Oizumi T, et al. Immune Checkpoint Inhibitor-Induced Diarrhea: Clinicopathological Study of 11 Patients. *Dig Endosc* (2020) 32:616–20. doi: 10.1111/den.13555
7. Krishna S, Lowery FJ, Copeland AR, Bahadiroglu E, Mukherjee R, Jia L, et al. Stem-Like CD8 T Cells Mediate Response of Adoptive Cell Immunotherapy Against Human Cancer. *Science* (2020) 370:1328–34. doi: 10.1126/science.abb9847
8. Chapuis AG, Roberts IM, Thompson JA, Margolin KA, Bhatia S, Lee SM, et al. T-Cell Therapy Using Interleukin-21-Primed Cytotoxic T-Cell Lymphocytes Combined With Cytotoxic T-Cel L Lymphocyte Antigen-4 Blockade Results

in Long-Term Cell Persistence and Durable Tumor Regression. *J Clin Oncol* (2016) 34:3787–95. doi: 10.1200/JCO.2015.65.5142
9. Wen S, Lu H, Wang D, Guo J, Dai W, Wang Z. TCF-1 Maintains $CD8^+$ T Cell Stemness in Tumor Microenvironment. *J Leukoc Biol* (2021) 3:585–90. doi: 10.1002/JLB.5MR1120-778R
10. Sade-Feldman M, Yizhak K, Bjorgaard SL, Ray JP, de Boer CG, Jenkins RW, et al. Defining T Cell States Associated With Response to Checkpoint Immunotherapy in Melanoma. *Cell* (2018) 175:998–1013.e20. doi: 10.1016/j.immuni.2018.12.021
11. Pais Ferreira D, Silva JG, Wyss T, Fuertes Marraco SA, Scarpellino L, Charmoy M, et al. Central Memory $CD8^+$ T?cells Derive From Stem-Like Tcf7hi Effector Cells in the Absence of Cytotoxic D Ifferentiation. *Immunity* (2020) 53:985–1000.e11. doi: 10.1016/j.immuni.2020.09.005
12. Austin PC, Steyerberg EW. Events Per Variable (EPV) and the Relative Performance of Different Strategies for Estimating the Out -of-Sample Validity of Logistic Regression Models. *Stat Methods Med Res* (2017) 26:796–808. doi: 10.1177/0962280214558972
13. Camp R, Dolled-Filhart M, Rimm D. X-Tile: A New Bio-Informatics Tool for Biomarker Assessment and Outcome-Based Cut-Point Optimization. *Clin Cancer Res an Off J Am Assoc Cancer Res* (2004) 10:7252–9. doi: 10.1158/1078-0432.Ccr-04-0713
14. Chow LQM, Haddad R, Gupta S, Mahipal A, Mehra R, Tahara M, et al. Antitumor Activity of Pembrolizumab in Biomarker-Unselected Patients With Recurrent and/or Metastatic Head and Neck Squamous Cell Carcinoma: Results From the Phase Ib KEYNOTE-012 Expansion Cohort. *J Clin Oncol* (2016) 34:3838–45. doi: 10.1200/JCO.2016.68.1478
15. Willinger T, Freeman T, Herbert M, Hasegawa H, McMichael AJ, Callan MF. Human Naive CD8 T Cells Down-Regulate Expression of the WNT Pathway Transcription Factors Lymphoid En Hancer Binding Factor 1 and Transcription Factor 7 (T Cell Factor-1) Following Antigen Encounter. *Vitro vivo J Immunol* (2006) 176:1439–46. doi: 10.4049/jimmunol.176.3.1439
16. Jeannet G, Boudousqui¨¦ C, Gardiol N, Kang J, Huelsken J, Held W. Essential Role of the Wnt Pathway Effector Tcf-1 for the Establishment of Functional CD8 T Cell Memor Y. *Proc Natl Acad Sci USA* (2010) 107:9777–82. doi: 10.1073/pnas.0914127107
17. Siddiqui I, Schaeuble K, Chennupati V, Fuertes Marraco SA, Calderon-Copete S, Pais Ferreira D, et al. Intratumoral $Tcf1^+PD\text{-}1^+CD8^+$ T Cells With Stem-Like Properties Promote Tumor Control in Response to Va Ccination and Checkpoint Blockade Immunotherapy. *Immunity* (2019) 50:195–211.e10. doi: 10.1016/j.immuni.2018.12.021
18. Kratchmarov R, Magun AM, Reiner SL. TCF1 Expression Marks Self-Renewing Human $CD8^+$ T Cells. *Blood Adv* (2018) 2:1685–90. doi: 10.1182/bloodadvances.2018016279
19. Kurtulus S, Madi A, Escobar G, Klapholz M, Nyman J, Christian E, et al. Checkpoint Blockade Immunotherapy Induces Dynamic Changes in PD-1-$CD8^+$ Tumor-Infiltrating T Cells. *Immunity* (2019) 50:181–94.e6. doi: 10.1016/j.immuni.2018.11.014
20. Plesca I, Tunger A, M¨¹ller L, Wehner R, Lai X, Grimm MO, et al. Characteristics of Tumor-Infiltrating Lymphocytes Prior to and During Immune Checkpoint Inhibitor The Rapy. *Front Immunol* (2020) 11:364. doi: 10.3389/fimmu.2020.00364
21. Li Y, Liang L, Dai W, Cai G, Xu Y, Li X, et al. Prognostic Impact of Programed Cell Death-1 (PD-1) and PD-Ligand 1 (PD-L1) Expression in Cancer Cells and Tumor Infiltrating Lymphocytes in Colorectal Cancer. *Mol Cancer* (2016) 15:55. doi: 10.1186/s12943-016-0539-x
22. Nie W, Qian J, Xu MD, Gu K, Qian FF, Hu MJ, et al. A Non-Linear Association Between Blood Tumor Mutation Burden and Prognosis in NSCLC Patients Receivin G Atezolizumab. *Oncoimmunology* (2020) 9:1731072. doi: 10.1080/2162402X.2020.1731072
23. Wu X, Jiang Y, Ge H, Diao P, Wang D, Wang Y, et al. Predictive Value of Prognostic Nutritional Index in Patients With Oral Squamous Cell Carcinoma. *Oral Dis* (2020) 26:903–11. doi: 10.1111/odi.13318
24. Zeng Z, Wei F, Ren X. Exhausted T Cells and Epigenetic Status. *Cancer Biol Med* (2020) 17:923–36. doi: 10.20892/j.issn.2095-3941.2020.0338
25. Wu T, Ji Y, Moseman EA, Xu HC, Manglani M, Kirby M, et al. The TCF1-Bcl6 Axis Counteracts Type I Interferon to Repress Exhaustion and Maintain T Cell Stemness. *Sci Immunol* (2016) 1:eaai8593. doi: 10.1126/sciimmunol.aai8593
26. LaFleur MW, Nguyen TH, Coxe MA, Miller BC, Yates KB, Gillis JE, et al. PTPN2 Regulates the Generation of Exhausted $CD8^+$ T Cell Subpopulations and Restrains Tumor Immunity. *Nat Immunol* (2019) 20:1335–47. doi: 10.1038/s41590-019-0480-4
27. Kallies A, Zehn D, Utzschneider DT. Precursor Exhausted T Cells: Key to Successful Immunotherapy? *Nat Rev Immunol* (2020) 20:128–36. doi: 10.1038/s41577-019-0223-7
28. Alfei F, Kanev K, Hofmann M, Wu M, Ghoneim HE, Roelli P, et al. TOX Reinforces the Phenotype and Longevity of Exhausted T Cells in Chronic Viral Infection. *Nature* (2019) 571:265–9. doi: 10.1038/s41586-019-1326-9
29. Mann TH, Kaech SM. Tick-TOX, It's Time for T Cell Exhaustion. *Nat Immunol* (2019) 20:1092–4. doi: 10.1038/s41590-019-0478-y
30. Bai M, Zheng Y, Liu H, Su B, Zhan Y, He H. $CXCR5^+$ $CD8^+$ T Cells Potently Infiltrate Pancreatic Tumors and Present High Functionality. *Exp Cell Res* (2017) 361:39–45. doi: 10.1016/j.yexcr.2017.09.039
31. E J, Yan F, Kang Z, Zhu L, Xing J, Yu E. $CD8^+CXCR5^+$ T Cells in Tumor-Draining Lymph Nodes Are Highly Activated and Predict Better Prognosis in Colorectal Cancer. *Hum Immunol* (2018) 79:446–52. doi: 10.1016/j.humimm.2018.03.003

Conflict of Interest: The authors declare that the research was conducted in the absence of any commercial or financial relationships that could be construed as a potential conflict of interest.

Publisher's Note: All claims expressed in this article are solely those of the authors and do not necessarily represent those of their affiliated organizations, or those of the publisher, the editors and the reviewers. Any product that may be evaluated in this article, or claim that may be made by its manufacturer, is not guaranteed or endorsed by the publisher.

frontiers | Frontiers in Oncology

ORIGINAL RESEARCH
published: 29 April 2022
doi: 10.3389/fonc.2022.788801

NSUN2 Promotes Tumor Progression and Regulates Immune Infiltration in Nasopharyngeal Carcinoma

Xinya Tong[1†], Yilan Xiang[2†], Yuanbo Hu[1,3†], Yingying Hu[1,4], He Li[5], Huilin Wang[1], Kong-Nan Zhao[1], Xiangyang Xue[1] and Shanli Zhu[1*]*

[1] Wenzhou Collaborative Innovation Center of Gastrointestinal Cancer in Basic Research and Precision Medicine, Wenzhou Key Laboratory of Cancer-related Pathogens and Immunity, Department of Microbiology and Immunology, Institute of Molecular Virology and Immunology, School of Basic Medical Sciences, Wenzhou Medical University, Wenzhou, China, [2] Department of Radiology, the First Affiliated Hospital of Wenzhou Medical University, Wenzhou, China, [3] Department of Gastrointestinal Surgery, Second Affiliated Hospital and Yuying Children's Hospital of Wenzhou Medical University, Wenzhou, China, [4] Department of Obstetrics and Gynecology, The Second Affiliated Hospital and Yuying Children's Hospital of Wenzhou Medical University, Wenzhou, China, [5] Department of Otolaryngology-Head and Neck Surgery, First Affiliated Hospital of Wenzhou Medical University, Wenzhou, China

OPEN ACCESS

Edited by:
Pablo Parente-Arias, A Coruña University Hospital Complex (CHUAC), Spain

Reviewed by:
Dakang Xu, Shanghai Jiao Tong University, China
Carolina Pena Álvarez, Centro Oncológico de Galicia, Spain

***Correspondence:**
Xiangyang Xue
wzxxy@wmu.edu.cn
Shanli Zhu
wenzhouzsl@126.com

[†]These authors have contributed equally to this work

Specialty section:
This article was submitted to Head and Neck Cancer, a section of the journal Frontiers in Oncology

Received: *03 October 2021*
Accepted: *31 March 2022*
Published: *29 April 2022*

Citation:
Tong X, Xiang Y, Hu Y, Hu Y, Li H, Wang H, Zhao K-N, Xue X and Zhu S (2022) NSUN2 Promotes Tumor Progression and Regulates Immune Infiltration in Nasopharyngeal Carcinoma. Front. Oncol. 12:788801. doi: 10.3389/fonc.2022.788801

Nasopharyngeal carcinoma (NPC) is one of the most common malignancies in the head and neck with a complex etiology, such as environmental factors, genetic factors, and Epstein–Barr virus infection. The NOP2/Sun domain family, member 2 (NSUN2) is a methyltransferase of m5C methylation modification that has been reported to be involved in the occurrence and progression of various tumors, but its role in NPC remains unclear. In this study, we found that NSUN2 was upregulated in NPC and predicted a poor prognosis for NPC patients in both GEO datasets and our tissue microarrays containing 125 NPC tissues. Next, we demonstrated that NSUN2 promoted the proliferation, migration, and invasion of NPC cells *in vitro*. Additionally, the differential expression genes between NSUN2-high and low expression patients were mainly enriched in multi-immune cell activation and proliferation. Furthermore, NSUN2 negatively regulates immune cell infiltration in the tumor microenvironment (TME) of NPC, which indicates that the NSUN2 level may be negatively correlated with the sensitivity of immunotherapy and chemotherapy. In conclusion, our findings highlight that NSUN2 might act as an important oncogene involved in NPC progression and serve as a potential biomarker to predict poor prognosis and drug sensitivity of NPC patients.

Keywords: nasopharyngeal carcinoma, NSUN2, oncogene, tumor immune microenvironment, immune infiltration

INTRODUCTION

Nasopharyngeal carcinoma (NPC) is a malignancy that occurs in the nasopharyngeal epithelium and is highly metastatic and aggressive (1). It is very common in Southeast Asia and southern China, and its incidence is closely related to Epstein–Barr virus (EBV) infection, genes, race, and environmental factors (2).The current treatment is a combination of radiotherapy and chemotherapy, which has greatly improved the prognosis of NPC patients. However, the 5-year

survival rate for patients with advanced nasopharyngeal cancer is still very low (1, 3). Therefore, exploring the pathogenesis of NPC and finding novel biomarkers plays a crucial role in finding appropriate treatment strategies.

RNA modification plays an indispensable role in the occurrence and development of malignancy. Currently, more than 100 RNA modifications have been reported (4). Among them, 5-methylcytosine (m5C), one of the most important types of post-transcriptional modifications, was first found in tRNAs and rRNA, and has recently been found in mRNA and non-coding RNA (5). Similar to the N6-methyladenosine (m6A) modification, the m5C modification has its own methyltransferase "Writer," demethylase "Eraser," and binding protein "Reader" (5, 6). NSUN2, a methyltransferase of m5C, is responsible for the m5C modification in the mRNA of mammals (7). Currently, published data have shown that NSUN2 is overexpressed in various tumors, such as breast cancer, colorectal cancer, and gallbladder carcinoma, and is associated with a series of malignant phenotypes such as tumor proliferation and migration (8–10). NSUN2 and its reading protein Y-box binding protein 1 (YBX-1) are highly expressed in human urothelial carcinoma of the bladder (UCB) and act as oncogenes in an m5C-dependent manner, promoting the development of UCB by increasing the mRNA stability of heparin-binding growth factor (HDGF) (7, 11). NSUN2 inhibits the translation of p27 by methylating the 5'-untranslated region (UTR) region of p27 mRNA. Overexpression of NSUN2 can reduce the expression of p27 and increase the level of cyclin-dependent kinase 1 (CDK1), thus promoting cell proliferation in human diploid fibroblasts (12). NSUN2 upregulates the TEAD1 expression in an m5C mediated methylation-promoted proliferation and migration of hypopharyngeal squamous cell carcinoma cells (13). A team headed by Lu has reported that NSUN2 expression was elevated in squamous cells of head and neck carcinoma (HNSC), including NPC (14). Another study showed that NSUN2 expression was negatively associated with T-cell activation and its expression level might act as a potential immunotherapy marker in HNSC (15). However, few studies have focused on the biological role of NSUN2 in NPC.

In this study, we used the three data entities of the Gene Expression Omnibus (GEO) database to identify the expression levels of 10 m5C regulators in NPC and found that NSUN2 was generally upregulated in NPC tissues and predicted a poor prognosis for NPC patients. Next, we analyzed the expression level of NSUN2, clinicopathological characteristics, and prognosis in tissue microarrays (TMA) containing 125 NPC tissues by immunohistochemistry (IHC). Additionally, we demonstrated that NSUN2 could promote the proliferation, migration, and invasion of NPC cells *in vitro*. Furthermore, based on the GEO database and bioinformatics analysis, we found that the expression level of NSUN2 was negatively associated with the degree of immune cell infiltration, immune checkpoint blockades (ICBs), and chemotherapeutic sensitivity in NPC. Together, our study identified that NSUN2 might serve as a predictive biomarker for poor prognosis and drug sensitivity of NPC patients and may play a vital role in NPC progression.

MATERIALS AND METHODS

NPC Dataset Source and Bioinformation Analysis

The raw data and corresponding clinical information were sourced from the Gene Expression Omnibus Database (GEO) (https://www.ncbi.nlm.nih.gov/geo/). The expression array data (GSE53819) contained 18 NPC tissues and 18 non-cancerous nasopharyngeal tissues, GSE12452 contained 31 NPC tissues and 10 non-cancerous nasopharyngeal tissues, and GSE61218 contained 10 NPC tissues and 6 non-cancerous nasopharyngeal tissues. The high throughput sequencing data GSE102349 containing 113 NPC tissues and corresponding progress-free survival (PFS) information were used for subsequent analysis.

Identification of Differentially Expressed m5C-Related Regulators in NPC

Ten m5C-related regulators were selected for differential expression analysis. Differential expression of m5C RNA methylation regulatory factors in NPC was performed using the Wilcoxon test from GSE53819 and GSE12452. $^{*}P$ <0.05, $^{**}P$ <0.01, and $^{***}P$ <0.001 are significant.

Survival Analysis

The R packages survival and survminer were used for the survival analysis. A total of 88 out of 113 patients from GSE102349 with detailed progress-free survival information were included for survival analysis. A Kaplan–Meier analysis was used to plot the survival curve, and log rank was used as the statistical significance test.

Immunohistochemistry (IHC)

The TMA with 125 NPC patients were purchased from Superbiotek (Shanghai, China). IHC determined the expression of NSUN2 in NPC and normal tissues as previously described (16). After deparaffinizing and blocking endogenous peroxidase, the slides were incubated with antibody against NSUN2 (1:800 dilution, 20854-1-AP, Proteintech, Wuhan, China). Arrays were then washed with PBS and incubated for 30 min with the EnVision™+ Dual Link System-HRP (Dako, Carpinteria, CA). After rinsing thrice with PBS for 3 min each time, the slides were incubated with DAB reagent (Dako, Carpinteria, CA) for 3–5 min and evaluated under a light microscope. The TMA were then counter-stained with hematoxylin and observed under a Leica microscope (DM4000b, Wetzlar, Germany). The results were evaluated independently by two blinded pathologists according to the following scoring criteria: 0, negative; 1, weak; and 2–3, strong. The degree of staining was scored as the proportion of the positive staining area relative to the whole cancerous area: 0, <5%; 1, 5–25%; 2, 26–50%; 3, 51–75%; and 4, >75%.

Reagents and Cell Culture

Human NPC cell lines C666-1 and CNE were purchased from the Chinese Academy of Medical Sciences Cell Bank (Shanghai, China). Both were cultured in RPMI-1640 (Gibco, Thermo

Fisher Scientific) medium supplemented with 10% fetal bovine serum (FBS, Gibco) at 37°C.

Plasmid and siRNA Transfection

The full-length coding sequence (CDS) of NSUN2 with an HA tag was subcloned into the EcoR I and XhoI restriction sites of the pcDNA3.1(+) vector. The construct was confirmed by DNA sequencing. RiboBio (Guangzhou, China) synthesized the small interfering RNA (siRNA) against NSUN2 (si-NSUN2-1,5'-GAAGCATCGTGCTGAAGTA-3'; si-NSUN2-2,5'-GGGTTATCCTCACAAATGA-3'). Plasmids and siRNA transfection was performed using Lipofectamine 2000 (Invitrogen Life Technologies®, Carlsbad, Calif., USA) according to the instructions. The expression level of NSUN2 was tested by Western blot with anti-NSUN2 and anti-HA-Tag (#2367, Cell Signaling Technology (CST), Danvers, MA, USA) antibodies, respectively.

Western Blot

Total proteins were extracted from the transfected cells with RIPA lysis buffer (Beyotime, Haimen, China) containing a protease and phosphatase inhibitor mixture. The proteins were separated by sodium dodecyl sulfate-polyacrylamide gel (SDS-PAGE), transferred to a polyvinylidene fluoride (PVDF) membrane (Bio-Rad, Hercules, CA) and blocked with 5% skim milk at room temperature for 1 h. The membranes were respectively incubated with primary mouse antibody against-HA (1:1,000 dilution), rabbit anti-NSUN2 (1:1,000 dilution), and mouse anti-GAPDH (1:1,000 dilution, AB-M-M001, Good Here, Hangzhou, China) overnight at 4°C. After washing thrice with TBST, the membranes were incubated with secondary antibodies (HRP-conjugated goat anti-rabbit IgG or HRP-conjugated goat anti-mouse IgG) at room temperature for 1 h. After three washes with TBST, the protein bands were visualized using enhanced chemiluminescence detection reagents.

Cell Proliferation and Clone Formation Assays

Cell proliferation was performed by using a Cell Counting Kit-8 (CCK8) and clone formation experiments. The NPC cell lines, C666-1 and CNE, were transfected with siRNA or pcDNA3.1 (+)/NSUN2 plasmid. After 48 h, 3,000/well transfected cells were seeded into a 96-well plate in quintuplicate. After 1, 2, 3, and 4 days, the medium was discarded and replaced with fresh complete medium with 10% CCK8 (Solarbio Science & Technology Co., Ltd., Beijing, China) solution that was added to each well. After incubation at 37 °C for 3 h, the OD value was measured at 450 nm. For the colony formation, transfected cells were evenly spread in a 6-well plate (300/well), and the medium was changed every four days for 10–14 days. After removing the medium, the cells were washed twice with PBS, fixed with 4% paraformaldehyde for 15 min and stained with 0.1% crystal violet (Beyotime Biotechnology, Shanghai, China) for 15 min. The number of colonies was counted under a microscope. The experiments were repeated three times.

Transwell Migration and Invasion Analysis

The Transwell system was used to assess the ability of cells to migrate and invade. In the migration assay, the cells were seeded in a 6-well plate overnight and transfected with siRNA or NSUN2 plasmid, respectively. After 24 h, the cells were trypsinized and 1×10^5 transfected cells suspended in 200 μl of serum-free medium were seeded in the upper chamber, and 600 μl of complete medium with 10% FBS was added to the lower chamber. After 28 h (C666-1) or 24 h (CNE), the upper chambers with residual cells were removed, and the cells under the surface were fixed with 4% paraformaldehyde for 15 min, and then stained with 0.1% crystal violet for 15 min. Five areas were randomly selected for counting under a microscope (Leica, London, UK). In the invasion assay, the chambers were coated with Matrigel (BD Pharringen, San Jose, CA). Similar protocols were followed as for the above-mentioned migration assay.

Generation of Differential Expression Genes (DEGs) Between NSUN2-High and Low Expression Groups

A total of 88 patients from GSE102349 were divided into NSUN2-high expression and low expression groups based on the survival analysis. Package limma was used to determine the DEGs between the two groups. DEGs with $|\log2FC| > 0.5$ and a false discovery rate (FDR) <0.05 were considered significant.

Functional Enrichment Analysis of the DEGs Between the NSUN2-High and Low Expression Groups

GO and KEGG analyses were performed using the package cluster Profiler, enrichplot, and ggplot2. Only the terms with a *P*-value of <0.05 were considered significantly enriched.

Estimation of Immune Infiltration of NPC

Immune and stromal scores were calculated by applying the ESTIMATE algorithm, which can reveal the enrichment of stromal and immune cell gene signatures. The microenvironment cell population-counter (MCP counter) and single-sample GSEA (ssGSEA) algorithm were performed to evaluate the absolute abundance of immune and stromal cells. The enrichment score of 16 immune cells was analyzed using the R package GSVA.

Chemotherapeutic Response Prediction

The R package pRRophetic was used to estimate the chemotherapeutic response determined by the half maximal inhibitory concentration (IC50) of each NPC patient on the Genomics of Drug Sensitivity in Cancer (GDSC) website (17, 18).

Statistical Analysis

All statistical analyses were performed using the R software (version 4.0.2), GraphPad Prism 8.0, or SPSS 20.0 software (SPSS, version 20.0, IBM, New York, USA). Data are presented as mean ± standard deviation (SD) or percentage (%). Comparisons between two groups were made using a two-tailed Student's t-test or χ^2 test. A P-value of <0.05 was considered statistically significant.

RESULTS

Expression Profile of m5C RNA Methylation Regulators and its Correlations With Overall Survival in NPC

The common m5C regulators included 8 "writers" (NOP2, NSUN2-7, TRDMT1), 1 "eraser" (TET2), and 1 "reader" (YBX1). To investigate whether m5C regulators were aberrantly expressed in NPC, two GEO datasets (GSE53819, containing 18 NPC tissues and 18 non-cancerous nasopharyngeal tissues, and GSE12452, containing 31 NPC tissues and 10 non-cancerous nasopharyngeal tissues) were analyzed. As shown in **Figures 1A–C** and **S1A**, NOP2, NSUN2, and YBX1 were significantly upregulated in NPC compared with normal tissues in the three datasets. Thus, NOP2, NSUN2, and YBX1 were selected for survival analysis in GSE102349. As shown in **Figures 1D–F**, NOP2 and NSUN2 were associated with PFS, and high levels of NOP2 and NSUN2 predicted a poor prognosis in NPC patients in the GSE102349 cohort. Taken together, the writer of m5C regulators were mainly dysregulated in NPC, and the levels of NOP2 and NSUN2 could predict a poor prognosis for NPC patients. Considering NSUN2 is the major methyltransferase catalyzing m5C modification of mammalian mRNAs (19, 20), we chose NSUN2 for further investigation.

NSUN2 was a Biomarker to Predict Tumor Stage, Metastasis and Poor Prognosis in NPC Patients

To explore the role of NSUN2 in the development and progression of NPC, we examined the expression level of NSUN2 in tissue microarrays with 125 NPC patients by IHC. The results showed that NSUN2 was mainly expressed in the nucleus of NPC cells (**Figure 2A**), which is consistent with the localization of NSUN2 in other tumor cells. According to the intensity of the staining, we divided these patients into the NSUN2-high group (n = 40) and the NSUN2-low group (n = 85). The correlation between NSUN2 level and NPC clinicopathological features showed that the level of NSUN2 was not correlated with gender ($P = 0.873$), age ($P = 0.293$), tumor size ($P = 0.103$), but with TNM stage ($P = 0.001$), distant metastasis ($P < 0.001$), and recurrence ($P < 0.001$) of NPC patients (**Figure 2B**) (**Table 1**), which indicated that NSUN2 might act as a precise biomarker to predict NPC progression. Kaplan–Meier survival analysis showed that patients with high NSUN2 level had a poor prognosis both in overall survival (OS) and disease-free survival (DFS) (**Figures 2C, D**). Univariate and multivariate Cox analyses showed that NSUN2 was an independent risk factor for OS ($P = 0.001$, HR = 3.993, 95% CI = 1.721–9.263) and DFS ($P < 0.003$, HR = 2.538, 95% CI = 1.384–4.652) in NPC (**Table 2**). In conclusion, these results indicated that NSUN2 was closely associated with malignant progression and was a key factor in the poor prognosis of NPC patients in our own cohorts.

NSUN2 Promotes the Proliferation of NPC Cells *In Vitro*

To further investigate the potential biological role of NSUN2 in the development of NPC, NSUN2 was either knocked down using siRNA or overexpressed using pcDNA3.1(+)/NSUN2-HA plasmid in two NPC cell lines (C666-1 and CNE). As shown in **Figures 3A, C**, the level of NSUN2 was significantly downregulated or upregulated in both NPC cell lines after transfection. Further, CCK-8 results showed that knockdown of NSUN2 could significantly inhibit the proliferation of NPC cells (**Figure 3B**), while overexpression of NSUN2 could promote the proliferation of NPC cells (**Figure 3D**). Additionally, colony formation assays were performed to determine the long-term impact of NUSN2 on NPC cell proliferation. There were more colonies formed after NSUN2 overexpression, whereas fewer colonies formed after NSUN2 knockdown. Together, these results indicate that NSUN2 promotes proliferation of NPC cells *in vitro*.

NSUN2 Promote the Migration and Invasion of NPC Cells *In Vitro*

Because the NSUN2 level was closely related to the TNM stage and distant metastasis of NPC, we presumed that NSUN2 might prominently influence the migration and invasion ability of NPC cells. The transwell assay showed that knockdown of NSUN2 in C666-1 cells reduced the number of cells crossing the compartment and significantly reduced the invasiveness of the cells (**Figure 4A**). In contrast, overexpression of NSUN2 increased the number of cells crossing the compartment and promoted NPC cell invasion (**Figure 4C**). Additionally, similar results were observed in the CNE cell lines (**Figures 4B, D**). These results indicate that NSUN2 can promote NPC cell migration and invasion *in vitro*.

NSUN2 has a Potential to Negatively Regulate Immune Cell Infiltration in the TME

To further investigate the carcinogenic mechanism of NSUN2 in NPC, 88 patients in GSE102349 were divided into the NSUN2-low expression group (n = 61) and the NSUN2-high expression group (n = 27). The comparison analysis of the transcriptome between high- and low-NSUN2 expression samples was carried out. **Figures 5A, B** show that 519 genes were upregulated and 812 genes were downregulated (|logFC (fold change)| ≥0.5 and adj. $P < 0.05$). The most significantly upregulated genes were *NSUN2*, *TRIP13*, *CCT5*, *TOMM40*, and *LSM4*, whereas the most significantly downregulated genes were *CALCOCO1*, *TXNIP*, *RASA3*, *SERPINF1*, and *KCTD12*. Furthermore, the 1,331 differential expression genes (DEGs) were submitted to GO and KEGG pathway analyses, and the results showed that the DEGs between the NSUN2 high- and low-groups were mainly enriched in immune response, namely, T cell activation, lymphocyte and mononuclear cell differentiation, multi-immune cell proliferation, and so on (**Figure 5C**). Additionally, KEGG enrichment analysis showed that DEGs were mainly enriched in cell adhesion molecules, chemokine signaling pathways, cell cycle, and T cell receptor signaling pathways (**Figure 5D**).

These results above indicate that the level of NSUN2 may influence cell infiltration of TME in NPC. Therefore, we first assessed the immune and stromal scores in NPC and found a significant difference in immune and stromal scores between

TABLE 1 | Clinicopathological features and NSUN2 in NPC.

Variables	All patients (n = 125)	Low (n = 85)	High (n = 40)	*P*-value
Gender				0.873
Female	45	31	14	
Male	80	54	26	
Age				0.293
<50	49	36	13	
≥50	76	49	27	
Tumor size				0.103
<1.2 cm	57	43	14	
≥1.2 cm	68	42	26	
TNM stage				0.001*
I + II	71	57	14	
III + IV	54	28	26	
Distant metastases				<0.001*
No	75	61	14	
Yes	50	24	26	
Recurrence				<0.001*
No	71	57	14	
Yes	54	28	26	

**Statistically significant (P <0.05).*

these two groups by applying the ESTIMATE algorithm (**Figure 6A**). NPC tissues with high NSUN2 levels represented lower immune and stromal scores. Next, we analyzed immune infiltration and characterized the immunologic landscape between the two groups. The MCP-counter and ssGSEA algorithms were used to calculate the abundance of 16 immune-related cell types in NPC patients (**Figure 6B**). As shown in **Figure 6C**, patients with high NSUN2 levels had a lower abundance of 12 immune cell populations (T cells, CD8 T cells, Cytotoxic lymphocytes, B lineage, NK cells, Monocytic lineage, Myeloid dendritic cells, Neutrophils, Endothelial cells, Fibroblasts, Tcm, and Tem), whereas they had a higher abundance of 1 immune cell population (Th2 cells). Considering the significant difference between the NSUN2 high- and low-expression groups, we further investigated whether NSUN2 level influences the immune checkpoint genes. As shown in **Figure 6D**, NPC patients with NSUN2 high-expression represented a lower level of seven targetable check-point genes (CD4, CXCR4, PDCD1, CD247, PDCD1LG2, CTLA4, and TLR9) than the NSUN2 low-expression group. Additionally, we found that most human leukocyte antigen (HLA) genes were also expressed at higher levels in the NSUN2 low-expression group, which indicated a potential association between the NSUN2 expression level and immunotherapy efficacy in NPC patients (**Figure 6E**). Furthermore, the R package pRRophetic was used to analyze the response to chemotherapy in GSE102349 NPC patients with the NSUN2 low- and high-expressions. We found that 55 chemotherapeutic drugs showed a significant difference in estimated IC50 between these two groups, and patients in the NSUN2-low group displayed higher sensitivity to most of the chemotherapeutic drugs than those in the NSUN2-high group (**Figure 6F**). At present, cisplatin, 5-fluorouracil, and paclitaxel are first-line chemotherapy drugs

TABLE 2 | Univariate and multivariate Cox regression analyses of overall survival in patients with NPC.

Variables	OS Univariate Cox analysis		OS Multivariate Cox analysis		DFS Univariate Cox analysis		DFS Multivariate Cox analysis	
	HR (95% CI)	*P*-value	HR (95% CI)	*P*-value	HR (95% CI)	*P*-value	HR (95% CI)	*P*-value
Gender (male vs. female)	1.45 (0.95–2.20)	0.082	1.080 (0.476–2.452)	0.854	1.046 (0.593–1.846)	0.875	0.461 (0.233–0.911)	0.026
Age (≥50 vs. <50)	3.34 (1.31–9.00)	0.012*	2.600 (0.953–7.093)	0.062	2.062 (1.135–3.748)	0.018*	1.961 (1.019–3.773)	0.044*
Tumor size (≥1.2 cm vs. <1.2 cm)	1.984 (0.903–4.357)	0.088	0.684 (0.275–1.699)	0.684	2.959 (1.608–5.446)	<0.001*	0.573 (0.288–5.780)	0.113
TNM stage (III + IV vs. I + II)	25.415 (6.026–107.189)	<0.001*	7.001 (1.560–31.413)	0.011*	6.607 (3.608–12.100)	<0.001*	2.894 (1.449–5.780)	0.003*
Distant metastases (yes vs. no)	60.907 (8.268–448.653)	<0.001*	1.097 (0.125–9.620)	0.934	52.010 (18.513–146.115)	<0.001*	76.151 (22.311–269.918)	<0.001*
NSUN2 expression (high vs. low)	5.840 (2.705–12.609)	<0.001*	3.993 (1.721–9.263)	0.001*	3.938 (2.244–6.913)	<0.001*	2.538 (1.384–4.652)	0.003*

**Statistically significant (P <0.05).*

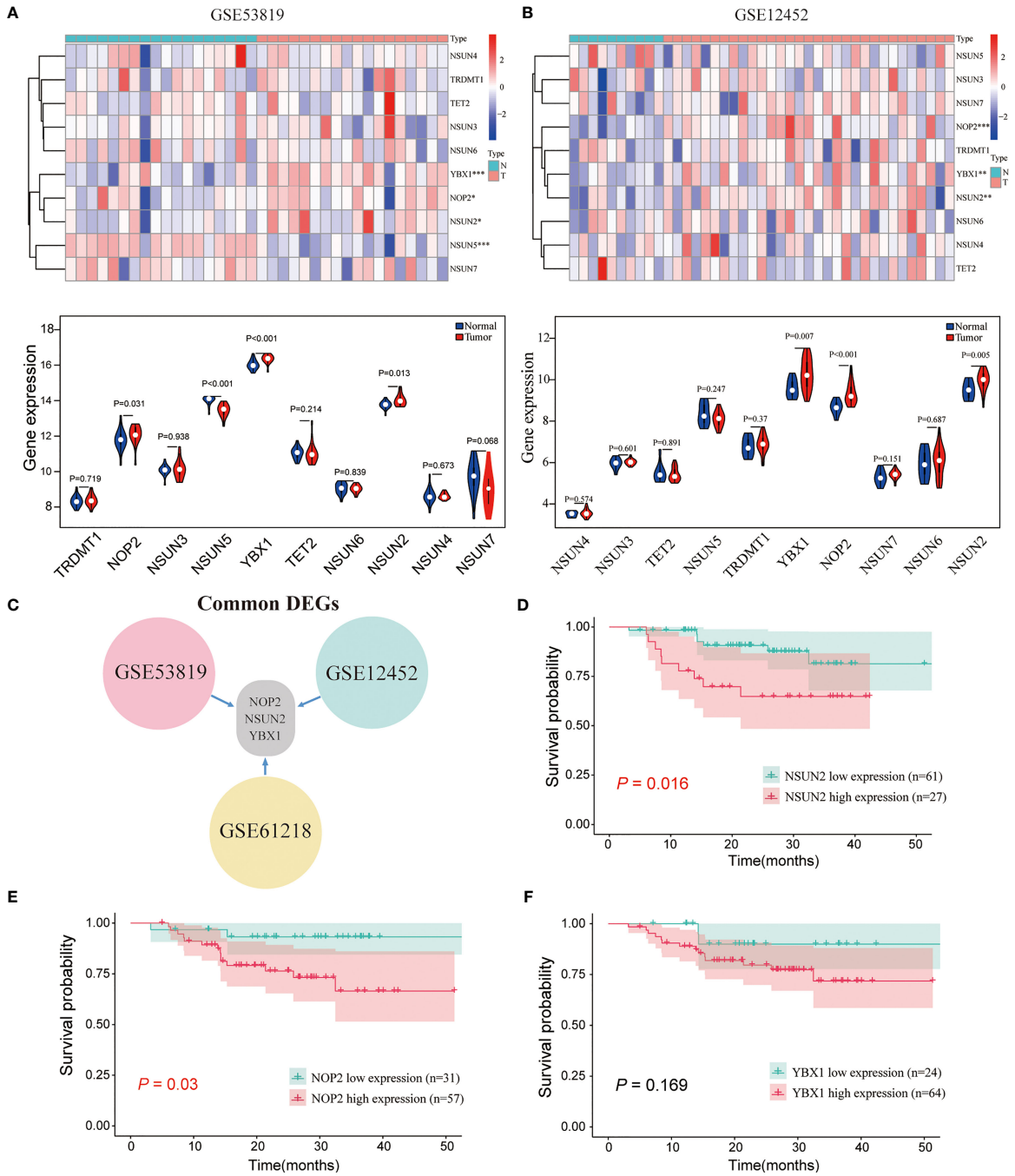

FIGURE 1 | The expression landscape of m5C regulators and the correlations of their expression with the survival of patients with NPC. **(A, B)** The expression levels of m5C genes in GSE53819 and GSE12452. **(C)** The common differentially expressed m5C regulators in GSE53819, GSE12452, and GSE61218. Kaplan–Meier curves of PFS for high-and low-NSUN2 **(D)**, NOP2 **(E)**, and YBX1 **(F)** in GSE102349. *$P < 0.05$, **$P < 0.01$, and ***$P < 0.001$.

for the clinical treatment of NPC (21). Moreover, studies have found that new chemotherapy drugs such as trametinib, docetaxel, and oxaliplatin can inhibit the growth of NPC cells, providing an experimental basis for the clinical treatment of NPC patients (22–24). We conducted an *in vitro* drug sensitivity test on NPC cells with different levels of NSUN2, and the results showed that the cells with a high level of NSUN2 were more resistant to oxaliplatin than those with low levels (**Supplementary Figure 1B**). Taken together, these results reveal that NSUN2 has the potential to negatively regulate immune cell infiltration in TME and is closely related to chemotherapy resistance.

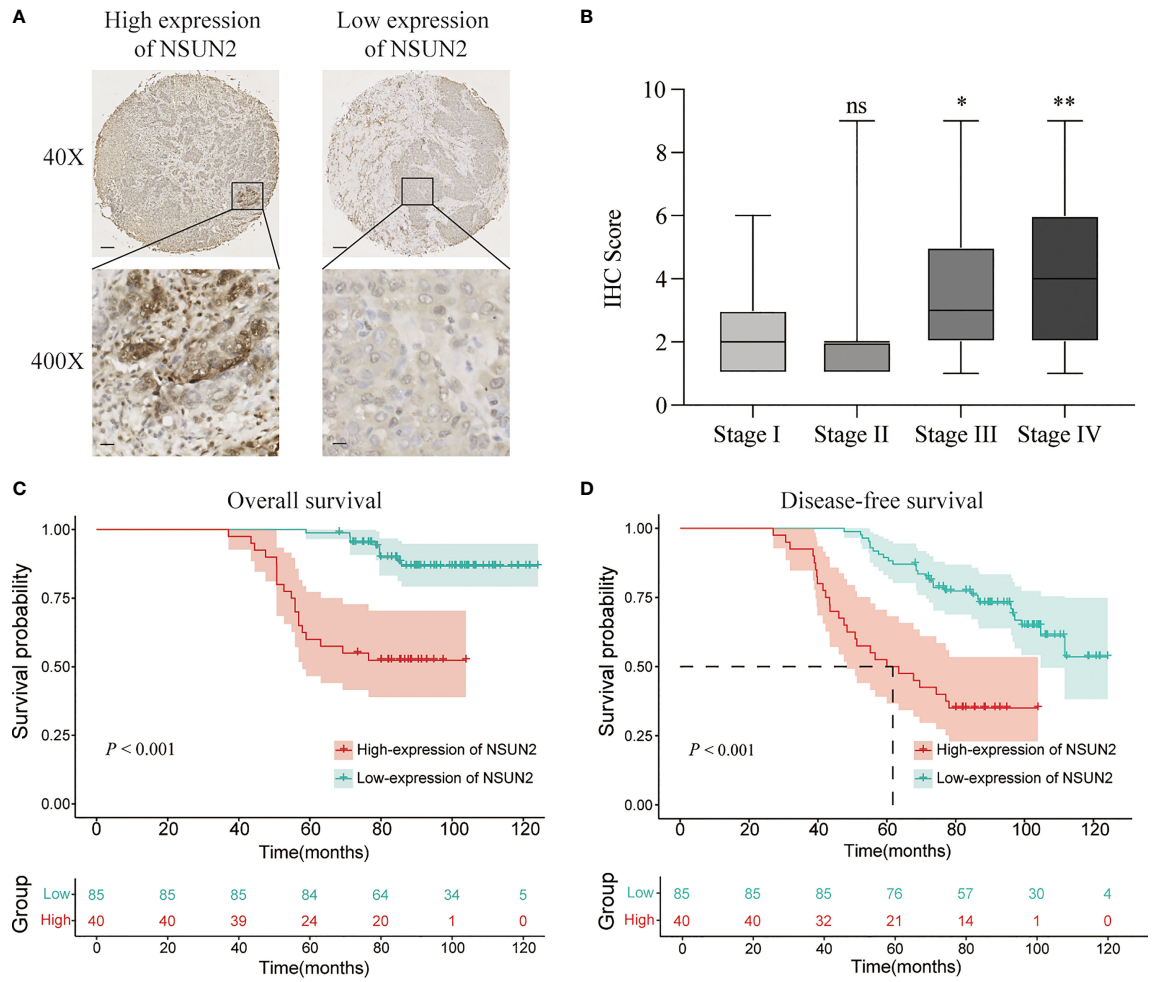

FIGURE 2 | NSUN2 is expressed in the nucleus and predicts a poor prognosis of NPC patients. **(A)** Representative immunohistochemical staining of NSUN2 in NPC TMA. Brown indicates positive staining (×40: scale bar = 100 μm; ×400: scale bar = 10 μm). **(B)** Correlation between the NSUN2 expression and TNM stage. Kaplan–Meier curves for OS **(C)** and DFS **(D)** of NPC patients with NSUN2 expression. *$P < 0.05$ and **$P < 0.01$. ns, no significance.

DISCUSSION

Different from other HNSC, NPC has its own unique biological characteristics, epidemiology (25), and etiology (26). Approximately 70% of all NPC patients are locally advanced at initial diagnosis because of the lack of obvious symptoms in the early period (27). Although treatments based on radiotherapy and chemotherapy have significantly improved for treating non-metastatic NPC (28), distal metastasis remains the major cause of death in NPC (29). Therefore, it is critical to find reliable tumor markers for early diagnosis and molecular targeted therapy for NPC. In this study, we demonstrated that NSUN2 was highly expressed in NPC and might predict a poor prognosis because it was closely correlated with the tumor stage and distant metastasis in the GEO database and our own cohorts. Moreover, NSUN2 promotes the malignancy of NPC cells *in vitro* and might negatively regulate the infiltration of immune cells into TME.

Increasing evidence has demonstrated that post-transcriptional modifications of RNA, such as m6A and m5C, have played a vital role in the progression of multiple cancers. Previous studies have reported that regulators of these RNA modifications dysregulate expression in most cancers and mediate multiple oncogenic pathways. However, few studies have reported the expression level and the biological role of m5C regulators in head and neck malignancies, especially NPC. Here, we displayed the landscape of the expression levels of m5C regulators in NPC and normal tissues based on the GSE53819, GSE12452, and GSE61218 datasets. By taking the intersection of three datasets, NOP2, NSUN2, and YBX1 were all upregulated in NPC compared with normal tissues. Next, we analyzed the survival information of the three genes in the NPC-based GSE102349 dataset and found only NOP2 and NSUN2 were correlated with poor survival of NPC patients, among which NSUN2 had more impact on prognosis. Moreover, NSUN2 is also the main m5C modification methyltransferase of

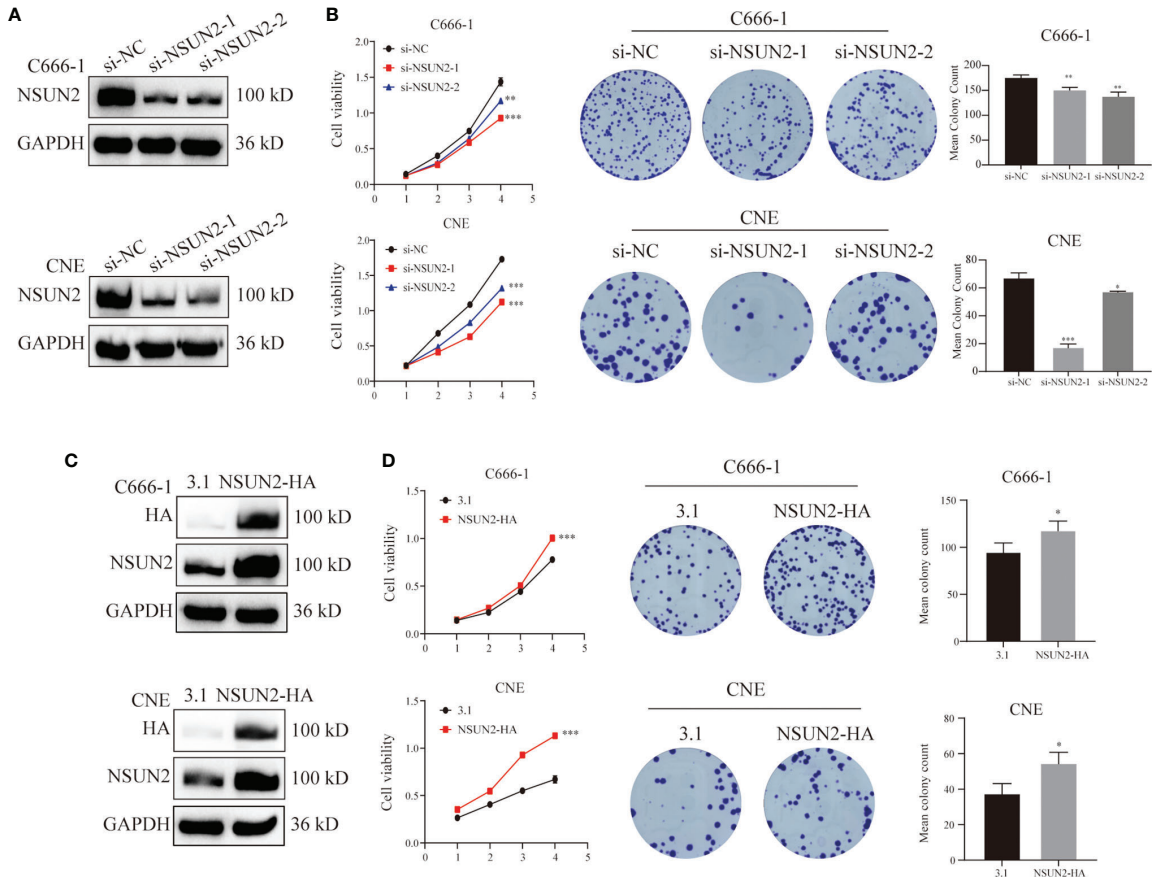

FIGURE 3 | NSUN2 promote the proliferation of NPC cells. **(A, C)** Western blot analysis showed the efficiency of NSUN2 knockdown and overexpression in C666-1 and CNE cells. GAPDH as an internal reference. **(B, D)** The effects of knockout and overexpression of NSUN2 on the proliferation of NPC cells were evaluated by CCK8 and clone formation assay. *$P < 0.05$, **$P < 0.01$, and ***$P < 0.001$.

mammalian mRNA. Therefore, we anchored NSUN2 as our target gene for further study of NPC.

As a writer of m5C RNA modification, NSUN2 has been reported to be closely related to the spliceosome, RNA degradation, cell cycle, and RNA polymerase (30). Accumulated evidence has demonstrated that NSUN2 is overexpressed in various tumors such as low-grade glioma (31), gastric cancer (27), triple-negative breast cancer (30), and so on. In this study, NSUN2 was highly expressed in NPC tissues, which was consistent with other tumors reported. Moreover, an increasing number of studies have confirmed that NSUN2 plays a carcinogenic role in tumorigenesis. For example, NSUN2 methylation can promote ATX exudation, enhance mRNA transcription, and influence the migration of glioma cells U87 through the NSUN2–ATX–LPA axis (32, 33). Mei et al. found that NSUN2 acts as an oncogene to inhibit p57 in an m5C-dependent manner in gastric cancer (27). Another study suggested that NSUN2 has a high mutation rate in gastric and esophageal cancers and has more protein alteration sites (34). In hepatocellular carcinoma, NSUN2 affects the biological function of hepatocellular carcinoma cells and methylates lncRNA H19RNA and methylated H19 recruits oncogene G3BP1 to promote the occurrence and development of tumors (35). Here, we demonstrated that NSUN2 was closely associated with poor prognosis and advanced pathological stages of NPC by IHC in our cohort, and future studies with large samples must confirm our findings. Meanwhile, NSUN2 could significantly promote the carcinogenicity of NPC cells because we observed that NSUN2 enhanced the proliferation and colony formation of NPC cells and promoted the migration and invasion of NPC cells, followed previous studies on other tumors. To explore the mechanism of NSUN2 expression and malignant progression and poor prognosis of NPC, we divided NPC patients into the NSUN2-low and NSUN2-high expression groups based on the group of Kaplan–Meier analysis in GSE102349. We found a significant difference in the transcriptome expression between these two groups. For example, common oncogenes, such as TRIP13 (36) were highly expressed in the NSUN2-high expression group, whereas the recognized tumor suppressor, TXNIP (37) was mainly expressed in the NSUN2-low expression group. Surprisingly, the GO and KEGG enrichment analyses showed that the DEGs between the NSUN2-high and

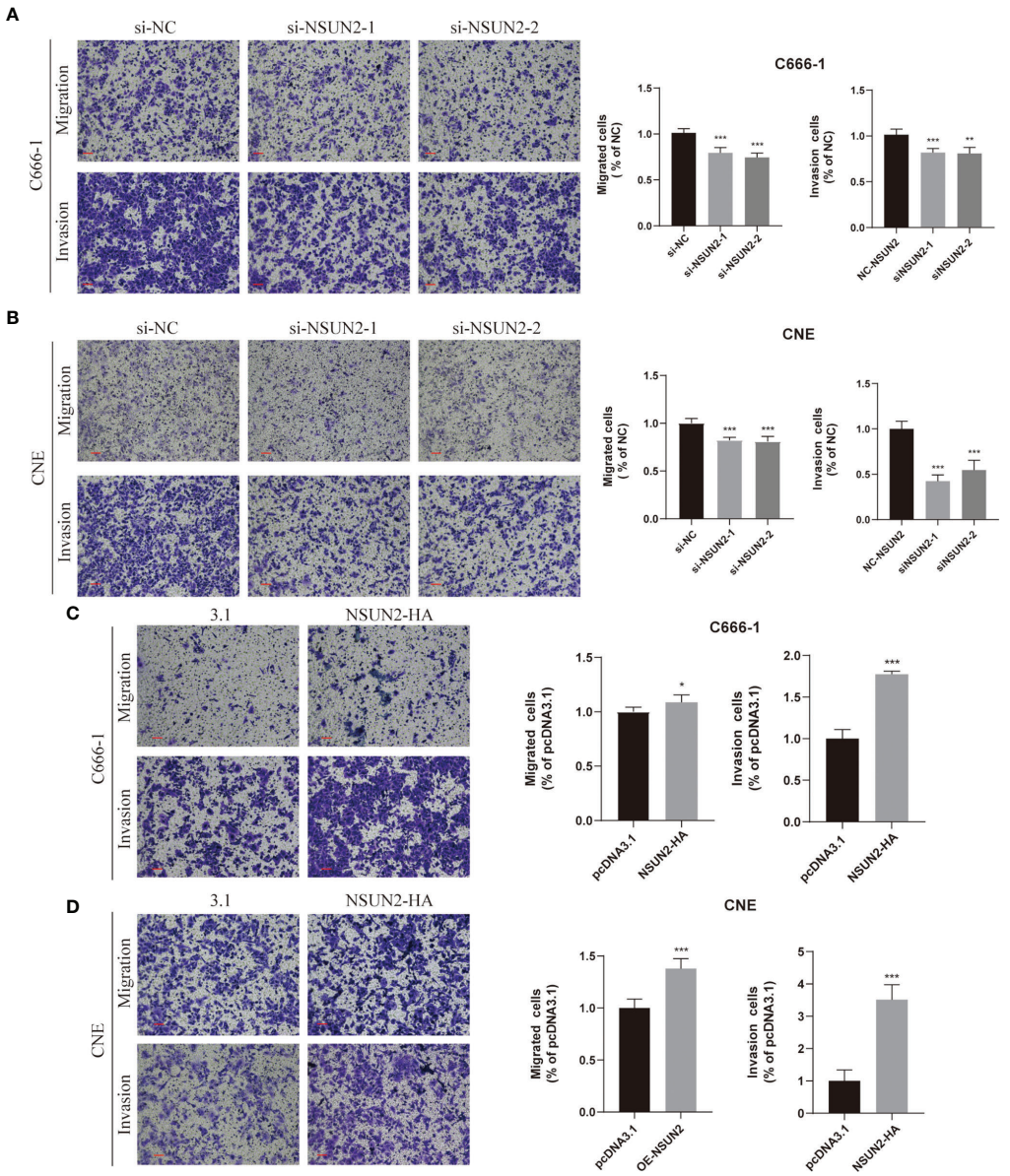

FIGURE 4 | NSUN2 promotes the migration and invasion of NPC cells. Representative images of Transwell assays with C666-1 and CNE cells under NSUN2 knockdown **(A, B)** or overexpression **(C, D)**. The numbers of migrating and invading cells are presented in the right panel. Scale bar, 100 μm. *$P < 0.05$, **$P < 0.01$, and ***$P < 0.001$.

-low groups were mainly enriched in multi-immune cell activation, differentiation, and proliferation, which indicated that NSUN2 is closely related to the infiltration of immune cells into NPC tissues.

Tumor progression was previously considered to be involved only in genetic and epigenetic variations of tumor cells (38). Recently, various studies showed that other cells in the TME such as immune cells, fibroblasts, inflammatory cells, and glial cells, also play essential roles in tumor progression, immune escape, and even drug resistance (39). Immunotherapy based on the TME of tumors has also gained widespread attention in cancer treatment (40, 41). NPC is a heterogeneous epithelial tumor characterized by EBV infection and severe lymphocyte infiltration (42). These special characteristics suggest an important role for TME in its progression. Therefore, we assessed the proportion of immune and stromal components in the NSUN2-high and low groups and found that both the ImmuneScore and StromalScore were significantly higher in the NSUN2-low expression group than in the NSUN2-high group, which implied numerous immune components in the NSUN2-low group. Additionally, we analyzed the degree of 16 immune-related cell type infiltration in the two NPC groups. Most of these immune cells were consistently highly infiltrated in the NSUN2-low group. Studies have shown that the degree of immune infiltration is

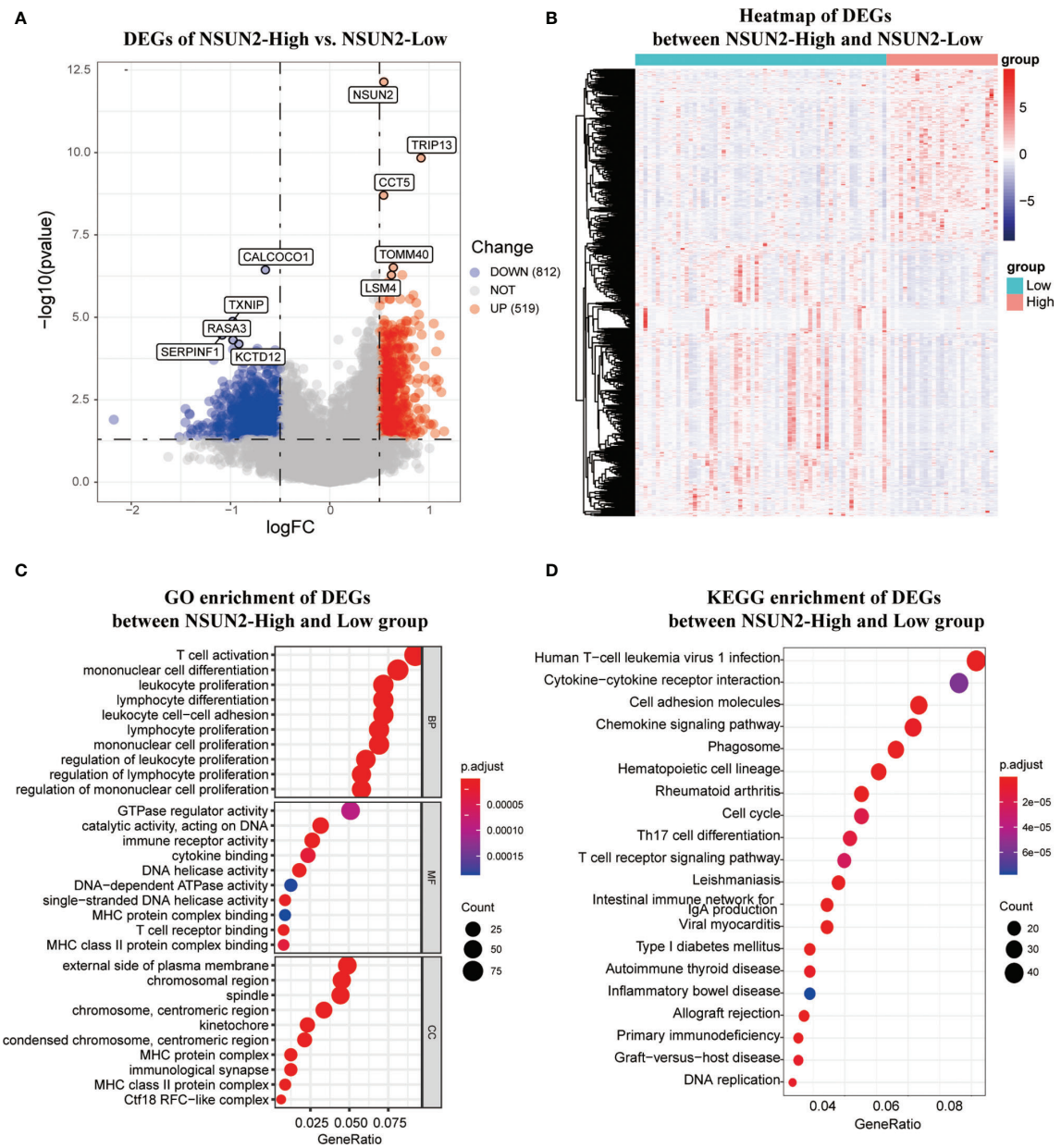

FIGURE 5 | The differentially expression analysis of samples with NSUN2 high and low expression. **(A)**The volcano plot of DEGs between the NSUN2 high expression and low groups. Red points mean upregulated genes, and blue points means downregulated genes. The top 5 significant differential expressed genes were notated. **(B)** The heatmap of DEGs between the NSUN2 high and low expression groups. The GO enrichment **(C)** and KEGG enrichment **(D)** analysis of the DEGs between the NSUN2 high and low expression groups.

related to the prognosis of patients, and a high level of immune infiltration generally predicts a better prognosis (43). Meanwhile, immune infiltration is closely associated with the response of tumors to immunotherapy (44). Predicting the response of immunotherapy based on the infiltration characteristics of TME is a crucial step to improving the success rate of existing immunotherapy and developing new immunotherapy strategies. For example, immunotherapies, such as immune checkpoint blockade against PD-1 and CTLA-4, have become a promising strategy for treating various malignancies (45, 46). Hence, we evaluated the expression level of common immune checkpoint genes and found that most of these genes were highly expressed in the NSUN2-low group, suggesting that it responds positively to these treatments. Furthermore, as an independent factor of tumor-associated antigen presentation, the HLA family plays an important role in anti-tumor immune response and neoplastic progression (47). Theoretically, diverse HLA with distinct binding specificity lead to the presentation of diverse epitopes by different

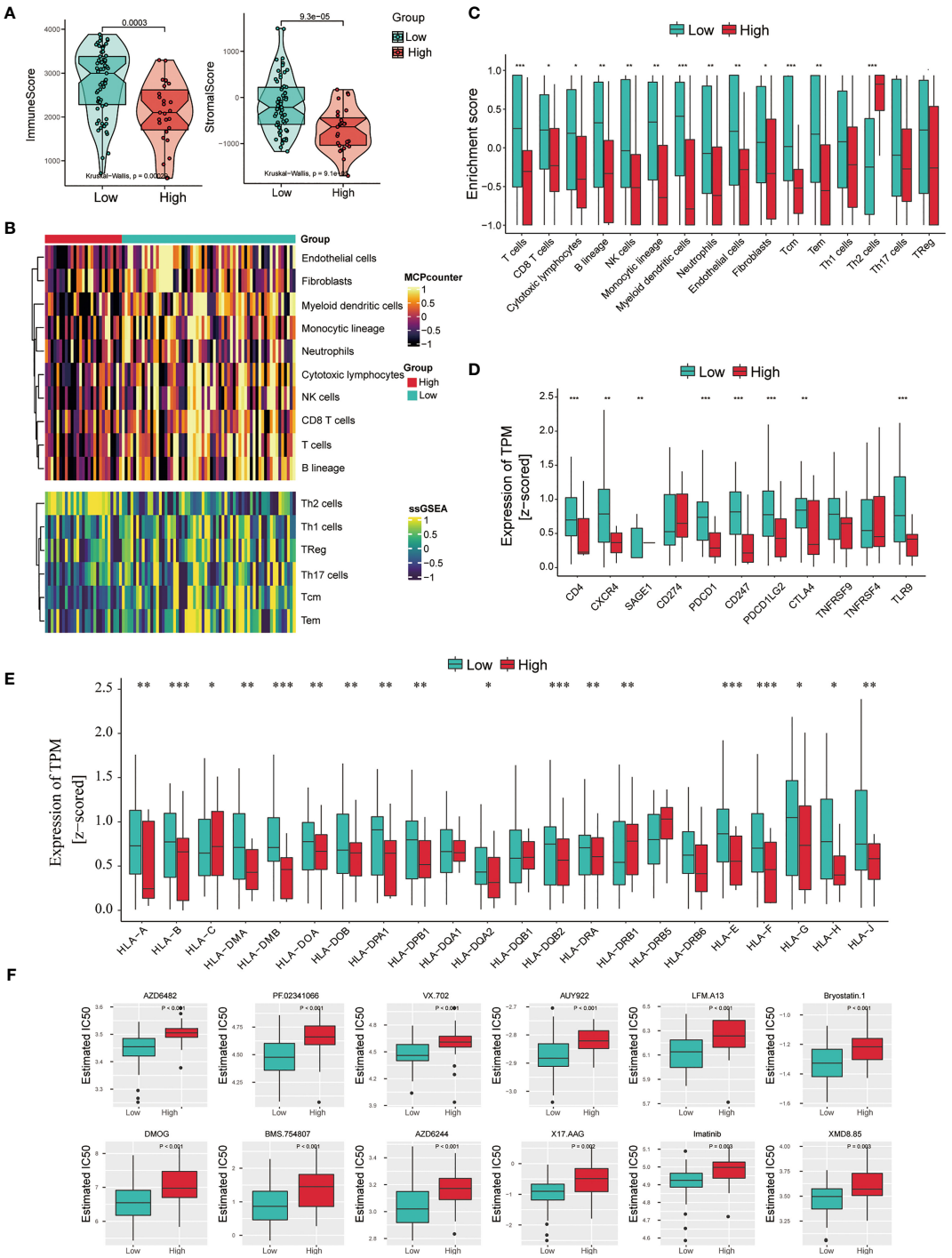

FIGURE 6 | Association between immune infiltration and NSUN2 expression in NPC. **(A)** Boxplot of the ImmuneScore and StromalScore from ESTIMATE of the NSUN2 high and low expression groups. **(B)** Heatmap of the abundance of immune and stromal cell populations in the NSUN2 high and low expression groups. **(C)** Boxplot of the enrichment score of the immune cells in these two groups. **(D)** Expression level of 11 immune checkpoint genes and **(E)** HLA genes in two groups. **(F)** The sensitivity of chemotherapeutic drugs in the NSUN2 high and low expression groups. *$P < 0.05$, **$P < 0.01$, and ***$P < 0.001$.

individuals which increases the possibility of presenting more immunogenic antigens, and increases the possibility of benefiting from ICBs (47, 48). Here, we showed that most HLA genes were highly expressed in the NSUN2-low groups, which also indicated that NSUN2 might be negatively associated with the efficacy of immunotherapy. Chemotherapy is one of the main treatments for NPC. Clinically, gemcitabine combined with cisplatin is an effective combination for treating patients with locoregionally advanced NPC (49, 50). However, chemotherapy resistance invariably develops and results in cancer recurrence and malignant progression. Here, we estimated the relationship between NSUN2 expression and the sensitivity of chemotherapy and found that NPC cell lines with lower NSUN2 expression are more sensitive to most chemotherapy. For example, AZD6482 is an inhibitor of PI3Kβ and exerts an anti-tumor role by inhibiting the proliferation and inducing apoptosis of human glioma cells (51). PF.02341066, a c-Met inhibitor, has been reported to be one of the effective therapeutic strategies for patients with lung cancer (52). We found that NPC cell lines with low expression of NSUN2 had higher sensitivity to AZD6482 and PF.02341066, which may provide a new choice for selecting chemotherapy drugs for NPC patients. Taken together, the above results suggest that NSUN2 has the potential to negatively regulate immune cell infiltration in the TME and was negatively correlated with the sensitivity of immunotherapy and chemotherapy drugs for NPC. Therefore, NSUN2 may act as a predictive biomarker of drug resistance in clinical chemotherapy and immunotherapy.

In summary, we found that NSUN2 was highly expressed in NPC tissues and the level of NSUN2 was closely correlated with tumor stage and distant metastasis. It might serve as a poor prognosis for NPC patients. Furthermore, we confirmed that NSUN2 significantly promoted the malignant phenotype of NPC cells *in vitro*. Additionally, NSUN2 might be negatively associated with multi-immune cell proliferation and infiltration in TME. Based on the level of immune checkpoint genes and the results of drug sensitivity tests *in vitro*, we speculated that patients with high levels of NSUN2 showed worse benefits from chemotherapy and immunotherapy. Overall, NSUN2 might act as an oncogene and predict poor prognosis and poor drug sensitivity in NPC patients.

DATA AVAILABILITY STATEMENT

The original contributions presented in the study are included in the article/**Supplementary Material**. Further inquiries can be directed to the corresponding author.

AUTHOR CONTRIBUTIONS

SZ, XX, and KZ designed the overall study and revised the paper. XT, YX, and YH drafted the manuscript and performed the experiments. XT, YYH, and HL participated in the data collection and analysis. XT and HW acquired the data and material support. All authors listed have made a substantial, direct, and intellectual contribution to the work and approved it for publication.

FUNDING

This research was supported by the Zhejiang Provincial Natural Science Foundation of China under Grant No. LY22H160015.

ACKNOWLEDGMENTS

The authors would like to express their sincere appreciation to the reviewers for their helpful comments on this article and the research groups for the GEO, which provided data for this collection.

SUPPLEMENTARY MATERIAL

The Supplementary Material for this article can be found online at: https://www.frontiersin.org/articles/10.3389/fonc.2022.788801/full#supplementary-material

REFERENCES

1. Chen WH, Cai MY, Zhang JX, Wang FW, Tang LQ, Liao YJ, et al. FMNL1 Mediates Nasopharyngeal Carcinoma Cell Aggressiveness by Epigenetically Upregulating Mta1. *Oncogene* (2018) 37:6243–58. doi: 10.1038/s41388-018-0351-8
2. Chen Y-P, Chan ATC, Le Q-T, Blanchard P, Sun Y, Ma J. Nasopharyngeal Carcinoma. *Lancet* (2019) 394:64–80. doi: 10.1016/S0140-6736(19)30956-0
3. Su L, She L, Shen L. The Current Role of Adjuvant Chemotherapy in Locally Advanced Nasopharyngeal Carcinoma. *Front Oncol* (2020) 10:585046. doi: 10.3389/fonc.2020.585046
4. Xuan JJ, Sun WJ, Lin PH, Zhou KR, Liu S, Zheng LL, et al. RMBase V2.0: Deciphering the Map of RNA Modifications From Epitranscriptome Sequencing Data. *Nucleic Acids Res* (2018) 46:D327–34. doi: 10.1093/nar/gkx934
5. Yang X, Yang Y, Sun BF, Chen YS, Xu JW, Lai WY, et al. 5-Methylcytosine Promotes mRNA Export - NSUN2 as the Methyltransferase and ALYREF as an M(5)C Reader. *Cell Res* (2017) 27:606–25. doi: 10.1038/cr.2017.55
6. Han Z, Yang B, Wang Y, Zeng X, Tian Z. Identification of Expression Patterns and Potential Prognostic Significance of M(5)C-Related Regulators in Head and Neck Squamous Cell Carcinoma. *Front Oncol* (2021) 11:592107. doi: 10.3389/fonc.2021.592107
7. Chen X, Li A, Sun BF, Yang Y, Han YN, Yuan X, et al. 5-Methylcytosine Promotes Pathogenesis of Bladder Cancer Through Stabilizing mRNAs. *Nat Cell Biol* (2019) 21:978–90. doi: 10.1038/s41556-019-0361-y
8. Kaakoush NO, Man SM, Mitchell HM. Functional Relationship Between Campylobacter Concisus and the Stomach Ecosystem in Health and Disease. *ISME J* (2013) 7:2245–7. doi: 10.1038/ismej.2013.115
9. Chen RX, Chen X, Xia LP, Zhang JX, Pan ZZ, Ma XD, et al. N(6)-Methyladenosine Modification of Circnsun2 Facilitates Cytoplasmic Export and Stabilizes HMGA2 to Promote Colorectal Liver Metastasis. *Nat Commun* (2019) 10:4695. doi: 10.1038/s41467-019-12651-2
10. Gao Y, Wang Z, Zhu Y, Zhu Q, Yang Y, Jin Y, et al. NOP2/Sun RNA Methyltransferase 2 Promotes Tumor Progression *via* its Interacting Partner RPL6 in Gallbladder Carcinoma. *Cancer Sci* (2019) 110:3510–9. doi: 10.1111/cas.14190
11. Nombela P, Miguel-Lopez B, Blanco S. The Role of M(6)A, M(5)C and Psi RNA Modifications in Cancer: Novel Therapeutic Opportunities. *Mol Cancer* (2021) 20:18. doi: 10.1186/s12943-020-01263-w

12. Atala A. Re: 5-Methylcytosine Promotes Pathogenesis of Bladder Cancer Through Stabilizing mRNAs. *J Urol* (2020) 203:884–5. doi: 10.1097/JU.0000000000000781
13. Chen L, Ding J, Wang B, Chen X, Ying X, Yu Z, et al. RNA Methyltransferase NSUN2 Promotes Hypopharyngeal Squamous Cell Carcinoma Proliferation and Migration by Enhancing TEAD1 Expression in an M(5)C-Dependent Manner. *Exp Cell Res* (2021) 112664. doi: 10.1016/j.yexcr.2021.112664
14. Lu L, Zhu G, Zeng H, Xu Q, Holzmann K. High tRNA Transferase NSUN2 Gene Expression Is Associated With Poor Prognosis in Head and Neck Squamous Carcinoma. *Cancer Invest* (2018) 36:246–53. doi: 10.1080/07357907.2018.1466896
15. Lu L, Gaffney SG, Cannataro VL, Townsend J. Transfer RNA Methyltransferase Gene NSUN2 mRNA Expression Modifies the Effect of T Cell Activation Score on Patient Survival in Head and Neck Squamous Carcinoma. *Oral Oncol* (2020) 101:104554. doi: 10.1016/j.oraloncology.2019.104554
16. Hu Y, Chen C, Tong X, Chen S, Hu X, Pan B, et al. NSUN2 Modified by SUMO-2/3 Promotes Gastric Cancer Progression and Regulates mRNA M5c Methylation. *Cell Death Dis* (2021) 12:842. doi: 10.1038/s41419-021-04127-3
17. Geeleher P, Cox N, Huang RS. Prrophetic: An R Package for Prediction of Clinical Chemotherapeutic Response From Tumor Gene Expression Levels. *PloS One* (2014) 9:e107468. doi: 10.1371/journal.pone.0107468
18. Azuaje F. Computational Models for Predicting Drug Responses in Cancer Research. *Brief Bioinform* (2017) 18(5):820–9. doi: 10.1093/bib/bbw065
19. Liu J, Huang T, Zhang Y, Zhao T, Zhao X, Chen W, et al. Sequence- and Structure-Selective mRNA M(5)C Methylation by NSUN6 in Animals. *Natl Sci Rev* (2021) 8:nwaa273. doi: 10.1093/nsr/nwaa273
20. Guo G, Pan K, Fang S, Ye L, Tong X, Wang Z, et al. Advances in mRNA 5-Methylcytosine Modifications: Detection, Effectors, Biological Functions, and Clinical Relevance. *Mol Ther Nucleic Acids* (2021) 26:575–93. doi: 10.1016/j.omtn.2021.08.020
21. Wang Y, Wang ZQ, Jiang YX, Wang FH, Luo HY, Liang Y, et al. A Triplet Chemotherapy Regimen of Cisplatin, Fluorouracil and Paclitaxel for Locoregionally Recurrent Nasopharyngeal Carcinoma Cases Contraindicated for Re-Irradiation/Surgery. *Expert Opin Pharmacother* (2016) 17:1585–90. doi: 10.1080/14656566.2016.1204293
22. Takamizawa S, Honma Y, Murakami N, Mori T, Oka H, Yamamoto S, et al. Short-Term Outcomes of Induction Chemotherapy With Docetaxel, Cisplatin, and Fluorouracil (TPF) in Locally Advanced Nasopharyngeal Carcinoma. *Invest New Drugs* (2021) 39:564–70. doi: 10.1007/s10637-020-00999-y
23. Gong X, Fan L, Wang P. MEK Inhibition by Trametinib Overcomes Chemoresistance in Preclinical Nasopharyngeal Carcinoma Models. *Anticancer Drugs* (2021) 32:978–85. doi: 10.1097/CAD.0000000000001092
24. Pan F, Ruan Z, Li J, Pang X, Zhang Y, Zou L, et al. Radiotherapy Combined Docetaxel and Oxaliplatin Chemotherapy Is Effective in Patients With Locally Advanced Nasopharyngeal Carcinoma. *Med Oncol* (2015) 32:252. doi: 10.1007/s12032-015-0698-4
25. Chang ET, Adami HO. The Enigmatic Epidemiology of Nasopharyngeal Carcinoma. *Cancer Epidemiol Biomarkers Prev* (2006) 15:1765–77. doi: 10.1158/1055-9965.EPI-06-0353
26. Tsao SW, Yip YL, Tsang CM, Pang PS, Lau VM, Zhang G, et al. Etiological Factors of Nasopharyngeal Carcinoma. *Oral Oncol* (2014) 50:330–8. doi: 10.1016/j.oraloncology.2014.02.006
27. Mei L, Shen C, Miao R, Wang JZ, Cao MD, Zhang YS, et al. RNA Methyltransferase NSUN2 Promotes Gastric Cancer Cell Proliferation by Repressing P57(Kip2) by an M(5)C-Dependent Manner. *Cell Death Dis* (2020) 11:270. doi: 10.1038/s41419-020-2487-z
28. Yang J-H, Sun X-S, Xiao B-B, Liu L-T, Guo S-S, Liang J-D, et al. Subdivision of *De-Novo* Metastatic Nasopharyngeal Carcinoma Based on Tumor Burden and Pretreatment EBV DNA for Therapeutic Guidance of Locoregional Radiotherapy. *BMC Cancer* (2021) 21(1):534. doi: 10.1186/s12885-021-08246-0
29. Yan Z, Xia L, Huang Y, Chen P, Jiang L, Zhang B. Nasopharyngeal Carcinoma in Children and Adolescents in an Endemic Area: A Report of 185 Cases. *Int J Pediatr Otorhinolaryngol* (2013) 77:1454–60. doi: 10.1016/j.ijporl.2013.06.005
30. Huang Z, Pan J, Wang H, Du X, Xu Y, Wang Z, et al. Prognostic Significance and Tumor Immune Microenvironment Heterogenicity of M5c RNA Methylation Regulators in Triple-Negative Breast Cancer. *Front Cell Dev Biol* (2021) 9:657547. doi: 10.3389/fcell.2021.657547
31. Li X, Meng Y. Expression and Prognostic Characteristics of M(5) C Regulators in Low-Grade Glioma. *J Cell Mol Med* (2021) 25:1383–93. doi: 10.1111/jcmm.16221
32. Xu X, Zhang Y, Zhang J, Zhang X. NSun2 Promotes Cell Migration Through Methylating Autotaxin mRNA. *J Biol Chem* (2020) 295:18134–47. doi: 10.1074/jbc.RA119.012009
33. Liu S, Umezu-Goto M, Murph M, Lu Y, Liu W, Zhang F, et al. Expression of Autotaxin and Lysophosphatidic Acid Receptors Increases Mammary Tumorigenesis, Invasion, and Metastases. *Cancer Cell* (2009) 15:539–50. doi: 10.1016/j.ccr.2009.03.027
34. Xiang S, Ma Y, Shen J, Zhao Y, Wu X, Li M, et al. M(5)C RNA Methylation Primarily Affects the ErbB and PI3K-Akt Signaling Pathways in Gastrointestinal Cancer. *Front Mol Biosci* (2020) 7:599340. doi: 10.3389/fmolb.2020.599340
35. Sun Z, Xue S, Zhang M, Xu H, Hu X, Chen S, et al. Aberrant NSUN2-Mediated M(5)C Modification of H19 lncRNA is Associated With Poor Differentiation of Hepatocellular Carcinoma. *Oncogene* (2020) 39:6906–19. doi: 10.1038/s41388-020-01475-w
36. Zeng L, Liu YM, Yang N, Zhang T, Xie H. Hsa_circRNA_100146 Promotes Prostate Cancer Progression by Upregulating Trip13 *via* Sponging miR-615-5p. *Front Mol Biosci* (2021) 8:693477. doi: 10.3389/fmolb.2021.693477
37. Karmi O, Sohn YS, Zandalinas SI, Rowland L, King S, Nechushtai R, et al. Disrupting CISD2 Function in Cancer Cells Primarily Impacts Mitochondrial Labile Iron Levels and Triggers TXNIP Expression. *Free Radic Biol Med* (2021) 20(176):92–104. doi: 10.1016/j.freeradbiomed.2021.09.013
38. Zhang B, Wu Q, Li B, Wang D, Wang L, Zhou YL. M(6)A Regulator-Mediated Methylation Modification Patterns and Tumor Microenvironment Infiltration Characterization in Gastric Cancer. *Mol Cancer* (2020) 19:53. doi: 10.1186/s12943-020-01170-0
39. Pitt JM, Marabelle A, Eggermont A, Soria JC, Kroemer G, Zitvogel L. Targeting the Tumor Microenvironment: Removing Obstruction to Anticancer Immune Responses and Immunotherapy. *Ann Oncol* (2016) 27:1482–92. doi: 10.1093/annonc/mdw168
40. Liu C, Chikina M, Deshpande R, Menk AV, Wang T, Tabib T, et al. Treg Cells Promote the SREBP1-Dependent Metabolic Fitness of Tumor-Promoting Macrophages *via* Repression of CD8(+) T Cell-Derived Interferon-Gamma. *Immunity* (2019) 51:381–97.e386. doi: 10.1016/j.immuni.2019.06.017
41. Zhang M, Fritsche J, Roszik J, Williams LJ, Peng X, Chiu Y, et al. RNA Editing Derived Epitopes Function as Cancer Antigens to Elicit Immune Responses. *Nat Commun* (2018) 9:3919. doi: 10.1038/s41467-018-06405-9
42. Zhao J, Guo C, Xiong F, Yu J, Ge J, Wang H, et al. Single Cell RNA-Seq Reveals the Landscape of Tumor and Infiltrating Immune Cells in Nasopharyngeal Carcinoma. *Cancer Lett* (2020) 477:131–43. doi: 10.1016/j.canlet.2020.02.010
43. Hollern DP, Xu N, Thennavan A, Glodowski C, Garcia-Recio S, Mott KR, et al. B Cells and T Follicular Helper Cells Mediate Response to Checkpoint Inhibitors in High Mutation Burden Mouse Models of Breast Cancer. *Cell* (2019) 179:1191–1206.e1121. doi: 10.1016/j.cell.2019.10.028
44. Santin AD, Bellone S, Buza N, Choi J, Schwartz PE, Schlessinger J, et al. Regression of Chemotherapy-Resistant Polymerase Epsilon (POLE) Ultra-Mutated and MSH6 Hyper-Mutated Endometrial Tumors With Nivolumab. *Clin Cancer Res* (2016) 22:5682–7. doi: 10.1158/1078-0432.CCR-16-1031
45. Thorsson V, Gibbs DL, Brown SD, Wolf D, Bortone DS, Ou Yang TH, et al. The Immune Landscape of Cancer. *Immunity* (2018) 48:812–30.e814. doi: 10.1016/j.immuni.2018.03.023
46. Ock CY, Hwang JE, Keam B, Kim SB, Shim JJ, Jang HJ, et al. Genomic Landscape Associated With Potential Response to Anti-CTLA-4 Treatment in Cancers. *Nat Commun* (2017) 8:1050. doi: 10.1038/s41467-017-01018-0
47. Kanakry CG, Fuchs EJ, Luznik L. Modern Approaches to HLA-Haploidentical Blood or Marrow Transplantation. *Nat Rev Clin Oncol* (2016) 13:10–24. doi: 10.1038/nrclinonc.2015.128
48. Hiraoka N, Ino Y, Hori S, Yamazaki-Itoh R, Naito C, Shimasaki M, et al. Expression of Classical Human Leukocyte Antigen Class I Antigens, HLA-E and HLA-G, Is Adversely Prognostic in Pancreatic Cancer Patients. *Cancer Sci* (2020) 111:3057–70. doi: 10.1111/cas.14514
49. Yang Q, Cao SM, Guo L, Hua YJ, Huang PY, Zhang XL, et al. Induction Chemotherapy Followed by Concurrent Chemoradiotherapy Versus Concurrent Chemoradiotherapy Alone in Locoregionally Advanced Nasopharyngeal Carcinoma: Long-Term Results of a Phase III Multicentre Randomised Controlled Trial. *Eur J Cancer* (2019) 119:87–96. doi: 10.1016/j.ejca.2019.07.007

50. Zhang Y, Chen L, Hu GQ, Zhang N, Zhu XD, Yang KY, et al. Gemcitabine and Cisplatin Induction Chemotherapy in Nasopharyngeal Carcinoma. *N Engl J Med* (2019) 381:1124–35. doi: 10.1056/NEJMoa1905287
51. Xu PF, Yang JA, Liu JH, Yang X, Liao JM, Yuan FE, et al. PI3Kbeta Inhibitor AZD6482 Exerts Antiproliferative Activity and Induces Apoptosis in Human Glioblastoma Cells. *Oncol Rep* (2019) 41:125–32. doi: 10.3892/or.2018.6845
52. Lu Q, Ni Y, Wang W, Wang L, Jiang T, Shang L. Dynamin 3 Inhibits the Proliferation of Non-Small-Cell Lung Cancer Cells by Suppressing C-MET-GBR2-STAT3 Complex Formation. *Front Cell Dev Biol* (2021) 9:641403. doi: 10.3389/fcell.2021.641403

Conflict of Interest: The authors declare that the research was conducted in the absence of any commercial or financial relationships that could be construed as a potential conflict of interest.

Publisher's Note: All claims expressed in this article are solely those of the authors and do not necessarily represent those of their affiliated organizations, or those of the publisher, the editors and the reviewers. Any product that may be evaluated in this article, or claim that may be made by its manufacturer, is not guaranteed or endorsed by the publisher.

frontiers | Frontiers in Oncology

TYPE Original Research
PUBLISHED 22 August 2022
DOI 10.3389/fonc.2022.815998

OPEN ACCESS

EDITED BY
Soldano Ferrone,
Massachusetts General Hospital and Harvard Medical School, United States

REVIEWED BY
Zhiqiang Liu,
Tianjin Medical University, China
Qi Shengcai,
Shanghai Stomatology Prevention Hospital, China

*CORRESPONDENCE
Rongtao Yuan
yuanrongtao@163.com
Hao Chen
chenhaoBGL2@xjtu.edu.cn

SPECIALTY SECTION
This article was submitted to Head and Neck Cancer, a section of the journal Frontiers in Oncology

RECEIVED 16 November 2021
ACCEPTED 01 August 2022
PUBLISHED 22 August 2022

CITATION
Qiu J, Tang Y, Liu L, Yu J, Chen Z, Chen H and Yuan R (2022) FOXM1 is regulated by DEPDC1 to facilitate development and metastasis of oral squamous cell carcinoma. *Front. Oncol.* 12:815998. doi: 10.3389/fonc.2022.815998

FOXM1 is regulated by DEPDC1 to facilitate development and metastasis of oral squamous cell carcinoma

Jing Qiu[1], Yongping Tang[1], Lan Liu[1], Jiangbo Yu[1], Zhenggang Chen[1], Hao Chen[2,3]* and Rongtao Yuan[1]*

[1]Department of Stomatology, Qingdao Municipal Hospital, Qingdao, Shandong, China, [2]Key Laboratory of Biomedical Information Engineering of Ministry of Education, Biomedical Informatics & Genomics Center, School of Life Science and Technology, Xi'an Jiaotong University, Xi'an, Shanxi, China, [3]Research Institute of Xi'an Jiaotong University, Hangzhou, Zhejiang, China

The Disheveled, EGL-10, Pleckstrin domain containing 1 (DEPDC1) is a new oncogene that has recently been described. The mechanisms and functions of its expression are yet to be determined in oral squamous cell carcinoma (OSCC). In the present study, the impact of DEPDC1 on the growth and development of OSCC was investigated using animal models, cell lines and human tissue samples. Elevated DEPDC1 expression within cancer cell lines and human OSCC has been identified. Mechanistic examination showed that restored DEPDC1 expression *in vivo* and *in vitro* stimulated OSCC tumour development. In addition, FOXM1 interacts with DEPDC1 as indicated by co-immunoprecipitation and immunofluorescence testing. Functionally, DEPDC1 facilitated Wnt/β-catenin signal transduction and β-catenin protein nuclear expression. In summary, the DEPDC1, interacting with FOXM1 *via* Wnt/β-catenin signaling, the closely regulated OSCC pathogenesis, suggesting that targeting the novel DEPDC1/FOXM1/β-catenin complex is an essential OSCC therapeutic approach.

KEYWORDS

oral squamous cell carcinoma, proliferation, migration, DEP domain containing 1, FoxM1

Introduction

An increasing malignancy worldwide, head and neck squamous cell carcinoma (HNSC) comprises 90% of all head and neck cancers (1). The primary subtype of HNSCs is oral squamous cell carcinoma (OSCC), one of the most common cancers worldwide (1, 2). Statistics for oral cancer are unreliable compared to other cancers because half of all oral cancers are not detected until cancer has spread to nearby tissues and around half of

the patients die within 5 years (3, 4). With over 90% of patients diagnosed with squamous cell carcinomas (SCC), most oral cancer originates from oral cavity neoplasms. OSCC therapeutic strategies include chemotherapy, radiation therapy and surgery (5). Despite the disease's alarming death and morbidity statistics, OSCC is one of the least studied malignancies, with limited understanding of its molecular pathophysiology. Hence, detailed studies must be carried out to identify the inherent mechanisms underlying tumour incidence to unveil potential OSCC therapies. DEPDC1 is a newly presented and well-preserved oncogene from mammals to *Caenorhabditis elegans* (6, 7). N terminal regions contain the DEP domain, and the gene for DEPDC1 is found at 1p31.3 in humans (6). DEPDC1 was first discovered at an abnormally raised expression in bladder cancer. It inhibited A20 transcription by associating with zinc-finger protein 224 (ZNF224), activating the anti-apoptotic pathway and stimulating the NF-κB pathway (8).

DEPDC1 is abnormally over-expressed in the prostate, hepatic, breast, and lung cancers, according to recent research, and can predict outcomes in lung and bladder cancer patients (9–12). Its activities in promoting tumour growth have also been gradually uncovered. DEPDC1 is primarily expressed throughout the cell cycle's interphase stage. It is necessary for normal metaphase division, as shown by drastic mitotic arrest when silencing it (7). Moreover, DEPDC1 regulates chemotherapy agents targeting microtubules to induce apoptosis by improving BCL-2 family protein MCL1's JNK-dependent degradation (6). Another study revealed that knocking down DEPDC1 caused a delay in nasopharyngeal cancer cell cycle progression, proliferation, and substantial migratory inhibition (13). However, in OSCC progression and growth, the functions and processes underlying DEPDC1 expression are yet to be elucidated. Forkhead box M1 (FOXM1) is a FOX superfamily transcription factor with a preserved DNA binding domain in the form of a winged helix (14).

Several studies have demonstrated that it plays a critical role in exacerbating metastatic activity, invasion, angiogenesis and cancer since FOXM1 is a crucial cell cycle proliferation regulator (15–17). We recently discovered that FOXM1's down-regulation prevents OSCC's invasion, migration and replication *in vitro* (17). In the nucleus, FOXM1 can trigger the expression of several genes that are involved in tumor initiation processes such as angiogenesis, cell proliferation, cellular migration and invasion (18). FOXM1 also synergizes with the canonical Wnt signaling pathway (often activated during tumorigenesis) by directing the nuclear translocation of β-catenin to induce transcription of several oncogenes (18). Additionally, increased FOXM1 expression induces changes in the methylation status similar to the epigenome in OSCC. Among those involved in OSCC progression and development, Wnt/β-catenin is one of the most efficient signaling mechanisms (19). Wnt ligands interact with Frizzled family receptors and cell surface co-receptors, blocking this pathway. Ligand binding inhibits the cytoplasmic degradation complex, including casein kinase 1, Axin, glycogen synthase kinase-3β, and adenomatous polyposis coli (APC) leading to β-catenin nuclear localization. Vector T-cell factor/lymphoid-enhancing factor is bound by β-catenin inside the nucleus to trigger downstream Wnt target genes, including matrix metalloproteinase 9 (MMP9), MMP2 and cyclin D1. Despite evidence indicating that Wnt/β-catenin signals alone are insufficient to cause cancer, such signaling has played a crucial role in the survival, chemoresistance, and development of cancer stem cells (20). FOXM1 is a relevant target for further characterization because FOXM1 regulates the expression of many genes and affects epigenetic controls that are involved in multiple oncogenic cellular processes. FOXM1 promotes the Wnt/β-catenin signaling pathway by promoting β-catenin nuclear translocation, according to newly published research (21).

Nevertheless, the biomechanical processes mediating that suppression and its role in the relationship between β-catenin and DEPDC1 remains unclear. The mechanisms and roles of DEPDC1 expression in OSCC migration and growth were determined in this study. We also observed that DEPDC1 expression was increased in OSCC cells and that DEPDC1 downregulation impaired the growth of OSCC cells and *in vivo* and *in vitro* metastasis. DEPDC1 downregulation is the cause of DEPDC1 interacting with FOXM1 and lowering the nuclear translocation of β-catenin.

Materials and methods

Collection of tumorous tissue

At the Qingdao Municipal Hospital, 42 related samples of tumorous tissue (central area of the lesion) and matched adjoining oral epithelial tissue were obtained post-surgically from patients with OSCC. All patients provided informed consent before sampling and had not received any treatment before surgery. All of the samples were kept at -80°C. The Ethical Committee of Qingdao Municipal Hospital authorized and approved this research (approval number 2018-0318).

Cell culture and cell transfection

The American Type Culture Collection (ATCC) supplied SCC-15, SCC-25, HaCaT, HEK29T and CAL-27 cell lines which were cultured in RPMI-1640 with streptomycin (100 μg/mL) (Solarbio, China), penicillin (100 U/mL) and 10% of fetal bovine serum (Gibco, USA). Overexpression vector-DEPDC1 (OV-DEPDC1), sh-DEPDC1, sh-FOXM1, OV-DEPDC1+ sh-FOXM1, OV-DEPDC1+ sh-NC, OV-NC + sh-FOXM1, OV-

NC+ sh-NC and negative control of the overexpression vector (OV-NC) were transfected into the cells. The GeneChem Company (Shanghai, China) developed these plasmids. The cells were grown on a 6-well plate for 48h and transfected upon reaching 70-80% confluent. The transfection was performed using an assay based on lipofectamine 3000 (Thermo Fisher Scientific, Massachusetts, USA). The medium was removed following an 8-hour transfection, and the cells were incubated for the specified times, then extracted and used for the designated experiments.

Bioinformatics analyses

Comparative investigations of DEPDC1 expression profiles were performed using multiple web-based bioinformatics techniques. The datasets from Gene Expression Omnibus (GEO, access #: GSE31056) were downloaded, assessed and used for calculations to obtain stored expression data and systematically interpret and combine datasets. GraphPad Prism software was utilized for mapping the expression profile. Gene Expression Profiling Digital Research (GEPIA, http://gepia2.cancer-pku.cn/) is a well-known tool for examining variations between cancerous and paired normal tissue mRNA levels expressed from particular genes (22). GEPIA was used to study mRNA levels in HNSC and paired normal tissues. UALCAN (http://ualcan.path.uab.edu/) was employed to test the DEPDC1 gene prognosis (23). Relative to normal RNA expression, cancer patients were classified into low and high expression groups for each gene, and the probability threshold $P < 0.05$ was considered significant for each difference. The OncoLnc (http://www.oncolnc.org/) database was first utilized to evaluate the prognostic value of DEPDC1 mRNA expression in HNSC (24).

RNA isolation and quantitative real-time polymerase chain reaction

Using TRIzol reagent (Thermo Fisher Scientific, Massachusetts, USA), we isolated whole-cell RNA from cell lines, normal tissues, and tumours (17). Takara (Shiga, Japan) supplied the PrimeScript RT Reagent Kit to generate cDNA at a 20 µL volume following manufacturer instructions. The cDNAs were subsequently used in qRT-PCR using SYBR® Premix Ex Taq™ kits according to manufacturer's instructions (Takara, Japan). QRT-PCR was performed in a FTC-3000 (Funglyn Biotech, Canada). The forward PCR primer used for DEPDC1 (225 bp) was: 5' -GTAAGCAGTAGTAGGTGCAGGAG-3' and the reverse primer was: 5'-GCTTGTGTGTGTTCCAC CA-30. For GAPDH (146 bp), the forward primer was: 5' -TCATGGTGGTGAACCAGAA-3' and the reverse primer was 5' -GCATGACTGTGCATGGATGAG-3.' We normalized the expression of each targeted gene to GAPDH (ΔCt), which was our housekeeping gene. Values for gene expression were then calculated using the $^{\Delta\Delta}$Ct method with the formula: R.Q. = $2^{-\Delta\Delta Ct}$. TaKaRa (Kyoto, Japan) provided the SYBR® Premix Ex Taq™ used for PCR amplification under the given parameters: 30 seconds at 95°C, then at 95°C again for forty cycles of 5 seconds each, followed by 30 seconds at 60°C. After that, a 15-second separation interval at 95°C, 60 seconds at 60°C, and finally 15 seconds at 95°C. The outcomes were calculated using the averages of three different reactions.

Sodium dodecyl sulphate polyacrylamide gel electrophoresis and western blotting

A proteinase inhibitor cocktail (Sigma, USA) was added to RIPA-lysis buffer (PBS, sodium deoxycholate (0.5%), NP40 (1%), Sodium dodecyl sulphate (SDS, 0.1%) and phenylmethylsulfonylfluoride (100µg/mL)) which was applied to isolate whole tissue or cell protein from surgical samples or cell lines for 30 minutes on ice. The supernatant was harvested from centrifuged lysates. SDS-PAGE was carried out, and the segregated proteins were moved to a fluoride polyvinylidene fluoride (PVDF) membrane. Membranes were blocked for 1 hour at room temperature with 5% powdered skimmed milk, then incubated with primary antibodies overnight at 4°C. The following primary rabbit antibodies were diluted at 1:1000 (Cell Signaling Technology, Massachusetts, USA): anti-Lamin B1, anti-β-catenin and anti-FOXM1. Rabbit anti-GAPDH, also from Cell Signaling, was diluted at 1:3000. Mouse anti-DEPDC1 (1:200) was from Santa Cruz Biotech, Texas, USA). Abcam supplied anti-mouse secondary IgG H&L antibodies labelled with horseradish peroxidase (HRP, diluted 1:2000) incubated with the membrane for one hour. Bio-Rad (California, USA) supplied the Clarity Western ECL Blotting Substrates used to visualize protein locations on the membranes developed with the ChemiDoc XRS+ Bio-Rad imaging system. Our loading controls were GAPDH and Lamin B1.

Measurement of cell colony forming capacity

Cells were seeded in 6-well plates 24 hours after transfection to examine colony-forming capacity, then incubated for approximately 14 days. Crystal violet (0.1%) and paraformaldehyde (4%) were employed to stain and fix the cells for 15 minutes at room temperature. The cell colonies were photographed and counted.

Cell counting kit-8

We used Cell counting kit-8 (CCK-8) assays acquired from Dojindo Laboratories (Kumamoto, Japan) to measure cell proliferation. For CCK-8 assays, a 96-well plate was filled with equivalent numbers of the stated OSCC cells. The CCK-8 was used to test absorbance every 22 hours per the manufacturer's instructions.

Wound healing assessment

The end of a pipette was used to injure cells growing in monolayers. PBS was used to rinse off non-adhering cells before adding fresh media. Cell migration was measured as the decline in the area of the wounded region in each field image. We photographed a minimum of three fields for each measurement on each occasion, and ImageJ software was used to measure the area.

Transwell migration assay

A Transwell assay was utilized to quantify cell migration capability. A 24-well plate separating the top and bottom chambers were used to house the Transwell chamber fitted with a polycarbonic membrane (8 μm pores, Costar, Corning, USA). The top chamber was loaded with 1×10^5 OSCC cells which migrated towards fetal bovine serum (20%) in RPMI-1640 medium added to the lower chamber. Following 24 hours of incubation at 37°C, crystal violet (0.1%) was added for half an hour to stain cells in the lower chamber. Migrant cell pictures were taken under a microscope.

Tumour growth in nude mice *in vivo*

The Beijing Critical River Laboratory provided the nude BALB/C mice (weigh t= 18.0 ± 2 g, age = 6 weeks) and were randomly divided into the stated groups. Grouped mice were injected subcutaneously with cells expressing controls or shRNA. A Vernier calliper was used to record the tumour volume (TVol) every couple of days using the equation TVol (mm^3) = $(x \times y^2)/2$, where y and x represent the smallest and largest diameters. Tumours were scheduled for further testing after weighing and removal, which occurred when all animals were slaughtered 24 days after injection. At necropsy, animals were sacrificed by CO_2 exposure followed by cervical dislocation. All procedures involving these animals were conducted in compliance with the Institutional Animal Care and Use Committee of Qingdao Municipal Hospital. The facilities and laboratory animal program of Qingdao Municipal Hospital are accredited by the Association for the Assessment and Accreditation of Laboratory Animal Care.

Co-immunoprecipitation assay

In 12-well plates, HEK293 T cells were cultured at 1.5×10^5 cells per well and incubated for 24 hours in RPMI-1640, as outlined above. Lipofectamine 3000 was applied to transfect the cells for 48 hours with DEPDC1-V5 and FOXM1-Flag plasmids. Cells were subjected to 500 μL of RIPA lysis buffer and then a protease inhibitor mixture (Thermo Science, Ontario, Canada) at 4°C for 30 minutes. For 10 minutes, the lysates were centrifuged at 4°C at 10,000 g, and 450 μL of the supernatant was reserved for the following step, whereas 50 μL was added to the 2 × SDS loading buffer as a complete extract to measure levels of the desired protein. Anti-DEPDC1 (Santa Cruz Biotech, Texas, USA), FOXM1, normal IgG, anti-V5 and anti-FLAG (all monoclonal antibodies were acquired from Cell Signaling Technology, Massachusetts, USA) were incubated with the 450 μL of supernatant while rotating at 4° C for 1 hour rotating before overnight incubation with protein G beads (Pierce, Illinois, USA) with further rotation at 4°C. Brief centrifugation at 4°C at 10,000 g then pelleted the beads, treated with 4 × RIPA buffer washes and used for Western blotting in 2 × SDS lysis buffer (50 μL).

Co-habitation examination using immunofluorescence

The overnight cell growth on coverslips at 4°C was followed by a 1h blocking incubation with 5% milk, then incubation with the following antibodies, all diluted at 1:100: DEPDC1, Flag and FOXM1. Anti-V5 primary antibody from Cell Signaling was used at 1:50 dilution. 4',6-diamidino-2-phenylindol (DAPI) and either Alexa Fluor 555 goat anti-mouse Ig G or Alexa Fluor 488 goat anti-mouse IgG (both diluted 1:1000, Cell Signaling Technology, Massachusetts, USA)) were subsequently applied to the coverslips. The TCS SP5 confocal microscope from Leica Microsystems (Germany) was used to obtain cell photographs.

Statistical analysis and data presentation

The visual presentation was done with GraphPad Prism 6.0 software, while the statistical tests were performed with Statistical Package for Social Sciences (SPSS v.18.0) software. The relationship between the patient's clinical pathology and the expression of DEPDC1 was studied by the Chi-square test. Using a Spearman rank correlation coefficient, we examined bivariate relationships between study variables. The Kaplan-Meier method was used to construct survival curves, and the

logarithmic rank test was applied to compare them. The results are presented as means ± standard deviation, and the data were analyzed using Tukey's *post hoc* test or the student's *t-test*. Statistically significant differences were considered at probability (P) values of * $P < 0.05$.

Results

DEPDC1 overexpression is associated with poor OSCC prognosis

To determine whether DEPDC1 was involved in OSCC development and progression, DEPDC1 modifications were initially examined in the GSE31056 microarray data set collected from GEO comparing OSCC and non-tumour tissues (25). The results revealed that DEPDC1 was downregulated in the GEO datasets (Figure 1A).

Three online sources, including GEPIA2, UALCAN and OncoLnc, were consecutively used to analyze the level of mRNA expression of DEPDC1 in human patients. Analysis of DEPDC1 expressions in human tumour tissues from the UALCAN database indicated that SSRP1 is upregulated in several tumour tissues (Supplementary Figure 1A). In addition, in normal tissue, HNSC and TCGA RNA sequencing data showed through GEPIA2 and UALCAN analysis that expression of DEPDC1 is upregulated in tumour tissues compared to normal tissue (Supplementary Figures 1B, D), whereas stages were significantly associated with DEPC1 expression (Supplementary Figure 1C). Moreover, Kaplan-Meier survival analysis revealed that patients with elevated levels of DEPDC1 had a poor overall (O.S.) survival relative to those with reduced levels (Supplementary Figure 1E).

To confirm the potential therapeutic utility of DEPDC1 expression, 42 samples were obtained for this study, including normal neighbouring and OSCC tissues. The levels of DEPDC1 expression in non-cancerous and OSCC tissues were compared. The levels were greater in OSCC tissues than in neighbouring non-cancerous ones, as revealed by qRT-PCR assay results (Figure 1B). The detailed clinical characteristics, including diagnosis at age, gender, lymphatic metastasis, blood glucose and TNM Stage, are shown in Table 1. All patients were between 35 and 82 years of age (57.47 ± 11.03 years). Table 2 summarizes the associations between DEPDC1 expression and clinicopathological features. There was a significant correlation between the DEPDC1 expression and the lymphatic metastasis parameters (P = 0.030), TNM stage (P = 0.032), while there was no correlation between the DEPDC1 and other parameters

TABLE 1 Clinicopathological characteristics of OSCC patient samples.

Characteristics	No. of case (%)
Age	
<60	16 (38.1)
≥60	26 (61.9)
Gender	
Male	37 (88.1)
Female	5 (11.9)
Lymphatic metastasis	
Yes	32 (76.2)
No	10 (23.8)
Blood glucose (mmol/L)	
Normal	34 (81.0)
High	8 (19.0)
TNM stage	
stage I	28 (66.7)
stage II	4 (9.5)
stage III	10 (23.8)

OSCC, oral squamous cell carcinoma; TNM, tumor-node-metastasis.

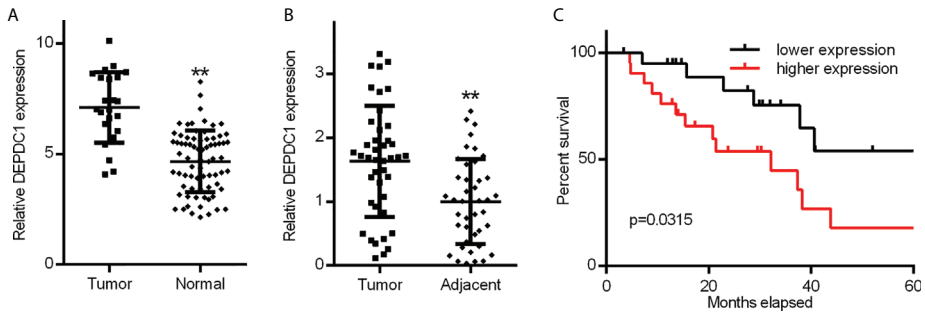

FIGURE 1
Increased OSCC tissue expression of DEPDC1. **(A)** Discovery in OSCC tissue samples of DEPDC1 expression *via* qRT-PCR by GSE31056 dataset. (normal n = 73, tumor n = 23). **(B)** DEPDC1 mRNA expression identification in OSCC tissue and neighbouring qRT-PCR samples (n = 42). **(C)** The general survival (O.S.) rate by Kaplan-Meier analysis is shown for OSCC patients with low or high DEPDC1 expression. (** $P < 0.01$). The data are presented as the mean ± SD. Replicate assays were performed three times.

TABLE 2 Correlation between DEPDC1 expression and clinicopathologic characteristics of OSCC patients.

Characteristics DEPDC1	DEPDC1 expression		
	Low no. cases	High no. cases	p value
Age			
<60	10	6	0.204
≥60	11	15	
Gender			
Male	17	20	0.153
Female	4	1	
Lymphatic metastasis			
Yes	2	8	**0.030**
No	19	13	
Blood glucose (mmol/L)			
Normal	18	16	0.432
High	3	5	
TNM stage			
stage I	18	10	**0.032**
stage II	1	3	
stage III	2	8	

P values were calculated using chi-square test. Bold numbers indicate significant differences (P < 0.05). OSCC oral squamous cell carcinoma, TNM tumor-node-metastasis.

including age (P = 0.204), gender (P = 0.153), blood glucose (P = 0.432), lymph node metastasis (P = 0.773), TNM stage (P = 0.861), radiotherapy (P = 0.624), chemotherapy (P = 0.569), relapse (P = 0.174), differentiation (P = 0.514).

Spearman's analysis of the correlation between DEPDC1 and clinicopathological features revealed that the expression of DEPDC1 was significantly associated with lymphatic metastasis (P = 0.030) and TNM stages (P = 0.008). Additionally, we examined the relative risks indicated by DEPDC1 in the OSCC prognostic. The Cox regression analysis was performed to determine if DEPDC1 could be a potential risk factor. As shown in Table 3, high expression of DEPDC1 and blood glucose was associated with a significantly elevated risk of death in OSCC patients (P = 0.039 and P = 0.022) compared to those with low DEPDC1 expression by univariate Cox regression analysis (Table 4). Multivariate Cox regression analysis revealed that blood glucose could be a factor in predicting poor survival (P = 0.019) (Table 4). These results indicate a significant correlation between the expression of DEPDC1 with the prognosis of OSCC.

The Kaplan-Meier analysis showed that patients with reduced expression of DEPDC1 had a markedly longer overall survival (O.S.) rate (O.S.: 71.43% *vs* 38.09%) than patients with high expression of DEPDC1; taking the DEPDC1 mid-level value as the cut-off point in 42 patients (Figure 1C). The findings suggest that DEPDC1 may be overexpressed and associated with poor OSCC prognosis.

DEPDC1 promotes *in vitro* OSCC cell metastasis and proliferation

In order to determine DEPDC1's biological function in OSCC cells, we analyzed DEPDC expression levels in the HaCaT immortalized keratinocyte cell line and three OSCC cell lines (Figure 2A). According to our findings, in each OSCC

TABLE 3 Spearman analysis of correlation between DEPDC1 and clinicopathological.

Variables	DEPDC1 expression level	
	Spearman correlation	p value
Age (years, <60 vs. ≥60)	0.196	0.213
Gender (male/female)	-0.221	0.16
Lymphatic metastasis (yes/no)	0.335	**0.03**
Blood glucose (normal vs high)	0.121	0.444
TNM stage (I+II vs III)	0.402	**0.008**

Bold numbers indicate significant differences (P < 0.05). OSCC oral squamous cell carcinoma, TNM tumor-node-metastasis.

TABLE 4 Univariate and multivariate analyses of various prognostic parameters in patients with OSCC Cox-regression analysis.

	Univariate analysis			Multivariate analysis		
	p value	Hazard Ratio	95% confidence interval	p value	Hazard Ratio	95% confidence interval
DEPDC1	**0.039**	2.779	1.052-7.342	0.095	2.436	0.857-6.919
Lymphatic metastasis (yes/no)	0.392	1.529	0.578-4.046	0.431	1.601	0.496-5.168
Blood glucose (normal vs high)	**0.022**	3.316	1.188-9.257	**0.019**	4.087	1.262-13.238

Bold numbers indicate significant differences ($P < 0.05$). OSCC oral squamous cell carcinoma, TNM tumor-node-metastasis.

cell line, DEPDC1 expression was greater than that of HaCaT cells. CAL-27 had the lowest concentration of DEPDC1, whereas SCC-25 had the highest concentration. Then, DEPDC1 was downregulated in SCC-25 cells and increased in CAL-27 cells, respectively (Supplementary Figures 2A, B). To investigate the biological function of DEPDC1 on OSCC progression, CCK-8 and colony formation assays were performed. Compared to the controls transfected with sh-NC, the SCC-25 cells transfected with sh-DEPDC1 had considerably lower cell viability (Figure 2B, C) (negative control). The propagation of OV-DEPDC1-transfected CAL-27 cells was better than that of OV-NC-transfected CAL-27 cells (Figure 2B, C).

We conducted Transwell and wound healing experiments to investigate how OSCC cell migration was affected by DEPDC1. Wound healing test results showed that DEPDC1 ectopically expressing CAL-27 cells had faster closure of wounds than control cells (Figure 2D), whereas the abolition of SCC-25 cell DEPDC1 expression delayed closure of wounds relative to controls (Figure 2D). The knockdown of DEPDC prevents the migration of SCC-25 cells, as demonstrated by the Transwell test, which also showed that DEPDC1 overexpression caused cell migration (Figure 2E). We next investigated the impact of DEPDC1 on nude mouse tumour growth to obtain confirmation that DEPDC1 enhanced tumour progression and found that DEPDC1 knockdown shrank the tumours (Figure 2F, **left**). In contrast, increased *in vivo* tumour size was observed following the overexpression of DEPDC1 in CAL-27 tumours (Figure 4F, **right**). Together, these results showed that in OSCC, DEPDC1 plays a cancer-inducing role *in vivo* and *in vitro*.

DEPDC1 associates with FOXM1

The GEPIA2 website was utilized to investigate related genes, find those associated with DEPDC1 and show the biomolecular mechanisms by which DEPDC1 improved OSCC tumorigenicity. Figure 3A shows the FOXM1-associated proteins that have been discovered. Because of FOXM1's crucial role in carcinogenesis in our earlier study, we decided to investigate it further (20). Following Genecards (https://www.genecards.org/) to analyze protein positions, the two potentially associated protein location sites were strongly coincidental (Supplementary Figure 3B). Therefore, a co-immunoprecipitation approach was used with cultured cell lysates to confirm the presumed physical interactions between FOXM1 and DEPDC1. The vectors DEPDC1-V5 and FOXM1-Flag were generated (Supplementary Figure 3C). SCC-25 cells revealed the interaction between endogenous FOXM1 and DEPDC1 (Figure 3B). Moreover, DEPDC1 (red) and FOXM1 (green) immunofluorescence staining showed that the two proteins co-habited in the nucleus (Figure 3C). These findings suggest that DEPDC1 is a validated interacting protein for FOXM1.

DEPDC1 accelerates OSCC cell growth *via* regulating FOXM1

As mentioned above, DEPDC1 was verified to play critical roles in promoting growth in OSCC cells. We suppressed FOXM1 endogenous expression in CAL–27 cells overexpressing DEPDC1 to see if DEPDC1-mediated FOXM1 regulation promotes tumour growth. We determined that DEPDC1 inhibited cell migration and proliferation under these conditions (Figures 4A–D). To further explore whether DEPDC1 promoted OSCC growth, the xenograft experiments were established in nude mice. Xenograft experiments frequently indicated that the consequences of over-expressing DEPDC1 were rescued by suppressing FOXM1 levels, resulting in the reduced progression of tumours (Figures 4E, F). Together, these results show that DEPDC1 stimulated tumour development by FOXM1 regulation.

DEPDC1 activates Wnt signaling in OSCC

Since our previous study revealed that a positive correlation exists between FOXM1 and Wnt signaling, we decided to focus efforts on FOXM1 since it is a critical transcriptional coactivator of Wnt signaling, which is tightly linked to tumor growth and metastasis (17). DEPDC1 has already been reported to regulate the Wnt/β-catenin pathway (10). Additionally, Wnt/β-catenin stimulation can increase OSCC cell invasion and proliferation (26). As a result, we hypothesized that DEPDC1 might promote OSCC malignancy by initiating a Wnt/β-catenin signaling cascade. Western blot experiments were used to test this

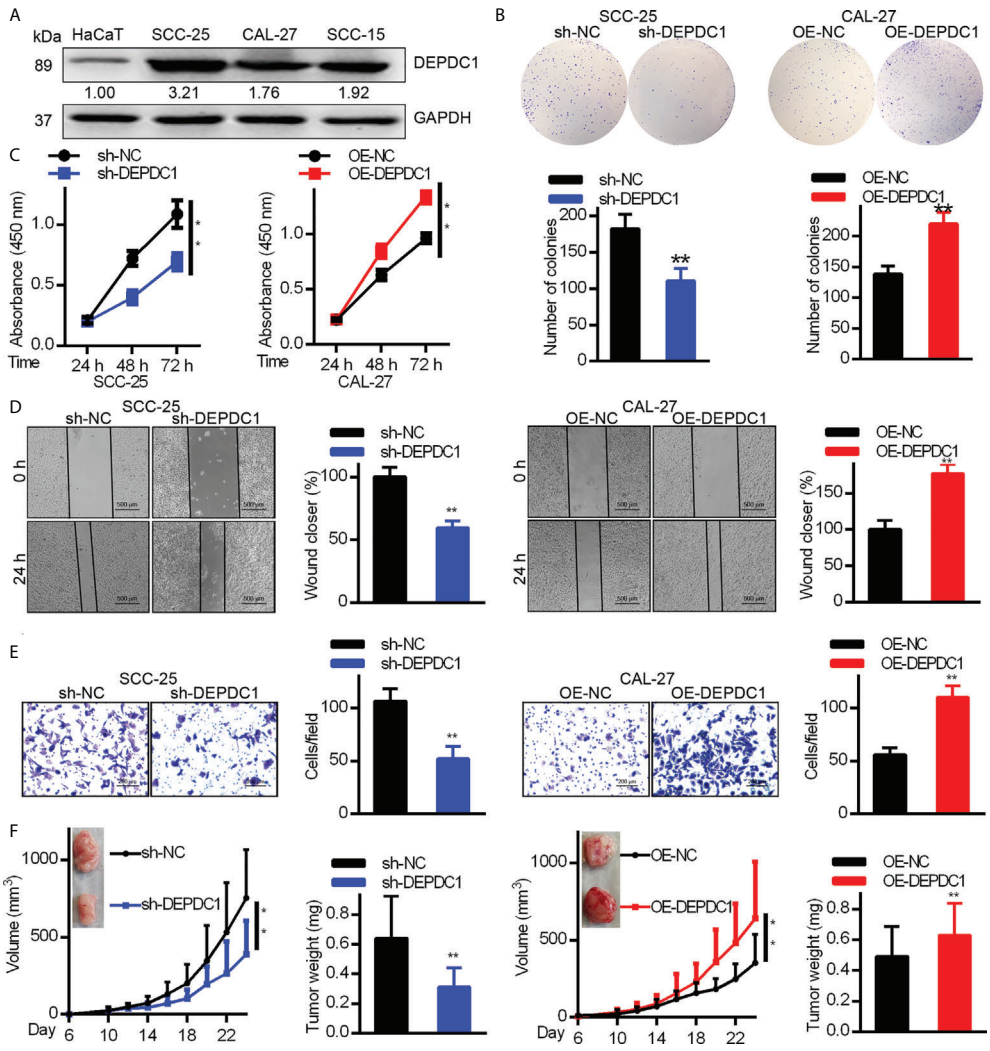

FIGURE 2
DEPDC1 promotes human OSCC cell tumorigenicity. **(A)** The expression of DEPDC1 in the HaCaT immortal keratinocyte cell line and three cell lines of OSCC (SCC-15, CAL-27 and CAL-25) was assessed with Western blot. Results were standardized to the GAPDH loading control. **(B)** SCC-25 cells had DEPDC1 knocked down, while in CAL-27 cells, it was overexpressed. **(B, C)** The colony formation study was studied by the Cell counting kit 8 (CCK-8). **(D)** A wound-healing test was performed. **(E)** Migration was measured using a Transwell assay. The figure-panels quantify and compare the number of cells going through the membrane and the proportion of wound closure. Scale bars are 500 μm **(D)** and 200 μm **(E)**. The results are shown as mean ± S.D. $P < 0.05$, ** $P < 0.01$, $N = 3$. **(F)** Each of 6 nude mice aged 6 weeks had 1×10^6 control or DEPDC1-knockdown SCC-25 cells injected under their skin. Weights and volumes of tumours were analyzed. Similarly, 1.5×10^6 control or DEPDC1-knockdown CAL-27 cells were injected under the skin of 6 nude mice. The weights and volume of the tumours were analyzed. For **(F)** A student's *t-test* was used to compare tumor weights between 2 groups, whereas the two-way ANOVA was performed for larger groups. The data are presented as the mean ± SD, and are representative of at least 3 independent experiments.

theory. Results showed that SCC-25 cell DEPDC1-downregulation decreased protein expression in the Wnt/β-catenin pathway, particularly the aggregation of β-Catenin in the nucleus (Figure 5A). Furthermore, immunofluorescence staining data shows that after DEPDC1 has been downregulated, β-catenin moves to the cytoplasm from the nucleus in SCC-25 cells (Figure 5B). When taken together, the results demonstrate that DEPDC1 employs Wnt/β-catenin signaling to promote malignant OSCC progression.

Discussion

Our findings provide compelling evidence for DEPDC1's important function in OSCC development regulation. DEPDC1 promotes the development and proliferation of human OSCC cells *via* Wnt/β-catenin signaling. DEPDC1 interacted with FOXM1, which led to the nuclear localization of β-catenin, the most important indicator for Wnt pathway activation. The level of DEPDC1 expression was also highly correlated with the level

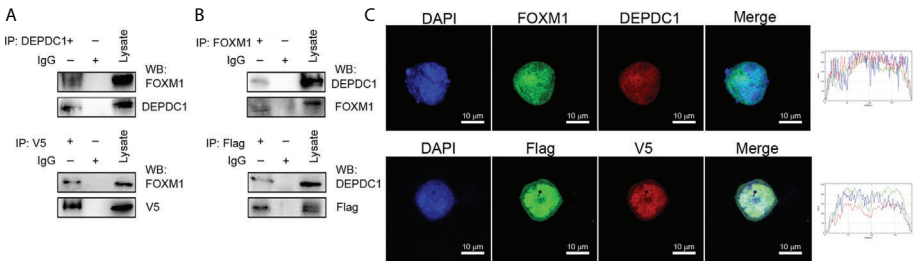

FIGURE 3
DEPDC1 associates with FOXM1. **(A)** FOXM1-expressing plasmids tagged with FLAG and DEPDC1 plasmids with V5 tags were both transfected into HEK293 T cells. Co-immunoprecipitation of transfected cell lysates using anti-V5 or anti-DEPDC1 antibodies bound to beads. Western blotting was then used to identify DEPDC1 is labelled with V5 using anti-V5 or anti-DEPDC1 antibodies. **(B)** Reverse immunoprecipitation. We transfected HEK293T cells with controls or FLAG-bound FOXM1 and V5-bound DEPDC1. Anti-V5 or anti-FOXM1 antibodies were used to Co-immunoprecipitate cell lysates. Anti-FLAG or anti-FOXM1 antibodies were used for Western blotting to detect immunoprecipitated products **(C)**. The subcellular sites of DEPDC1-V5 and FOXM1-Flag were transfected into SCC-25 cells. One day after transfection, cells were fixed, penetrated and incubated with green FLAG, red V5, green FOXM1 and red DEPDC1 Confocal microscopy were performed to analyze nuclei stained with DAPI (blue). Graphs of the intensity profile are shown at the bottom of the image (x-axis, length [in microns]; y-axis, intensity). The bar is set to scale: 10 μm. The data are representative of at least 3 independent experiments.

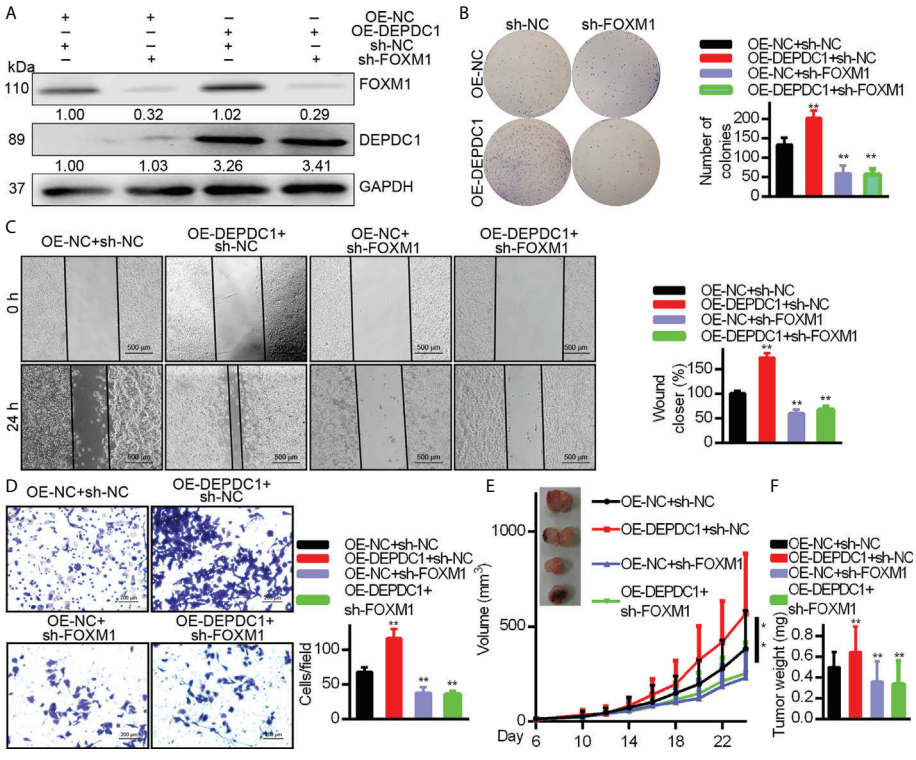

FIGURE 4
DEPDC1 facilitates the OSCC cell migration and growth via FOXM1. DEPDC1-over-expressing CAL-27 cells had FOXM1 knocked down. The indicated antibodies were used for Western blotting cell lysates **(A)**. Colony formation **(B)**, wound healing (500 μm scale bar) **(C)**, and Transwell (100 μm scale bar) assays **(D)** have been studied in cell growth and migration. The results shown for (**B–D**) are mean ± S.D. N = 3 separate tests. Data were analyzed with the student's *t-test*. In the CAL-27 cells, FOXM1 was knocked down with high or low over-expression of DEPDC1 and 1.5×10^6 cells were injected under the skin of 6-week nude mice (n = 6). The development of tumours was studied. The data are shown as mean ± S.D. The student's *t-test* **(F)**, Two-way ANOVA procedure **(E)** and been used to assess statistical significance. The data are representative of at least 3 independent experiments * $P < 0.05$, ** $P < 0.01$..

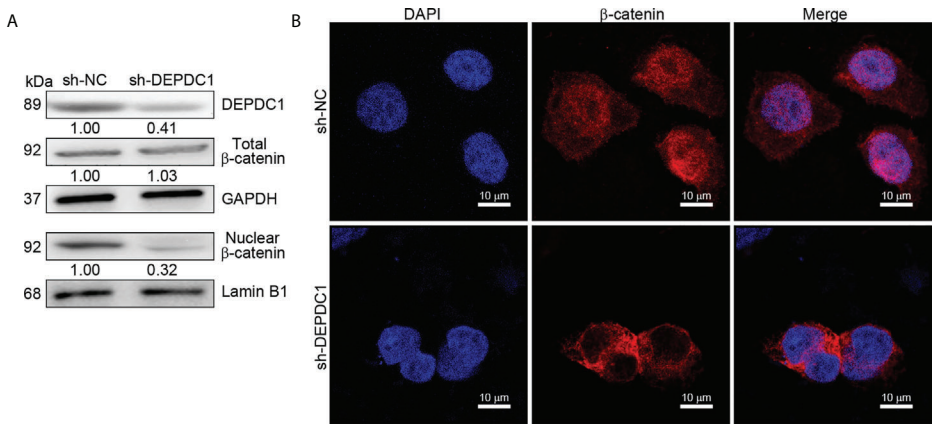

FIGURE 5
DEPDC1 downregulations in oral squamous cell carcinoma inhibit the Wnt/β-catenin signaling pathway. **(A)** DEPDC1 has been tested for its effect on the Wnt/β-catenin signaling pathway in SstainingstainingstainingCC-25 cells using a Western blot assessment. **(B)** The nuclear translocation of β-catenin was mediated by DEPDC1-immunofluorescence-stained β-catenin in sh-DEPDC1 treatment of SCC-25 cells. The data are presented as the mean ± SD, and are representative of at least 3 independent experiments.

of FOXM1 expression in human OSCCs in online databases. DEPDC1 has since been discovered to play a role in cancer progression and is widely regarded as a possible oncogene.

The most common cancer type in which DEPDC1 was shown to play a function was bladder cancer (8, 27). Studies have shown that DEPDC1 is significantly elevated in bladder cancer and is important for cancer cell proliferation (8). DEPDC1 was revealed as one of the most activated genes in breast cancer by analyzing microarray data (28). The TCGA, open-access data, are used to evaluate the function of breast cancer genes, providing scientists with a valuable research tool and novel techniques for cancer prevention, treatment, and diagnostics (29). This report examined DEPDC1's transcription profiles in the GEO and TCGA datasets. Our findings showed that levels of expression of DEPDC1 protein and mRNA in OSCC tissue were considerably increased, and a progressive improvement in the tumour stage was recorded. DEPDC1 expression was lower in normal adjacent tissue relative to OSCC tissue. In addition, several studies have found that longer survival in patients with multiple myeloma and hepatocellular carcinoma was significantly correlated with a lower DEPDC1 expression, suggesting that DEPDC1 may be a new diagnostic marker (30, 31). According to these reports, increased DEPDC1 in OSCC cancer significantly correlated with shorter patient survival times.

Cancer development and proliferation are promoted by abnormal gene expression (32). In nasopharyngeal carcinomas, suppressing DEPDC1 slows the cell cycle and significantly reduces invasion, migration, and proliferation (13). A separate study showed that DEPDC1 inhibits A549 cell proliferation by blocking cell apoptosis (33). Overexpression of DEPDC1 constantly increased the possibility of cancer development and proliferation in breast cancer cells, which was prevented by its deletion. In addition, TCGA datasets revealed that DEPDC1 was a new, highly expressed gene contributing to HNSC migration and proliferation. Together, the results suggest that DEPDC1 mediates a cancer-inducing function in OSCC cells in addition to facilitating OSCC progression through modulating the OSS cell growth environment. In OSCC cancer cells, correlations between DEPDC1 and FOXM1 were also discovered. FOXM1 is a critical regulator of chemoresistance, metastasis, and oncogenesis (16). Our previous reports found that FOXM1 is overexpressed in OSCC cells (17).

Nonetheless, the expression regulators upstream of FOXM1 remain unknown. Merlin has been demonstrated to regulate FOXM1 expression in pancreatic tumours by ubiquitin-labelling and degradation of FOXM1 (34). Here, we also observed that DEPDC1 interacts with FOXM1. It was recently reported that DEPDC1 is mainly found in cancer cell nuclei (8). However, the accumulation of FOXM1 in the nucleus attracts β-catenin to the Wnt gene promoter, thereby inducing Wnt signaling (35). By managing the structural changes in FOXM1, DEPDC1 can make it more stable. Despite these facts, a better understanding of the complicated mechanisms involved in DEPDC1-mediated FOXM1 stability regulation is needed.

The molecular processes behind the function of DEPDC1 remain uncertain. In cancer, Wnt/β-catenin pathways are usually disrupted and are key OSCC tumorigenesis mediators (36). Nuclear migration and stability of β-catenin are important processes for the continuous stimulation of this signaling. The results from gene enrichment examination suggest that general and WNT/β-catenin-specific cancer signaling pathways related to HCC cancer genes had a positive correlation with DEPDC1 expression (10). In earlier studies, Zhang et al. showed that

nuclear translocation of β-catenin was enhanced by direct FOXM1 binding (37). This is the first time that a blocked Wnt/β-catenin signal and β-catenin nuclear translocation have been reported in OSCC cells due to DEPDC1 downregulation. Since Wnt/β-catenin signaling is an important contributor to OSCC development and spread, identifying pathological molecular mechanisms behind OSCC will be aided by discovering a DEPDC1/FOXM1/β-catenin signaling complex.

Conclusion

These findings show that DEPDC1 overexpression is linked to poor clinical outcomes and tumour progression in OSCC patients. FOXM1 interacts with DEPDC1, which causes cancer in OSCC cells, according to these fundamental *in vitro* data. Furthermore, this study describes a novel regulatory signaling pathway driven by DEPDC1 that enhances cancer characteristics by leveraging the Wnt/β-catenin OSCC. Our findings add to our understanding of the pathogenesis of OSCC cancer tumorigenesis.

Data availability statement

The original contributions presented in the study are included in the article/Supplementary Material. Further inquiries can be directed to the corresponding authors.

Ethics statement

This study was approved by the Ethics and Research Committee of Qingdao Municipal Hospital and conducted according to the ethical guidelines of the 1975 Declaration of Helsinki. The animal study was reviewed and approved by the Institutional Animal Care and Use Committee of Qingdao Municipal Hospital. Approval reference number QMHAS20180812. Written informed consent was obtained from the individual(s) for the publication of any potentially identifiable images or data included in this article.

Author contributions

JQ, YT, HC and RY performed most of the experiments included in this study. HC and RY wrote the first draft of the manuscript. LL completed and formatted the manuscript for submission. JY and ZC helped in analyzing the data. All authors contributed to the article and approved the submitted version.

Funding

This work was supported by Natural Science Foundation of Zhejiang Province of China (LGF19H160014) and Natural Science Basic Research Program Shaanxi Province (2020JM-008).

Acknowledgments

We appreciate researchers who have developed and maintained public databases such as GEPIA2, UALCAN, and OncoLnc (http://www.oncolnc.org/), which will accelerate the understanding and treatment of human cancer.

Conflict of interest

The authors declare that the research was conducted in the absence of any commercial or financial relationships that could be construed as a potential conflict of interest.

Publisher's note

Supplementary material

The Supplementary Material for this article can be found online at: https://www.frontiersin.org/articles/10.3389/fonc.2022.815998/full#supplementary-material

SUPPLEMENTARY FIGURE 1
Expression and overall survival (O.S.) of DEPDC1 family in HNSC patients from the GEPIA, UALCAN and OncoLnc databases. **(A)** UALCAN database displays DEPDC1 is in a high expression status in multiple tumour types. **(B)** Expression of DEPDC1 in patients with HNSC in the UALCAN database. **(C)** DEPDC1 is associated with clinical stages (UALCAN) in HNSC. **(D)** Expression of DEPDC1 in patients with HNSC in the GEPIA database. **(E)** HNSC Patients in the OncoLnc sample were assessed using The Kaplan-Meier approach, which was used to classify patients into a group of high expression with ≥25% above the median. Meanwhile, the low expression had ≤25% less than the median.

SUPPLEMENTARY FIGURE 2
SCC-25 cell DEPDC1 was knocked down and overexpressed in the CAL-27 cells. **(A)** Detection of DEPDC1 expression in SCC-25 cells after down-regulated by sh-DEPDC1. **(B)** Detection of DEPDC1 expression in CAL-27 cells after upregulated by OE-DEPDC1. **P < 0.01. The data are presented as the mean ± SD, and are representative of at least 3 independent experiments.

SUPPLEMENTARY FIGURE 3
Identification of the DEPDC1 interacting proteins. **(A)** The FOXM1 protein expression correlated with DEPDC1 by Pearson correlation coefficient (PCC) analysis. **(B)** The intracellular location of DEPDC1 and FOXM1 was shown on the GeneCards website. **(C)** Construction map of FOXM1-Flag and DEPDC1-V5 vectors.

References

1. Siegel RL, Miller KD, Fuchs HE, Jemal A. Cancer statistics, 2022. *CA Cancer J Clin* (2022) 72:7–33. doi: 10.3322/caac.21708

2. Leemans CR, Snijders P, Brakenhoff RH. The molecular landscape of head and neck cancer. *Nat Rev Cancer*. (2018) 18:269–82. doi: 10.1038/nrc.2018.11

3. Zeng H, Chen W, Zheng R, Zhang S, Ji JS, Zou X, et al. Changing cancer survival in china during 2003-15: a pooled analysis of 17 population-based cancer registries. *Lancet Glob Health* (2018) 6:e555–67. doi: 10.1016/S2214-109X(18)30127-X

4. Sung H, Ferlay J, Siegel RL, Laversanne M, Soerjomataram I, Jemal A, et al. Global cancer statistics 2020: globocan estimates of incidence and mortality worldwide for 36 cancers in 185 countries. *CA Cancer J Clin* (2021) 71:209–49. doi: 10.3322/caac.21660

5. Su CW, Lin CW, Yang WE, Yang SF. Timp-3 as a therapeutic target for cancer. *Ther Adv Med Oncol* (2019) 11:432488009. doi: 10.1177/1758835919864247

6. Sendoel A, Maida S, Zheng X, Teo Y, Stergiou L, Rossi CA, et al. Depdc1/let-99 participates in an evolutionarily conserved pathway for anti-tubulin drug-induced apoptosis. *Nat Cell Biol* (2014) 16:812–20. doi: 10.1038/ncb3010

7. Mi Y, Zhang C, Bu Y, Zhang Y, He L, Li H, et al. Depdc1 is a novel cell cycle related gene that regulates mitotic progression. *Bmb Rep* (2015) 48:413–8. doi: 10.5483/bmbrep.2015.48.7.036

8. Harada Y, Kanehira M, Fujisawa Y, Takata R, Shuin T, Miki T, et al. Cell-permeable peptide depdc1-znf224 interferes with transcriptional repression and oncogenicity in bladder cancer cells. *Cancer Res* (2010) 70:5829–39. doi: 10.1158/0008-5472.CAN-10-0255

9. Li Y, Tian Y, Zhong W, Wang N, Wang Y, Zhang Y, et al. Artemisia argyi essential oil inhibits hepatocellular carcinoma metastasis *via* suppression of depdc1 dependent wnt/beta-catenin signaling pathway. *Front Cell Dev Biol* (2021) 9:664791. doi: 10.3389/fcell.2021.664791

10. Qu D, Cui F, Lu D, Yang Y, Xu Y. Dep domain containing 1 predicts prognosis of hepatocellular carcinoma patients and regulates tumor proliferation and metastasis. *Cancer Sci* (2019) 110:157–65. doi: 10.1111/cas.13867

11. Zhang L, Du Y, Xu S, Jiang Y, Yuan C, Zhou L, et al. Depdc1, negatively regulated by mir-26b, facilitates cell proliferation *via* the up-regulation of foxm1 expression in tnbc. *Cancer Lett* (2019) 442:242–51. doi: 10.1016/j.canlet.2018.11.003

12. Gong Z, Chu H, Chen J, Jiang L, Gong B, Zhu P, et al. Depdc1 upregulation promotes cell proliferation and predicts poor prognosis in patients with gastric cancer. *Cancer biomark* (2021) 30:299–307. doi: 10.3233/CBM-201760

13. Feng X, Zhang C, Zhu L, Zhang L, Li H, He L, et al. Depdc1 is required for cell cycle progression and motility in nasopharyngeal carcinoma. *Oncotarget*. (2017) 8:63605–19. doi: 10.18632/oncotarget.18868

14. Kopanja D, Chand V, O'Brien EM, Mukhopadhyay NK, Zappia MP, Islam A, et al. Transcriptional repression by foxm1 suppresses tumor differentiation and promotes metastasis of breast cancer. *Cancer Res* (2022) 82:2458–71. doi: 10.1158/0008-5472.CAN-22-0410

15. Xing S, Tian Z, Zheng W, Yang W, Du N, Gu Y, et al. Hypoxia downregulated mir-4521 suppresses gastric carcinoma progression through regulation of igf2 and foxm1. *Mol Cancer*. (2021) 20:9. doi: 10.1186/s12943-020-01295-2

16. Kalathil D, John S, Nair AS. Foxm1 and cancer: faulty cellular signaling derails homeostasis. *Front Oncol* (2020) 10:626836. doi: 10.3389/fonc.2020.626836

17. Qiu J, Zhao J, Zuo A, Liu L, Liu Q, Pan H, et al. Lentiviral rna interference-mediated downregulation of forkhead box m1 expression suppresses growth of oral squamous cell carcinoma. *vitro*. *Oncol Lett* (2019) 17:525–31. doi: 10.3892/ol.2018.9536

18. Borhani S, Gartel AL. Foxm1: a potential therapeutic target in human solid cancers. *Expert Opin Ther Targets*. (2020) 24:205–17. doi: 10.1080/14728222.2020.1727888

19. Ramos-Garcia P, Gonzalez-Moles MA. Prognostic and clinicopathological significance of the aberrant expression of beta-catenin in oral squamous cell carcinoma: a systematic review and meta-analysis. *Cancers (Basel)*. (2022) 14:479. doi: 10.3390/cancers14030479

20. Bugter JM, Fenderico N, Maurice MM. Mutations and mechanisms of wnt pathway tumour suppressors in cancer. *Nat Rev Cancer*. (2021) 21:5–21. doi: 10.1038/s41568-020-00307-z

21. Hsu CC, Liao WY, Chang KY, Chan TS, Huang PJ, Chiang CT, et al. A multi-mode wnt- and stemness-regulatory module dictated by foxm1 and aspm isoform i in gastric cancer. *Gastric Cancer*. (2021) 24:624–39. doi: 10.1007/s10120-020-01154-5

22. Tang Z, Kang B, Li C, Chen T, Zhang Z. Gepia2: an enhanced web server for large-scale expression profiling and interactive analysis. *Nucleic Acids Res* (2019) 47:W556–60. doi: 10.1093/nar/gkz430

23. Chandrashekar DS, Bashel B, Balasubramanya S, Creighton CJ, Ponce-Rodriguez I, Chakravarthi B, et al. Ualcan: a portal for facilitating tumor subgroup gene expression and survival analyses. *Neoplasia*. (2017) 19:649–58. doi: 10.1016/j.neo.2017.05.002

24. Zheng H, Zhang G, Zhang L, Wang Q, Li H, Han Y, et al. Comprehensive review of web servers and bioinformatics tools for cancer prognosis analysis. *Front Oncol* (2020) 10:68. doi: 10.3389/fonc.2020.00068

25. Reis PP, Waldron L, Perez-Ordonez B, Pintilie M, Galloni NN, Xuan Y, et al. A gene signature in histologically normal surgical margins is predictive of oral carcinoma recurrence. *BMC Cancer*. (2011) 11:437. doi: 10.1186/1471-2407-11-437

26. Qiao C, Qiao T, Yang S, Liu L, Zheng M. Snhg17/mir-384/elf1 axis promotes cell growth by transcriptional regulation of ctnnb1 to activate wnt/beta-catenin pathway in oral squamous cell carcinoma. *Cancer Gene Ther* (2022) 29:122–32. doi: 10.1038/s41417-021-00294-9

27. Wang Y, Wu J, Luo W, Zhang H, Shi G, Shen Y, et al. Alpk2 acts as tumor promotor in development of bladder cancer through targeting depdc1a. *Cell Death Dis* (2021) 12:661. doi: 10.1038/s41419-021-03947-7

28. Colak D, Nofal A, Albakheet A, Nirmal M, Jeprel H, Eldali A, et al. Age-specific gene expression signatures for breast tumors and cross-species conserved potential cancer progression markers in young women. *PLoS One* (2013) 8:e63204. doi: 10.1371/journal.pone.0063204

29. Tomczak K, Czerwinska P, Wiznerowicz M. The cancer genome atlas (tcga): an immeasurable source of knowledge. *Contemp Oncol (Pozn)*. (2015) 19:A68–77. doi: 10.5114/wo.2014.47136

30. Zhang L, Li Y, Dai Y, Wang D, Wang X, Cao Y, et al. Glycolysis-related gene expression profiling serves as a novel prognosis risk predictor for human hepatocellular carcinoma. *Sci Rep* (2021) 11:18875. doi: 10.1038/s41598-021-98381-2

31. Zhang J, Liu X, Zhou W, Lu S, Wu C, Wu Z, et al. Identification of key genes associated with the process of hepatitis b inflammation and cancer transformation by integrated bioinformatics analysis. *Front Genet* (2021) 12:654517. doi: 10.3389/fgene.2021.654517

32. Oren Y, Tsabar M, Cuoco MS, Amir-Zilberstein L, Cabanos HF, Hutter JC, et al. Cycling cancer persister cells arise from lineages with distinct programs. *Nature*. (2021) 596:576–82. doi: 10.1038/s41586-021-03796-6

33. Bolomsky A, Heusschen R, Schlangen K, Stangelberger K, Muller J, Schreiner W, et al. Maternal embryonic leucine zipper kinase is a novel target for proliferation-associated high-risk myeloma. *Haematologica*. (2018) 103:325–35. doi: 10.3324/haematol.2017.172973

34. Quan M, Cui J, Xia T, Jia Z, Xie D, Wei D, et al. Merlin/nf2 suppresses pancreatic tumor growth and metastasis by attenuating the foxm1-mediated wnt/beta-catenin signaling. *Cancer Res* (2015) 75:4778–89. doi: 10.1158/0008-5472.CAN-14-1952

35. Chen Y, Li Y, Xue J, Gong A, Yu G, Zhou A, et al. Wnt-induced deubiquitination foxm1 ensures nucleus beta-catenin transactivation. *EMBO J* (2016) 35:668–84. doi: 10.15252/embj.201592810

36. Xie J, Huang L, Lu YG, Zheng DL. Roles of the wnt signaling pathway in head and neck squamous cell carcinoma. *Front Mol Biosci* (2020) 7:590912. doi: 10.3389/fmolb.2020.590912

37. Zhang N, Wei P, Gong A, Chiu WT, Lee HT, Colman H, et al. Foxm1 promotes beta-catenin nuclear localization and controls wnt target-gene expression and glioma tumorigenesis. *Cancer Cell* (2011) 20:427–42. doi: 10.1016/j.ccr.2011.08.016

Advantages of publishing in Frontiers

OPEN ACCESS
Articles are free to read for greatest visibility and readership

FAST PUBLICATION
Around 90 days from submission to decision

HIGH QUALITY PEER-REVIEW
Rigorous, collaborative, and constructive peer-review

TRANSPARENT PEER-REVIEW
Editors and reviewers acknowledged by name on published articles

Frontiers
Avenue du Tribunal-Fédéral 34
1005 Lausanne | Switzerland

Visit us: www.frontiersin.org
Contact us: frontiersin.org/about/contact

REPRODUCIBILITY OF RESEARCH
Support open data and methods to enhance research reproducibility

DIGITAL PUBLISHING
Articles designed for optimal readership across devices

FOLLOW US
@frontiersin

IMPACT METRICS
Advanced article metrics track visibility across digital media

EXTENSIVE PROMOTION
Marketing and promotion of impactful research

LOOP RESEARCH NETWORK
Our network increases your article's readership